Department of Molecular & Clinical Cancer Medicine

Deregulation of DNA methylation and retrotransposon reactivation in NSCLC

Thesis submitted in accordance with the requirements
of the University of Liverpool for the degree of Doctor in Philosophy by
Alexandros Daskalos

February 2011

Supervisors: Triantafillos Liloglou & John K Field

To my wife Anna

Acknowledgements:

I am heartily thankful to my supervisors, Dr Triantafillos Liloglou and Professor John K Field, whose encouragement, guidance and support from the initial to the final step in this study, enabled me to develop my understanding on the subject and complete this thesis.

I am also grateful to my colleagues Dr George Xinarianos, Mr George Nikolaidis, Mrs Urszula Oleksiewicz, Dr Julie Bryan, Mrs Jennie Goggin, Miss Stephanie Unsworth and all the members of the Liverpool Lung Project team for their help and support throughout these three years. Special thanks to Mrs Beverley Green for taking care of all the administrative issues involved.

Finally I would like to express gratitude to the Roy Castle Lung Cancer Foundation. This study would not have been possible without their financial and moral support.

Disclaimer:

All of the work presented in this thesis, unless otherwise stated, is the work of the author.

Table of Contents

Abstract

Lung cancer has the highest mortality among all human neoplasias and non-small cell lung cancers (NSCLC) comprise approximately 85% of all lung cancer cases. DNA methylation deregulation, reflected by both global hypomethylation and regional hypermethylation, appears to play a major role in lung tumour development. Global hypomethylation affects repeated DNA sequences as well as CpG poor regions and imprinted genes and is linked to re-expression of embryonic genes and retro-transposable elements, loss of imprinting chromosomal instability and tumour formation. Regional hypermethylation involves in a great extent CpG islands of promoter regions and can promote carcinogenesis through the transcriptional silencing of multiple tumour-suppression genes (TSGs).

This study aims to elucidate some important aspects of DNA methylation deregulation in the development of NSCLC. In particular it was sought to: 1) explore the molecular mechanisms involved in the observed deregulation of DNA methylation and 2) measure the extent of global DNA hypomethylation in NSCLC and investigate its links with genomic instability and reactivation of retrotransposition.

In order to identify possible causes for the observed deregulation of DNA methylation patterns we have evaluated the mRNA expression levels of key players of the DNA methylation machinery (UHRF1, DNMT1, DNMT3A and DNMT3B) in primary non-small cell lung carcinomas by qPCR. The methylation status of two TSGs (CDKN2A and RASSF1) promoters was examined by pyrosequencing in the same set. In addition UHRF1 was knocked down by shRNA in A549 lung adenocarcinoma cells. All four genes were overexpressed in a coordinated manner in the lung tumour tissues and their expression correlated with that of E2F1. Higher UHRF1 expression in tumour tissues correlated with the hypermethylation of

CDKN2A and RASSF1 promoters while the relationship with a combined epigenotype was even stronger. DNMTs expression was also significantly higher in samples with either a hypermethylated RASSF1 or CDKN2A promoter. When UHRF1 was knocked down in A549 lung adenocarcinoma cells lower methylation levels of RASSF1, CYGB and CDH13 promoters were observed. Furthermore, UHRF1 knockdown clones demonstrated reduced proliferation and decreased cell migration properties. Our data demonstrate that UHRF1 is a key epigenetic switch, which controls cell cycle in NSCLC through its ability to sustain the transcriptional silencing of tumour suppressor genes by maintaining their promoters in a hypermethylated status.

Towards our second aim, we evaluated global DNA methylation by pyrosequencing, measuring the DNA methylation levels of LINE-1 and Alu transposable elements in primary non-small cell carcinomas and their paired adjacent tissues. We demonstrated a significant reduction of the methylation levels of both elements in a coordinated manner suggesting a possible common mechanism for their methylation maintenance. Genomic instability was assessed utilizing eleven fluorescent microsatellite markers located on lung cancer hot-spot regions such as 3p, 5q 9p, 13q and 17p. Hypomethylation of both transposable elements was associated with increased genomic instability. The reduction of the methylation index of LINE-1 and Alu elements following treatment of three lung cell lines with a demethylating agent consistently resulted in increased expression of both elements. We have also demonstrated, utilising a construct which carries a full LINE-1 element tagged with a reporter cassette, that unmethylated LINE-1 can retrotranspose successfully in a lung cancer cell line. Our study demonstrates the strong link between hypomethylation of transposable elements with genomic instability in non-small cell lung cancer and provides early evidence for a potential active role of these elements in lung neoplasia.

Findings of this study have been published in the following manuscripts:

A Daskalos, Urszula Oleksiewicz, A Filia, G Nikolaidis, G Xinarianos, JR Gosney, A Malliri, JK Field, T Liloglou. UHRF1-mediated tumour suppressor gene inactivation in non-small cell lung cancer. Cancer. 2010 Nov 8. [Epub ahead of print]

Daskalos A, Nikolaidis G, Xinarianos G, Paraskevi P, Cassidy A, Zakopoulou R, Kotsinas A, Gorgoulis V, Field JK, & Liloglou T. Hypomethylation of retrotransposable elements correlates with genomic instability in non-small cell lung cancer. Int J Cancer, 124: 81-87, 2009

A Daskalos, S Logotheti, S Markopoulou, G Xinarianos, JR Gosney, V Zoumpourlis, AN Kastania, JK Field and T Liloglou. Global DNA hypomethylation-induced ΔNp73 transcriptional activation in non-small cell lung cancer. Cancer Lett. 2011 Jan 1;300(1):79-86.

Logotheti S, Michalopoulos I, Sideridou M, **Daskalos A**, Kossida S, Spandidos D, Field JK Vojtesek B, Liloglou T, Gorgoulis V and Zoumpourlis V. Sp1 binds to the external promoter of the p73 gene and induces the expression of TAp73 γ isoform in lung cancer. FEBS J. 277: 3014-3027, 2010

Also communicated in the following research meetings:

A Daskalos, A Filia, G Nikolaidis, G Xinarianos, V Gorgoulis, A Kotsinas, J Field, T Liloglou. UHRF1 overexpression correlates with hypermethylation in non-small cell lung cancer. B104. NCRI Cancer Conference, 4-7 Oct 2009, Birmingham, UK.

G Xinarianos, **A Daskalos**, G Nikolaidis, P Savvari, A Cassidy, R Zakopoulou, A Kotsinas, V Gorgoulis, J Field, T Liloglou. Hypomethylation of LINE-1 and Alu-PV retrotransposble elements in lung cancer. NCRI Annual Meeting 2008, Birmingham, UK, 5-8 Oct 2008, A138

G Xinarianos, U Babiszkiewicz, **A Daskalos**, G Nikolaidis, A Filia, J Gosney, J Field, T Liloglou. Cytoglobin-mediated epigenetic reprogramming of non-small cell lung carcinomas. B112. NCRI Cancer Conference, 4-7 Oct 2009, Birmingham, UK.

Liloglou T, **Daskalos A**, Nikolaidis G, Xinarianos G, Field JK. Aberrant methylation of both Tp73 promoters in non-small cell lung cancer. 99th AACR Annual Meeting, San Diego, CA, April 12-16, 2008, P4268

Abbreviation table

Symbol	Description
AII	allelic imbalance index
CCD	charge coupled device
AZA	5-azacytidine
DNMTs	DNA methyltransferases
EGF	epidermal growth factor
EGFR	epidermal growth factor receptor
EN	endonuclease
FAL	fractional allele loss
FBS	foetal bovine serum
FHIT	fragile histine triad
GWAS	genome-wide association study
HDACs	histone deacetylases
HER2	heregulin receptor
ICF	Immunodeficiency, Centromere instability and Facial anomalies
LINEs	long interspersed nuclear elements
LLP	Liverpool Lung Project
LOH	loss of heterozygosity
LTR	long-terminal repeats
MBPs	methyl-binding proteins
MDB2	methyl-binding domain 2
MDS	myelodysplastic syndromes
MtI	methylation index
MTT	(3-(4,5-dimethy1–2-thioazoyl) 2,5-diphenyltetrazolium bromide)
NEO	neomycin
NSCLC	non-small cell lung cancer
ORF	open reading frame
OWA	open wound area
PCNA	proliferating cell nuclear antigen
PSQ	pyrosequencing
RQ	relative quantification
RT	reverse transcriptase
RTKs	receptor tyrosine kinases
SCC	squamous cell carcinoma
SCLC	small-cell lung cancer
SINEs	short interspersed nuclear elements
SRA	SET and RING associated
TDG	thymine DNA glycosylase
TPRT	target primed reverse transcription
TSA	Trichostatin-A
TSG	tumour-suppressor gene
UTR	untranslated region

Chapter 1. Lung Cancer

1.1 Epidemiology

1.1.1 Incidence

Lung cancer is a global health threat. In the year 2002, more than 1.3 million people worldwide were diagnosed with lung cancer [Parkin, 2005]. In the United Kingdom it is the second most commonly diagnosed cancer, following breast cancer, with 39,027 new cases observed in the year 2006. Lung cancer has the second higher incident rates in men, after prostate cancer, with 22,381 new cases observed in the year 2006 in the UK. In woman it is the third most commonly diagnosed cancer, following breast and colorectal cancer, with 16,646 new cases in the year 2006 in the UK [Cancer Stats, CRUK website, 2007] (Figure 1). In the United States lung cancer is the most commonly diagnosed cancer with an estimate of up to 219,440 new cases in 2009, with 116,090 cases for men and 103,350 cases for women [Jemal, 2009]. In Europe, lung cancer is the secondly most commonly diagnosed cancer in men after prostate cancer with 292,200 cases in 2006. In women lung cancer rated fourth with 94,100 cases after breast cancer, colorectal cancer and cancer of the uterus in the year 2006. Lung cancer is the third most commonly diagnosed cancer in Europe in both sexes (386,300) after breast and colorectal cancer in the year 2006 [Ferlay, 2007].

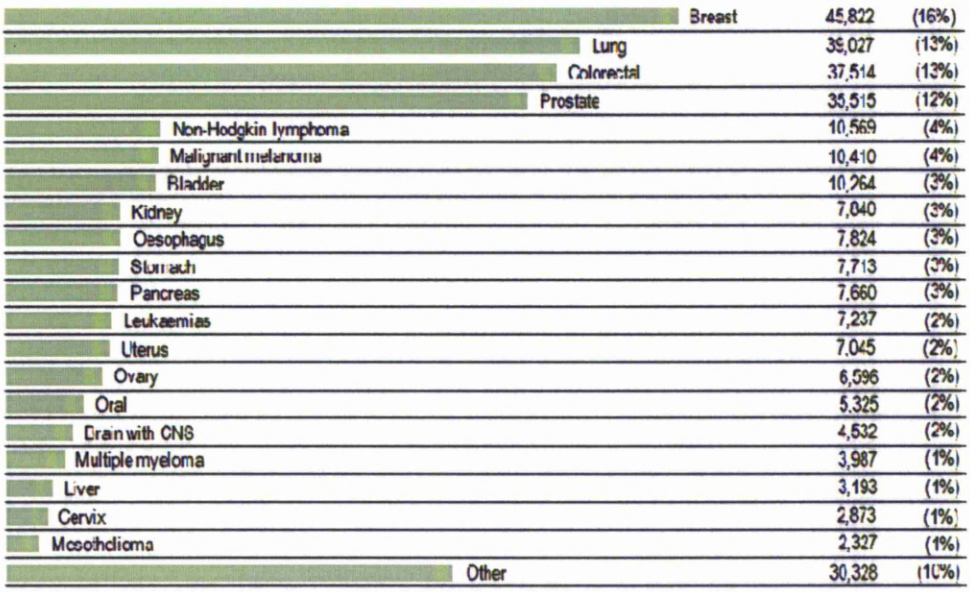

Figure 1. Incidence rates for the 20 most frequently diagnosed cancer types for the year 2006 in the UK. Number of cases includes both sexes. Lung cancer is the second most frequent cancer type with 39,027 cases. (Figure adapted without permission by Cancer Stats, CRUK website, 2007).

1.1.2 Survival - Mortality

Lung cancer is the leading cause of cancer-related deaths worldwide. In the United Kingdom for the year 2007, lung cancer mortality accounted for 22% of all cancer related deaths with 34,509 cases. It is of note that lung cancer mortality rates are more than two times higher than the next most common cause of cancer related death, colorectal cancer (Figure 2). Mortality rates are higher in men with 19,637 cases, compared to female mortality rates with 14,872 cases in 2007 in UK [Cancer Stats, CRUK website, 2007]. In the United States lung cancer is estimated to be the cause of 159,390 deaths (88,900 for men and 70,490 for women) for the year 2009 alone [Jemal, 2009]. The situation is similar in Europe where lung cancer related deaths account for 253.300 cases in men and 81.500 cases in woman, totalling 334.800 deaths in 2006 [Ferlay, 2007].

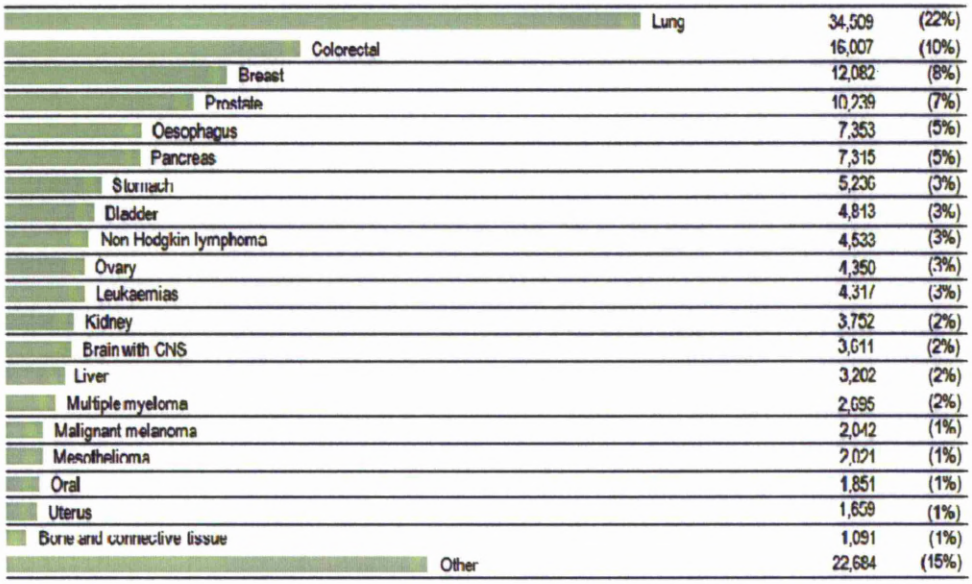

Figure 2 Mortality rates for the 20 most common causes of cancer-related death for the year 2007 in UK. Number of cases includes both sexes. Lung cancer is the most frequent cause of cancer-related death with 34,509 cases. (Figure adapted without permission by Cancer Stats, CRUK website, 2007).

The overall five-year survival after diagnosis of the disease has increased from 12.4% for the period 1974-1976 to 15% for the period 1996-2002 reflecting the limited advances in screening and treatment of lung cancer [Schwartz, 2007]. The poor 5 year-survival rates are mainly due to the late diagnosis of lung cancer cases combined with the failure of current therapeutic regimes to cure advanced disease [Breuer, 2005]. In the United States the 5 year survival rates are at 16% for 1996-2004 diagnoses, demonstrating an increase from 13% compared to the periods 1975-1977 and 1984-1986 [Jemal, 2009]. In England and Wales the 5 year survival rates are significantly lower, remaining bellow 10% for both men and women [Cancer Stats, CRUK website, 2007].

1.1.3 Risk Factors

The most important risk factor for lung cancer is long term exposure to inhaled tobacco smoke [Bruske-Hohlfeld, 2009]. Almost 87% of lung cancer cases are caused by cigarette smoking although only 20% of smokers will eventually get lung cancer [Hecht, 2002]. The risk of developing lung cancer is affected by smoking duration, level of consumption and tar content. However, the risk is much more dependent on duration of smoking rather than consumption. In addition, starting smoking at young age carries additional risks of lung damage [Cancer Stats, CRUK website, 2007].

The particulate phase of tobacco smoke contains more than 3500 chemical compounds, at least 55 of which have been identified as carcinogens. The two major classes of carcinogens are polycyclic aromatic hydrocarbons and tobacco-specific nitrosamines [Shields, 2002]. Tobacco induced carcinogenesis is a complex and multistep process. In general, tobacco smoking leads to increased carcinogen-DNA adduct formations which cause accumulating damage on the DNA of the pulmonary epithelial cells after a long latency period [Shields, 2002], [Hecht, 2002]. Other risk factors of lung cancer include; (i) exposure to industrial carcinogens such as asbestos, arsenic, chromium, nickel, cadmium, radon, particulate air pollution and others [Bruske-Hohlfeld, 2009]; (ii) respiratory diseases such as COPD, chronic bronchitis, emphysema and tuberculosis [Littman, 2004], [Schabath, 2005]; and (iii) family history [Matakidou, 2005] and genetic background [McKay, 2008], [Bailey-Wilson, 2004].

1.1.4 The LLP project

The Liverpool Lung Project (LLP) is a large population study, funded by the Roy Castle Foundation. It aims to reduce lung cancer mortality by developing early detection and

intervention schemes [Field, 2005]. LLP utilises epidemiological data and has developed a 5-year absolute risk assessment model for predicting lung cancer development [Cassidy, 2008]. The LLP participated in a large international consortium undertaking a genome-wide association study (GWAS) to identify SNPs that may be responsible for increased lung cancer risk [Hung, 2008], [McKay, 2008], [Lips, 2010]. Currently genetic and epigenetic biomarkers are being integrated into the model in order to increase its prediction efficiency. In parallel, a number of projects relevant to the genetics and biology of lung cancer development are undertaken, the present thesis being among them.

1.2 Pathology

1.2.1 Histological subtypes

The majority of lung tumours are classified into four major types: squamous cell carcinomas, adenocarcinomas, large cell carcinomas and small cell carcinomas. The remaining malignant epithelial tumours include adenosquamous carcinomas, sarcomatoid carcinomas, carcinoid tumours and other [Beasley, 2005]. The WHO classification of epithelial lung tumours is provided in Table 1 [Beasley, 2005]. Apart from tumours of epithelial origin lung cancer includes tumours with neuroendocrine morphology such as low grade typical carcinoids (TC) and intermediate grade atypical carcinoids (AC), sarcomatoid carcinomas such as pleomorphic carcinomas, spindle cell carcinomas and carcinosarcomas, and other pulmonary tumours including mucoepidermoid carcinomas (MEC) and adenoid cystic carcinomas [Beasley,2005]. For practical therapeutic reasons epithelial tumours are divided in two main categories: small cell lung cancers (SCLCs) and non-small cell lung cancers (NSCLCs) which account for

approximately 75% of lung tumours and include squamous cell carcinomas, adenocarcinomas and large cell carcinomas [Risch, 2008].

Table 1 2004 WHO Classification of malignant epithelial lung tumours (adapted without permission Beasley, 2005).

Squamous cell carcinoma	**Large cell carcinoma**
Variants	Variants
Papillary	Large cell neuroendocrine carcinoma
Clear cell	Combined large cell neuroendocrine carcinoma
Small cell	Basaloid carcinoma
Basaloid	Lymphoepithelioma-like carcinoma
Small cell carcinoma	Clear cell carcinoma
Variant	Large cell carcinoma with rhabdoid phenotype
Combined small cell carcinoma	**Adenosquamous carcinoma**
Adenocarcinoma	**Sarcomatoid carcinoma**
Adenocarcinoma, mixed subtype	Pleomorphic carcinoma
Acinar adenocarcinoma	Spindle cell carcinoma
Papillary adenocarcinoma	Giant cell carcinoma
Bronchioloalveolar carcinoma	Carcinosarcoma
Nonmucinous	Pulmonary blastoma
Mucinous	**Carcinoid Tumour**
Mixed nonmucinous and mucinous or indeterminate	Typical carcinoid
Solid adenocarcinoma with mucin production	Atypical carcinoid
Variants	**Salivary Gland Tumours**
Fetal adenocarcinoma	Mucoepidermoid carcinoma
Mucinous ("colloid") carcinoma	Adenoid cystic carcinoma
Mucinous cystadenocarcinoma	Epithelial-myoepithelial carcinoma
Signet ring adenocarcinoma	
Clear cell adenocarcinoma	

Squamous cell carcinoma (SCC) is the most frequent lung cancer pathology in Europe [Hoffman, 2000]. The great percentage of squamous cell carcinomas (75%) usually occurs as central masses while the remaining carcinomas are normally located peripherally [Beasley, 2005]. SCCs are usually associated with lobar collapse, obstructive pneumonia and haemoptysis and demonstrate late development of distant metastasis [Hoffman, 2000]. Figure 3 depicts the morphology of a typical squamous cell carcinoma under microscopic examination demonstrating keratinisation or intercellular bridges [Beasley, 2005].

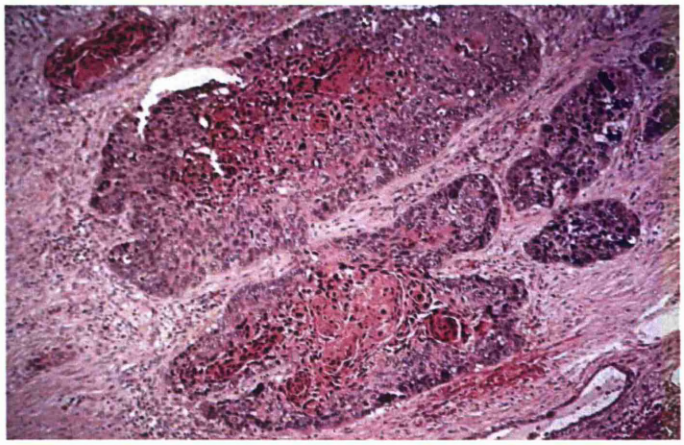

Figure 3 Photo of a squamous cell carcinoma. The tumour cells demonstrate keratinisation and squamous pearls (adapted without permission from Beasley, 2005)

Adenocarcinomas are usually present as peripheral nodules and are quite often heterogeneous containing more than one subtype [Beasley, 2005]. They are characterised by early development of metastases and are associated with smoking in a lesser extend compared to squamous cell carcinomas [Hoffman, 2000]. There are a number of different subtypes of adenocarcinomas as seen in Table 1. The morphology of acinar and bronchioloalveolar carcinoma types are distributed in figure 4.

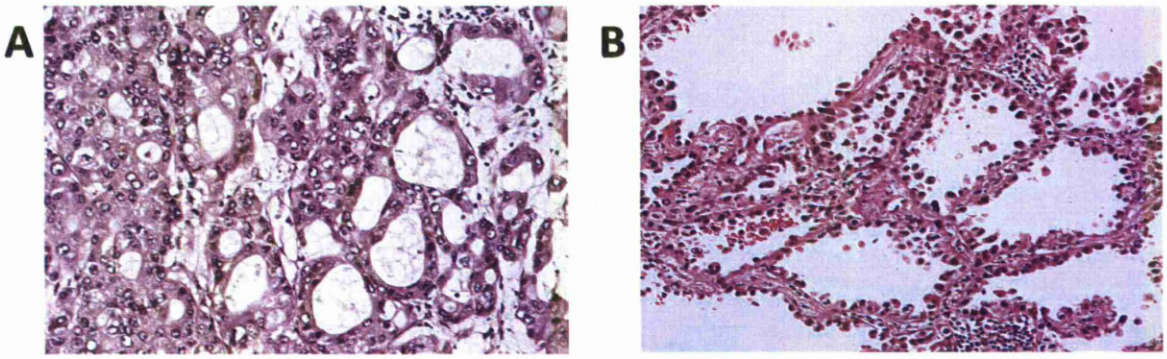

Figure 4 Subtypes of adenocarcinomas. A: Acinar adenocarcinomas. Tumour cells form glands or acini indicating adenocarcinomas differentiation. B:Nonmucinous type of bronchioloalveolar carcinoma (adapted without permission from Beasley, 2005)

Small-cell lung carcinomas are neuroendocrine tumours with small cell cytological features, oval shaped cells with scant cytoplasm and hyperchromatic nuclei and considered to be the most aggressive type of lung cancers (Figure 5) [Beasley, 2005], [Jackman, 2005]. They are strongly associated with smoking, they have a rapid growth rate and are characterised by early metastasis [Jackman, 2005] [Hoffman, 2000].

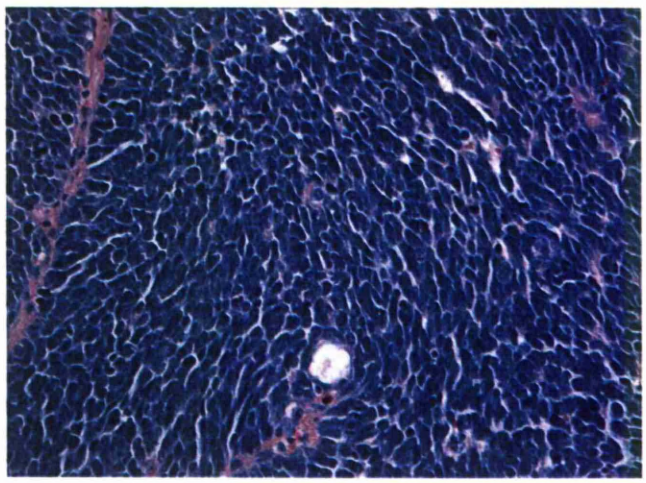

Figure 5 Small-cell lung cancer. The tumour demonstrates typical scant cytoplasm, increased mitotic index and spindling (adapted without permission from Jackman, 2005)

1.2.2 Symptoms and Treatment

Lung cancer patients present a variety of symptoms that may be associated with the primary tumour or mediastinal spread of the tumour, metastasis or paraneoplastic syndrome. Symptoms include dyspnoea, cough, haemoptysis, chest pain, loss of appetite and weight loss [Hamilton, 2005]. Lung cancer primary tumours can metastasise in many different sites including the brain, bone, liver, pleural cavity and skin [Hoffman, 2000].

Treatment differs for NSCLC and SCLC. Surgery is the main curative treatment for NSCLC patients, although the tumour may not be operable in many cases [Hoffman, 2000]. The five

year survival rates for stage I (T1N0, T2N0) patients treated with radical surgery are between 40%-67% [Hoffman, 2000]. Depending on the stage of the disease and patient's general health status, radical radiotherapy may be used instead of surgery but with a poorer outcome. Stage II (T1N1, T2N1, T3N0) patients have a 5 year survival rate of 25-55% after surgery. Surgery is also performed when possible, combined with radiotherapy and/or chemotherapy, for patients with advanced NSCLC (stage III), [Hoffman, 2000], [Burris, 2009].

In contrast, surgery for SCLC is rarely an option. Combined chemotherapy is the main treatment option with active drugs including cisplatin, etoposide, carboplatin and others while chest radiotherapy may also be applied in certain patients [Jackman, 2005]. 85-95% of patients with limited disease respond to combined chemotherapy with a median survival of 14-20 months and 5-year cancer free survival of 12-25%. 75-80% of patients with extensive disease respond to combined chemotherapy with a median survival of 7-10 months and 5-year cancer free survival of 2% [Jackman, 2005] [Hoffman, 2000].

1.3 Molecular Pathogenesis

Transformation of normal lung cells into cancer cells is a multistep procedure. This includes multiple genetic and epigenetic changes and result in some form of growth or cellular survival advantage [Breuer, 2005]. Genetic studies in lung cancer tissues and cell lines have shown that the key events causing lung carcinogenesis, as in all cancers, include (proto)oncogene activation and tumour-suppression gene (TSG) inactivation. Oncogene activation usually occurs through a mechanism such as chromosome translocation, gene amplification or point mutation [Breuer, 2005], [Risch, 2008]. TSGs inactivation is believed to take place in a two-step process affecting both alleles [Breuer, 2005]. Inactivation may take place due to loss of

heterozygosity (chromosomal deletion or translocation), point mutation or epigenetic changes such as silencing by hypermethylation or homozygous deletion [Breuer, 2005], [Risch, 2008]. The landscape of genetic and epigenetic changes across the complicated network of oncogenes and tumour suppressor genes involved in cancer development is massive. A small number of such representative gene changes are given below in the following paragraphs.

1.3.1 Oncogene activation

Proto-oncogene activation is a frequent phenomenon in lung cancers. Among the most frequently activated oncogenes observed are the RAS family proto-oncogenes. Usually activated due to point mutations, RAS family oncogene activation is detected in 15-20% of NSCLCs with K-RAS activation being the most frequent event [Aviel-Ronen, 2006]. Ras activated oncogenes induce the RAF1MEK/ERK pathway which is associated with transformation of cells and tumour progression [Sekido, 2003]. Genes of another proto-oncogene family, the Myc family (comprised of the MYC, MYCN and MYCL genes) are frequently activated either by gene amplification or transcriptional deregulation in lung cancers [Sekido, 2003], [Breuer, 2005]. At least one member of the MYC family is activated in 18% of SCLCs and 8% of NSCLCs [Richardson, 1993].

The receptor tyrosine kinases (RTKs) mediate cell signalling in response to extracellular growth factors. Members of this family, including the epidermal growth factor receptor (EGFR) and Heregulin receptor (HER2), are frequently deregulated in lung cancer and are associated with malignant transformation [Sharma, 2007], [Breuer, 2005]. EGFR is overexpressed in approximately 60% of NSCLCs, most frequently in squamous cell carcinomas, and is associated with poor prognosis [Sharma, 2007]. Heregulin receptor (HER2/neu) is overexpressed in approximately 30% of NSCLCs and is most frequent in adenocarcinomas and is also associated

with poor survival [Sekido, 2003]. Furthermore, the GRP growth hormone and its receptors are found to be overexpressed in 20%-50% of SCLCs promoting the growth of this lung cancer type [Sekido, 2003].

1.3.2 Tumour suppressor gene inactivation

P53 protein is one of the most studied proteins due to its clear function as a tumour suppressor gene. It is responsible for the maintenance of genome integrity preventing the accumulation of genetic damage in daughter cells. Activated by various stress signals, such as DNA damage, hypoxia, oncogene activation and others, it acts mainly as a transcription factor regulating a number of responsive genes, mediating cell-cycle arrest, senescence, DNA repair, apoptosis and many more functions of the cell [Vousden, 2007] (Figure 6). P53 is the most frequently mutated TSG in human cancers with alterations observed in 75%-100% of SCLCs and in 47% of NSCLCs [Sekido, 2003].

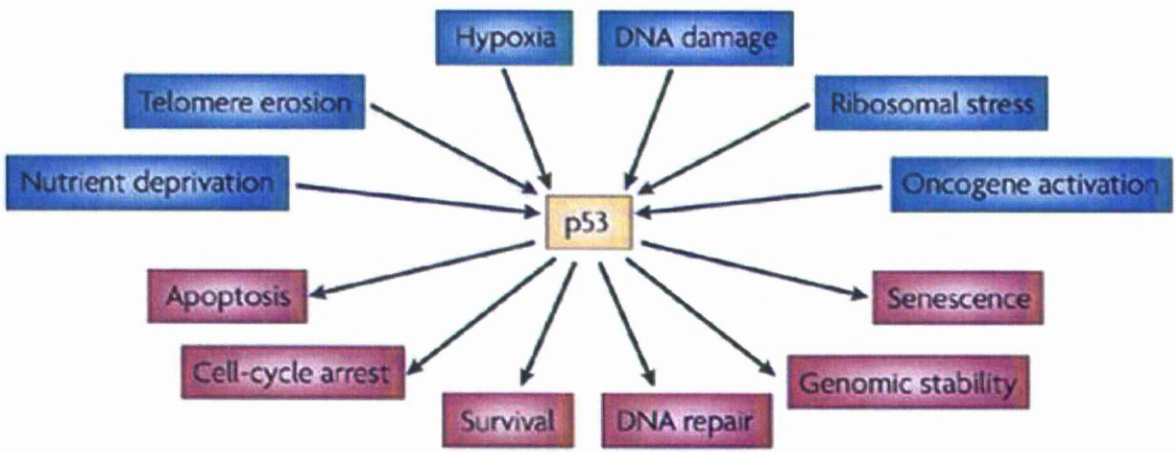

Figure 6 P53: the guardian of the human genome. P53 expression is induced by a variety of stress signals (blue boxes). Acting mainly as a transcription factor, p53 transactivates a variety of molecules affecting many different cell processes (pink boxes)(Figure adapted without permission from Vousden, 2007).

Inactivating mutations are the most frequent cause of p53 inactivation in lung cancers [Hollstein, 1991]. Other molecules that are part of the p53 pathway either as p53 regulators or upstream and downstream targets and are frequently deregulated in lung cancers include p21, p14ARF and MDM2 [Sekido, 2003].

The CDKN2A^{ink4a}-cyclin D1-CDK4-RB pathway, which is critical in controlling the G1 to S phase transition of the cell, is also widely disturbed in lung cancers. Two out of the four main compounds of this pathway, CDKN2A and Rb, are widely affected. The CDKN2A gene is inactivated due to either hypermethylation of its 5' promoter or due to inactivating mutations that occur in approximately 30%-70% of NSCLCs. The Rb protein, in its hypophosphorylated form, binds and blocks on the transition transcription factors E2F1, E2F2 and E2F3 which are essential for the G1 to S phase transition of the cell cycle. Inactivation of pRb due to deletion, nonsense mutations and splicing abnormalities appear in almost 90% of SCLCs and in 15-30% of NSCLCs [Sekido, 2003].

Frequent homozygous deletions at chromosome region 3p14.2 in lung cancers lead to the inactivation of the fragile histine triad (FHIT) TSG [Geradts, 2000]. In addition the FHIT gene is also silenced due to promoter hypermethylation in almost 50% of primary lung cancers [Zochbauer-Muller, 2001]. Other tumour suppressor genes that are frequently inactivated in cancers due to hypermethylation include RASSF1 which is inactivated in more than 90% of SCLCs and about 50% of NSCLCs [Sekido, 2003], [Vaissiere, 2009], CYGB [Xinarianos, 2006], and RAR-b [Virnani, 2000], [Risch, 2008].

Chapter 2. DNA methylation

2.1 Cancer Epigenetics

Epigenetic changes are defined as heritable changes in gene expression that occur independent of any alterations on the DNA sequence [Esteller, 2008]. Most of these changes are established during differentiation and reflect the epigenome of a cell. They include methylation of the cytosine residues of DNA, post-translational modifications of histone proteins and positioning of nucleosomes along the DNA [Sharma, 2010]. The epigenome of a cell is maintained through cell divisions, while failure to do so can potentially lead to the activation or de-activation of signalling pathways resulting quite frequently in catastrophic results regarding the proper function of the cell. Epigenetic reprogramming of the cell is studied in a great extent in human tumours and is believed to play a crucial role in carcinogenesis and tumour progression [Jones, 2002], [Jones, 2007], [Esteller, 2008], [Sharma, 2010]. In the following paragraphs we will study the role of DNA methylation in cancers while we will not stress out the other epigenetic changes observed in human cells.

2.2 DNA methylation

DNA methylation is probably the best studied epigenetic change in humans as yet. It involves the addition of a methyl group at the 5' site of a cytosine residue which, most of the times, is located prior to a guanidine residue (CpG dinucleotide) on the DNA chain [Cheng, 2008]. The addition of methyl groups does not occur randomly on CpG sites. It takes place mainly on stretches of DNA that include a great proportion of CpG sites, called CpG islands, and regions of large repetitive sequences (centromeric repeats, retrotransposable elements, satellite DNA). CpG islands can be found in the vicinity of about 76% of human promoters, their length

is between 0.4-3 kb, they have a rich C-G content (>55%) and CpG sites in greater frequency compared to the rest of the human genome with an observed/expected ratio of >0.6 [Goll, 2005]. While repetitive sequences are usually heavily methylated in normal tissues, CpG islands which are associated with both tissue-specific and housekeeping genes, are usually unmethylated or lightly methylated [Sharma, 2010], [Goll, 2005].

It is now well established that DNA methylation causes transcriptional repression, especially when affecting CpG islands in the vicinity of gene promoters. This is accomplished either by blocking the binding of transcription factors on the 5' end promoters of genes or by the recruitment of methyl-binding proteins, such as MeCp2, which mediate transcriptional repression through the subsequent recruitment of a histone deacetylase (HDACs) containing complex [Jones, 1998], [Sharma, 2010], [Boyes, 1991], [Nan, 1998]. Apart from its role on transcriptional repression, DNA methylation has others effects on the human genome. It is responsible for X chromosome inactivation, genomic imprinting, genome integrity and stability, for the maintenance of telomere length and normal development [Robertson, 2001], [Okano, 1999], [Brena, 2007], [Gonzalo, 2006]. The importance of the proper maintenance of methylation patterns, which are established during development, is obvious in genetic models were DNA methyltransferases (DNMTs) knockouts, the enzymes responsible for the methylation of DNA, can lead to genome instability [Brown, 2007] and tumour formation [Gaudet, 2003].

2.3 DNA methyltransferases

Methylation of the human genomic DNA is undertaken by DNMTs. In brief, when DNMTs bind to DNA, the target cytosine is extruded from the double helix into the active site of the enzyme where the transfer of a methyl group from the Ado-Met substrate takes place (Figure 7) [Cheng, 2001], [Cheng, 2008].

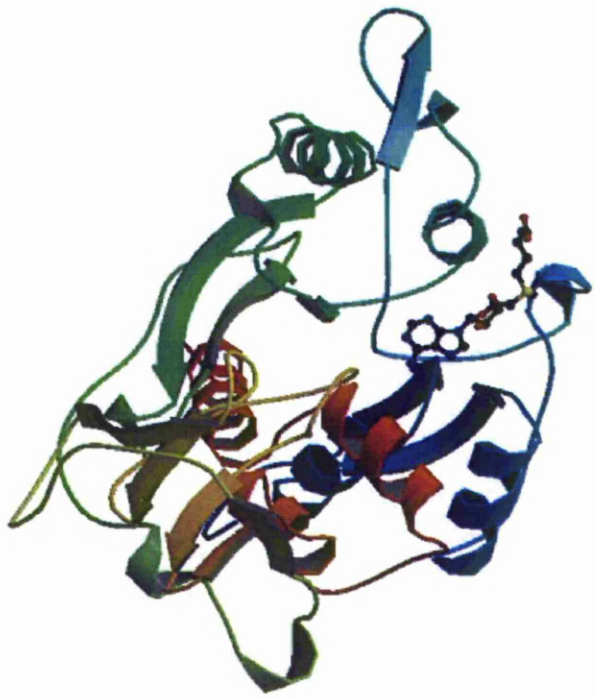

Figure 7 Crystal structure of the DNA (cytosine-5)-methyltransferase, M.HhaI (recognition sequence: GCGC) complexed with S-adenosyl-L-methionine. The core of the structure is dominated by sequence motifs conserved among all DNA (cytosine-5)-methyltransferases, and these are responsible for cofactor binding and methyltransferase function. Figure adapted without permission from Protein Data Bank (PDB file 1HMY, Cheng, 1993)

There are three DNMTs with proven de novo methylase activity; DNMT1, DNMT3A and DNMT3B [Bestor, 2000] while a fourth DNA methyltransferase DNMT3L appears to have an accessory function in de novo methylation, despite lacking itself any catalytic methylation activity [Cheng, 2008]. DNMT2 methylates cytosine 38 in the anticodon loop of $tRNA^{asp}$ while it has only a weak and ambiguous enzymatic activity on DNA substrate [Goll, 2006], [Hermann,

2003]. DNMT3 methyltransferases can be grouped in two distinct structurally and functionally families compared to DNMT1 or DNMT2 as seen in Figure 8 [Cheng, 2008].

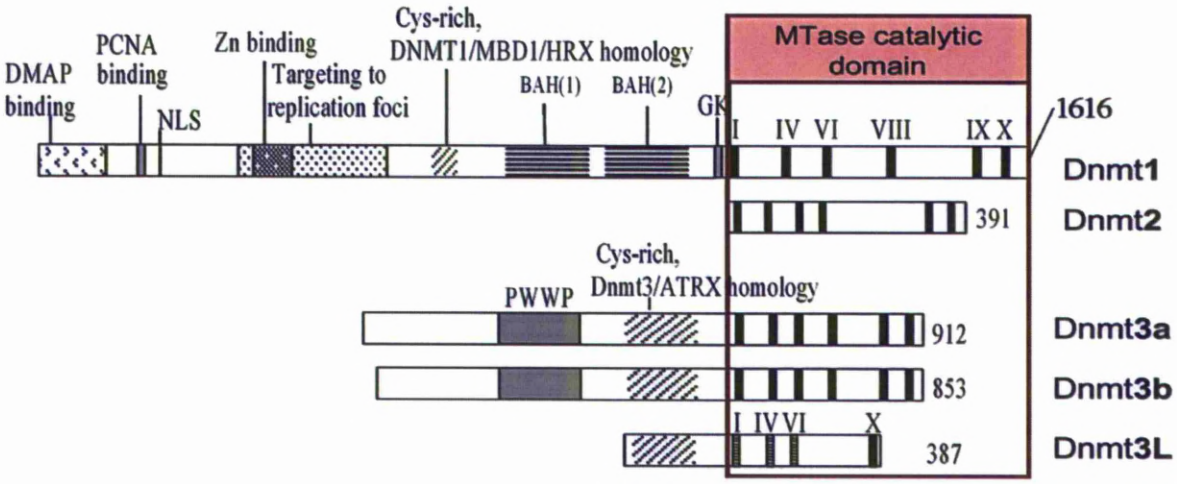

Figure 8 Architectural structure of the human DNA methyltransferases. The methyltransferase (MTase) catalytic domain can be seen in the pink box. DNMT3L has only a small part of the MTase domain lacking methyltransferase activity. Different domains such as PWWP, PCNA and ZN binding domains are marked on each gene. DNMT3A and DNMT3B share great homology (Figure adapted without permission from Cheng, 2008).

2.3.1 DNMT1

DNMT1 was the first methyltransferase to be identified [Bestor, 1988]. It is a large protein comprised of a 1616 amino acid sequence. At the C-terminal domain lays the catalytic centre (MTase catalytic domain) responsible for the methyltransferase activity of the enzyme. At the N-terminal part of the enzyme lie several individual domains, including the proliferating cell nuclear antigen (PCNA) binding domain, that are responsible for regulating the enzyme's activity (Figure 8)[Jeltsch, 2006].

DNMT1 is responsible mainly for maintaining methylation patterns during replication of DNA [Chen, 2006] and repair [Mortusewicz, 2005] demonstrating a thirty to forty fold preference for hemimethylated substrates compared to unmethylated substrates [Cheng, 2008] [Yoder,

1997]. However, de novo methylation activity of the enzyme cannot be excluded since DNMT1 is the only methyltransferase that was purified and cloned on the basis of its ability for de novo methylation and since its specific activity on unmethylated DNA is greater than the two main de novo methyltransferases DNMT3A and DNMT3B [Goll, 2005], [Cheng, 2008]. Additional features of DNMT1, supporting a maintenance methyltransferase character, are its ability to localise on replication foci via several independent domains and interact with the PCNA [Robertson, 2001].

DNMT1 expression is a prerequisite for proper embryonic development, imprinting, and X chromosome inactivation as demonstrated by DNMT1 knockout mice [Robertson, 2001] [Brown, 2007]. In addition, genetic studies of DNMT1 demonstrate a link between DNA methylation and tumourigenesis. This subject will be discussed in a following chapter.

2.3.2 The DNMT3 family

The DNMT3 family consists of the DNMT3A, DNMT3B and DNMT3L proteins. DNMT3A and DNMT3B can catalyse CpG methylation and are considered as the main de novo methyltransferases [Okano, 1999] while DNMT3L lacks any methyltransferase activity and functions only as a regulatory factor in germ cells [Goll, 2005]. The structure of DNMT3A and DNMT3B proteins is very closely related. On the C-terminus lies the catalytic centre of the proteins with the methyltransferase activity (MTase catalytic domain). The N-terminal tails of both proteins contain a PWWP domain and a cysteine-rich zinc-binding region related to that of DNMT1 and some of the methyl-binding proteins (MBPs) (Figure 8).

The two proteins can catalyse the transfer of methyl-group in unmethylated and hemimethylated substrates at equal rates and are expressed in a variety of adult tissues but in

lower rates compared to DNMT1 [Goll, 2005]. Double knockout mice of either DNMT3A or DNMT3B demonstrated global demethylation of the genome although in a lesser extent compared to DNMT1 knockout mice. In addition the inactivation of both genes blocks de novo methylation on embryonic stem cells and early mice embryos demonstrating that these proteins are essential for de novo methylation [Okano, 1999]. However, embryonic cells with no DNMT3B or DNMT3A activity demonstrate a mild demethylation which suggests that these two enzymes may also play a role in methylation maintenance assisting in a sense DNMT1 [Chen, 2003], [Okano, 1999], [Liang, 2002].

It is also worth noting that point mutations in human DNMT3B are responsible for the human ICF (**I**mmunodeficiency, **C**entromere instability and **F**acial anomalies) syndrome. This syndrome is caused by the hypomethylation of classical satellite DNA at the pericentromic regions of chromosomes 1, 9 and 16. These regions, following demethylation, demonstrate high rates of gains and losses of long arms and result in chromosomes with multiple long arms and single short arms [Goll, 2005], [Bestor, 2000].

DNMT3L is related to the other two proteins of the DNMT3 family in its C-terminal (MTase catalytic domain) and its N-terminal domain (cysteine-rich domain) but lacks the PWWP domain (Figure 8) [Goll, 2005]. It is expressed specifically in germ cells [Aapola, 2000] and as we already mentioned it lacks any methyltransferase activity [Aapola, 2000]. However DNMT3L co-localises with both DNMT3A and DNMT3B enhancing their de novo methylation enzymatic activity and is essential for the methylation of most imprinted loci and dispersed retrotransposons in germ cells [Bourc'his, 2004], [Webster, 2005], [Cheng, 2008].

2.4 UHRF1

Although DNMT1 demonstrates a 30-40 fold preference for hemimethylated DNA in vitro, it is questioned whether this ability is enough to explain the high fidelity observed in the inheritance of DNA methylation patterns [Ooi, 2008]. UHRF1 (also known as ICBP90) is a protein that has recently been found to play an important part in methylation maintenance assisting DNMT1 [Bostick, 2007], [Ooi, 2008]. It binds hemi-methylated DNA through its SRA (SET and RING associated) domain [Arita, 2008], [Avvakumon, 2008] and subsequently facilitates the loading of DNMT1 onto the replicating heterochromatic regions [Sharif, 2007], [Bostick, 2007]. UHRF1 knockout derivatives of mouse embryonic stem cells exhibit significant loss of genomic methylation demonstrating the important role of UHRF1 in the maintenance of DNA methylation patterns [Bostick, 2007].

Based on structural data Arita and colleagues [Arita, 2008] have suggested a model according to which UHRF1 facilitates the work of DNMT1 by recruiting it and in a sense offering the target sequence. In brief, after the recognition and binding of UHRF1 onto a hemi-methylated sequence, the methyl-cytosine base is flipped out of the DNA helix in the SRA-DNA complex and fits tightly into a protein pocket on the concave surface. The successive flip out of the pre-existing methylated cytosine and the target cytosine to be methylated is associated with the coordinated transfer of the hemi-methylated CpG site from UHRF1 to DNMT1 (Figure 9) (Arita, 2008).

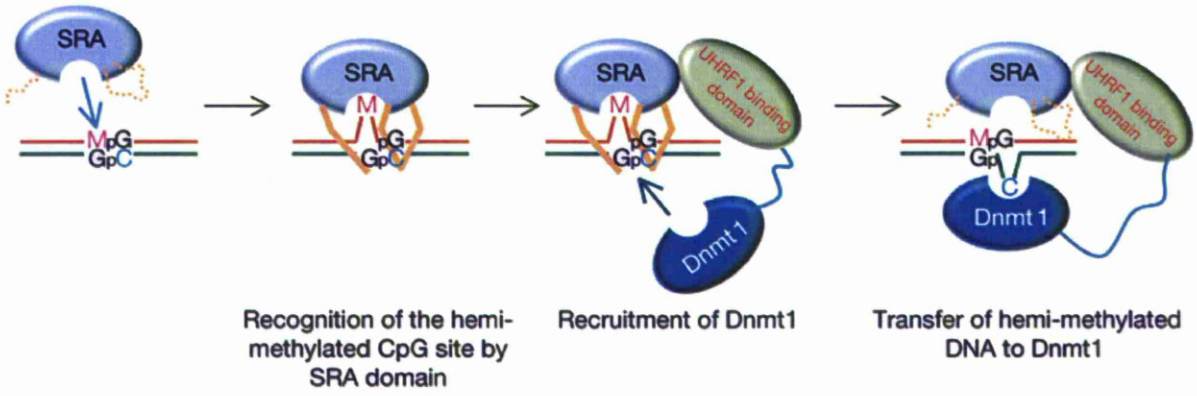

Figure 9 Proposed model for the role of UHRF1 in methylation maintenance. The SRA domain of the UHRF1 protein recognises hemimethylated CpG sites. The methylcytosine base is flipped out of the DNA helix in the SRA-DNA complex and fits tightly into a protein pocket on the concave surface of UHRF1. After recruitment of DNMT1, UHRF1 'offers' the target cytosine to DNMT1 (Figure adapted without permission from Arita, 2008)

It is worth noting that a recent study demonstrates strong interactions between the UHRF1 protein and the de novo methyltransferases DNMT3A and DNMT3B. Apart from DNMT1 mediated DNA methylation maintenance, this study suggests that UHRF1, together with DNMT3A and DNMT3B, can mediate promoter silencing through histone modification followed by DNA methylation [Meilinger, 2009].

2.5 Demethylases

DNA methylation can be removed passively by blocking methylation during DNA replication [Stresemann, 2008], [Wild, 2010]. However there have been several studies which suggest an alternative mechanism towards DNA hypomethylation. The general hypothesis is that methyl groups can be taken out of the CpG sites through active demethylation, a process which can be undertaken by specific demethylating proteins. Although this mechanism was proven in plants were active demethylation is undertaken by a family of m^5C glycosylase, in mammals a similar mechanism has not been established yet [Ooi, 2008]. Nevertheless, several molecules such as thymine DNA glycosylase (TDG), methyl-binding domain 2 (MDB2) protein or

GADD45a have been suggested to act as DNA demethylases in the literature [Jost, 1993], [Bhattacharya, 1999], [Hamm, 2008], [Barreto, 2007], although the field of active demethylation still remains unclear [for a review read Ooi, 2008]. It is of note that two recent studies suggest that the demethylation process is initiated by the same enzymes responsible for de novo DNA methylation, DNA methyltransferases DNMT3A and DNMT3B [Kangaspeska, 2008], [Metivier, 2008].

Chapter 3. DNA methylation in cancer

The spectrum of DNA methylation pattern alterations during cell transformation and tumour progression is wide. These changes are only a part of a fundamental epigenetic reprogramming that takes place in human cancers [Esteller, 2008]. DNA methylation changes can be classified into two major categories: global DNA hypomethylation and regional hypermethylation. Despite the plethora of studies exploring the causes and the effects of these two phenomena in cancer initiation and progression, the landscape remains far from being clear as to what is the biochemical relationship between them as well as their timing [Esteller, 2008], [Wild, 2010].

3.1 Global hypomethylation

The decrease in the overall 5-methylcytocine context of tumour cells was one of the first epigenetic changes to be observed in human cancers [Feinberg, 1983]. This is a common feature of human cancers affecting predominantly repeated DNA sequences such as LINES(long interspersed nuclear elements), SINES (short interspersed nuclear elements) and satellite repeats or CpG poor regions and imprinted genes [Ehrlich, 2002], [Sharma, 2010]. It is suggested that the degree of hypomethylation is related to the tumour progression. As tumour progresses from a benign to an invasive form hypomethylation increases [Esteller, 2008], [Fraga, 2004].

The significance of hypomethylation is now well established, with experiments in animal and cell models demonstrating its capability of promoting chromosomal instability and tumour formation [Gaudet 2003], [Eden, 2003], loss of imprinting and oncogene re-activation [Esteller, 2008], [Feinberg, 2006]. One of the possible means by which DNA hypomethylation

is suggested to promote carcinogenesis is by the 'unmasking' of repetitive sequences [Esteller, 2008]. Hypomethylation of repeated sequences can lead to genomic instability by promoting chromosomal rearrangements [Eden, 2003]. In addition, hypomethylation of retrotransposable elements which are part of the repeated sequences affected, may lead to their reactivation, translocation to other parts of the genome and finally to genomic instability [Howard, 2008], [Gaudet, 2003]. Retrotransposable elements and their possible reactivation in human cancer will be discussed in the following chapter. It is worth mentioning that, although DNA hypomethylation in cancers was observed earlier than regional hypermethylation, its relation with repeated sequences which pose technical difficulties, made this mechanism less popular and less studied than its counterpart [Ehrlich, 2006].

3.2 The human hypermethylome

Regional hypermethylation in human cancers affects in a great extend the CpG islands of promoter regions and is a major event in carcinogenesis, promoting the transcriptional silencing of many tumour-suppression genes (TSGs) [Esteller, 2008], [Feinberg, 2006]. To date, there is a large list of genes which have been shown to be at least partially silenced by promoter hypermethylation in human cancers, i.e. CDKN2A, Rb, BRCA1, VHL, RASSF1, RARB2, GSTP1, DAPK1, APC, and many more [Esteller, 2007], [Robertson, 2001]. The affected TSGs are part of different cellular pathways including cell signalling, adhesion and invasion, cell cycle, angiogenesis, DNA repair and apoptosis all of which are involved in cancer development (Table 2) [Esteller, 2007]. It is of note that the profiles of hypermethylated TSGs are specific for the different cancer types (picture 10) [Costello, 2000], [Esteller, 2007].

Table 2. Representative genes that are frequently hypermethylated in human tumours and affected pathways (Table adapted without permission from Esteller, 2007)

Pathways	Representative hypermethylated genes
DNA repair	hMLH1, MGMT, WRN, BRCA1
Hormone response	Estrogen, progesterone, androgen, prolactin and thyroid-stimulating hormone receptors
Vitamin response	RARB2, CRBP1,
Ras signalling	RASSFIA, NOREIA
Cell cycle	$CDKN2A^{INK4a}$, $p15^{INK4b}$, Rb
P53 network	p14ARF, p73, HIC-1
Cell adherence and invasion	E-cadherin, H-cadherin, FAT cadherin, EXT-1, SLIT2, EMP3
Apoptosis	TMS1, DAPK1, WIF-1, SFRP1
Wnt signaling	APC, DKK-1, IGFBP-3
Tyrosine kinase cascades	SOCS-1, SOCS-3, SYK
Transcription factors	GATA-4, GATA-5, ID4
Homeobox genes	PAX6, HOXA9
Other pathways	GSTP1, LKB1/STK11, THBS-14, COX-2, SRBC, RIZ1, TPEF/HPP1, SLC5A8, Lamin A/C
microRNAs	miR-127 (targeting BCL6), miR-124a (targeting CDK6)

Lung cancer is affected, as all cancer types, by regional hypermethylation. Hypermethylation of a plethora of gene promoters such as RASSF1 [Vaissiere, 2009], CDKN2A [Esteller, 1999], [Zochbauer-Muller, 2001], CYGB [Xinarianos, 2006], EDNRB [Knight, 2009], RARbeta [Virnani, 2000], MGMT [Zochbauer-Muller, 2001] and CDH13 [Vaissiere, 2009], [Kim, 2007] has been demonstrated indicating the key role of aberrant methylation into the progression of the disease.

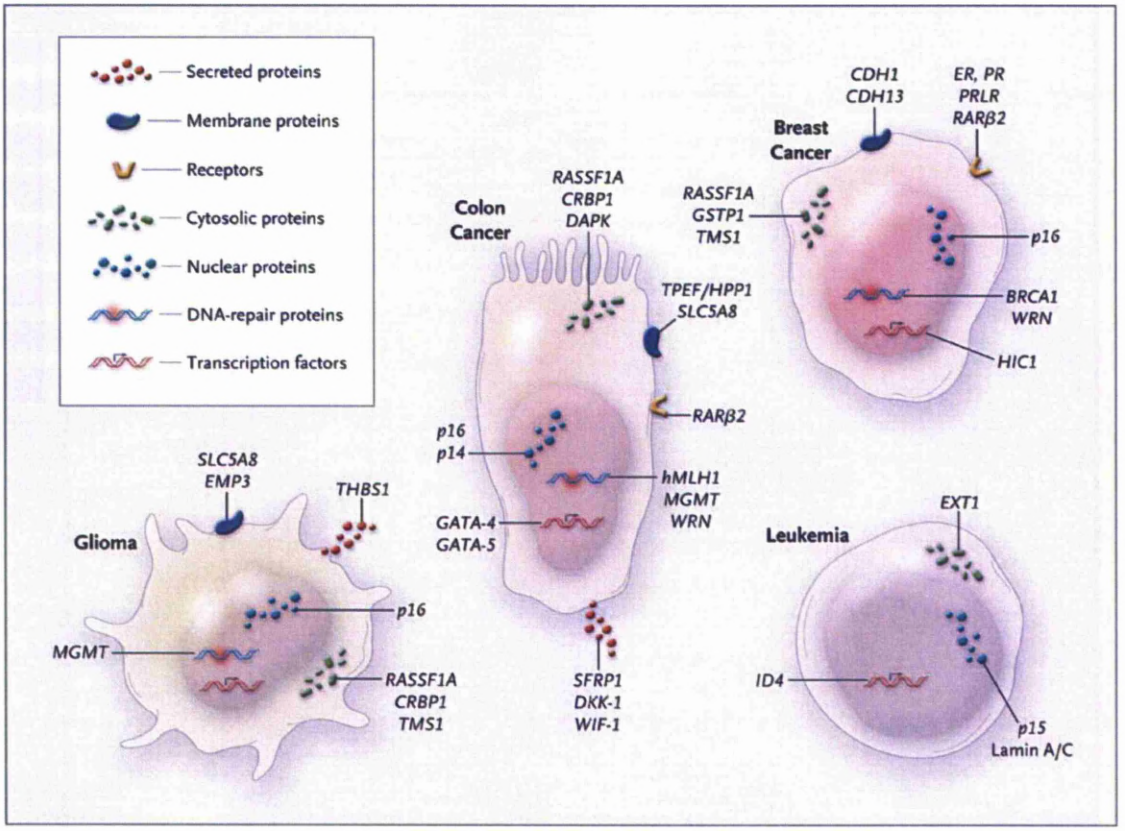

Figure 10 Frequently hypermethylated genes and their proteins in different cancer types (Figure adapted without permission from Esteller, 2008)

3.3 DNMTs and UHRF1 in human cancers

The majority of studies in human cancer tissues suggest that the expression levels of most DNMTs are increased [el-Deiry, 1991], [Robertson, 1999], [Robertson, 2001]. A study in lung cancer primary tissues demonstrates overexpression of all DNMT1, DNMT3A and DNMT3B while DNMT1 overexpression correlated with a poor prognosis [Lin, 2007]. Another study in NSCLC suggests that the predominant form of DNMT3B is the ΔDNMT3B isoform [Wang, 2006]. E2F1 can bind and regulate the expression of DNMT1 [Kimura, 2003], [McCabe, 2005]. It appears that the pRb/E2F pathway regulates the expression of DNMT1 increasing their

abundance during S and G2 phases [Vogel, 1988], [Jeanblanc, 2005] in order to replicate the DNA methylation patterns onto the newly synthesized strands.

Accumulated evidence suggests that UHRF1 has a putative oncogene function [Bronner, 2007]. In normal cells, UHRF1 is expressed in late G1 and during G2/M transition, however, in contrast, it is expressed throughout the cell cycle in cancer cell lines [Mousli, 2003] and overexpressed in breast carcinomas [Hopfner, 2000], [Jenkins, 2005], [Unoki, 2004] and pancreatic adenocarcinomas [Crnogorac-Jurcevic, 2005]. The UHRF1 gene is a target for the transcriptional activator E2F1 [Unoki, 2004], [Mousli, 2003] and its expression is associated with increased cell proliferation [Fujimori, 1998], [Hopfner, 2000]. Moreover, UHRF1 regulates the expression of topoisomerase II alpha and retinoblastoma genes, favouring cell entry into the S phase of the cell cycle [Jeanblanc, 2005], [Hopfner, 2000], [Hopfner, 2002]. In addition, UHRF1 expression knockdown leads to growth arrest [Arima, 2004], [Jenkins, 2005], [Bonapace, 2002], [Unoki, 2004]. There is limited information regarding the status of UHRF1 in lung cancer where overexpression of UHRF1 has been identified in the A549 cell line [Mousli, 2003] and in a small number (n=10) of primary lung tumours [Jenkins, 2005].

3.4 DNMTs, UHRF1 and aberrant methylation patterns

DNMT1, DNMT3A, DNMT3B and UHRF1 are the main molecules responsible for the generation and the maintenance of normal methylation patterns in human cells. This group of proteins may, therefore, provide a possible mechanism behind the aberrant methylation patterns observed in human cancers. A change in the expression levels of some of these proteins could potentially lead to the altered methylation profiles observed in cancers [Ehrlich, 2002]. In many cases the observed overexpression of DNMTs in primary human

tumours was analysed in comparison to the methylation status of several TSGs. Despite the lack of correlation between overexpression of DNMTs and hypermethylation of specific TSGs in some studies [Ehrlich, 2006], [Sato, 2002], [Park, 2006], other reports demonstrate associations between expression of specific DNMTs with hypermethylation status of specific genes. Overexpression of a specific DNMT3B isoform (ΔDNMT3B) in NSCLC is responsible for the hypermethylation of RASSF1 promoter but not CDKN2A promoter, suggesting that ΔDNMT3B can regulate methylation in a promoter specific manner [Wang, 2006], [Wang, 2007]. In addition DNMT1 overexpression correlates with hypermethylation of CDKN2A promoter [Lin, 2007], [Kim, 2006]. As already noted, UHRF1 is also overexpressed in many different cancer types. In a study in primary breast tumours, UHRF1 overexpression was found to be associated to BRCA1 promoter hypermethylation [Jin, 2009]. In addition, UHRF1 was found to be bound on methylated promoters of various tumour suppressor genes, including CDKN2A [Unoki, 2004].

The disruption of the activity of UHRF1 or any of the DNMTs in cell tissue models results into hypomethylation of the genome as previously discussed. Although primary tumours demonstrate global genomic hypomethylation, this cannot be connected to reduced or disrupted activity of DNMTs or UHRF1 since all these proteins tend to become overexpressed in human tumours. On the contrary, there is a report demonstrating that global hypomethylation correlates with overexpression of isoform DNMT3B4 in chronic myeloid leukaemia [Roman-Gomez, 2005]. It is also worth noting that there is a recent study suggesting that global hypomethylation, as measured by LINE-1 is inversely associated with CpG island methylator phenotype in colorectal cancer [Ogino, 2008]. However a study in

ovarian epithelial tumours suggests that there is no such association between the two phenomena [Ehrlich, 2002], thus the situation remains unclear.

3.5 Epigenetic cancer therapies.

Hypermethylation of TSGs is currently considered as a hallmark event in the tumour progression process [Esteller, 2007]. This notion has led to the use of hypomethylating agents for cancer treatment. The FDA has already approved the use of 5-azacytosine (azacytidine) and 2'-deoxy-5-azacytidine (decitabine) for the treatment of myelodysplastic syndromes [Plimack, 2007], [Issa, 2007].

Azacytidine and decitabine are nucleosidic analogs that cause hypomethylation in the same pattern. After cellular uptake, they are incorporated in the DNA during replication, where they substitute for cytosine. DNMTs recognise these nucleoside analogs as their normal substrate and initiate the methylation process by creating a covalent bond with their substrate. Although in the case of cytidine this bond is subsequently resolved and the enzyme is released, when either azacytidine or decitabine are present, this reaction is blocked and DNMT remains trapped on the DNA. This triggers DNA damage signalling and trapped DNMTs are being degraded. As a result hypomethylation occurs gradually during subsequent cycles of replication (Figure 11) [Stresemann, 2008], [Lyko, 2005].

Although azacytidine and decitabine act through the same mechanism, decitabine is believed to be more effective. This is a result of decitabine's ability to bind specifically on DNA while, on the contrary, azacytidine can be incorporated in high amounts (80-90%) into RNA [Li, 1970]. It is important to note that the effectiveness of these nucleoside analogs towards

demethylation of DNA is optimal in low doses while in higher doses, most probably due to cell cycle arrest, no demethylation is observed [Qin, 2007].

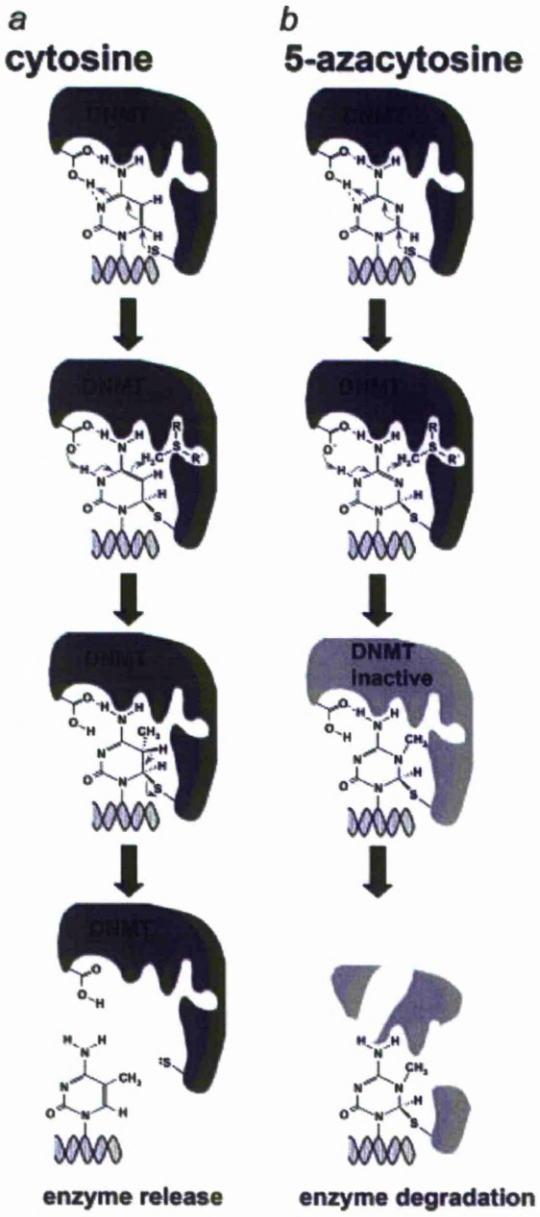

Figure 11 Azacytidine mechanism of DNMT depletion. (a) After binding, DNMT undertakes a nucleophilic attack at the C6 position of cytosine. Following, a methyl group from the methyl donor S-adenosyl-L-methionine is transferred through a covalent complex at position C6 between the DNA and the DNMT protein. A b-elimination reaction results in the resolve of the covalent complex and the subsequent release of the active DNA methyltransferase enzyme. (b) In the case of 5-azacytidine the covalent complex at C6 cannot be resolved through b-elimination because of the presence of a nitrogen atom at position 5. Covalently trapped DNMTs trigger DNA damage signalling which leads in the degradation of the enzymes (Figure adapted without permission from Stresemann, 2008)

To date demethylating agents show some results of clinical relevance in patients with myelodysplastic syndromes (MDS) where they have been introduced [Issa, 2007]. It was demonstrated that decitabine can cause hypomethylation of DNA in vivo [Momparler, 1984], which was connected in some patients with hypomethylation and re-expression of TSGs such as CDKN2B/$p15^{ink4B}$ [Daskalakis, 2002]. The molecular mechanisms behind the observed response of MDS patients to decitabine or azacytidine are not fully investigated and therefore it is still unclear at which extent toxicity of these substances to cells may cause this response [Lyko, 2005]. Possible molecular mechanisms suggested are the reactivation of TSGs due to hypomethylation and methylation-independent effects such as induction of p53 dependent DNA damage response [Santos, 2010], [Issa, 2009].

Although the use of demethylating agents in the treatment of MDS appears to be promising and there are a number of studies assessing the effect of this therapeutic option in other cancer types as well [Plimack, 2007], however the question remains as to the possible negative implications of global hypomethylation on human cells [see comments of Eden, 2003 and Yang, 2003]. It has been previously discussed that hypomethylation may potentially result in oncogene activation or reactivation of retrotransposable elements and also correlates with genomic instability and tumour formation [Gaudet, 2003], [Eden, 2003]. Although it is possible that the effect of demethylating agents may be favourable therapeutically, the need for further investigation into decitabine and other hypomethylating agent effects on the genome integrity is urgently required [Issa, 2007].

Chapter 4. Retrotransposable elements

4.1 Introduction

The initial sequencing and analysis of the human genome revealed that almost half of its content is derived from transposable elements (Figure 12) [Lander, 2001]. Transposable elements are divided into two major classes namely DNA transposons and retrotransposons.

DNA transposons can be excised from their specific location and be integrated into a different part of the genome by a cut and paste mechanism [Kazazian, 2004]. However these elements are currently considered to be inactive in the human genome [Lander, 2001].

Retrotransposons are transcribed into an RNA intermediate and through reverse transcription they are re-inserted into a new location of the genome, thereby duplicating themselves. They are further categorised into LTR retrotransposable elements (containing long-terminal repeats at both ends) and non-LTR retrotransposable elements (without long-terminal repeats but containing a polyadenylate sequence at their 3' end) [Kazazian, 2004]. LTR elements of the human genome are mainly endogenous retroviruses with limited activity of retrotransposition. Non-LTR retrotransposons include the LINE-1, ALU and SVA elements which account for the almost 30% of the human genome. These elements are currently active in the human genome resulting in different types of genetic disorders [Cordaux, 2009].

Retrotransposable elements are highly methylated in normal tissues while in human cancers they are affected by global hypomethylation. Since methylation is considered as one of the major mechanisms responsible for retaining their retrotransposition efficiency the next section will further describe in detail LINE-1 and Alu elements and explore their possible role in lung pathogenesis.

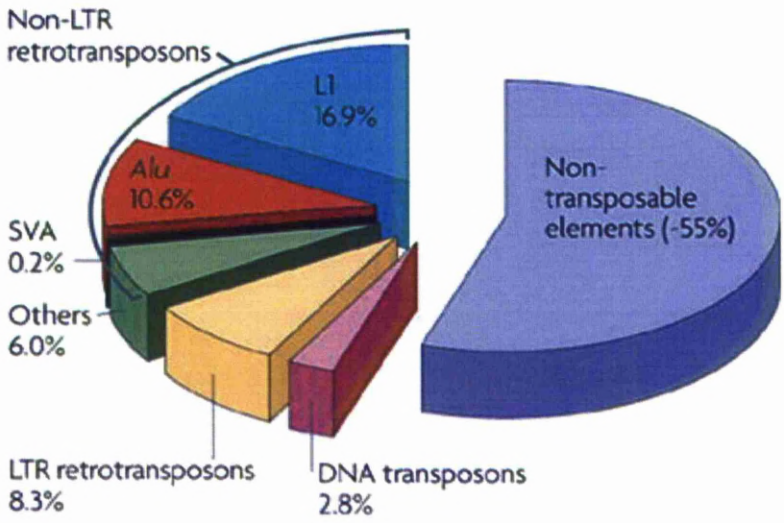

Figure 12 The proportion of transposable elements in the human genome. In total, transposable elements account for about 45% of the human DNA. Non-LTR retrotransposons (LINE-1, Alu, SV40 and related elements comprise the bulk of transposable elements which accounts for almost 34% of human DNA while LTR retrotransposons and DNA transposons are significantly less frequent. (Figure adapted without permission from Cordaux, 2009).

4.2 LINE-1 and Alu elements

LINE-1 elements (long interspersed nuclear elements, also termed LINE-1) are non-LTR retrotransposons accounting for about 17% of the human genome [Cordaux, 2009]. Although most of these elements are 5' truncated and therefore incapable of retrotransposition, there are an estimated number of 80-100 elements which are considered to be potentially active in the human genome [Brouha, 2003].

Full length LINE-1 elements are about 6 kb, and consist of a 5' UTR (untranslated region), two open reading frames(ORF) and a 3' UTR with a functional polyadenylation signal (Figure 13). The two open reading frames, ORF1 and ORF2, give rise to two proteins both of them required for retrotransposition. ORF1p is a 40 ~kDA protein with RNA binding and nucleic acid chaperone activities. During the retrotransposition event ORF1p facilitates complementary strand annealing, melting and strand displacement in mispaired DNA duplexes. ORF2p has an

endonuclease (EN) and a reverse transcriptase (RT) domain. The endonuclease domain is responsible for DNA cleavage with preference for the 5' TTTT AA 3' sequence [Babushok, 2007].

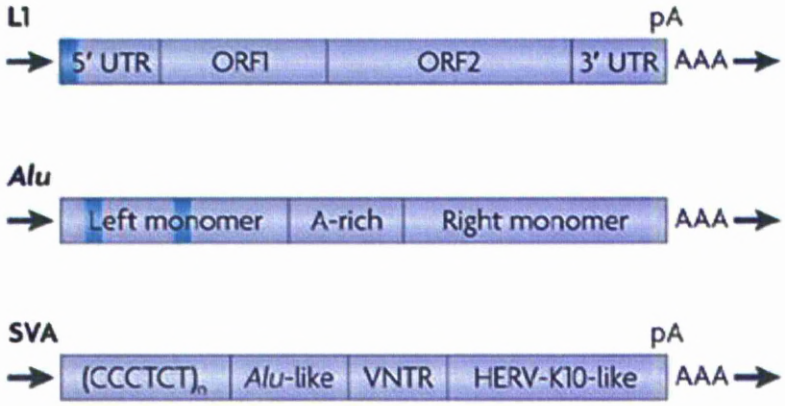

Figure 13 Structure of full human LINE-1 and Alu elements. LINE-1 is 6kb and contains a 910 bp 5' UTR region with promoter activity (blue box), an ORF1 region encoding a 40-kDa RNA-binding protein, an ORF2 region encoding for a 150 kDa protein with endonuclease (EN) and reverse transcriptase (RT) activities and a 3' UTR region which contains a functional polyadenylation signal. The Alu element is about 300 bp and consists of two similar 150 bp monomers separated by an A-rich linker region. The 5'end left monomer has a functional pol III promoter (blue boxes) while the 3'end ends in an oligo(dA)-rich tail. (Figure adapted without permission from Cordaux, 2009).

Although retrotransposition events of LINE-1 elements lacking the endonuclease domain were identified at atypical sites in DNA-repair deficient cell lines and at mammalian telomeres, it is less efficient and rarely found in vivo, underlying the need of the endonuclease domain for successful retrotransposition [Morrish, 2002], [Morrish, 2007]. LINE-1 elements retrotranspose through a target primed reverse transcription (TPRT) mechanism. In brief, the endonuclease domain of the ORF2 protein nicks the host genome preferentially at a 5' TTTT AA 3' site. The RT domain then uses the free 3' hydroxyl group as a primer and polymerises a cDNA copy of the LINE-1 RNA. The next steps most likely include second strand cleavage, LINE-1 RNA cleavage and second strand synthesis but are less understood (Figure 15) [Kazazian, 2004].

Alu elements are of even higher copy number in the human genome with more than 10^6 copies, comprising about 11% of the genome. The Alu consensus sequence is about 300 bp and consists of two similar 150 bp monomers with a 3' variable oligo dA tail. There is a functional pol III promoter in the left monomer (Figure 13) [Mighell, 1997]. Alu elements do not encode for specific proteins. It is thus suggested that their retrotransposition relies on other retrotransposable elements' machinery. The most likely candidate is LINE-1 element. There is a report demonstrating the ability of LINE-1 sequences to mediate retrotransposition of ALU sequences [Dewannieux, 2003]. This together with other data [Ostertag, 2001] suggest that ALU sequences use LINE-1 machinery in order to complete retrotransposition.

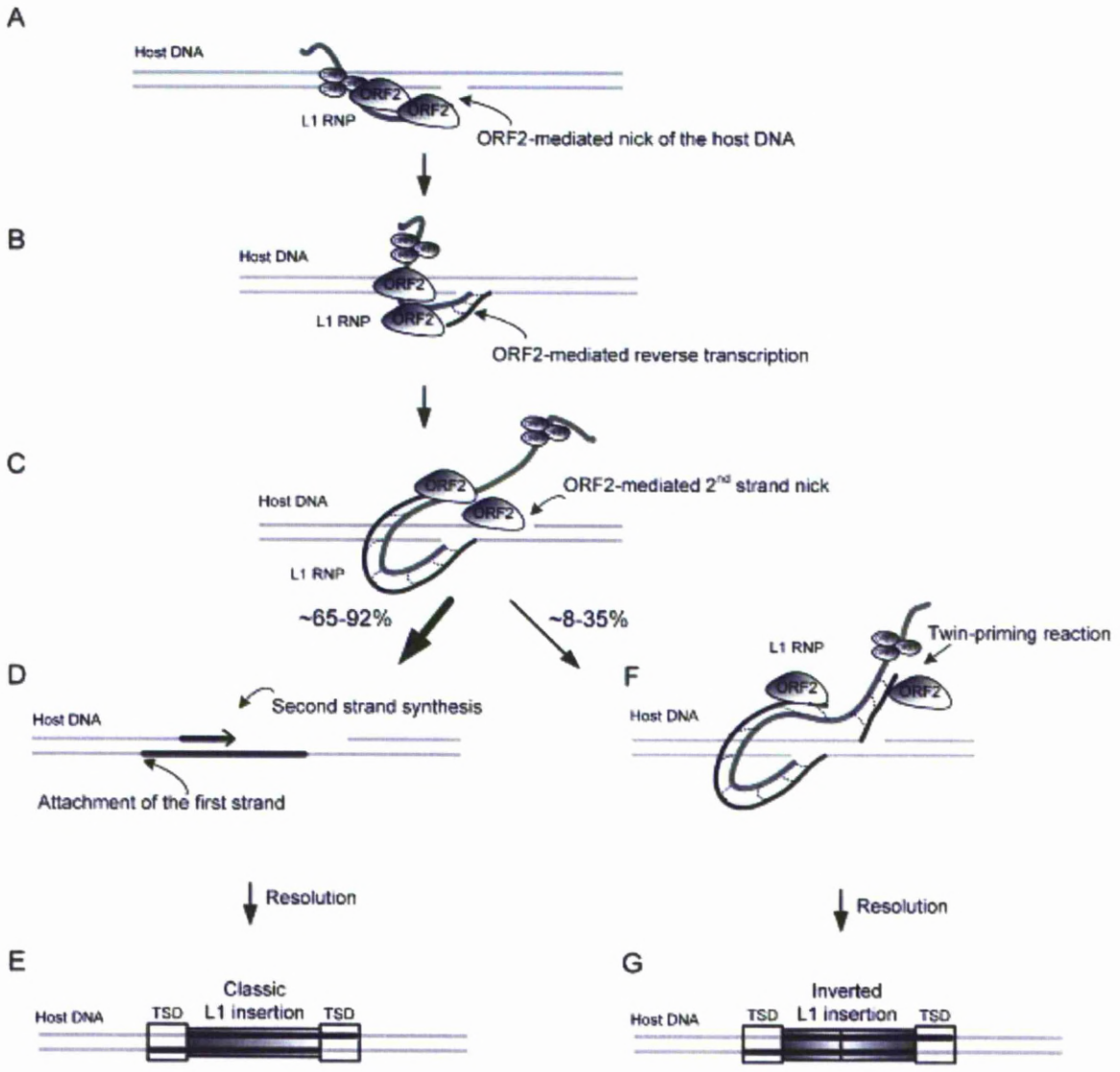

Figure 14 Proposed model of LINE-1 integration reaction. A: EN domain of the ORF2 protein nicks the host genome preferentially at a 5' TTTT AA 3' site. B: The RT domain of ORF2 then uses the free 3' hydroxyl group as a primer and polymerises a cDNA copy of the LINE-1 RNA. C-G: The next steps include second strand cleavage, LINE-1 RNA cleavage and second strand synthesis leading to either classic or inverted insertion of the LINE-1 sequence but are less understood (Figure adapted without permission from Progress in Understanding the Biology of the Human Mutagen LINE-1, Babushok, 2007)

4.3 Retrotransposition capacity and implications on the human genome

In normal cells, LINE-1 and Alu retrotransposition is rare. The LINE-1 promoter and the Alu sequences contain heavily methylated CpG islands, creating a condensed inaccessible form to the transcriptional machinery of the cells. The heavy methylated state of these elements also prevents recombination [Schulz, 2006].

Apart from the restriction of these elements' activities at the DNA level there are further barriers to their activity, at the RNA level. There are reports demonstrating inhibition of LINE-1 element retrotransposition by specific siRNAs that are produced by its 5'antisense promoter. These siRNAs act through RNAi machinery reducing LINE-1 transcripts in the culture models [Yang, 2006], [Soifer, 2006]. In addition, it is considered that the transcriptional elongation of the LINE-1 element is inadequate, thus leading to poor expression [Han, 2004]. Alu element's retrotransposition is inhibited by the editing of its RNA by APOBEC3G, although the restriction mechanism remains unclear [Esnault, 2005]. Alu elements are widely edited in the human transcriptome and the above report indicates towards a protective role of adenosine-to-inocine nucleoside modification against retrotransposition [Levanon, 2005]. Furthermore, there are reports demonstrating protection against activation of these elements at the retrotransposition step, with cells carrying intact p53 undergoing apoptosis [Haoudi, 2004].

The restriction mechanisms of normal cells posed on retrotransposable elements are required to keep them constrained, as their activation has been proved to be destructive for a cell. There are a number of human genetic disorders such as Neurofibromatosis [Wallace, 1991] and beta-thalassemia that were caused by LINE-1 and Alu elements through unequal homologous recombination or direct retrotransposition into gene areas [Ostertag, 2001].

Full LINE-1 elements have been studied in cell culture models were they were exogenously introduced. Their overexpression has been found to cause chromosome breaks and translocations, promoting genomic instability of the cells [Symer, 2002], [Kazazian, 2002], [Gilbert, 2002]. Successful retrotransposition of LINE-1 elements in active genes or in the proximity of these genes may alter completely their expression either by inducing or decreasing transcription or by giving rise to premature and variant transcripts [Babushok, 2007]. They can also promote carcinogenesis through illegitimate and homologous recombination [reviewed in Schulz, 2006]. Apart from sharing the same potential negative effects regarding their retrotransposition events as LINE-1 elements, Alu sequences are more liable to homologous recombination, being responsible for chromosomal aberrations, and disease causing mutations [Kolomietz, 2002], [Ostertag, 2001]. The observations currently point towards a destructive potential of these elements, should they become unleashed [Kazazian, 2004]. In human cancers, their main restriction mechanism, methylation, in most cases is not present, thus enabling a potential reactivation of these elements.

4.4 LINE-1 and Alu elements in human cancers

It has already been previously discussed that LINE-1 and Alu elements are largely affected by DNA hypomethylation in many types of cancers. LINE-1 hypomethylation has been found in prostate, bladder, teratocarcinoma, renal and colorectal cancers [Schulz, 2006], [Suter, 2004], [Ehrlich, 2002], [Chalitchagorn, 2004], [Cho, 2007], [Wilson, 2007]. Hypomethylation of Alu elements has been reported in neuroendocrine tumours [Choi, 2007], colorectal carcinomas [Rodriguez, 2008], prostate cancer [Cho, 2007] and other types of tumours [Weisenberger, 2005].

Since methylation of these elements is one of the main restriction mechanisms for their activity, it has been suggested that they may become reactivated in human cancers [Howard, 2008]. This hypothesis is supported by a number of findings demonstrating increased LINE-1 expression in cancers after hypomethylation of the LINE-1 sequences. LINE-1 expression was observed following hypomethylation in chronic myeloid leukaemias [Roman-Gomez, 2005] and urothelial carcinomas [Florl, 1999].

However, the available evidence on LINE-1 and Alu expression in human cancers is limited and as yet it is inconclusive to confirm their reactivation in neoplasia. It is possible that, even when methylation is absent as a restriction mechanism for these sequences, other mechanisms previously mentioned, can fully constrain their reactivation. Nonetheless, there are reports on a breast cancer case in which BRC2 gene was interrupted by an Alu sequence [Miki, 1996] and a colon cancer case where the APC gene was interrupted by a LINE-1 element [Miki, 1992]. It is of note that there is some data connecting LINE-1 activity in a cancer cell line with increased apoptosis [Belgnaoui, 2006]. In addition, a further study demonstrates that LINE-1 retrotransposition induces apoptosis in cancer cells with intact p53 protein [Haoudi, 2004].

Further investigations are required to demonstrate the potential re-expression in the RNA and protein level (for LINE-1) of these elements in clinical samples, however, potential retrotransposition events, in contrast to cell lines, are difficult if possible to identify in clinical samples. PCR and sequencing approaches have been shown to have specific difficulties when targeting LINE-1 and Alu elements, mainly due to their presence in multiple copies but also due to the degeneracy of their sequences [Schulz, 2006].

4.5 DNMTs, UHRF1 and retrotransposable elements

LINE-1 and Alu elements are mainly restricted by methylation and, as previously described, the molecules mainly responsible for the generation and maintenance of the methylation patterns are DNMTs and UHRF1. Although there is some data connecting specific DNMTs with the methylation of repeated elements [Bourc'his, 2004], it is more likely that DNMTs cooperate in order to maintain the methylation patterns of these sequences [Liang, 2002]. Double knockdowns of DNMT1 and DNMT3B in a cancer cell line have been shown to reduce the genome methylation up to 95% affecting repeated sequences including Alu [Rhee, 2002] and LINE-1 [Weisenberger, 2005].

Taking this evidence into account one would expect that the observed hypomethylation of LINE-1 and Alu elements in human tumours would be due to the inactivation of DNMT1 and DNMT3B. However this is not the case, at least regarding the mRNA levels of DNMTs, for clinical samples, where as we already mentioned DNMTs are usually overexpressed and no connection between low expression of DNMTs and retrotransposable elements hypomethylation has been established so far [Ehrlich, 2006]. On the contrary hypomethylation of LINE-1 elements have been found to correlate with overexpression of DNMT3B4 transcripts [Roman-Gomez, 2005].

In addition, it has been shown that UHRF1 knockout results in global hypomethylation and LINE-1 elements are greatly affected [Bostick, 2007], however, this situation cannot mimic the primary tissues environment, since UHRF1 protein is overexpressed in most cancer types studied, where at the same time LINE-1 hypomethylation is apparent. The observed hypomethylation of LINE-1 and Alu elements and global hypomethylation in primary tumours cannot be connected to the loss of activity of DNMTs or UHRF1 [Ehrlich, 2006].

4.6 AIMS and OBJECTIVES of this study

Given the already evident abnormalities of the genome and epigenome of NSCLCs, this study had a two-fold aim:

1. To investigate the possible causes leading to the deregulation of the DNA methylation maintenance machinery in NSCLC and
2. To establish a link between global hypomethylation, retrotransposition and genomic instability in NSCLC development

To address these aims this study was organised to contain an observational (*ex vivo*) component and a functional (*in vitro*) one.

The specific objectives included:

a. Measure the expression of individual components of the DNA methylation machinery in primary NSCLC and investigate possible causes of transcriptional deregulation.

b. Examine the methylation status of retrotransposable elements which simultaneously provide a measure of global hypomethylation.

c. Investigate genomic instability utilising microsatellite markers at chromosomal loci shown to be hot-spots for loss of heterozygosity in NSCLC.

d. Examine the associations among variables established in a-c and investigate their potential clinical relevance.

e. Confirm hypomethylation-mediated activation of retrotransposable elements *in vitro*.

f. Assess the impact of alterations in the expression of UHRF1, a recently discovered methylation maintenance factor, in the regional hypermethylation of TSGs both in primary NSCLC tissue and *in vitro*.

Chapter 5. Materials and methods

5.1 Human tissues

Two different set of tissues were used for this study. The first set consisted of forty eight NSCLCs (24 adenocarcinomas and 24 squamous carcinomas) and paired adjacent normal tissues. Twenty six (54%) patients were male and twenty two female (46%). Age ranged between 46 and 80 years (mean=64). All specimens were of advanced stage (43 T2, 4 T3 and 1 T4). The second set consisted of 105 NSCLCs (55 adenocarcinomas and 50 squamous cell carcinomas), as well as 50 adjacent normal lung tissues. Fifty seven patients were males and forty eight were females. Specimens comprised the following pathological stages (pT): ten T1, eighty one T2, ten T3 and four T4. All tissues from both sets were obtained from Liverpool Heart and Chest Hospital (Liverpool, UK). Ethical approval has been obtained from Liverpool Ethics Committee for this study and informed consent was obtained from each individual.

5.2 Cell lines

Nine cell lines of lung cancer origin and one normal lung fibroblast cell line were examined in this study (Table 3). Cells were grown in DMEM: F12 medium supplemented with L-glutamine and 10% foetal bovine serum (FBS). In addition one immortalised - non tumourigenic lung epithelial cell line (HBEC 3KT – kindly donated by A. Gazdar was analyzed. This cell line was grown in Keratinocyte serum free medium (Keratinocyte-SFM medium, Invitrogen) supplemented with epidermal growth factor (EGF) and pituitary extract (Supplements for K-SFM medium, Invitrogen). All cells were grown at 37°C supplemented with 5% CO2.

Table 3 Cells lines used in this study and their histological type

Cell lines	Histological type
CRL-5802	squamous cell carcinoma
SKMES	squamous cell carcinoma
A549	adenocarcinoma
SKLU-1	adenocarcinoma
CALU-3	adenocarcinoma
CRL-5935	adenocarcinoma
DMS-53	small cell carcinoma
CORL-23	large cell carcinoma
CALU-6	anaplastic carcinoma
IMR-90	normal lung fibroblast

5.3 DNA extraction

DNA extraction from primary tissues was undertaken utilising 20×40 µm sections which were cut from frozen tissue. The first and last sections underwent pathological review to ensure an at least 80% tumour cell content. DNA extraction of the samples was performed using the DNeasy kit (96-well protocol) (Qiagen) following the manufacturer's protocol. Briefly, tissue was lysed with 360 µl of ATL reagent and 40 µl of Proteinase K solution (Qiagen) and incubated at 55°C overnight in an orbital shaking incubator at 200rpm. 820 µl of premixed AL buffer with ethanol were added and after mixing, lysates were transferred in two "twin" 96-well plates with silica based membranes. The samples were then centrifuged at 4,000 g for 10min and washed once with 500µl buffer AW1. After centrifugation at 4,000 g the samples were washed again with 500µl buffer AW2. After centrifugation at 4,000 g 55µl of AE buffer pre-warmed at 60°C were added to each sample and DNA was recovered by centrifugation at 4,000 g for 5 min.

For the DNA extraction from cell lines the DNeasy kit (Spin column protocol) (Qiagen) was used. A maximum of $5x10^6$ cells were pelleted at 300 x g for 5minutes and the pellet was re-suspended in 200 µl PBS. 20 µl proteinase K and 4 µl of RNase A (100 mg/ml) (Qiagen) were

added, the lysate was then mixed by vortexing and incubated at room temperature for 10 minutes. Subsequently 200 µl Buffer AL were added and the lysate was mixed thoroughly by vortexing and incubated at 56°C for 10 min. 200 µl of ethanol (96–100%) were added to the sample which was mixed thoroughly by vortexing. The mixture was transferred into the DNeasy Mini spin column (which carries a silica based membrane) placed in a 2 ml collection tube, and was centrifuged at 6000 x g for 1 min. 500 µl of Buffer AW1 were added, and the sample was centrifuged for 1 min at 6000 x g . 500 µl of Buffer AW2 were then added and the sample was centrifuged for 3 min at 20,000 x g to dry the DNeasy membrane. The DNeasy mini spin column was then placed in a 1.5 ml microcentrifuge tube and the DNA was recovered into 200 µl Buffer AE with centrifuging at 6000 x g for 1 min. DNA quality and quantity was assessed by spectrophotometry at 260/280 nm wavelength.

5.4 RNA extraction

Two different kits were used in this study for RNA extraction. RNA from tissues and from cell lines which was used for the study of LINE-1.2 and Alu-PV sequences was extracted using the RNeasy kit (DNAse digest protocol, Qiagen). Approximately less than $<5 \times 10^6$ pelleted cells were disrupted in 350 µl of Buffer RLT and the pellet was mixed by vortexing. The lysate was directly transferred into a QIAshredder spin column which was placed in a 2 ml collection tube and centrifuged for 2 min at 8000 x g. 350 µl of 70% ethanol were added to the homogenized lysate and mixed well by pipetting. 700 µl of the sample were then transferred to an RNeasy spin column which was placed in a 2 ml collection tube and was centrifuged for 15 s at 8000 x g (10,000 rpm). 350 µl of Buffer RW1 were then added to the RNeasy spin column and the column was centrifuged at 8000 x g (10,000 rpm) for 15 sec. The DNase I incubation mix (10 µl

of DNase I stock solution and 70 µl Buffer RDD) was added directly to the RNeasy spin column and incubated at room temperature (20–30°C) for 15 min. 350 µl of Buffer RW1 were added to the RNeasy spin column which was centrifuged for 15 s at 8000 x g (10,000 rpm). 500 µl Buffer RPE were added to the RNeasy spin column which was centrifuged for 15 s at 8000 x g (10,000 rpm). Subsequently, 500 µl of Buffer RPE were added to the RNeasy spin column and the column was centrifuged for 2 min at 8000 x g (10,000 rpm). 50 µl of DNase/RNase-Free water were added directly to the spin column membrane which was following centrifuged for 1 min at 8000 x g (10,000 rpm) to elute the RNA. An aliquot of each RNA was used for Agilent chip analysis in order to check its quality and quantity while the remaining RNA was stored at -80°C for future use.

RNA from cell lines that was used for the expression study of all other genes except for LINE-1.2 and Alu-PV sequences was performed using the Mini RNA Isolation II Kit™ (ZymoResearch). Cells were lysed directly in the culture container by removing liquid medium and replacing with 600 µl ZR RNA. The lysate was then transferred with the help of a pipette into a Zymo-Spin™ Column which was placed in a collection tube. The sample was spun in a microcentrifuge at ≥7,000 g for 1 minute and flow through was discarded. Following, 350 µl of RNA Wash Buffer were added to the column which was subsequently centrifuged at ≥7,000 g for 1 minute. The flow-through was discarded and the wash step with RNA wash buffer was repeated once more. After discarding the flow through the column was transferred to an RNase-free 1.5 ml microcentrifuge tube. 50 µl of DNase/RNase-Free water were added directly to the membrane of the column, and, after 2 minutes, the column was centrifuged at ≥7,000 g for 1 minute to elute the RNA. An aliquot of each RNA was used for Agilent chip analysis in order to check its quality and quantity while the remaining RNA was stored at -70°C for future use.

5.5 Agilent RNA 6000 Nano kit

RNA quality and quantity was assessed by capillary electrophoresis on an Agilent 2100 Bioanalyser (Agilent Technologies). In brief 550 µl of Agilent RNA 6000 Nano gel matrix were placed into the top receptacle of a spin filter. The spin filter was centrifuged for 10 minutes at 1500 g ± 20 % and 65 µl filtered gel were used per each chip. RNA 6000 Nano dye concentrate was vortexed and 1 µl of RNA 6000 Nano dye concentrate was added to a 65 µl aliquot of filtered gel. The gel and dye mix was vortexed thoroughly and spun for 10 minutes at room temperature at 13000 g. 9.0 µl of the gel-dye mix were pippeted at the bottom of the well marked in a RNA Nano chip. The gel and dye mix was spread throughout the chip under air pressure using a syringe for 30 seconds. After 5 seconds, the plunger of the syringe was slowly pulled back, the chip priming station was opened and 9.0 µl of the gel-dye mix were pipetted in each of the marked wells. Subsequently 5 µl of the RNA 6000 Nano marker were pipetted into the well marked with the ladder symbol and each of the 12 sample wells. To minimize secondary structure, RNA ladder and samples were heat denatured at 70°C for 2 minutes before loading on the chip.1 µl of the RNA ladder was pippeted into the well marked with the ladder symbol and 1 µl of each sample into each of the 12 sample wells. The chip was placed horizontally in the adapter of the IKA vortex mixer and was vortexed for 60 seconds at 100 g. Finally the chip was inserted in the Agilent 2100 Bioanalyzer and the run started in the following five minutes.

5.6 TURBO DNA-free Procedure

RNA from cell lines in which the expression of retrotransposable elements (LINE-1.2, Alu-PV) were examined, were treated with TURBO DNAse (Ambion) before cDNA preparation, in

order to eliminate the possibility of DNA carry over. TURBO DNA-*free* reactions were conducted in 0.5 mL tubes to facilitate removal of the supernatant after treatment with the DNase Inactivation Reagent. 5 µl of 10X TURBO DNase Buffer and 1 µL TURBO DNase were added to approximately 2 µg of RNA in a 0.5 ml tube and was mixed gently. The mixture was incubated at 37°C for 30 min and 5 µl of the re-suspended DNase Inactivation Reagent was added and the sample was incubated for 5 min at room temperature. The tube was flicked 2–3 times during the incubation period to re-disperse the DNase Inactivation Reagent. After incubation the mixture was centrifuged at 10,000 x g for 1.5 min and the supernatant, which contained the RNA, was carefully transferred without disturbing the pellet into a fresh tube.

5.7 cDNA preparation

Two different kits were used for the cDNA preparation. For cDNAs in which the expression of LINE-1.2 or Alu-PV elements expression was going to be measured, we used the Quantitect reverse transcription kit (Qiagen) following the manufacturer's protocol. This kit was selected as it includes an initial gDNA elimination step, minimizing the possibility of gDNA carry over into the produced cDNA. Briefly 1 µg of RNA was mixed with gDNA wipe-out buffer and RNase free water and was incubated at 42°C for 2 min. Quantiscript reverse transcriptase, Quantiscript RT buffer and RT primer mix were added, mixed and then incubated at 42 °C for 30 min with a final incubation at 95°C for 3 min to inactivate Quantiscript reverse transcriptase.

For all other cDNAs that were used in this study the High-Capacity cDNA Reverse Transcription kit (Applied biosystems) was used following the manufacturer's protocol. Briefly 1 µg of RNA (10 µl) was mixed with 2 µl of 10x RT Buffer, 0.8 µl of dNTP Mix (100 mM), 2 µl of RT Random

Primers, 1 µl of MultiScribe™ Reverse Transcriptase and 4.2 µl of Nuclease-free H_2O. After mixing by pippeting and centrifugation the reaction of the reverse transcription took place using a thermal cycler and performing the following steps: 10 min at 25 ^{0}C, 120 min at 37^{0}C and a last step of 5 sec at 85 ^{0}C. cDNAs were diluted one time and 2 µl or 1.5 µl were used for the Quantitive PCR reactions.

5.8 Bisulphite treatment of DNA

In order to identify the methylation status of the different promoters and element's tested in this study, we have bisulphite treated our DNAs. 1 µg DNA from primary tissues was bisulphite treated using the EZ-96 DNA Methylation-Gold™ Kit, (Shallow-Well Format) (ZymoResearch) following the manufacturer's protocol.

The CT Conversion Reagent was prepared prior to use by adding 7.88 ml of water, 440 µl of M-Dissolving Buffer, and 2.63 ml of M-Dilution buffer. It was then mixed at room temperature by shaking for 15 minutes. The M-Wash Buffer was prepared by adding 144 ml of 100% ethanol to the 36 ml M-Wash Buffer concentrate. 130 µl of the CT Conversion Reagent were added to 20 µl (1 µg) of each DNA sample in a Conversion Plate and samples were mixed by pipetting up and down. The plate was sealed, transferred to a thermal cycler and the following steps were performed: 98°C for 10 minutes, 64°C for 2.5 hours. The samples from the Conversion Plate were then transferred to the wells of the Silicon-A™ Binding Plate mounted on a Collection Plate, together with 400 µl of M-Binding Buffer. The plate was centrifuged at 3,000 x *g* for 5 minutes and the flow-through was discarded. 400 µl of M-Wash Buffer were added to each well of the plate and it was then centrifuged at 3,000 x *g* for 5 minutes. 200 µl of M-Desulphonation Buffer were then added to each well and the plate was left at room

temperature (20 °C – 30 °C) for 20 minutes. After the incubation, it was centrifuged at 3,000 x *g* for 5 minutes, and the flow-through was discarded. 400 µl of M-Wash Buffer were added to each well of the plate, which was then centrifuged at 3,000 x *g* for 5 minutes, and the flow-through was discarded. Another 400 µl of M-Wash Buffer were added and the plate was centrifuged at 3,000 x *g* for 10 minutes. The Silicon-A™ Binding Plate was then placed onto an Elution Plate and 35µl of M-Elution Buffer were added directly to each well. After 5 minutes, it was centrifuged at 3,000 x *g* for 3 minutes to elute the DNA. 3 µl of bisulphite treated DNA was used for each PCR reaction.

One µg DNA from cell lines was bisulphite treated using the EZ DNA Methylation-Gold Kit™ (Zymo Research) following the manufacturer's protocol. The CT Conversion Reagent was prepared prior to use by the addition of 900 µl of ddH_2O, 50 µl of M-Dissolving Buffer and 300 µl of M-Dilution Buffer to a tube of CT Conversion Reagent. The mixture was dissolved at room temperature with intermittent, brief vortexing for a total of 10 minutes. The M-Wash Buffer was prepared by adding 24 ml of 100% ethanol to the M-Wash Buffer concentrate. 130 µl of the CT Conversion Reagent solution were added to 20 µl of DNA (1 µg) sample in a PCR tube and the sample was mixed by pipetting. The sample tube was placed in a thermal cycler and the following steps were performed: 98°C for 10 minutes, 64°C for 2.5 hours. After incubation the sample was loaded into the Zymo-Spin IC™ Column containing 600 µl of the M-Binding Buffer, and the column was placed onto a provided Collection Tube. The mixture was centrifuged at full speed (>10,000 x g) for 30 seconds and the flow-through was discarded. 100 µl of M-Wash Buffer were added to the column which was then spun at >10,000 x g for 30 seconds. 200 µl of M-Desulphonation Buffer were then added to the column which was incubated at room temperature (20 °C – 30 °C) for 15-20 minutes. After the incubation, the column was spun at >10,000 x g for 30 seconds and the flow through was discarded. 200 µl of

M-Wash Buffer were added to the column which was following spun at >10,000 x g for 30 seconds. Another 200 µl of M-Wash Buffer were added and the column was spun at >10,000 x g for 2 minutes to ensure complete removal of alcohol traces. Finally 10 µl of M-Elution Buffer were added directly to the column matrix, the column was placed into a 1.5 ml tube and spun briefly at >10,000 x g to elute the DNA. 3 µl of bisulphite treated DNA was used for each PCR reaction.

5.9 Pyrosequencing Methylation Analysis (PMA).

Pyrosequencing (PSQ) is a method that can identify the sequence from small DNAs efficiently and with high fidelity. The procedure of the technique can be divided into two parts. The first part is the preparation of the samples that are to be sequenced. The target DNA sequence is amplified by PCR using primers that are generated by the pyrosequencing software. One of the two primers is biotinylated. After the examination of the product's quality in an agarose gel, the PCR products are mixed with the binding buffer, which contains sepharose streptavidin beads and buffer, and then are transferred into a 96 well PSQ plate.

With the help of a tool that uses vacuum, the beads, in which the PCR product is bound, are held against a filter. The beads are then washed successively with ethanol, NaOH and wash buffer. NaOH denatures and separates the strands, while the wash buffer neutralises the immobilised strand. As a result, at the end of the above procedure, in the tool remain only the streptavidin beads with the biotinylated strand of the PCR products. The beads are then released in a new 96 well PSQ plate together with the annealing buffer which contains the sequencing primers.

The second part of the technique takes place in the 96MA Pyrosequencer (Qiagen) instrument. The template DNA together with the sequencing primer, are incubated with the enzymes DNA polymerase, ATP sulfurylase, lusiferase and apyrase, and the substrates adenosine 5' phosphosulfate (APS) and luciferin. The first of the four triphosphates (dNTPs) is injected into the reaction. DNA polymerase catalyses the incorporation of the first dNTP into the DNA strand if it is complementary to the base in the template strand. Each incorporation event is accompanied by release of pyrophosphate (PPi) in a quantity equimolar to the amount of incorporated nucleotide. ATP sulfurylase converts PPi to ATP in the presence of APS. This ATP drives the lusiferin to oxyluciferin that generates visible light in amounts that are proportional to the amount of the ATP. The light produced in the luciferase- catalysed reaction is detected by a charge coupled device (CCD) camera and seen as a peak in a pyrogram. The height of each peak (light signal) is proportional to the number of nucleotides incorporated (Figure 15).

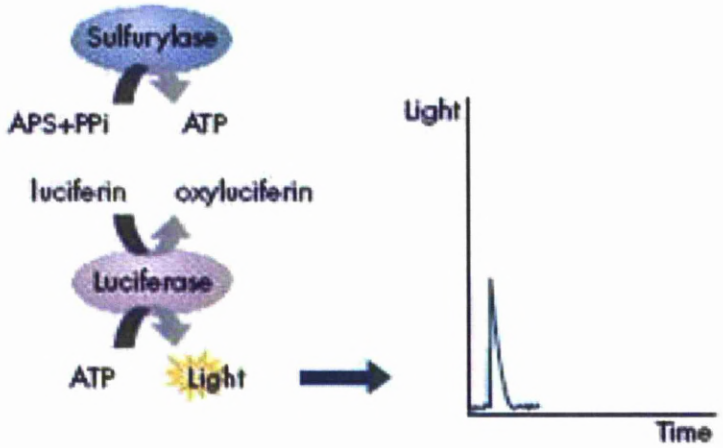

Figure 15 Nucleotide incorporation generates light seen as peak in the program (Figure adapted without permission from Qiagen website)

Apyrase, a nucleotide degrading enzyme, continuously degrades ATP and unincorporated dNTPs. This switches off the light and regenerates the reaction solution. The next dNTP is then added. The dNTPs are added one at a time. As the process continuous, the complementary DNA strand is built up and the nucleotide sequence is determined from the signal peaks in the pyrogram. An example is shown in Figure 16.

Pyrosequencing has applications in genetic variation (SNPs, haplotypes), in mutation detection (point mutations, insertions/deletions, known/unknown positions), quantification (allele frequency quantification, loss of heterozygosity, CpG methylation) and sequence analyses (viral/bacterial typing, clone checking, sequence identification). For the needs of this project we used the pyrosequencing technique for methylation analysis.

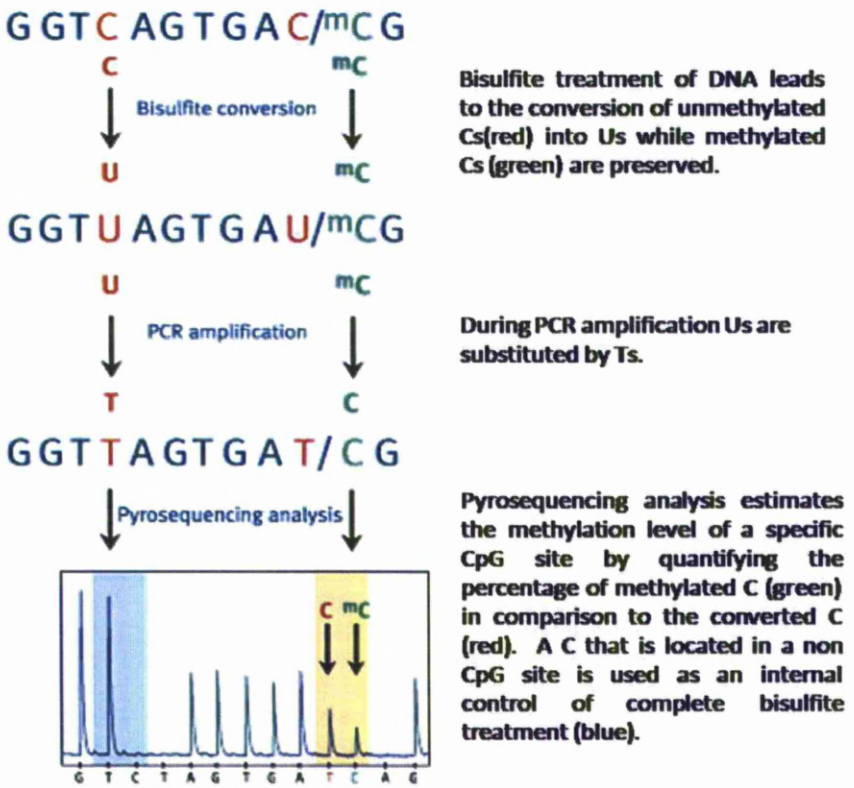

Figure 16 An example of a DNA sequence, and its conversion by bisulphite treatment, with further amplification by PCR. By pyrosequencing, unmethylated cytosine C is measured as the relative content of T at the CpG site, and methylated cytosine, ^{m}C, is measured as the relative content of C at the CpG site (Figure adapted without permission from Qiagen website).

Using the standard treatment of genomic DNA with bisulphite (described in the previous paragraph), unmethylated Cytosine (C) is converted to Uracil (U), whereas methylated Cytosine (^{m}C) remains unchanged. Using PCR, Uracil (U) is amplified to Thymine (T), whereas methylated Cytosine (^{m}C) is amplified to Cytosine (C). Discrimination between ^{m}C and C is thereby achieved by transforming ^{m}C and C to appear as a C/T SNP (Figure 16).

5.9.1 LINE-1 and Alu assays

In order to identify the methylation status of LINE-1 and ALU elements in NSCLCs and cell lines we used the LINE-1.2 (Genebank accession no M80343) and the Alu-PV (Genebank accession no Z49816) as targets sequences. Those two sequences were specifically chosen as they belong to retrotranspositionally active families and there are published data on their ability to retrotranspose [Sassaman, 1997], [Wallace, 1991]. For the LINE-1.2 element a target region inside the CpG island of the 5' internal promoter including 6 CpGs was chosen while for the Alu-PV element we selected a target region in the CpG island near its 3' end encompassing 4 CpG sites. All primers were designed using the Assay Design Software (Qiagen) and synthesized by MWG (Germany) (Table 4).

Table 4 Primers designed with Assay Design Software for LINE-1 and Alu-PV pyrosequencing assays. BIO: biotinylated end.

Promoter	Forward primer (5'→3')	Reverse primer (5'→3')	Sequencing primer (5'→3')
LINE-1	BIO-TAGGGAGTGTTAGATAGTGG	AACTCCCTAACCCCTTAC	CAAATAAAA CAATACCTC
ALU-PV	GAGGTTGAGGTAGGAGAA	BIO- CCCAAACTAAAATACAATAAC	GTTGAGGTAGGAGAA

PCR amplifications were performed using Qiagen HotStarTaq Plus Master Mix Kit, 5μM biotinylated primer, 10 μM non-biotinylated primer and 3 μl (approximately 60ng) of bisulphite treated DNA. In order to avoid any biotinylated primer remains which could

possibly cause problems during the pyrosequencing reaction we have used the non-biotinylated primer in excess. For the same reason we overcycled (40 cycles) our products. Thermal profiles for LINE-1 and Alu-PV amplification are shown in Tables 5 and 6 respectively.

Table 5 Thermal profile for LINE-1 amplification PCR reactions

Step	Temperature (°C)	Time	No of cycles
Taq Activation	95	5 min	
Denaturation	94	30 sec	
Annealing	58	45 sec	40
Extension	72	45 sec	
Final extension	72	10 min	

Table 6 Thermal profile for ALU-PV amplification PCR reactions

Step	Temperature (°C)	Time	No of cycles
Taq Activation	95	5 min	
Denaturation	94	30 sec	
Annealing	49	45 sec	40
Extension	72	45 sec	
Final extension	72	10 min	

The PCR product quality and quantity was confirmed by agarose gel (2%) electrophoresis UV visualisation on a UVP VisionWorks LS instrument prior to clean up and Pyrosequencing analysis. For the latter the SQA kit was used following the suppliers protocol (Qiagen) and the reaction was performed on a 96MA Pyrosequencer (Qiagen). The methylation index (MtI) for the LINE-1 and Alu elements was calculated as the mean value of $^{m}C/(^{m}C+C)$ for all examined CpGs in the elements.

5.9.2 DNMTs and UHRF1 assays

DNMTs are often aberrantly expressed in cancers. Interestingly, using the EMBOSS CpGPlot program (EBI) we have identified CpG islands in the promoter region of all DNMTs and the

UHRF1 genes. In order to investigate the potential epigenetic regulation of DNMTs and UHRF1 in our lung cancer cell panel, we designed pyrosequencing assays for DNMT1, DNMT3A, DNMT3B and UHRF1. For DNMT1 (Genebank gene id: 1786) we have selected a target region inside the CpG island of the promoter including 5 CpGs (Figure 17). For DNMT3A (Genebank gene id: 1788) we have selected a target region inside the CpG island of the promoter including 6 CpGs (Figure 17). For DNMT3B (Genebank gene id: 1789) we have selected a target region inside the CpG island of the promoter including 9 CpGs (Figure 17). For UHRF1 (Genebank gene id: 29128) we have selected a target region inside the CpG island of the promoter including 6 CpGs (Figure 17).

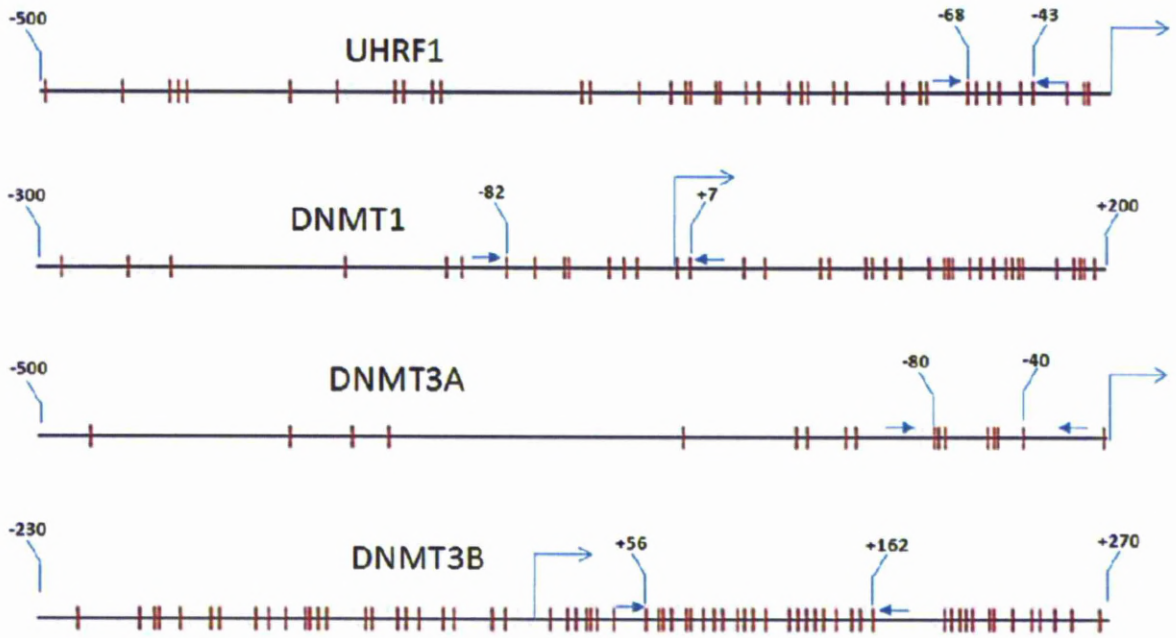

Figure 17 Diagrammatic map of the DNMTs and UHRF1 promoter regions examined. CpGs are represented by vertical lines and primers as arrows. Numbering refers to the transcriptions start site depicted by the gamma-shaped arrow.

All primers were designed using the Assay Design Software (Qiagen) and synthesized by MWG (Germany) (Table 7).

Table 7 Primers designed with Assay Design Software for DNMT1, DNMT3A, DNMT3B and UHRF1 pyrosequencing assays. bio: biotinylated end.

Promoter	Forward primer (5'→3')	Reverse primer (5'→3')	Sequencing primer (5'→3')
DNMT1	GATATTTTGTGTAGAAGGATGGAA	bio –ACCCACCTCCCAACAAAC	ATTTTGTGTAGAAGGATG
DNMT3A	GATTTTGGTTTTGTAGAGTAGAG	bio -TCTACCTACCTCAACACTAAAACT	ATTTTGGTTTTGTAGAGTA
DNMT3B	GAGTTAGGTTTATTTGGGTTAT	bio -CTTCCTCCCAACAACTACT	TTATTTGGGTTATTTAA
UHRF1	GGTTAATTAGGAGGTAGG	bio -ACTCCACATTTAAAAATTAC	GGTTAATTAGGAGGTAG

In order to avoid any biotinylated primer remains which could possibly cause problems during the pyrosequencing reaction we have used the non-biotinylated primer in excess. For the same reason we overcycled (40 cycles) our products. PCR amplifications were performed using Qiagen HotStarTaq Plus Master Mix Kit, 5 μM biotinylated primer, 10 μM non-biotinylated primer and 3 μl (approximately 60ng) bisulphite treated DNA. Thermal profiles for the different targets are seen in Table 8.

Table 8 Thermal profile for DNMT1, DNMT3A, DNMT3B and UHRF1 amplification PCR reactions

Step	Target	Temperature (°C)	Time	No of cycles
Taq Activation		95	5 min	
Denaturation		94	30 sec	40
Annealing	DNMT1	57	30 sec	
	DNMT3A	54		
	DNMT3B	57		
	UHRF1	51		
Extension		72	30 sec	
Final extension		72	10 min	

The PCR product quality and quantity was confirmed by agarose gel (2%) electrophoresis and UV visualisation on a UVP VisionWorks LS instrument prior to clean up and Pyrosequencing

analysis. The methylation index (MtI) was calculated as the mean value of $^{m}C/(^{m}C+C)$ for all examined CpGs in the target regions of the promoters.

5.9.3 Assays for frequently hypermethylated tumour suppressor genes

Regional hypermethylation is a common feature of human cancers which often affects promoters of tumour suppressor genes. In this study we have examined using pyrosequencing the methylation status of the CDKN2A, RASSF1, CDH13 and CYGB promoters. These genes were chosen as they are known from the literature to be frequently hypermethylated in lung cancers. We have designed primers specific for target areas that are located on the promoters of these genes (Figure 18).

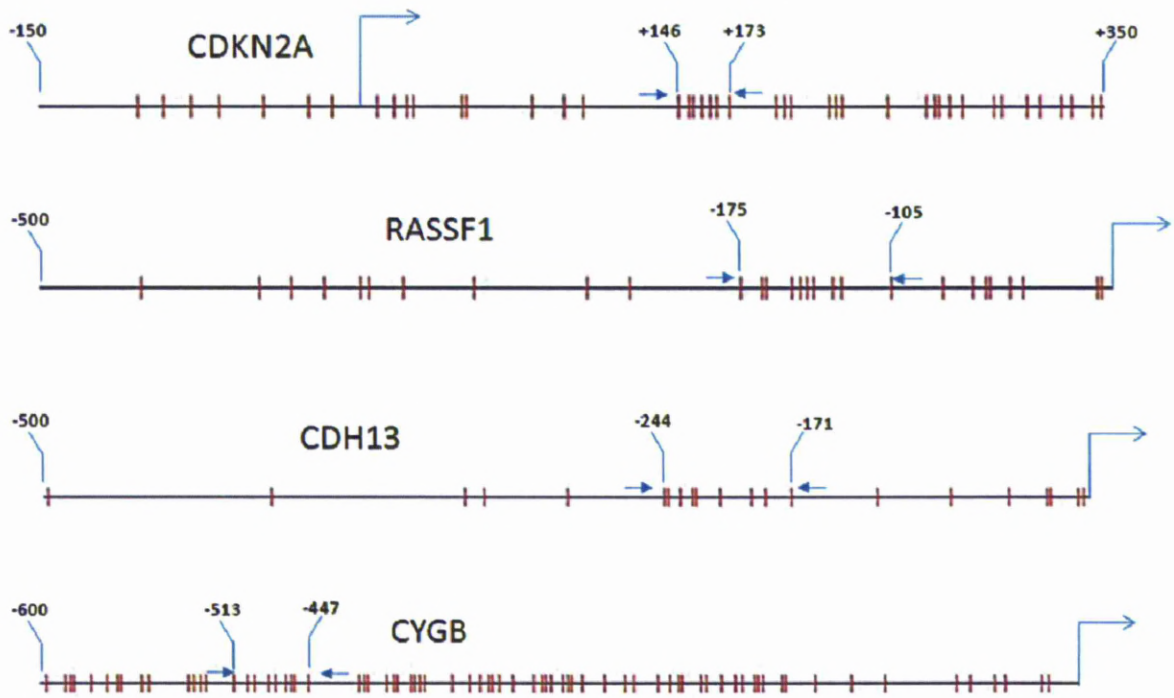

Figure 18 Diagrammatic map of the promoter regions examined. CpGs are represented by vertical lines and primers as arrows. Numbering refers to the transcriptions start site depicted by the gamma-shaped arrow.

Primers were designed using the Assay Design Software (Qiagen) and synthesized by MWG (Germany) (Table 9).

Table 9 Primers designed using the Assay Design Software for RASSF1, CDKN2A, CDH13 and CYGB pyrosequencing assays. bio: biotinylated end.

Promoter	Forward primer (5'→3')	Reverse primer (5'→3')	Sequencing primer (5'→3')
RASSF1	AGTATAGTAAAGTTGGTTTTTAGAAA	bio-CCCTTCCTTCCCTCCTT	AAGTTGGTTTTTAGAAATA
CDKN2A	AGGGGTTGGTTGGTTATTAG	bio-CTACCTACTCTCCCCCTCTC	GGTTGGTTATTAGAGGGT
CDH13	bio-TTAGGGAAAATATGTTTAGTGTAGT	ACCCCTCTTCCCTACCTA	ACCCCTCTTCCCTACCT
CYGB	bio-GGGAATTGATTTAAAGTTTA	AAAAAACCCAACTAAATCCAC	ACCCAACTAAATCCAC

In order to avoid any biotinylated primer remains which could possibly cause problems during the pyrosequencing reaction we have used the non-biotinylated primer in excess. For the same reason we overcycled (40 cycles) our products. PCR amplifications were performed using Qiagen HotStarTaq Plus Master Mix Kit, 5 μM biotinylated primer, 10 μM non-biotinylated primer and 3 μl (approximately 60ng) bisulphite treated DNA. Thermal profiles for the different targets are seen in Table 10:

Table 10 Thermal profile for RASSF1, CDKN2A, CYGB and CDH13 amplification PCR reactions

Step	Target	Temperature (°C)	Time	No of cycles
Taq Activation		95	5 min	
Denaturation		94	30 sec	
Annealing	RASSF1	50	30 sec	40
	CDKN2A	55		
	CYGB	50		
	CDH13	52		
Extension		72	30 sec	
Final extension		72	10 min	

The PCR product quality and quantity was confirmed by agarose gel (2%) electrophoresis UV visualisation on a UVP VisionWorks LS instrument prior to clean up and Pyrosequencing analysis. The methylation index (MtI) was calculated as the mean value of $^{m}C/(^{m}C+C)$ for all examined CpGs in the target regions of the promoters.

5.9.4 Pyrosequencing assay for the LRE3 element

To explore the effect of DNA methylation on LINE-1 retrotransposition in lung cancer we have collaborated with Dr John V. Moran and utilised the KS-101 plasmid he kindly provided us with. The KS-101 plasmid contains a full length human retrotransposition competent LINE-1 element (LRE3) tagged with a retrotransposition cassette and is cloned into a pBluescript backbone (Stratagene). Complete information on this construct is shown in paragraph 5.12.1. In order to investigate the methylation status of the LRE3 element after its insertion to mammalian cell lines we have designed primers that will specifically amplify the LRE3 element that is part of the construct and not some other LINE-1 homologous element. One of the primers was designed to anneal on the backbone of the pBluescript near the promoter of the LRE3 element while the second primer was designed to anneal in the promoter region of the LRE3 element (Figure 19).

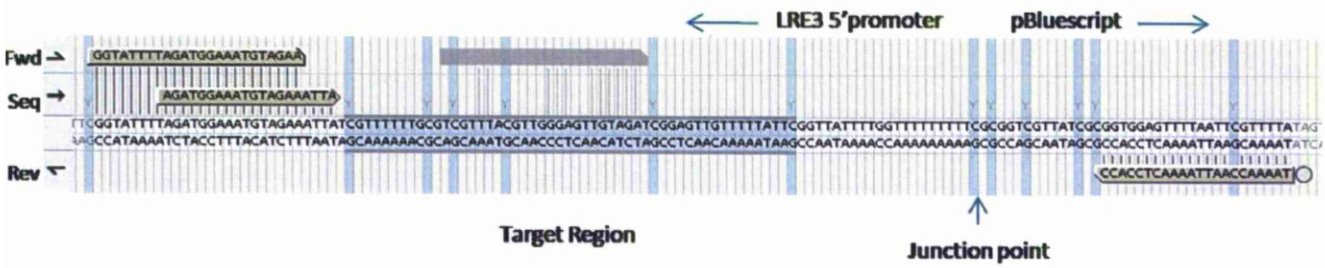

Figure 19 Primer design for LRE3 pyrosequencing analysis using the Assay Design software on the KS-101 construct sequence. The sequence shown contains a part of the LRE3 5'promoter (left side) and a small part of the pBluescript backbone (right side). The junction site is indicated with a blue arrow. The reverse biotinylated primer is designed to bind on the pBluescript region while the forward and sequencing primers are designed to bind on the 5-end LRE3 promoter. The target sequence inside the 5-end CpG island is marked as a grey zone and contains 6 CpG sites (blue strips).

Primers were designed using the Assay Design Software (Qiagen) and synthesised by MWG (Germany) forward primer: 5'-GGTATTTTAGATGGAAATGTAGAA-3', reverse primer: 5'-bio-GGTGGAGTTTTAATTGGTTTTA -3', sequencing primer: 5'- AGATGGAAATGTAGAAATTA-3'. The reverse primer which was the one to anneal on the specific pBluescript backbone was

designed with a slightly higher annealing temperature (Tm: 53.8) compared to the non specific forward primer (Tm: 52.4) in order to achieve maximum specificity. Moreover, the reverse specific primer was chosen to be biotinylated so as to obtain only specific templates for the pyrosequencing reaction. In order to avoid any biotinylated primer remains which could possibly cause problems during the pyrosequencing reaction we have used the non-biotinylated primer in excess. For the same reason we overcycled (40 cycles) our products. PCR amplifications were performed using Qiagen HotStarTaq Plus Master Mix Kit, 5 μM biotinylated primer, 10 μM non-biotinylated primer and 3 μl (approximately 60ng) bisulphite treated DNA. The optimised thermal profile for the LRE3 amplification reaction is shown in Table 11.

Table 11 Thermal profile for the LRE3 amplification PCR reactions

Step	Temperature (°C)	Time	No of cycles
Taq Activation	95	5 min	
Denaturation	94	30 sec	
Annealing	53	30 sec	40
Extension	72	30 sec	
Final extension	72	10 min	

The PCR product quality and quantity was confirmed by agarose gel (2%) electrophoresis UV visualisation on a UVP VisionWorks LS instrument prior to clean up and Pyrosequencing analysis. The methylation index (MtI) was calculated as the mean value of $^{m}C/(^{m}C+C)$ for all examined CpGs in the target regions of the promoters.

5.10 Quantitative Real-Time PCR expression assays

5.10.1. LINE-1 and ALU-PV expression assays

In order to investigate the expression status of the LINE-1 and Alu elements in our cell lines we used LINE-1.2 (Genebank accession no M80343) and the Alu-PV (Genebank accession no Z49816) as targets sequences. Those two sequences were specifically chosen as they belong to retrotranspositionally active families and there are published data on their ability to retrotranspose [Sassaman, 1997], [Wallace, 1991].

As Alu and LINE-1 sequences do not contain introns, the primers for the expression assays are unable to distinguish between the DNA sequences and the corresponding mRNA. Thus, an on column DNAse digestion step was included in the RNA extraction, extra DNAse treatment was performed on the extracted RNA and cDNA preparation encompassed an additional gDNA elimination step in order to ensure that no gDNA contaminants were carried over. In addition, control PCR reactions using primers for the p21 promoter sequence were carried in order to check for any gDNA contamination of the cDNAs prepared.

We have designed qPCR (real time) Taqman assays using the Primer Express v 2.0 software (Applied Biosystems) (Table 12). Primers were synthesized by MWG (Germany). The probes were labelled at the 5' end with FAM dye while the 3' end of the probe was labelled with TAMRA dye.

Table 12 Primers designed for the detection of LINE-1 and Alu-PV RNA sequences.

Target	Forward primer (5'→3')	Reverse primer (5'→3')	probe (FAM labelled)
LINE-1	GAGAGGATGCGGAGAAATAGGA	GGATGGCTGGGTCAAATGGT	CAACCATTGTGGAAGTCAGTGTGGCG
Alu-PV	GAGGCGGGCGGATCAC	GTTTCACCGTTTTAGCCAGGAT	AGGTCAGGAGATCGAG

The amplicon size of LINE-1 primers was 131 bps while the amplicon size of Alu-PV primers was 58 bps. Primers and probe (labelled with VIC dye) amplifying the actin cDNA (Applied Biosystems, assay Id: 4326315E) with amplicon size 171 bps were used as endogenous control. The different dyes between our target and endogenous control enabled the identification of the target and endogenous control expression in the same reaction tube. Primers for LINE-1 and Alu-PV elements had a smaller amplicon size compared to the amplicon size of the endogenous control in order to check for cDNA integrity. Assays were performed in a final reaction volume of 20 μl containing 10 μl of 2x TaqMan® Gene Expression Master Mix (Applied Biosystems), 900 nM of each primer and 250 nM probe (LINE-1 or Alu-PV primers), 900 nM of each primer and 250 nM probe of the endogenous control ACTB-VIC (Applied Biosystems) and approximately 50 ng of cDNA following the universal conditions (2 min at 50°C, 95 °C for 10 min, 50 cycles of 94 °C for 30 sec, 60 °C for 45 sec) on an Applied Biosystems 7500 real time PCR machine. The assays' efficiency regarding reproducibility and robustness was tested over 5-logs of cDNA concentration. The 7500 Software v2.0.1 (Applied Biosystems) was used for data analysis. RNA levels were expressed as relative quantification values (RQ) which were calculated as: $RQ=2^{(-\Delta\Delta Ct)}$, where the mRNA expression of IMR-90 cells was used as a calibrator in each run. All assays were run in duplicate and the mean values were used for the analysis.

5.10.2 UHRF1, MBD2, E2F1 and DNMTs assays.

In order to investigate the expression levels of the DNMT1, DNMT3A, DNMT3B, UHRF1 and E2F1 in tissues and cell lines, we used off-the-shelf assays (Applied Biosystems) to reduce the optimisation times. The assay Ids for each gene and additional details are shown in Table 13.

Table 13 Ids and additional information for the assays used for examining expression levels of DNMT1, DNMT3A, DNMT3B, UHRF1 and E2F1 genes.

GENE	Assay Id	DYE	Unigene Id	Amplicon length (bp)
DNMT1	Hs00945898_g1	FAM	Hs.202672	102
DNMT3A	Hs01027167_g1	FAM	Hs.515840	65
DNMT3B	Hs01003404_g1	FAM	Hs.643024, Hs.713611	74
UHRF1	Hs00273589_m1	FAM	Hs.108106	105
E2F1	HS01566605_g1	FAM	Hs.654393	66
ACTIN	4326315E	VIC	Hs.520640	171

ACTB-VIC (Applied Biosystems) was used as an endogenous control. Since its probe was labelled with a different dye (VIC) it was used in the same reaction tube with the target assays. The length of the endogenous control amplicon (171) was greater compared to the amplicon lengths of out targets enabling for an internal control of cDNA integrity. Assays were performed in a final reaction volume of 20 µl containing 10 µl of 2x TaqMan® Gene Expression Master Mix (Applied Biosystems), 900 nM of each primer and 250 nM probe, 900 nM of each primer and 250 nM probe of the endogenous control ACTB-VIC (Applied Biosystems) and approximately 50 ng of cDNA following the universal conditions (2 min at 50°C, 95 °C for 10 min, 50 cycles of 94 °C for 30 sec, 60 °C for 45 sec) on an Applied Biosystems 7500 real time PCR machine. The 7500 Software v2.0.1 (Applied Biosystems) was used for data analysis. RNA levels were expressed as relative quantification values (RQ) which were calculated as: $RQ=2^{(-\Delta\Delta Ct)}$, where the mRNA expression of IMR-90 cells was used as a calibrator in each run. All assays were run in duplicates and the mean values were used for the analysis.

5.11 Microsatellite analysis

The microsatellite marker panel reaction was carried out in a multiplex fashion using the Qiagen Multiplex PCR Master Mix (Qiagen, UK). Primers were selected from the LMS High Density Panel set (Applied Biosystems) and were custom synthesized with 5' biotinylated reverse primers. These 11 microsatellite markers were chosen as they have been previously shown to be hot spots for loss of heterozygosity (LOH) in lung tumours [Liloglou, 2000] [Liloglou, 2001]. The microsatellite markers used were D3S1566, D3S1289, D9S161, D13S153, D13S171, D13S263, D3S1300, D3S1263, D9S157, D5S644 and D17S938.

The reaction mix was prepared using Qiagen Multiplex PCR Master Mix (Qiagen, UK), 200nmol of each primer, 50 ng of DNA and ddH_20 in a total volume of 20 µl. The thermal profile is shown in Table 14.

Table 14 Thermal profile used for the amplification of the target microsatellite markers

Step	Temperature (°C)	Time	No of cycles
Taq Activation	95	15 min	
Denaturation	94	30 sec	
Annealing	56	90 sec	30
Extension	72	60 sec	
Final extension	72	30 min	

PCR products were cleaned using Streptavidin coated Dynabeads (Invitrogen, UK). Immobilized PCR products were washed with 200 µl 70% ethanol and dissolved in 4 µl loading buffer containing formamide: dextran blue: ROX400 size standard (Applied Biosystems) in a 10: 2: 1.5 ratio. The mixture was denatured at 95 °C for 5 min, cooled on ice, and loaded on a 4.2% denaturing polyacrylamide gel on a 377 ABI PRISM automated sequencer. Peak area analysis was undertaken using the GeneScan and Genotyper software (Applied Biosystems). The allelic imbalance index (AII) was calculated for each sample as follows: AII=

(A1/A2)T/(A1/A2)N. The LOH threshold was calculated based on the 99% reference range (=mean ± 3×SD) created by values produced by multiple repetition of normal blood DNA samples [Liloglou, 2000].

5.12 Vectors and constructs

5.12.1 KS101 and KS105 vectors

In order to measure the retrotransposition ability of a full LINE-1 element in a lung cancer environment we collaborated with Dr Moran of the University of Michigan who has provided us with the KS-101 and KS-105 plasmids [Garcia-Perez, 2007]. The KS-101 plasmid is approximately 11.5 Kb and contains an 8.7 kb NotI-SalI fragment cloned into a pBluescript backbone (Stratagene). This fragment contains a full length human retrotransposition competent LINE-1 element (LRE3) tagged with a neomycin (NEO) retrotransposition cassette and a SV40 late polyadenylation signal in its 3' end. This element is located on chromosome 2q24.1 on the human genome and is one of the most actively retrotransposing LINE-1 elements [Brouha, 2002].The NEO retrotransposition cassette consists of the neomycin phosphotransferase gene interrupted by an intronic sequence, and has a CMV promoter in its 3 end before the SV40 polyadenylation signal at the antisense direction. A graphic map of the plasmid can be seen in Figure 20.

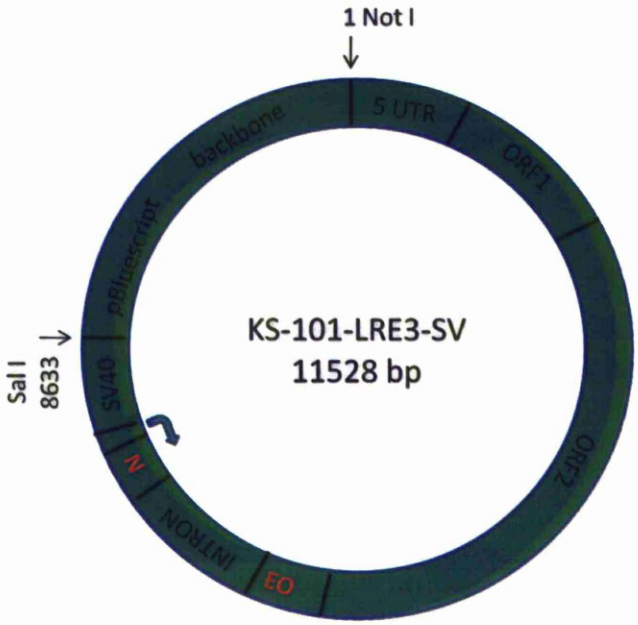

Figure 20 Graphic map of the KS-101 plasmid. The Not I-Sall fragment is cloned into the backbone of pBluescript. The different parts of the LRE3 element are shown. LRE3 contains an internal promoter at 5 UTR as all full LINE-1 elements. Between the SV 40 polyadenylation signal and ORF2 lies the neo gene sequence interrupted by an intronic sequence. The neo gene runs in the antisense direction under the regulation of a CMV promoter (blue arrow).

The KS-101 plasmid is used to demonstrate the ability of the cloned LINE-1.3 element to retrotranspose in a host cell line [Garcia-Perez, 2007]. The LRE3 element is under the regulation of its native 5'UTR promoter. The retrotransposition cassette becomes activated only if spliced LRE3 mRNA undergoes a successful round of retrotransposition. When this occurs, the neomycin gene is activated and the cell demonstrates resistance in the presence of G418 antibiotic. Therefore after transfection of a cell line with the KS-101 plasmid, the number of colonies that will appear, after selection with G418, stand for the number of cells where the LRE3 element completed at least a full cycle of retrotransposition. A detailed presentation of the activation of the retrotransposition cassette can be seen in Figure 21.

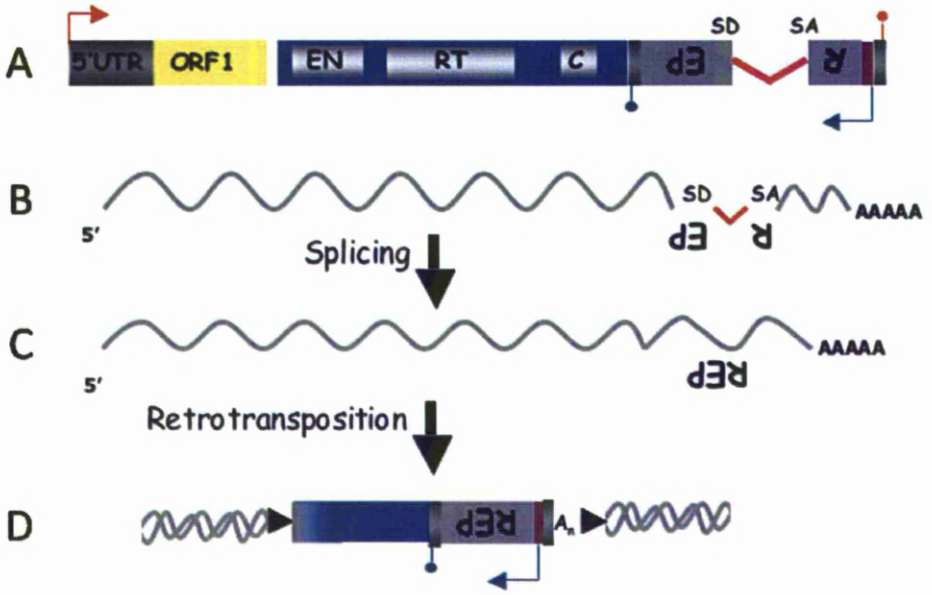

Figure 21 Graphic representation of the KS-101 construct reporter cassette. A: the sequence of the LRE3 element and the reporter cassette are shown. The reporter gene (neo) runs in the antisense direction and is interrupted by an intronic sequence with a splice donor (SD) and a splice acceptor (SA) arm. The CMV promoter is active but any product at the current stage will give rise to an interrupted NEO gene and therefore will not confer resistance to G418 antibiotic. B,C: When the LRE3 element is transcribed then the intronic sequence is excised from the reporter gene during splicing of the RNA. D: After a full retrotransposition cycle the LRE3 element is inserted to a new location in the genome carrying the intact neo gene and therefore conferring resistance to the cell after selection with G418 antibiotic. (Figure adapted without permission from Garcia-Perez, 2007).

The KS-105 vector is the same with the KS-101 vector except from the fact that it contains a missense mutation in the RT active site [Garcia-Perez, 2007]. Therefore, its LRE3 element is not capable for retrotransposition and the KS-105 plasmid can be used as a mock control.

5.12.2 Construction of the KS101B and KS105B vectors

The KS-101 plasmid can be used to demonstrate the ability of a retrotransposition competent LRE3 element to retrotranspose under the regulation of its own promoter in a cell line. However it has a specific limitation. No selection marker is available on the plasmid and therefore the transformation efficiency cannot be estimated. In order to be able to isolate

colonies which have obtained the KS-101 plasmid, we have inserted a blasticidin resistance marker in the KS-101 and KS-105 plasmids.

We have purchased from Invitrogen the pCMV/Bsd vector. This vector carries the blasticidin resistance gene under the regulation of a CMV and EM7 promoters followed by an SV40 polyA tail. The fragment carrying the blasticidin gene and its regulatory sequences is flanked by polylinker sequences enabling the excision of the desired fragment using different restriction enzymes (Figure 22).

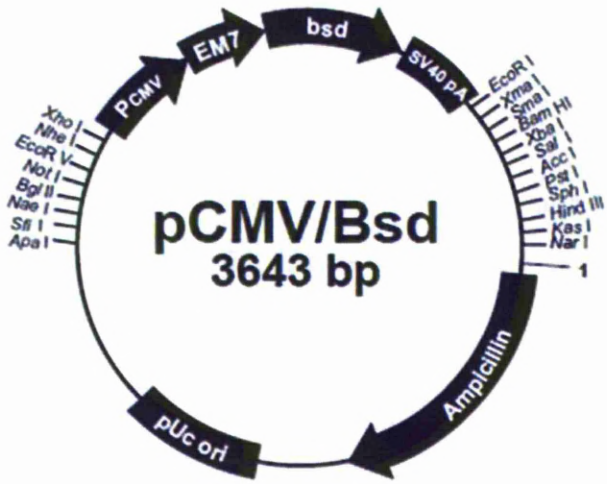

Figure 22 Graphic map of the pCMV/Bsd vector.

The pCMV/Bsd vector was digested with Sal I. 2.4 µg of plasmid were digested with 60 units of Sal I (NEB) in 1x NEB buffer 3 in a total reaction volume of 30 µl at 37 ^{0}C for 2 hrs. After digestion the linear vector was cleaned using the Qiaquick removal kit (Qiagen, see paragraph **5.12.4**). The vector was eluted in 30 µl ddH2O and was further digested with 100 units of Apa I (NEB) in 1x NEB buffer 4 in a total reaction volume of 40 µl at 25 ^{0}C for 2 hrs. After incubation the reaction mix was loaded in a 1% low melting point agarose gel made with TAE buffer. Electrophoresis separated the two fragments of the CMV vector and the desired fragment

carrying the blasticidin gene (1333 bp) was cut out from the gel using a scalpel, obtained using the Qiaquick gel extraction kit (Qiagen, see paragraph **5.12.5)** and eluted at 20 µl ddH_2O.

The KS-101 and KS-105 vectors were digested with Sal I and Apa I restriction enzymes (Figure 23). 2.5 µg of plasmid were digested with 60 units of Sal I (NEB) in 1x NEB buffer 3 in a total reaction volume of 30 µl at 37 ^{0}C for 2 hrs. After digestion the linear vector was cleaned using the Qiaquick removal kit (Qiagen). The vector was eluted in 30 µl ddH2O and was further digested with 100 units of Apa I (NEB) in 1x NEB buffer 4 in a total reaction volume of 40 µl at 25 ^{0}C for 2 hrs. The vector was cleaned using the Qiaquick removal kit (Qiagen) and eluted in 20 µl ddH_2O.

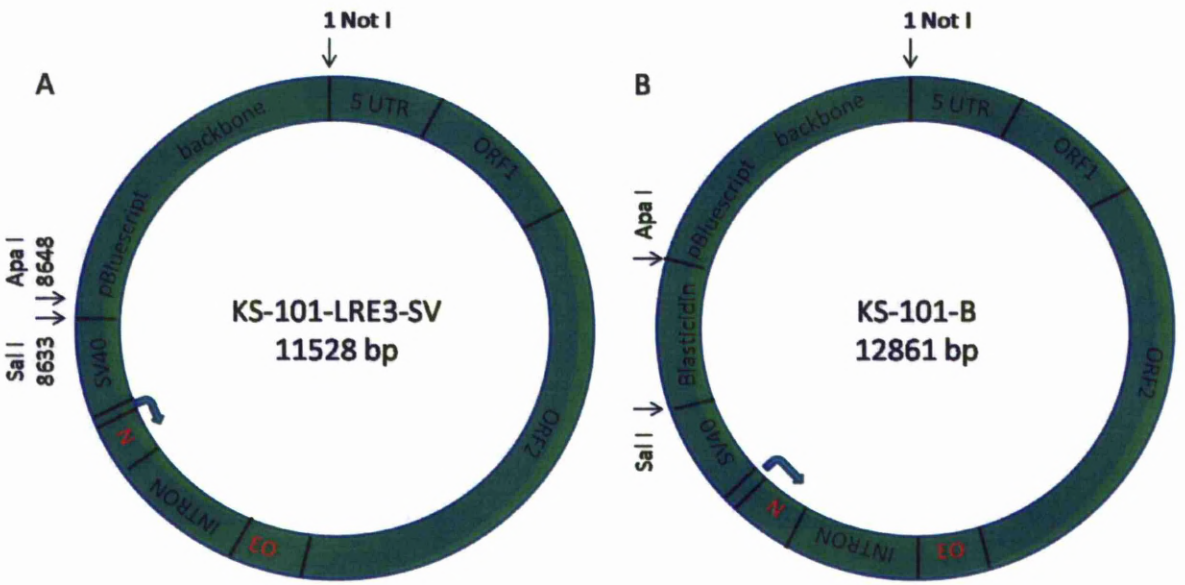

Figure 23 Graphic presentation of KS-101 and KS-101B constructs. A: The KS-101 plasmid and the recognition sites for SalI and ApaI restriction enzymes. B: KS-101B plasmid after the insertion of the blasticidin fragment from the pCMV.BSD vector.

The blasticidin fragment was ligated with the KS-101 and KS105 vectors using T4 ligase. I µl of the KS-101 and KS105 vectors were mixed with 5 µl of the blasticidin fragment, 1 µl of T4 DNA ligase (NEB) and 1 µl of 1x T4 ligase reaction buffer (NEB) in a total reaction volume of 10 µl. In

order to have approximately the same copy number of the KS-101 or KS105 and blasticidin fragment and since the KS-101 and KS105 fragments are ~11.5 kb and the blasticidin fragment is ~1.4 kb we have used the blasticidin fragment in excess (5 times more than the KS-101/KS-105 plasmids). The reaction mix was incubated for 30 min at room temperature. After incubation, 2 µl of the ligation mix were transformed into One Shot® TOP10 Chemically Competent *E. coli* bacteria (Invitrogen) following the manufacturer's protocol for chemical transformation (see paragraph 5.12.6). The transformed bacteria were spread on labelled LB agar plates containing 50 µg/µl ampicillin. The plates were incubated at 37 ^{0}C overnight. Twenty five resistant colonies were picked up for each vector and minipreparation of the plasmids was undertaken utilising the Qiagen 96 prep kit as described in paragraphs 5.12.7. Plasmid DNA was digested using Sal I and ECOR I which were both one-cutter enzymes for the KS-101 plasmid while they do not cut into the blasticidin fragment. 17 µl of KS-101B and KS105B plasmid were mixed with 10 units of Sal I (NEB) and 10 units ECOR I (NEB) 1x NEBuffer 3 and dd_2HO in a final volume of 20 µl. The reaction mix was incubated for 2 hrs at 37 ^{0}C. In addition approximately 500 ng of KS-101 were digested as described above in order to serve as controls. After incubation 5 µl of the reaction were run in a 1% agarose gel in TBE buffer and the cut plasmids were visualised using Safeview (NBS Biologicals) under UV lighting. The bacteria carrying the selected clones were grown in 150 ml liquid LB growth medium containing ampicillin (50 µg/µl) at 37 ^{0}C with shaking at 220 rpm. After 20-22 hrs maxipreperation of plasmid was undertaken using the using the Zyppy™ Plasmid Maxiprep Kit (Zymo Research, see paragraph 5.12.8) while 5 ml of the bacterial culture were used to create glycerol stock which was stored at -80 ^{0}C.

5.12.3 Construction of the PAXUHRF1 vector

In order to investigate the effect of UHRF1 expression on regional hypermethylation and hypomethylation of cancer cells we have used an inducible shRNA system to silence the expression of UHRF1 in a lung cancer cell line. The shRNA inducible knockdown system was a generous gift from Dr Malliri (Paterson institute).

The system is based on two vectors. The first one is comprised of an engineered pGEM T-easy vector which carries the H1 promoter and a Tet operator upstream of the position where the desired shRNA sequence is inserted. After insertion of the desired shRNA sequence in the pGEM T-easy vector, the shRNA module (H1 promoter, Tet operator and shRNA) is excised and ligated into the vector backbone of the pN1p_actin-rtTA^{2S}-M2-IRESEGFP plasmid [Welman et al. 2006] containing the tetracycline repressor. Dr Malliri also provided us with a ready to transfect final PA-1 vector which contains a scrambled shRNA sequence and can therefore be used as a mock control.

5.12.3.1 Preparation of UHRF1 shRNA oligo

The following DNA oligo sequence which carries a UHRF1 siRNA sequence (Qiagen) was designed and synthesised by MWG:

5'- GATCCCGGACGGCGCGGGAACTCTATTCAAGAGATAGAGTTCCCGCGCCGTCCTTTTTGGAAA- 3'

5'- AGCTTTTCCAAAAAGGACGGCGCGGGAACTCTATCTCTTGAATAGAGTTCCCGCGCCGTCCGG- 3'

5' GATCCCGGACGGCGCGGGAACTCTATTCAAGAGATAGAGTTCCCGCGCCGTCCTTTTTGGAAA 3'

3'GGCCTGCCGCGCCCTTGAGATAAGTTCTCTATCTCAAGGGCGCGGCAGGAAAAACCTTTTCGA 5'

The DNA oligos carrying the UHRF1 shRNA sequence were annealed as follows. A 20 µl reaction mix was prepared with 400 pmol of each oligo, 3 µl PCR buffer (Roche), 6 µl of betaine (Sigma Aldrich) and 13 µl of ddH_2O. The mixture was incubated at 95^0C for 5 minutes and then let to cool down at room temperature. The DNA oligo was analysed on a 4% TAE low melting point agarose gel, cut out, cleaned using Qiaquick nucleotide removal kit (Qiagen) and eluted at 20 µl ddH_2O.

5.12.3.2 Ligation of the UHRF1 shRNA sequence with the vector carrying the shRNA module

The pGEM T-easy shuttle vector containing the H1 promoter and Tet operator was digested with Bgl II and Hind III restrictive enzymes as follows. 500 ng of pGEM T-easy were mixed with 2 µl of Buffer 2 (NEB), 20 U of Hind III, 20 U of Bgl II and ddH_2O in a final volume of 20 µl. The reaction mix was incubated for 2 hrs at 37^0C and subsequently cohesive ends were melted by incubating at $65\ ^0C$ for 10 minutes. The mixture was then loaded and visualised on a 2% 1xTAE low melting point agarose gel. The vector was cut out, cleaned using the Qiaquick gel extraction kit (Qiagen), and eluted in 20 µl ddH_2O.

The target DNA oligo sequence was subsequently ligated with the open pGEM T-easy shuttle vector using 1 µl of T4 DNA ligase (NEB), 1 µl of 1x T4 ligase reaction buffer (NEB), 1 µl of open pGEM T-easy shuttle vector, 1 µl of oligo and ddH_2O in a total reaction volume of 10 µl. The reaction mix was incubated for 30 min at room temperature. After incubation, 2 µl from the ligation mix was transformed in One Shot® TOP10 Chemically Competent *E. coli* bacteria (Invitrogen) following the manufacturer's protocol for chemical transformation. The transformed bacteria were spread on labelled LB agar plates containing ampicillin (50 µg/ µl) antibiotic.

The following day 20 colonies were picked up and cultured for 16 hrs in LB growth medium containing ampicillin (50 μg/ μl) antibiotic. Plasmid extraction of the colonies took place the following day using Qiagen 96 prep kit. Positives colonies were checked by Xho I digestion and electrophoresis. The vector carrying the shRNA insert was larger (~500 bp) than the empty vector (~450 bp). Plasmids were digested with Xho I (5 μl DNA, 1 μl buffer 4 (NEB), 1 μl Xho I, 3 μl ddH_2O) at 37^0C for 2hrs and then run in a 2% agarose gel. In order to verify the inserted sequence positive plasmids were sequenced (see paragraph 5.12.9) using T7/SP6 primers that flank the target DNA oligo of interest.

5.12.3.3 Transfer of the UHRF1 shRNA module in the final PA-1 vector

The next step was to transfer the UHRF1 shRNA module (H1 promoter, Tet operator and shRNA) to the pN1p_actin-rtTA^{2S}-M2-IRESEGFP plasmid [Welman, 2006] vector containing the tetracycline repressor. Approximately 500 ng from the selected PGEM T-easy vector carrying the verified UHRF1 shRNA sequence and 500 ng of the pN1p_actin-rtTA^{2S}-M2-IRESEGFP plasmid were digested using 20 U of Xho I, 2 μl buffer 3 (NEB) and ddH_2O for 2 hrs at 37 ^0C in a final reaction volume of 20 μl. After incubation the pN1p_actin-rtTA^{2S}-M2-IRESEGFP vector was treated with alkaline phosphatase (NEB). Since the enzyme is working on the same buffer (buffer 3, NEB) as Xho I enzyme, 10 U of alkaline phosphatase were added in the pN1p_actin-rtTA^{2S}-M2-IRESEGFP vector-Xho I digested mix and the new mix was incubated for an extra 1hrs at 37 ^0C. The Xho I digested vectors were separated on 2% 1 x TAE low melting point agarose gel. The desired Xho I-Xho I insert carrying the shRNA module and the Xho I digested vector were cut out and cleaned using the Qiaquick gel extraction kit (Qiagen) and eluted in 20 μl of ddH_2O.

2 µl of Xho I-Xho I insert carrying the shRNA module and 2 µl of Xho I digested vector were subsequently ligated using 1 µl of T4 DNA ligase (NEB), 1 µl of 1x T4 ligase reaction buffer (NEB) and ddH_2O in a total reaction volume of 10 µl. The reaction mix was incubated for 30 min at room temperature. After incubation, 2 µl from the ligation mix was transformed into One Shot® TOP10 Chemically Competent *E. coli* bacteria (Invitrogen) following the manufacturer's protocol for chemical transformation. The transformed bacteria were spread on labelled LB agar plates containing 50 µg/ µl Kanamycin. The following day 20 colonies were picked up and cultured for 16 hrs in LB growth medium containing kanamycin 50 µg/ µl antibiotic. Plasmid extraction of the colonies took place the following day using Qiagen 96 prep kit (see paragraph 5.12.7). Positives were checked by Xho I digestion and gel electrophoresis. In order to verify the shRNA sequence and positive clones were sequenced utilising H1 primers which flank the inserted oligo in the pN1p_actin-rtTA^{2S}-M2-IRESEGFP vector. The bacteria carrying the selected clones were grown in 150 ml liquid LB growth medium containing 50 µg/ µl kanamycin at 37 ^{0}C with shaking at 220 rpm. After 20-22 hrs maxi-preparation of plasmid was undertaken using the using the Zyppy™ Plasmid Maxiprep Kit (Zymo Research) while 5 ml of the bacterial culture were used to create glycerol stock which was stored at -80 ^{0}C. The constructed PAUHRF1 and a ready to transfect full PA-1 vector (carrying a scramble shRNA sequence and used as a mock control) were used for the transfection of the desired cell line.

5.12.4 DNA clean up from enzymatic reactions

In order to clean up DNA fragments from enzymatic reactions we have used the QIAquick Nucleotide Removal Kit (Qiagen) following the manufacturer's protocol. 500 µl of Buffer PN were added to a 50 µl enzymatic reaction sample and were mixed. A QIAquick spin column

was placed in a provided 2 ml collection tube. In order to bind DNA, the sample was applied to the QIAquick column and centrifuged for 1 min at 3000 g. The flow-through was discarded and the QIAquick column was placed into a new collection tube. To wash the QIAquick column, 700 µl of Buffer PE were added and the column was centrifuged for 1 min at 3000 g. The flow-through was discarded and the column was centrifuge for an additional 1 min at 17,000 *g* in order to completely remove residual ethanol from PE buffer. The QIAquick column was placed in a clean 1.5 ml microcentrifuge tube. To elute DNA, 50 µl of Buffer EB (10 mM Tris·Cl, pH 8.5) were applied to the centre of the QIAquick membrane and the column was centrifuged for 1 min at 17,000 *g*.

5.12.5 DNA fragments extraction from agarose gels and clean up

In order to extract and purify DNA fragments and vectors from low-melt TAE buffer agarose gels we have used the QIAquick Gel Extraction Kit (Qiagen) following the manufacturer's protocol. The desired DNA fragment was excised from the agarose gel with a clean, sharp scalpel and in order to minimize the size of the gel slice, extra agarose was removed. The gel slice was weighed in a colourless 1.5 ml tube and 3 volumes of Buffer QG were added to the tube to 1 volume of gel (100 mg ~ 100 µl). For example, 300 µl of Buffer QG were added to each 100 mg of gel. The maximum amount of gel slice per QIAquick column is 400 mg, so for gel slices >400 mg more than one QIAquick column were used. The mixture was incubated at 50°C for 10 min until the gel slice has completely dissolved. After the gel slice was completely dissolved, 1 gel volume of isopropanol was added to the sample and mixed. A QIAquick spin column was placed in a provided 2 ml collection tube and in order to bind DNA, the sample was applied to the column and centrifuged for 1 min. The flow-through was discarded and the QIAquick column was placed in a new collection tube. To wash the DNA fragment, 0.75 ml of

Buffer PE were added to the QIAquick column and centrifuged for 1 min. The flow-through was discarded and the QIAquick column was centrifuged for an additional 1 min at 17,000 *g* to remove any residual ethanol from the PE buffer. The QIAquick column was placed into a clean 1.5 ml microcentrifuge tube. To elute DNA, 50 µl of Buffer EB (10 mM Tris·Cl, pH 8.5) were added to the centre of the QIAquick membrane and the column was centrifuged for 1 min.

5.12.6 Transformation

For plasmid propagation the One Shot® TOP10 Chemically Competent *E. coli* bacteria (Invitrogen) were used following the manufacturer's protocol for chemical transformation. One 50 µl vial of One Shot® cells was thawed on ice for each transformation. Following, 1 to 5 µl of each ligation reaction or plasmid vector were transferred with a pipette directly into the vial of competent cells and mixed by tapping gently. The vials were incubated on ice for 30 minutes and then for exactly 30 seconds in a 42°C water bath. Subsequently the vials were removed from the 42°C bath and placed on ice. 250 µl of pre-warmed S.O.C medium was added to each vial. The vial(s) were placed in a micro-centrifuge rack on its side and shaken at 37°C for exactly 1 hour at 225 rpm in a shaking incubator.150 µl from each transformation vial were spread on separate, labelled LB agar plates containing 50 µg/ µl of the selection antibiotic (either ampicillin or kanamycin). The plate(s) were inverted and incubated at 37°C overnight. The following day colonies were selected for miniprep isolation.

5.12.7 Mini preparation of plasmid DNA

For the mini preparation of plasmid DNA two different kits based on alkaline lysis procedures, the R.E.A.L. Prep 96 Plasmid Kit (Qiagen) and the Zyppy Plasmid Miniprep kit (Zymo Research) were used following the manufacturer's protocols.

Utilising the R.E.A.L. Prep 96 Plasmid Kit (Qiagen), different colonies were grown in each well of a 96 square-well block in 1.3 ml LB growth medium containing the appropriate selective antibiotic (either kanamycin or ampicillin). A single bacterial colony was inoculated in each well and the cultures were incubated for 20–24 h at 37°C with shaking at 220 rpm. The bacterial cells were harvested in the block by centrifugation for 5 min at 1500 x *g* in a centrifuge with a rotor for 96-well microplates and the medium was removed by inverting the block. Subsequently, each bacterial pellet was re-suspended in 0.3 ml Buffer R1 (containing RNase A) and mixed by vortexing. 0.3 ml of Buffer R2 were added to each well, the block was mixed gently but thoroughly by inverting 10 times and incubated at room temperature for 5 min. 0.3 ml of Buffer R3 were added to each well, and the block was mixed immediately by inverting 10 times. The block was then placed in a boiling water bath for 5 min and then cooled at room temperature by incubating on ice for 10 min. The QIAfilter 96 plate was placed in the top plate of the QIAvac 96 manifold. A new square-well block was placed into the base and the manifold was reassembled. The lysates were transferred to the wells of the QIAfilter 96 plate and vacuum (–200 to –300 mbar) was applied until the lysates were completely transferred to the square-well block in the QIAvac base. 0.7 volumes of room-temperature isopropanol were then added to each well and the block was mixed immediately by inverting 3 times. Following, the block was centrifuged at 2500 x *g* for 15 min at room temperature to pellet the plasmid DNA and the supernatants were removed by quickly inverting the block over a waste container, then tapping the block firmly, upside down, onto a paper towel. Each

DNA pellet was then washed with 0.5 ml of 70% ethanol and the block was centrifuged at 2500 x *g* for 2 min to re-concentrate the pellets. The wash solutions were removed by inverting the block and the pellets were dried under vacuum for 10 min. The DNA pellets were then re-dissolved in 100 µl 10 mM Tris-Cl, pH 8.5. The plasmid purity and plasmid DNA yield was assessed by spectrophotometry at 260/280 nm wavelength.

In order to use the Zyppy Plasmid Miniprep kit (Zymo Research) we have first prepared the Neutralization Buffer by adding RNase A at a final concentration of 50 µg/ml and the Zyppy™ Wash Buffer concentrate by the addition of absolute ethanol. 1.5 ml of bacterial culture was centrifuge for 30 seconds at maximum speed. The supernatant was discarded and the bacterial cell pellet was re-suspended in 600 µl of water. The mixture was transferred to a 1.5 ml microcentrifuge tube, 100 µl of 7X Lysis Buffer (blue) were added and were mixed by inverting the tube 4-6 times. 350 µl of cold Neutralization Buffer (Yellow) were added and the mixture was mixed thoroughly. The sample turned yellow when the neutralization was complete and a yellowish precipitate formed. The sample was then centrifuged at 11,000 – 16,000 x g for 2-4 minutes. The supernatant (~900 µl) was transferred carefully without disturbing the cell debris pellet into the provided Zymo-Spin™ IIN column. The column was then placed into a Collection Tube and centrifuged for 15 seconds. The flow-through was discarded and the column was placed back into the same Collection Tube. 200 µl of Endo-Wash Buffer were added to the column which was subsequently centrifuged for 15 seconds at top speed. 400 µl of Zyppy™ Wash Buffer2 were added to the column another Centrifugation took place for 30 seconds at top speed. The column was transferred into a clean 1.5 ml microcentrifuge tube and 30 µl of Zyppy™ Elution Buffer were added directly to the column matrix and let stand for one minute at room temperature. Centrifugation for 15 seconds at

top speed took place for the elution of the plasmid DNA. The plasmid purity and plasmid DNA yield was assessed by spectrophotometry at 260/280 nm wavelength.

5.12.8 Maxi preparation of plasmid DNA

Maxi preparation of plasmids was undertaken using the Zyppy™ Plasmid Maxiprep Kit (Zymo Research) following the manufacturers protocol as follows. P1 buffer was prepared by the addition of RNAse A at a final concentration of 50 µg/ml and Zyppy™ Wash Buffer by the addition of 96 ml of absolute ethanol. We have used the vacuum manifold protocol and all the steps were carried at RT. Up to 150 ml of fresh bacterial culture was centrifuged at ≥ 3,400 x *g* for 10 minutes. The supernatant was discarded, 15 ml of P1 Buffer (Red) were added to the bacterial cell pellet and it was re-suspended completely by vortexing. 15 ml of P2 Buffer (Green) were added, mixed immediately by inverting the tube 4-6 times and the tube was let to stand for one minute to lyse the cells completely. 20 ml of P3 Buffer (Yellow) were added, mixed thoroughly and the mixture was incubated on ice for 5 minutes. The Zymo-Maxi Filter™/Zymo-Spin™ VI column assembly was placed onto a vacuum manifold. And the entire mixture was added into the blue Zymo-Maxi Filter™ column. After the cell debris floated to the surface, the vacuum was turned on until all of the liquid had passed completely through both columns. The blue Zymo-Maxi Filter™ column was removed and discarded from the top of the Zymo-Spin™ VI column. 10 ml of Endo-Wash Buffer were added to the Zymo-Spin™ VI column and the vacuum was turned on. After the Endo-Wash Buffer had completely passed through the Zymo-Spin™ VI column, 10 ml of Zyppy™ Wash Buffer2 were added, the vacuum was turned on and the vacuum was let on for an additional 5 minutes to remove all residual Zyppy™ Wash Buffer. The Zymo-Spin™ VI column was then transferred into a clean 50 ml

conical tube and 3 ml of Zyppy™ Elution Buffer were added to the column. The column was incubated at RT for one minute, and then centrifuged at ≥ 3,400 x *g* for 1 minute to elute the plasmid DNA. The plasmid purity and plasmid DNA yield was assessed by spectrophotometry at 260/280 nm wavelength.

5.12.9 Sequencing of plasmids

The pGEM/UHRF1 vector and the final PAUHRF1 plasmid were sequenced in order to verify correct inserts. Sequencing reactions were prepared as following. 10 µl from the plasmid DNA were incubated at 95 ^{0}C for 5 minutes then put on ice and spun at full-speed for 3 minutes. After centrifugation, 2.5 µl of plasmid DNA were taken from the top of the liquid and mixed with 8 µl BigDye® Terminator v3.1 Cycle Sequencing Kit (Applied Biosystems), 3.2 pmol of H1 primer and 8.5 µl ddH_2O in a total reaction of 20 µl. The cycle sequencing was performed in an Applied Biosystems 7500 PCR machine using the following thermal profile. The reaction mix was heated at 95°C for 5 minutes followed by 30 cycles of 95 °C for 30 sec (denaturation), 58 °C for 45 sec (annealing) and 60 °C (elongation) for 4 minutes.

After the sequencing reaction, the DNA fragments were precipitated using ethanol/EDTA method which produces consistent signal, while minimizing unincorporated dyes. Our samples were mixed with 5 µl of 125 mM EDTA. 60 µl of 100% ethanol were added, mixed and the tubes were incubated at room temperature for 15 min in the dark. Subsequently, the tubes were centrifuged for 15 min at 10.000 g and the supernatant was discarded using a pipette. 60 µl of 70% ethanol were added to each tube which was subsequently centrifuged for 5 min at 10.000 g. Supernatant was discarded using a pipette and the precipitates were dried under vacuum for 5 min. Finally the samples were re-suspended in 10 µl HDF (Applied Biosystems),

incubated at 95^0C for 5 minutes and cooled on ice for 1 minute. Sample electrophoresis took place on an ABI prism 3700 DNA analyzer.

5.13 Transfection of cell lines

For the transfection of prepared plasmids into the desired cell lines we used two different protocols. For the transfection of the PAXUHRF1 and PA-1 mock plasmids we have used the Attractene Transfection Reagent (Invitrogen) following the manufacturer's protocol. Plasmid DNA transfection was performed in 6-well plates. The day before transfection 5 x 10^5 cells were seeded per well in 2 ml of culture medium containing serum and antibiotics. Cells were incubated under normal growth conditions (typically 37 ^{o}C and 5% CO_2) until they reached 60%-80% confluence. On the day of transfection 1.2 μg of plasmid DNA was dissolved in medium without serum, proteins, or antibiotics to a total volume of 100 μl. 4.5 μ of Attractene Transfection Reagent were added to the DNA solution and mixed by pipetting. The samples were incubated for 15 min at room temperature (15-25 ^{o}C) to allow complex formation. While complex formation took place, the medium from the cells was gently aspirated and 2 ml of fresh medium (containing serum and antibiotics) were added to the cells. Subsequently the transfection complexes were added drop-wise onto the cells and the plate was gently swirled to ensure uniform distribution of the transfection complexes and cells were incubated under their normal growth conditions.

For the transfection of cells with KS-101, KS105, KS101B and KS-105B plasmids we have used the *Trans*IT®-2020 Transfection Reagent (Mirus) following the manufacturer's protocol. Plasmid DNA transfection was performed in 6-well plates. One day before transfection, 5 x 10^5 cells were plated per well in 2.5 ml complete growth medium containing serum and

antibiotics. Cells were incubated under normal growth conditions (typically 37 °C and 5% CO_2) until they reached 60%-80% confluence. The *Trans*IT-2020 Transfection Reagent was pre-warmed to room temperature and vortexed gently before being used. 2.5 µg of plasmid DNA were added to 250 µl of Opti-MEM®I Reduced Serum medium in a sterile polystyrene tube and mixed by pippeting. Subsequently, 7.5µl of *Trans*IT-2020 Transfection Reagent were added to the diluted DNA mixture and mixed by pippeting. The mixture was then incubated at room temperature for 30 minutes to allow sufficient time for the formation of complexes. The *Trans*IT-2020 Transfection Reagent: DNA complexes were added drop wise to different areas of the wells containing the plated cells. The culture vessel was gently rocked back and forth and from side to side to evenly distribute the *Trans*IT-2020 Transfection Reagent:DNA complexes and cells were incubated at normal conditions. As the *Trans*IT-2020 Transfection Reagent demonstrated minimum toxicity the complete growth medium was not replaced the following day with fresh medium.

5.14 Generation of A549 PAUHRF1 stable cell line clones

Screening of a panel of cell lines has demonstrated that A549 cells expressed the higher levels of UHRF1 mRNA and were therefore selected as the best candidates from UHRF1 downregulation experiments. A549 cells were transfected with the PAXUHRF1 plasmid which carries the neomycin resistance gene. In order to determine the optimal concentration of G418 for selection we have examined the kill curve of A549 cells in the presence of various concentrations of G418. Cells were seeded in 24 well plates at low density and were grown in the presence of different concentrations (400 µg/ml - 1.5 µg/ml) of G418 for two weeks. The lowest concentration of G418 that promoted complete death of A549 cells in less than two

weeks was 600 μg/ml. 48 hours post transfection of A549 cells with the PAXUHRF1 and the PA-1 mock plasmids, cells were passaged in complete growth medium containing 600 μg/ml of G418. Growth medium and antibiotic was replenished every 2-3 days. After 2 weeks of selection colonies were isolated using cloning cylinders, trypsinised and grown in new flasks under normal growth conditions and in the presence of selection antibiotic. Twenty different clones were checked for UHRF1 downregulation at both RNA (qPCR) and protein (western blot) level in the presence/absence of 1 μg/ml Doxycycline for up to 96 hrs. Colonies demonstrating the highest UHRF1 knockdown efficiency were grown and used for further analysis.

5.15 Western blot

5.15.1 Protein extraction and total protein concentration measurement

A549 cells were cultivated as described above until they reached 80% confluence. After two washes with DPBS, the cells were harvested using 50μl of RIPA buffer (Table 15) supplemented with protease inhibitors (1mM PMSF (Sigma Aldrich), 10μg/ml leupeptin (Sigma Aldrich), 10mM NaF (Fluka), 1mM Na_3VO_4 (Sigma Aldrich)).

Table 15 Reagents used for the preparation of RIPA buffer

RIPA buffer	
Tris-HCl pH 7.4	50mM
NaCl	150mM
EDTA	1mM
Nonidet P-40	1%
Deoxycholate sodium	0.1%
SDS	0.1%

Cells were lysed for 15min on ice, spun at 4^0C for 15min at 18.000 g and supernatant was stored at -20 ^{0}C until further analysis. Total protein concentration was measured with DC Biorad Assay (Biorad) using DU530 UV/VIS spectrophotometer (Beckman). Concentrations were read from a standard curve created from serial dilutions of fraction V BSA (Sigma Aldrich) prepared in RIPA buffer with protease inhibitors.

5.15.2 Protein electrophoresis

In order to prepare the samples for electrophoresis, 20 µg of total protein from A549 cells and clone derivatives were mixed together with 2.5 µg of (4x) NuPAGE® LDS Sample Buffer (Invitrogen), 1 µl of (10x) NuPAGE Reducing Agent (Invitrogen) and ddH_20 up to a total of 10 µl reaction volume. The mix was denatured by incubation at 70 ^{0}C for 10 minutes. For the electrophoresis of total protein we have used the 3-8% NuPAGE Novex Tris-Acetate Mini gels (Invitrogen). The gels were placed in the electrophoresis tank and the upper chamber was filled with 200 ml of 1x NuPAGE Tris-Acetate SDS running buffer (Invitrogen) mixed with 500 µl of NuPAGE® Antioxidant (Invitrogen), while the lower chamber was filled with 600 ml of 1x NuPAGE® Tris-Acetate SDS running buffer (Invitrogen).. After denaturation the samples were loaded on the gels together with Full Range Amersham™ Rainbow™ Marker (GE Healthcare). The gels were run at 150 V (40-55 mA gel start/ 25-40 gel end) for 1 hrs.

5.15.3 Electrotransfer, immunoblotting and detection.

For blotting of the electrophorised proteins we have used the iBLOT platform (Invitrogen). After electrophoresis, the gels were removed and trimmed, put onto the membrane of Anode Stack (Invitrogen) and covered with pre-wet (in ddH_20) blotting paper. The Cathode Stack

(Invitrogen) was then added on top of blotting paper and a white sponge was placed on the inner side of the lid. The iBLOT platform was switched on at program 3 (P3-7min). After 7min the membrane was removed from the iBLOT and placed in the blocking solution for 1h at room temperature (blocking solutions: 5% milk in PBS-T, 3% BSA in PBS-T or Protoblock solution from National Diagnostics). The gels were rinsed in ddH_20 water (3x 5min), stained with the Commassie Blue (e.g. Simple Blue SafeStain by Invitrogen), destained in water (3x 5 min or more) and pictures were captured using the UVP VisionWorks LS instrument. After one hour of blocking, the membrane was incubated overnight with 2 μg/ml of the primary anti-UHRF1 mouse antibody (ab57083, Abcam) at 4 ^{0}C. The membrane was washed with three changes of PBS-T every 10min and probed with HRP-rabbit anti-mouse secondary antibody (ab6728, Abcam) for 1h at room temperature. Membrane was then washed four times for 10 min in PBS-T and the bands were visualised using the ECL western blotting detection kit (Amersham). Anti-Tubuline primary antibody (SC31779, Santa Cruz) was used as an internal control of total protein concentration.

5.16 Examination of cells phenotypic characteristics

5.16.1 MTT proliferation assay

The viability of A549 parental and PAXUHRF1 knockdown clones was measured using the MTT proliferation assay. $5x10^3$ of A549 parental, mock, and clone derivative cells were seeded in 12 well plates. The next day cells were washed with PBS and incubated with fresh medium containing 0.5 mg/ml of MTT (3-(4,5-dimethy1–2-thioazoyl) 2,5-diphenyltetrazolium bromide) (Sigma-Aldrich) for 2.5 hours at 37 °C supplemented with 5% CO2. The medium was subsequently removed and cells were washed with PBS. The converted formazan was

solubilised by the addition of 1 ml of isopropyl alcohol–0.04 M HCl and pipette mixing. After five minutes, viability of the cells was determined by measuring the difference in absorbance at 570 nm with reference at 630 nm (optical density 570–655). Time point measurements were performed every 24 hrs for 5 subsequent days. The average proliferation rate was deducted from three biological replicates.

5.16.2 Wound healing assay

Wound-healing capacity of the A549 parental, mock and clone derivative cells was measured using scratch assays. Approximately 3-5x10^3 of A549 parental, mock, A549 PAXUHRF1 clone 1 and clone 2 cells were seeded in 24 well plates. Next day when cells had reached confluence, monolayers were scratched using a tip and time lapsed images were digitally captured at different time points over a period of 24 hrs with a CCD camera. The open wound area was calculated using TScratch software [Gebäck, 2009].

5.17 Treatment of cell lines with decitabine and trichostatin-A

We have utilised decitabine, a known DNA demethylating agent and Trichostatin-A (TSA), a known histone de-acetylase (HDAC) inhibitor, in order to examine the effect of epigenetic changes on retrotransposable elements. The optimal amount of decitabine which yields maximum levels of global hypomethylation, was established by the use of different decitabine concentrations for treatment of a non tumourigenic (HBEC 3kt) and a cancer (CRL5802)_cell line. Cells were seeded so as to cover about 15% of the flask surface before the first day of treatment. On the day of treatment we changed medium and added the following amount of decitabine: 0.01 μM, 0.05 μM, 0.1 μM, 0.5 μM, 1 μM, 1.5 μM, 2 μM, 5 μM, 10 μM, 20 μM.

Decitabine has a self-life time of 21 hrs at 37 ^{o}C [Stresemann, 2008] and therefore every 24 hrs the medium was changed and fresh decitabine was added. Since decitabine blocks DNMTs and promotes hypomethylation during DNA replication, treatment was carried on until the cells had undergone at least two duplications. The concentration which demonstrated the highest degree of global demethylation as measured by the methylation status of LINE-1 element was 0.1 μM. TSA was used at a concentration of 100 nM for 16 hrs. This dose for this period of time inhibits effectively the HDAC enzymes while it demonstrates low toxicity for the cells [Oyer, 2009].

DNA methylation/ histone acetylation inhibition experiments were carried out by treating A549, CRL5802 and HBEC3KT cell lines (one adenocarcinoma, one squamous and one non-tumourigenic respectively) with 5-aza-2'-deoxycytidine (Decitabine, Sigma-Aldrich, cat no11390) and TSA (Sigma-Aldrich, cat no T8552). Cells were seeded so as to cover about 15% of the flask surface. Four flasks were seeded for each cell line that we used; one served as a control; one was treated only with 100nM decitabine; one was treated only with 100nM TSA; one was treated with both chemical substances. Every 24 hrs the medium was changed and fresh decitabine was added. Treatment was carried on until the cells had undergone at least two cell divisions. TSA was added were applicable for the last 16 h prior to harvesting cells. When harvested cells from each flask were pelleted, split into two tubes and stored at -80 ^{0}C until DNA and RNA extraction. Observations were confirmed by triplicate experiments.

5.18 Transfection of different cell lines with KS-101 and KS-105 plasmids

In order to identify the retrotransposition ability of the LRE3 element in NSCLC and normal lung cell lines we have transfected IMR-90, A549, CRL5802, CRL5935, CALU-1 and CALU-6 cell

lines with KS-101 and KS-105 plasmids. As we have described above, after transfection with the KS-101 plasmid, cell will acquire resistance to G418 only after a full retrotransposition cycle. Therefore retrotransposition events can be visible in the number of colonies present after selection with G418.

In order to determine the optimal concentration of G418 for selection we have examined the kill curve of all different cell lines in the presence of various concentrations of G418. Cells were seeded in 24 well plates at low density and were grown in the presence of different G418 concentrations (400 μg/ml - 1.5 mg/ml) for two weeks. The lowest concentration of G418 that promoted complete death of IMR-90, A549, CRL5935, CALU-1 and CALU-6 cells in less than two weeks was 600 μg/ml while for CRL5802 the optimal concentration of G418 was 800 μg/ml.

The different cell lines were transfected with KS-101 and KS-105 plasmids as described in paragraph 5.13. 48 hrs post transfection cells were passaged in complete growth medium containing the optimal concentration of G418. Growth medium and antibiotic were replenished every 2-3 days. After 2 weeks of selection colonies were stained with 0.01% crystal violet, counted and photographed using the UVP VisionWorks LS instrument.

We have also examined the effect of decitabine on the retrotransposition capacity of L1.3 in these cell lines. After transfection with KS-101 and KS-105 plasmids, cells were passaged in a final confluence of approximately 20%. Treatment with decitabine was carried in half of the cells, as described in the previous paragraph until cells had undergone at least two duplications, while the rest were left untreated to serve as control. Subsequently the medium containing decitabine was subtracted from the cells and G418 selection took place in both decitabine treated and untreated cells as described above.

5.19 Transfection of different cell lines with KS-101B and KS-105B plasmids

We have transfected CRL5802 cells using KS-101B and KS-105B plasmids. These two plasmids allow for selection of transfected colonies using blasticidin (see paragraph 5.12.2). The selected clones carry the KS-101 plasmid and can be studied regardless of the retrotransposition ability of the L1.3 element they carry on the KS-101 plasmid.

In order to determine the optimal concentration of blasticidin for selection we have examined the kill curve of the CRL5802 cell line in the presence of different blasticidin concentrations (2-10 μg/ml). Cells were seeded in 24 well plates at low density and were grown in the presence of the different concentrations. The lowest concentration of blasticidin that promoted complete death of the CRL5802 cells in less than two weeks was 5 μg/ml.

Cell lines were transfected as described in paragraph 5.13. 48 hrs post transfection cells were passaged in complete growth medium containing 5 μg/ml of blasticidin. Growth medium and antibiotic was replenished every 2-3 days. After 2 weeks of selection colonies were isolated after trypsinization using cloning cylinders and were grown in new flasks under normal growth conditions and in the presence of selection antibiotic. DNA was extracted from each colony for methylation analysis of the LRE3 promoter. Colonies were examined for retrotransposition activity with or without decitabine as described in paragraph 5.18.

5.20 Statistical analysis

Q-Q plots and the one-sample Kolmogorov-Smirnof test were used to evaluate fitness to normal distribution of continuous parameters. Paired t-test was used to determine if there was a statistically significant change in the methylation status of LINE-1 and Alu-PV in primary NSCLC tumours. Depending on the fitness of parameters to normal distribution, the Pearson's

(parametric) or Spearman's (non-parametric) tests were used to analyze correlations between LINE-1 and Alu-PV methylation and genomic instability. Non-parametric tests such as Mann-Whitney and Wilcoxon's were used to analyze expression values among different groups of DNMTs, E2F1 and UHRF1 expression. Spearman's correlation was employed to assess the relationship between continuous values. $P<0.05$ was considered statistically significant. All statistical tests were performed by SPSS16.0 (SPSS Inc. Chicago, IL, USA).

Chapter 6. Deregulation of DNA methylation in lung cancer

The first aim of this study was to explore DNA methylation deregulation in lung cancer and identify potential causes behind this phenomenon. Towards this goal we have studied the expression of DNMTs and UHRF1, the proteins responsible for the establishment and maintenance of the methylation patterns, in a large set of primary tissues. In parallel, we identified in the same set the methylation status of particular TSG promoters bearing CpG islands and assessed global hypomethylation reflected by the methylation status of LINE-1 element. Analysis demonstrated the importance of UHRF1, DNMT1 and DNMT3B in the promotion and maintenance of the hypermethylation of TSGs. Since this role is new and less studied for UHRF1, we further examined the effect of UHRF1 in TSG maintenance by knocking down its expression in a lung adenocarcinoma cell line.

6.1 Expression status of DNMTs, UHRF1 and E2F1 in primary tumours and cell lines

We examined by qPCR the mRNA expression levels of DNMTs, UHRF1 and E2F1 in a set of 105 primary non-small cell lung carcinomas. RNA from paired normal adjacent tissues was available from 50 of these patients. RNA quality was examined on an Agilent Bioanalyser. The selection for the compilation of this set was based on a RIN value $\geq$ 6 (Figure 24). Representative qPCR runs for UHRF1 and DNMT1 are shown in Figures 25 and 26 respectively.

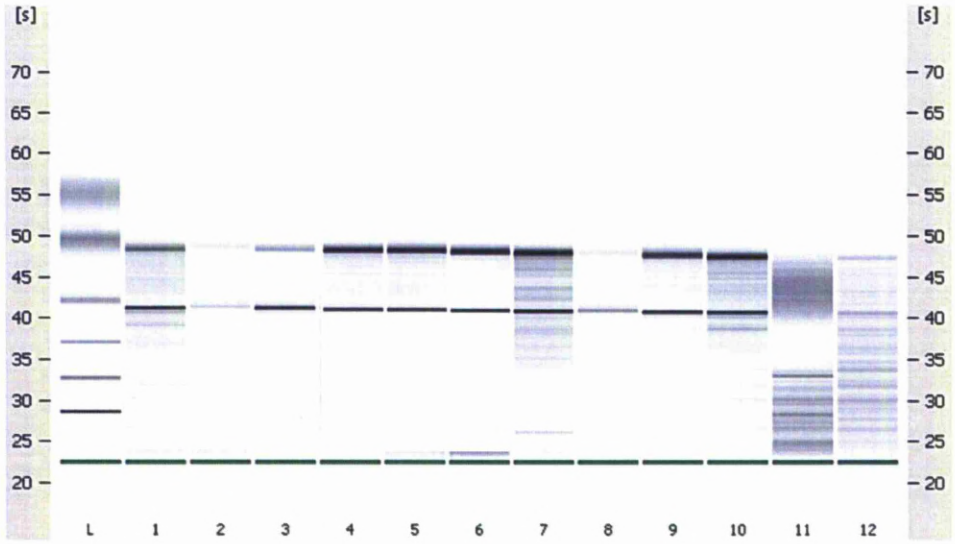

Figure 24 Total RNA electropherogram run on a Agilent Bioanalyser chip. The 18S and 28S peaks are clearly visible at 40 and 48 seconds, respectively. The examined lung tissue RNA set was constructed only with samples with adequate amount of RNA and a high RIN number (RIN>6, such as samples 4-7). Highly degrade RNAs (as in samples 11, 12) were not included in the set.

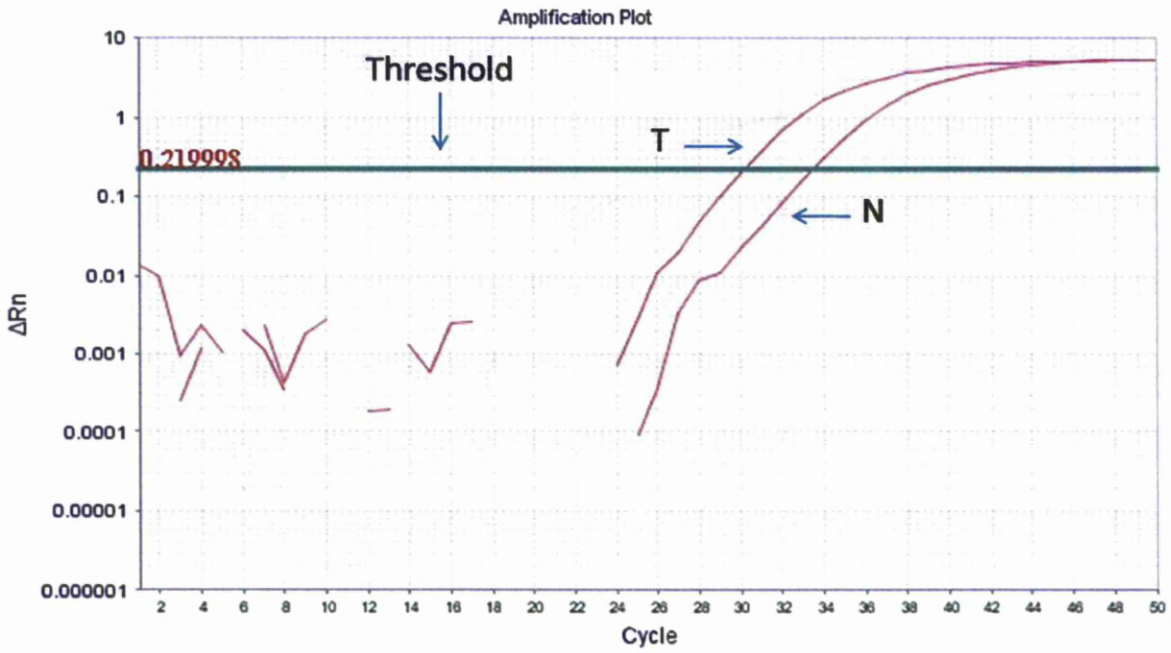

Figure 25 Representative amplification plot of UHRF1 gene on an Applied Biosystems 7500 real time PCR machine. The amplification curve of UHRF1 in a tumour and a corresponding adjacent normal sample are normalised to actin and superimposed in this plot. According to the threshold set, UHRF1 has a dCt value of 30 in the tumour sample while at the corresponding normal a dCt value of 34.

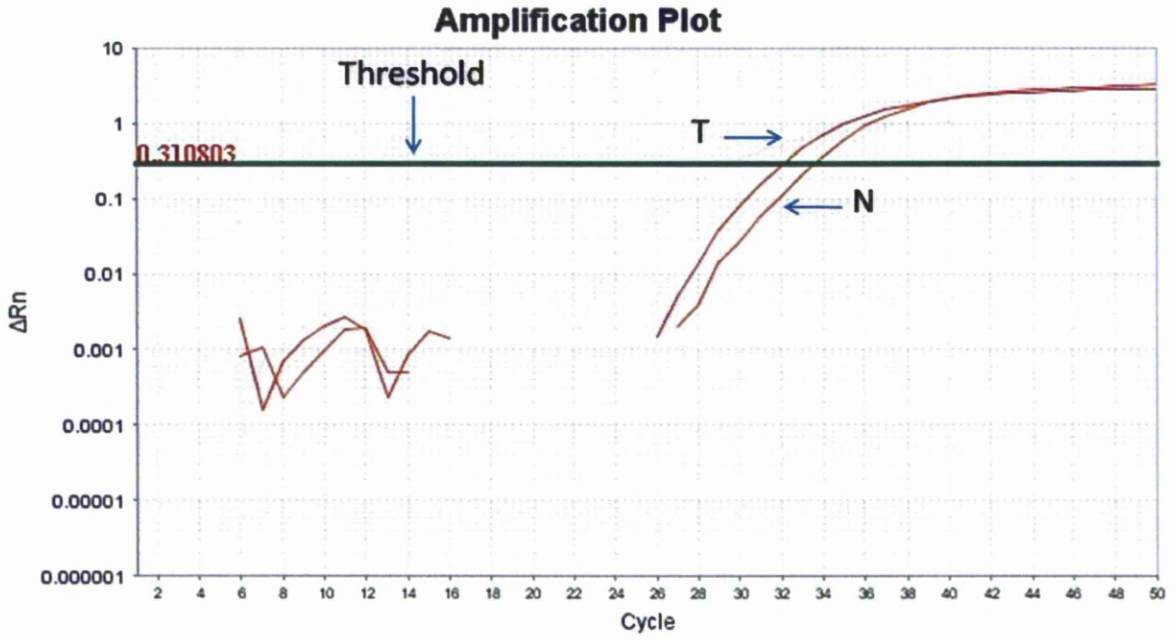

Figure 26 Representative amplification plot of DNMT1 gene on an Applied Biosystems 7500 real time PCR machine. The amplification curve of DNMT1 in a tumour and a corresponding adjacent normal sample are normalised to actin and superimposed in this plot. According to the threshold set, DNMT1 has a dCt value of 32 in the tumour sample while at the corresponding normal a dCt value of 34.

RNA levels were expressed as relative quantification values (RQ) which were calculated as: $RQ=2^{(-\Delta\Delta Ct)}$, where the mRNA expression of IMR-90 lung embryonic fibroblast cells was used as a calibrator in each run. All assays were run in triplicates and the mean value was used for the analysis. The mean RQ values of all genes in the examined set are available in the appendix.

We statistically compared the expression of these genes in tumour and adjacent normal tissues undertaking a non parametric test for paired analysis (Wilcoxon's). Analysis of normal/tumour paired tissue set demonstrated higher mRNA levels for UHRF1, DNMTs and E2F1 in the tumour samples (Table 16).

Table 16 mRNA expression of examined genes in lung tumour and paired normal lung tissue (n=50).

	mRNA expression (RQ values, mean ± SE)		
	Tumour	Normal lung	p-value (Wilcoxon's test)
UHRF1	3.9 ± 0.4	0.5± 0.1	1.7×10^{-9}
DNMT1	9.8 ± 0.8	5.8 ± 0.4	2.0×10^{-5}
DNMT3A	47.9 ± 7.4	32.9 ± 4.5	3.9×10^{-4}
DNMT3B	89.0 ± 16.7	31.8 ± 5.8	4.4×10^{-6}
E2F1	25.3 ± 3.8	9.5 ± 1.5	1.9×10^{-6}

RQ=Relative quantification value= $2^{-\Delta\Delta Ct}$. The expression of IMR90 lung fibroblasts has been used as calibrator in all genes. The mean value was deduced by two repeats.

Bivariate analysis (Spearman's correlation) of the expression levels of the above genes in the set of 105 tumours demonstrated significant correlations between all of them (Table 17).

Table 17 Coordinated expression of UHRF1, DNMTs and E2F1 in NSCLC (N=105)

	DNMT1	DNMT3A	DNMT3B	E2F1
UHRF1	0.633*	0.583	0.514	0.754
	4.5×10^{-13} **	6.6×10^{-11}	2.4×10^{-8}	1.5×10^{-20}
DNMT1		0.737	0.558	0.659
		3.2×10^{-19}	7.3×10^{-10}	2.3×10^{-14}
DNMT3A			0.688	0.744
			6.9×10^{-16}	1.1×10^{-19}
DNMT3B				0.732
				1.1×10^{-18}

* Spearman's correlation coefficient
** p-value

Expression of UHRF1, DNMTs and E2F1 was comparatively analyzed with the clinicopathological data of this set. UHRF1 was found to be expressed at higher levels in squamous carcinomas compared to adenocarcinomas (Mann-Whitney test, p=0.019), whilst no other clinical association (age, gender, T stage, nodal metastasis or differentiation) was observed for the rest of the genes. Furthermore, we have analysed the expression levels of the above genes in comparison to survival data which were available for a subset of tumours (n=54) (Appendix). DNMT3B mRNA overexpression correlated with poor prognosis. In

particular, patients with lower than median DNMT3B expression (RQ≤26.6) had a mean estimate survival of 70.2 ± 10.4 months while the corresponding figure for those with higher DNMT3B expression was 29.3 ± 5.7 months (Log rank test, p=0.013, Figure 27). The rest of the genes examined did not demonstrate any correlation with survival.

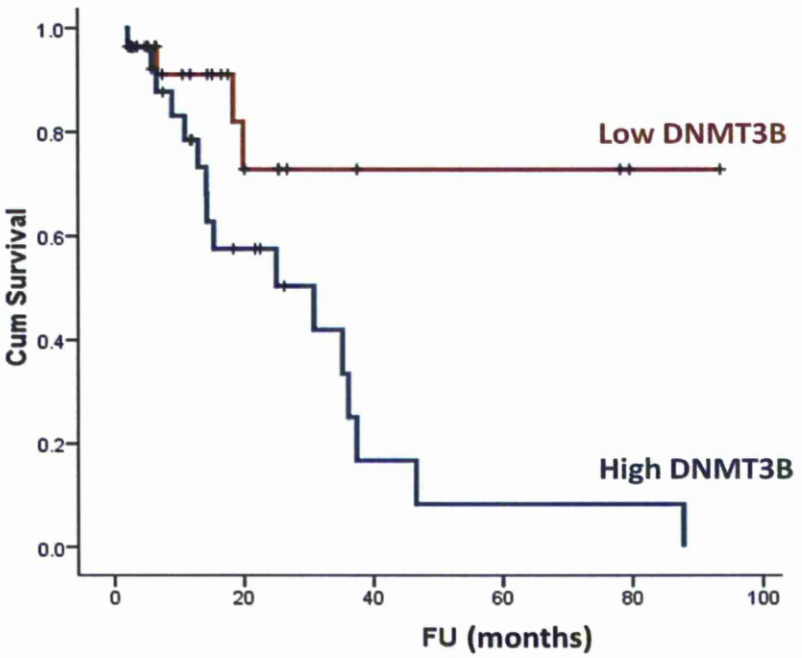

Figure 27 Kaplan-Meier survival analysis of NSCLC patients in relation to the DNMT3B mRNA expression. X axis represents follow-up (FU) time while cumulative survival is represented on the Y axis. Tumours with DNMT3B RQ value >26.1 (median) demonstrate a lower survival rate than those with lower than the median DNMT3B expression. It must be noted that none of the patients received post-operative chemo- or radiotherapy.

6.2 Methylation status of DNMTs and UHRF1 promoters in primary tumours

Bioinformatic analysis of the UHRF1 and all DNMTs promoters demonstrated the presence of CpG islands. This led us to investigate the potential epigenetic regulation of these molecules. Pyrosequencing assays were designed for each gene and used to identify the methylation status of their promoter in this normal and tumour set. Representative pyrograms for each gene are shown in Figure 28. The threshold for scoring hypermethylated samples was

conservatively set to 10%, which is higher to previously established threshold [Shaw, 2006], [Hall, 2008], in order to increase the prospect of the detected methylation for biologically relevance. All four promoters were found to be completely unmethylated with a methylation index below 5% in all normal and tumour tissues examined.

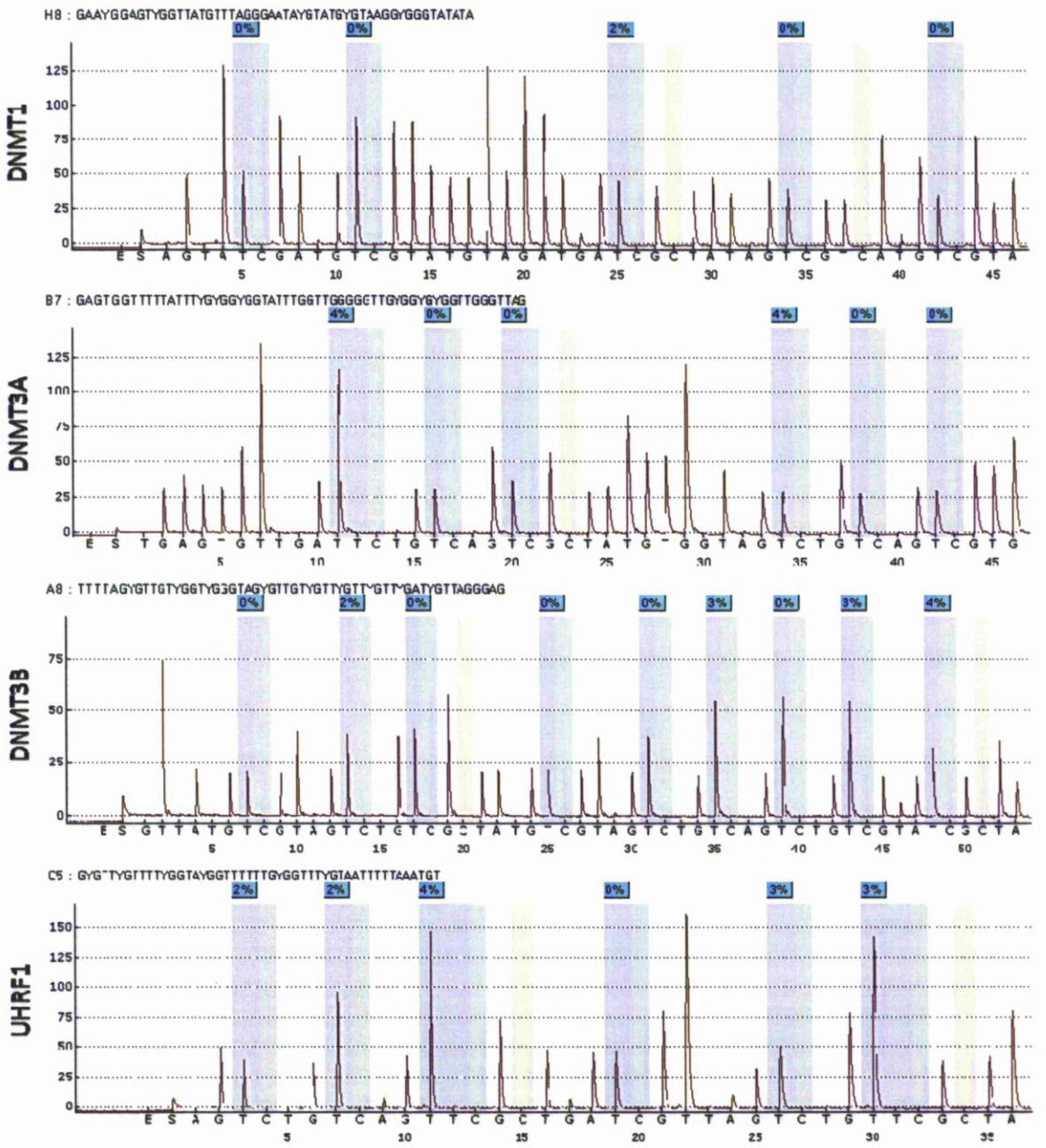

Figure 28 Representative pyrograms of DNMT1, DNMT3A, DNMT3B and UHRF1 promoter sequences examined in this study. The percentages in boxes represent the individual CpG methylation values. The methylation

index (MtI) is calculated as the average values of the examined CpGs. All gene promoters demonstrated low to methylation (less than 5%) DNMT1: MtI 0%, DNMT3A: MtI 1% DNMT3B: MtI 1%, UHRF1: MtI 2%. The bisulphite control dispensed nucleotides are shown in the yellow column.

6.3 Methylation status of CDKN2A and RASSF1 TSGs in primary lung carcinomas

In order to examine the potential relationship between DNMTs and UHRF1 expression and frequently hypermethylated genes in lung cancer, we have identified the methylation status of CDKN2A and RASSF1 genes. The methylation levels of CDKN2A and RASSF1 promoters were measured by Pyrosequencing in this set of 105 NSCLC tumour and 50 normal tissues. The threshold for scoring hypermethylated samples was conservatively set to 10%, which is higher to previously established thresholds [Shaw, 2006], [Hall, 2008], in order to increase the prospect of the detected methylation for biological relevance. DNA hypermethylation was observed in 32.4% of the tumours for RASSF1 and 26% of the tumours for CDKN2A (Appendix). Representative pyrograms for each gene are given in photos 29 for CDKN2A and 30 for RASSF1.

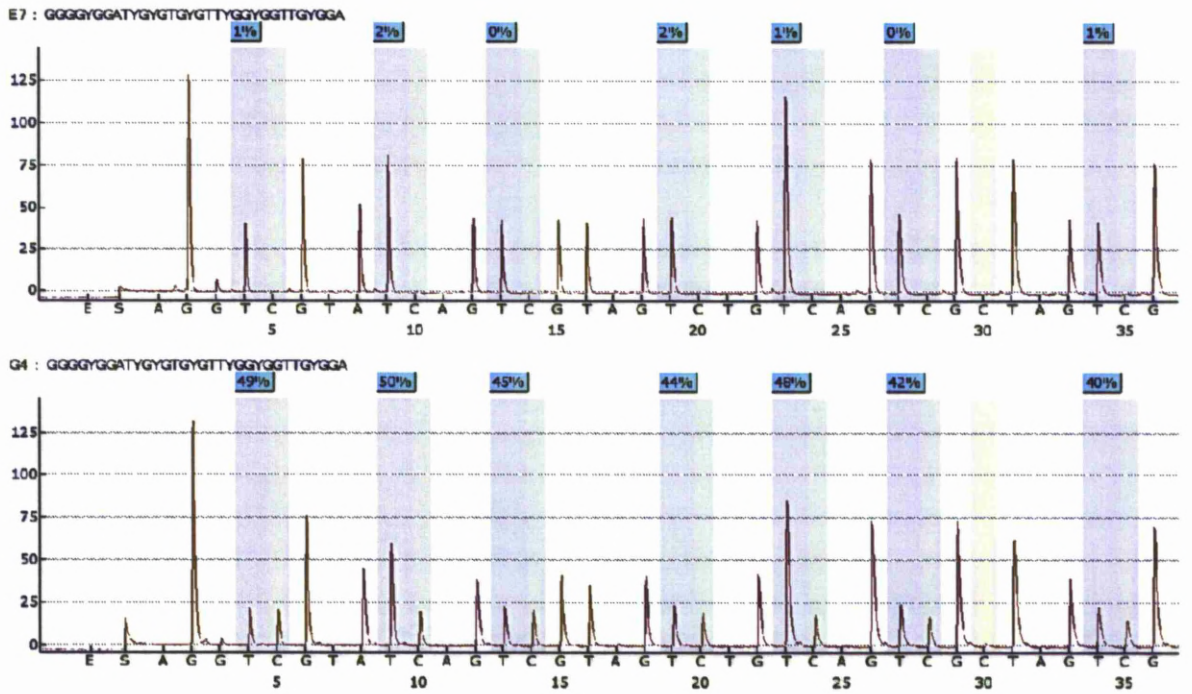

Figure 29 Representative pyrograms of the CDKN2A promoter sequence examined in this study. Upper: CDKN2A adjacent normal, MtI 0%. Lower: CDKN2A lung tumour, MtI 45%. The percentages in boxes represent the individual CpG methylation values. The methylation index (MtI) is calculated as the average values of the examined CpGs. The bisulphite control dispensed nucleotides are shown in the yellow column.

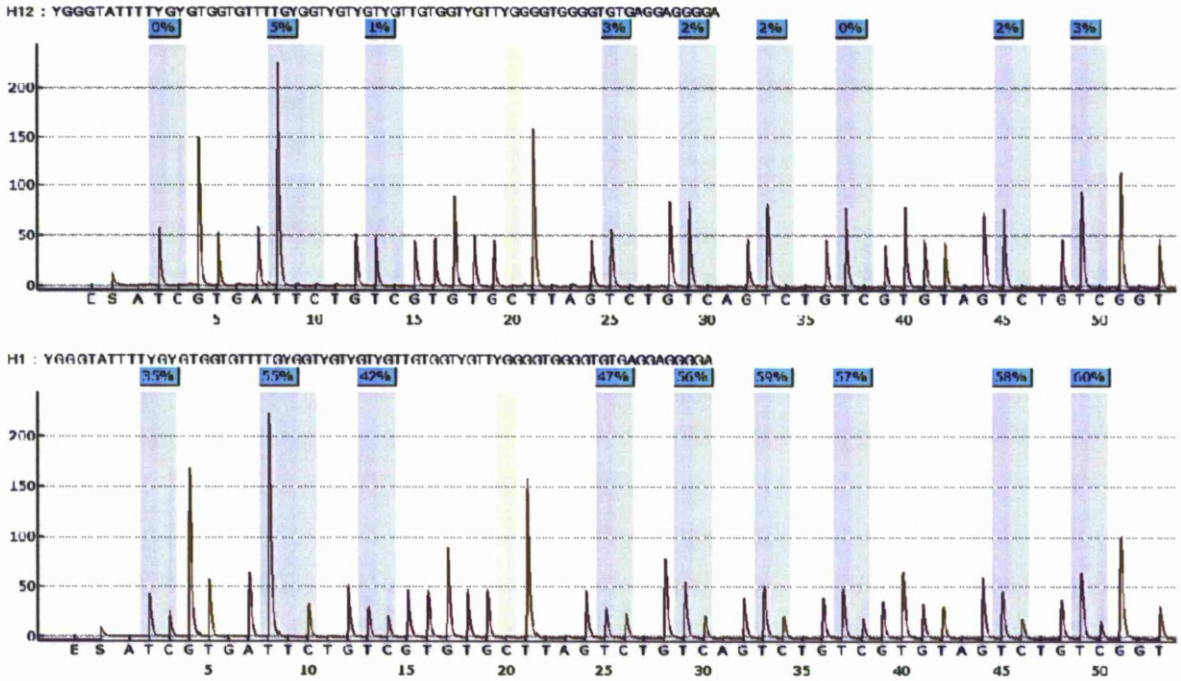

Figure 30 Representative pyrograms of the RASSF1 promoter sequence examined in this study. Upper: RASSF1 adjacent normal, MtI 2%. Lower: RASSF1 lung tumour, MtI 52%. The percentages in boxes represent the individual CpG methylation values. The methylation index (MtI) is calculated as the average values of the examined CpGs.

The methylation status of CDKN2A and RASSF1 promoter was analysed in comparison to clinicopathological data (age, gender, histological type, pTNM, differentiation). There was no significant association between the methylation status of either CDKN2A or RASSF1 promoters and clinicopathological data.

6.4 Relationships between UHRF1 and DNMTs expression with hypermethylation

The expression of the UHRF1 and DNMTs genes was analyzed in relation to the hypermethylation status of the TSGs (Appendix). Tumours with a hypermethylated CDKN2A promoter demonstrated higher levels of the DNMT1 (Mann-Whitney, p=0.018) and UHRF1 (p=0.005) expression compared to the CDKN2A-unmethylated tumours. In addition, tumours with hypermethylated RASSF1 promoter demonstrated higher levels of DNMT3B (Mann-

Whitney, p=0.043) and UHRF1 (p=0.034) expression. DNMT3A expression did not demonstrate a correlation with any of the two examined promoters. Interestingly, when combining the methylation status of both CDKN2A and RASSF1 (positive = at least one methylated) the correlation between UHRF1 expression and hypermethylation becomes more significant ($p=2.3\times10^{-4}$, Table 18). The same stands for DNMT3B (p=0.037) while DNMT1 expression shows no significant difference between the combined group and unmethylated samples (Table 18).

Table 18 mRNA expression levels of UHRF1, DNMT1, DNMT3A and DNMT3B in groups of NSCLCs with different methylation status of CDKN2A and RASSF1

	CDKN2A methylation			RASSF1 methylation			CDKN2A and/or RASSF1		
	0	1	p-value	0	1	p-value	0	1	p-value
UHRF1	2.9±0.4	3.9±0.4	**0.005**	2.8±0.3	4.1±0.7	**0.034**	2.4±0.3	4.1±0.5	**2.3×10^{-4}**
DNMT1	6.5±0.8	8.8±1.2	**0.018**	6.8±0.7	8.1±1.3	0.301	6.0±0.7	8.2±1.0	0.058
DNMT3A	26.4±3.2	35.3±9.6	0.604	31.7±5.3	31.4±4.9	0.314	23.7±3.6	33.3±5.9	0.151
DNMT3B	59.5±10.0	73.1±20.0	0.200	54.8±9.7	90.8±19.8	**0.043**	41.9±6.1	84.6±16.8	**0.037**

Values are presented as mean relative quantification (RQ) ± standard error. P values originate from Mann-Whitney tests.

6.5 Relationships between UHRF1, DNMTs expression and global hypomethylation

The LINE-1.2 methylation assay was utilised as a measure of global hypomethylation [Weisenberger, 2005] in the tumour samples of this NSCLCs set. Tumour samples of this set demonstrated a variable degree of hypomethylation in agreement to the findings of the second set (chapter 7) with a mean LINE-1.2 methylation index of 58.8% ± 0.9%. LINE-1.2 hypomethylation was more apparent in squamous carcinomas (mean Mtl: 55.9± 1.4) compared to adenocarcinomas (mean Mtl: 61.3± 1.1, Mann-Whitney test p= 0.002) (Figure

31). No other association was observed between the methylation status of LINE-1.2 promoter and clinicopathological data in this set.

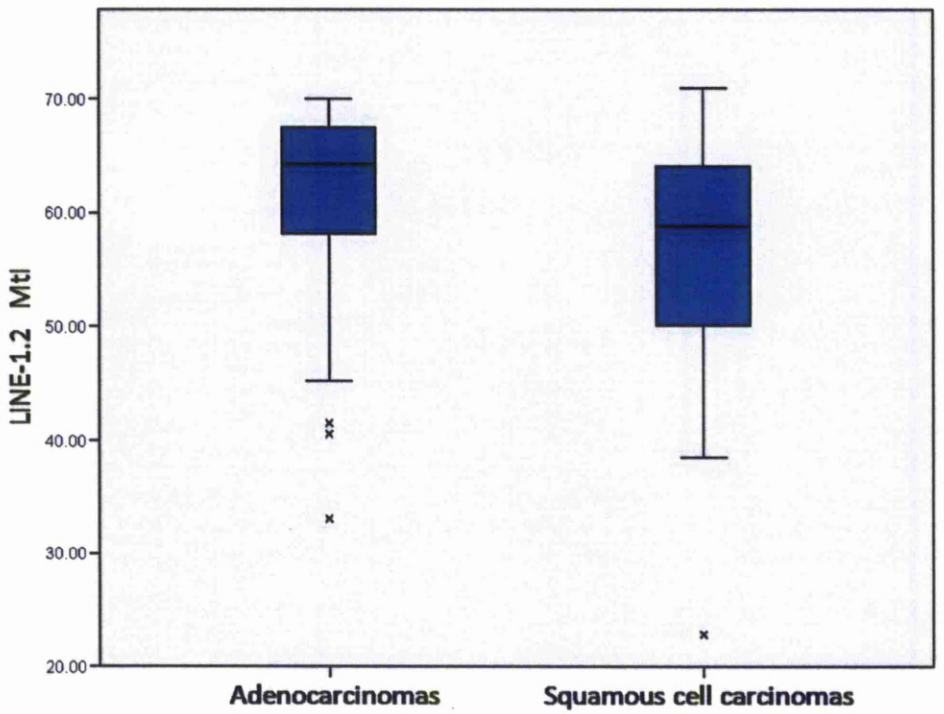

Figure 31 Box plot representation of LINE-1.2 methylation values in adenocarcinomas versus squamous cell carcinomas. LINE-1.2 element demonstrates greater hypomethylation in squamous cell carcinomas.

The expression of the UHRF1 and DNMTs genes and regional hypermethylation of CDKN2A and RASSF1 was subsequently analyzed in relation to the global methylation as measured by LINE-1 assay. Firstly, we compared the continuous values performing Spearman's correlation test for non-parametric values. An inverse correlation was observed between global methylation and the methylation status of RASSF1 while there was no correlation with the methylation status of CDKN2A promoter. An inverse correlation was also observed between LINE-1.2 methylation and E2F1, UHRF1 and DNMT1 expression. There was also an inverse correlation between LINE-1.2 methylation and DNMT3A or DNMT3B expression, however, with really low correlation coefficient. The results are summarized in Table 19.

Table 19 Correlation between LINE-1, CDKN2A, RASSF1 methylation and DNMTs, UHRF1, E2F1.

		expression levels (RQ values)					methylation status (Mtl)	
		DNMT1	DNMT3A	DNMT3B	UHRF1	E2F1	CDKN2A	RASSF1
LINE-1 (Mtl)	Correlation Coefficient	**-0.339**	**-0.198**	**-0.282**	**-0.491**	**-0.443**	-0.126	**-0.333**
	Sig. (2-tailed)	**$4x10^{-4}$**	**0.044**	**0.004**	**$1x10^{-6}$**	**$2.5x10^{-6}$**	0.215	**$5x10^{-4}$**
	N	104	104	103	104	104	99	104

In order to gain a wider view on the observed correlation of hypomethylation with hypermethylation and higher expression of the studied genes we have dichotomized our samples into two distinct groups according to their LINE-1 methylation status. The expression status of DNMTs, UHRF1 and E2F1 was compared in these two group using Mann-Whitney test for non-parametric samples. The expression levels of DNMT1, DNMT3B, UHRF1 and E2F1 were significantly higher in the group with lower LINE-1.2 methylation compared to that with higher LINE-1.2 methylation. The significance was higher for UHRF1 and E2F1 in accordance to the correlation results. The results are summarized in Table 20 and the differences in the mean expression values between the two groups can be seen in Figure 32.

Table 20 Expression of DNMTs, UHRF1 and E2F1 in high and low LINE-1 methylation groups

Examined Genes	LINE-1 methylation	N	Mean RQ value	Std. Error	Asymp. Sig. (2-tailed)
DNMT1	high	52	5.16	0.52	**0.003**
	low	52	9.05	1.05	
DNMT3A	high	52	22.18	2.42	0.174
	low	52	40.08	7.19	
DNMT3B	high	51	39.26	5.83	**0.004**
	low	52	90.16	16.54	
UHRF1	high	52	2.17	0.25	**$7x10^{-5}$**
	low	52	4.27	0.50	
E2F1	high	52	11.49	1.27	**$9x10^{-5}$**
	low	52	26.11	3.68	

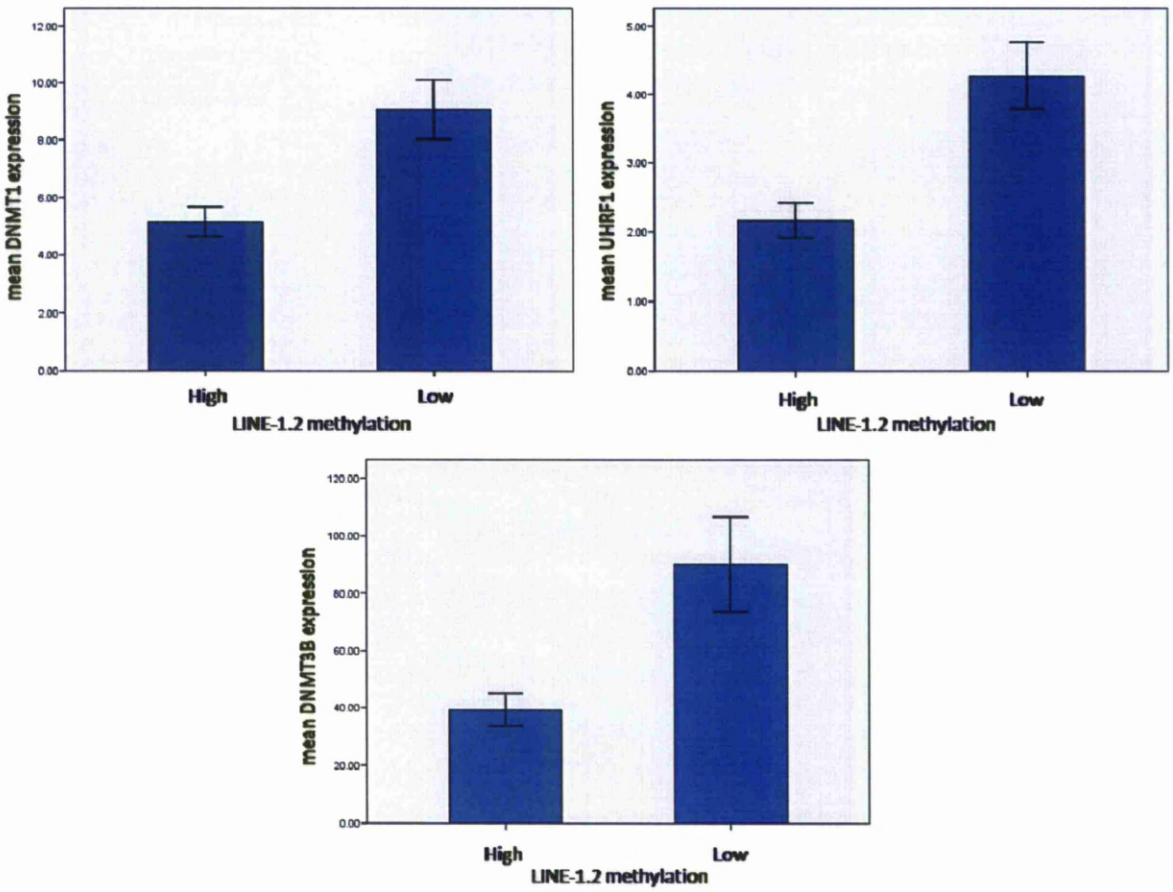

Figure 32 Bar representation of DNMT1, UHRF1 and DNMT3B mean expression between the lower and higher LINE-1.2 methylation groups. The Y-axis represents the mean expression in RQ values. Error bars represent standard error of the mean. The mean expression of DNMT1, DNMT3B and UHRF1 is higher in the group of patients with higher LINE-1 methylation

We have also examined the scored hypermethylated and unmethylated RASSF1 and CDKN2A samples with the two distinct groups of LINE-1.2 methylation. Since we wanted to compare ordinal values we performed chi square test. CDKN2A methylation status showed no difference between the two groups (Pearson chi-square p=0.78) while RASSF1 methylated samples were significantly more in the group with lower LINE-1.2 methylation (Pearson chi-square p=0.037)(Table 21). Furthermore, by using the assigned hypermethylated status, values were compared to the combined for both CDKN2A and RASSF1 phenotype with LINE-1.2 methylation status. Samples with CDKN2A and/or RASSF1 hypermethylated promoter

were significantly more frequent in the group with lower LINE-1.2 methylation (Pearson chi-square p=0.011) (Table 22).

Table 21 Tumour samples grouped according to the methylation status of LINE-1.2 and RASSF1.

		LINE-1.2 methylation		Total
		0	1	
RASSF1	0	40	30	70
methylation	1	12	22	34
Total		52	52	104

Table 22 Tumour samples grouped according to the methylation status of LINE-1.2 and a combined hypermethylation status of CDKN2A/RASSF1.

		LINE1.2 methylation		Total
		0	1	
CDKN2A/RASSF1	0	34	21	55
methylation	1	18	31	49
Total		52	52	104

6.6 UHRF1 downregulation leads to hypomethylation of TSGs in A549 cells

Following the observations regarding the relationship between UHRF1 expression, TSG hypermethylation and global hypomethylation in primary NSCLCs, we further investigated the role of the UHRF1 in a cell line model by knocking down UHRF1 in the A549 lung adenocarcinoma cell line and acquiring stable cell transfectants.

We have inserted an shRNA oligo that specifically knockdowns UHRF1 expression in a shRNA inducible vector. The inserted sequence was verified by sequencing of the construct. The various clones were examined for their UHRF1 knockdown efficiency under doxycycline

induction. Clones demonstrating inducible knockdown of UHRF1 did not succeed more than 45% reduction of the UHRF1 mRNA (Table 23).

Table 23 Expression of UHRF1 in A549 PAUHRF1 clones after induction with doxycyclin.

	UHRF1 expression (RQ)				
A549 PAUHRF1	Untreated	supplemented with doxycyclin			
		24 hrs	48 hrs	72 hrs	96 hrs
clone 1	1	0.64	0.60	0.54	0.65
clone 2	1	1.20	1.12	1.25	1.21
clone 3	1	0.62	0.65	0.60	0.58
clone 4	1	0.85	0.87	0.84	0.80
clone 5	1	1.22	1.15	1.18	1.14
clone 6	1	1.30	1.18	1.20	1.22
clone 7	1	1.10	1.05	1.04	1.03
clone 8	1	1.09	1.08	1.03	1.10
clone 9	1	1.07	1.09	1.11	1.12
clone10	1	0.97	0.95	0.90	0.92
clone 11	1	1.08	1.03	1.02	1.01
clone 12	1	1.30	1.23	1.21	1.32
clone 13	1	1.10	1.12	1.13	1.00
clone 14	1	0.55	0.60	0.55	0.57
clone 15	1	0.57	0.56	0.62	0.57

RQ=Relative quantification value= 2^{-ddCt}. The expression of the untreated corresponding clone has been used as calibrator. The mean value was deduced by triplicate experiments.

In contrast, two clones (named clone 1 and 2 thereafter) demonstrated constitutive, non-inducible >80% knockdown of UHRF1 mRNA compared to the parental and mock transfected A549 cells. Thus it was decided to proceed to the subsequent experiments with these two clones. Both derived clones demonstrated 80% knockdown at the RNA level (Figure 33A) while the protein was almost undetectable in western blotting (Figure 33B).

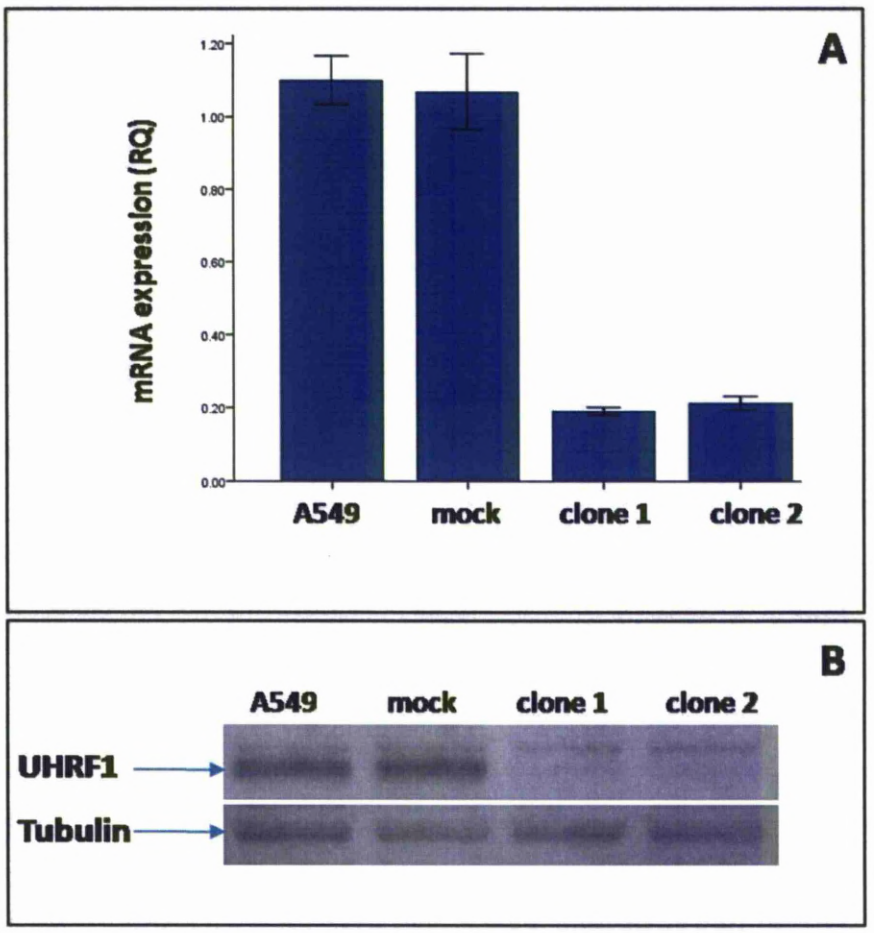

Figure 33 qPCR (A) and western blotting (B) demonstrating UHRF1 mRNA and protein expression respectively of the A549-derived UHRF1 knockdown clones. A >80% reduction of mRNA levels is observed in both clones while UHRF1 protein is hardly detectable in the western blot in comparison to the strong UHRF1 expression in A549 and mock cells.

In order to investigate the UHRF1 knockdown effect on regional hypermethylation, we screened, using previously designed pyrosequencing assays, a number of frequently hypermethylated TSGs promoters in lung cancer including the promoters of CDKN2A, RASSF1, CYGB, and CDH13. CDKN2A was completely unmethylated in A549 parental, mock cells and UHRF1 knockdown derived clones. Representative pyrograms from CYGB and CDH13 are shown in Figure 34.

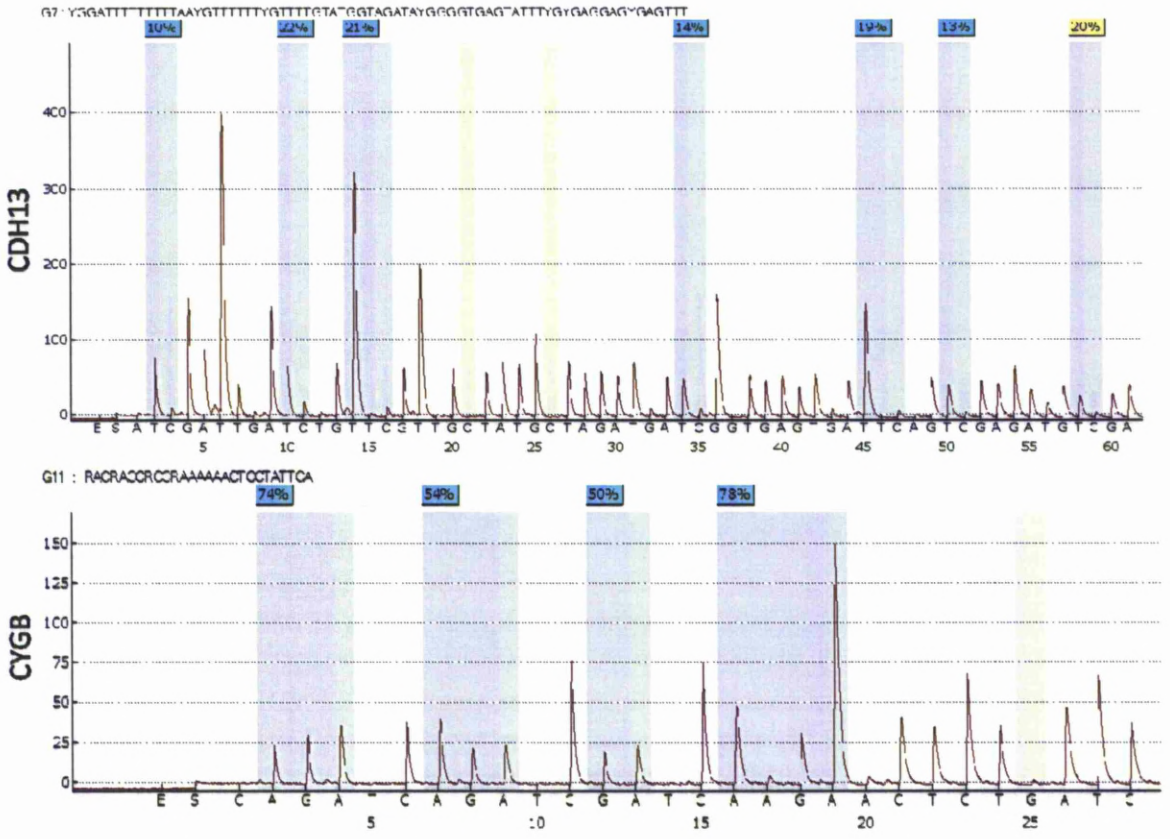

Figure 34 Representative pyrograms of the CDH13 and CYGB promoter sequences examined in this study. The percentages in boxes represent the individual CpG methylation values. The methylation index (MtI) is calculated as the average values of the examined CpGs. The bisulphite control dispensed nucleotides are shown in the yellow column.

While no difference was observed in the mock cell line, the methylation status of RASSF1, CYGB, and CDH13 promoters was consistently, although variably, reduced in both UHRF1 knock down clones (Figure 35).

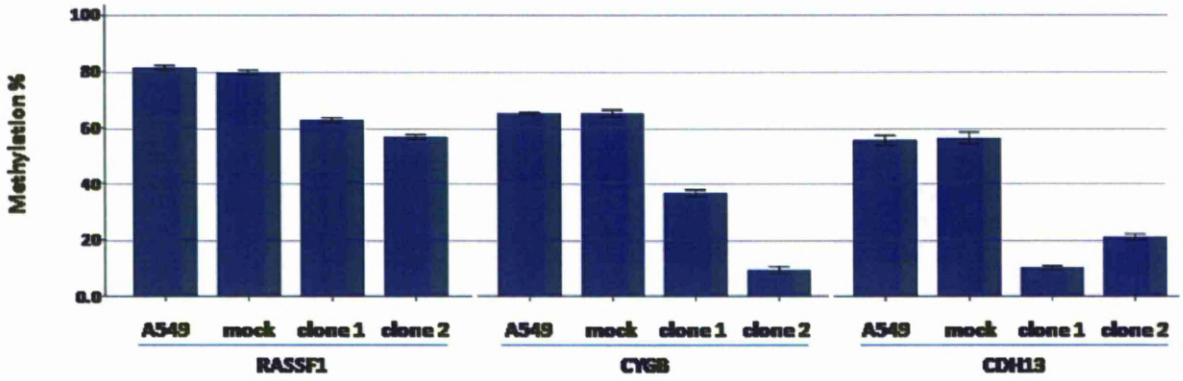

Figure 35 Effect of UHRF1 expression knockdown on the DNA methylation levels of RASSF1, CYGB and CHD13. A consistent reduction of the DNA methylation of all three promoters is observed across biological replicates in both UHRF1 knockdown clones. The Y-axis represents the mean methylation index detected by triplicate pyrosequencing experiments. Error bars represent standard error of the mean.

Furthermore, we used the LINE-1.2 assay in order to detect any changes in global hypomethylation caused by UHRF1 downregulation. Indeed, UHRF1 knockdown clones demonstrated decreased mean methylation compared to parental and mock cells (Figure 36).

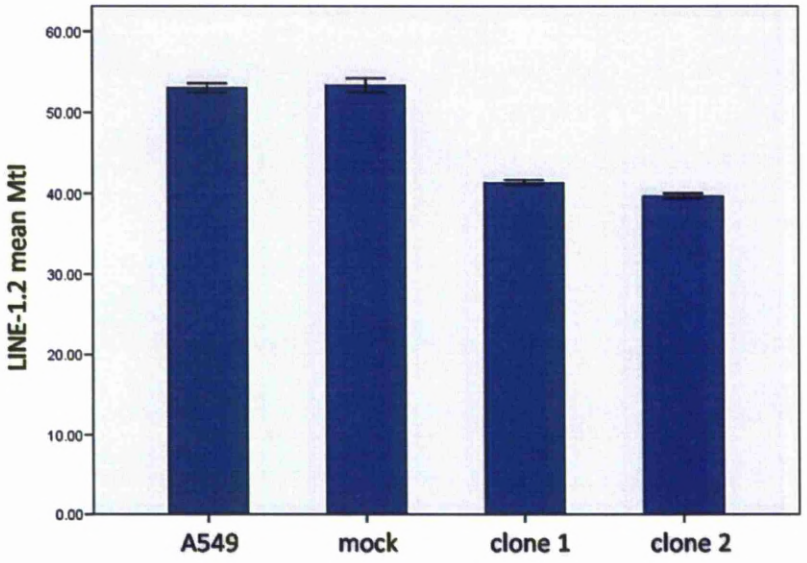

Figure 36 Bar representation of LINE-1.2 methylation (global methylation) in A549, mock and UHRF1 knockdown clones 1 and 2. The Y-axis represents the mean methylation index (MtI) detected by triplicate pyrosequencing experiments. Error bars represent standard error of the mean. UHRF1 knockdown clones demonstrate a significant decrease in their LINE-1.2 methylation levels.

In order to detect any changes in the expression levels of DNMTs in the derived clones we have examined by qPCR the mRNA levels of al DNMTs in the control, mock and derived clones. The mRNA expression levels of DNMT1, and DNMT3A demonstrated no significant changes between A459, the mock and the UHRF1 knockdown clones. In contrast, DNMT3B was up-regulated in both UHRF1 knockdown clones (Table 24). UHRF1 and DNMT promoters were unmethylated in the A549 cells and no change was observed in the UHRF1 knockdown clones (Table 24).

Table 24 mRNA expression and DNA methylation status of DNMTs in UHRF1 knock-down clones.

	mRNA expression (mean RQ ±SE)			Promoter Methylation Index			
	DNMT1	DNMT3A	DNMT3B	UHRF1	DNMT1	DNMT3A	DNMT3B
A549	1.00 ± 0.21	1.02 ± 0.08	1.02 ± 0.08	2%	1%	0%	1%
mock	1.07±0.19	0.96±0.04	1.2±0.13	3%	2%	1%	0%
Clone 1	0.78 ± 0.15	1.16 ± 0.06	**6.03 ± 0.39**	2%	0%	2%	1%
Clone 2	0.94 ± 0.18	1.27 ± 0.06	**4.15 ± 0.19**	2%	1%	1%	1%

RQ= relative quantification. Means and standard error (SE) have been calculated from 6 replicates (2 biological × 3 technical). The average value of the A549 cells was used as calibrator for calculating RQ.

6.7 Phenotypic effects of UHRF1 downregulation

The phenotypic characteristics of the UHRF1 knockdown clones were significantly different to those of A549 and mock cell lines. Proliferation of cells was measured using MTT assay for 5 subsequent days. Both UHRF1 knock down clones demonstrated reduced proliferation rates compared to the parental and mock cells (Figure 37).

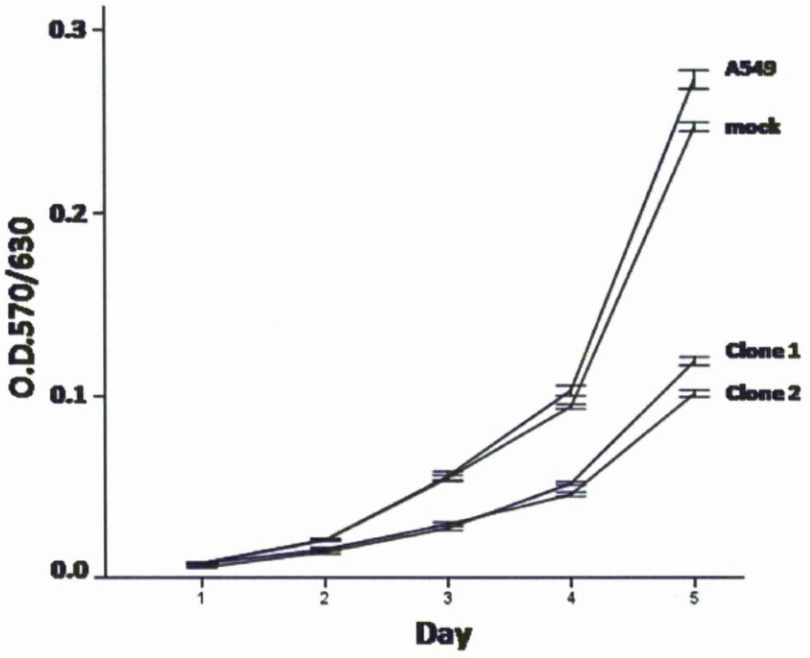

Figure 37 Proliferation rates over 5 days, measured by MTT experiments. Proliferation is significantly reduced in both UHRF1 knock down clones in comparison to A549 cells and mock (scrambled shRNA) cell lines.

In addition, scratch assays demonstrated lower migration efficiency of the UHRF1 knockdown clones (Figure 38). In particular, TScratch software analysis demonstrated that after 24 hours, the open wound area was 10.5% ± 1.3% in the parental A549, 14.1% ± 1.1% in mock cells, 71.9% ± 1.8% in UHRF1 clone 1 and 56.1% ± 1.8% in clone 2 (Figure 39).

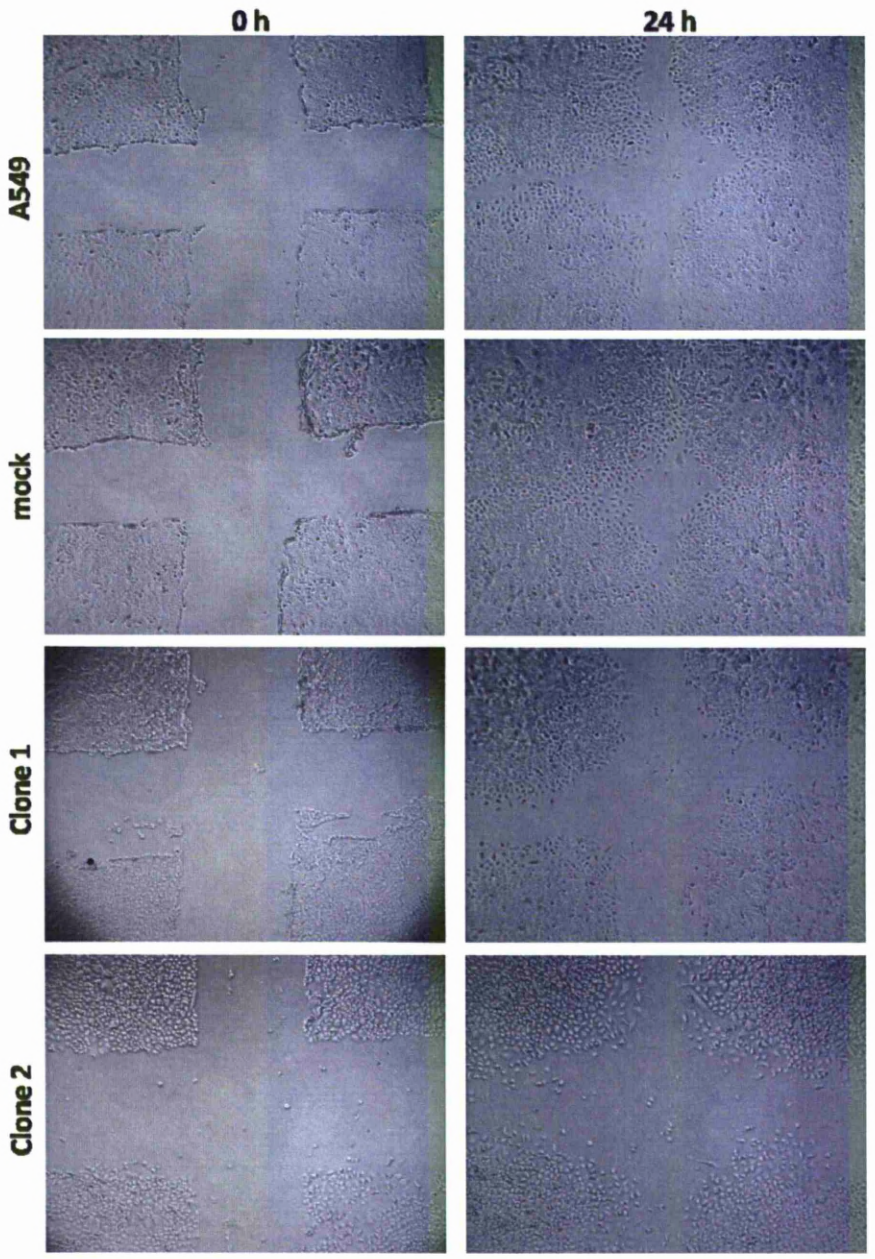

Figure 38 Scratch assays demonstrating the reduced migration efficiency of UHRF1 knock down clones in comparison to A549 cells and mock (scrambled shRNA) cell lines. Photographs of t=0 and t=24 hours are presented. The open wound area was quantified using TScratch software.

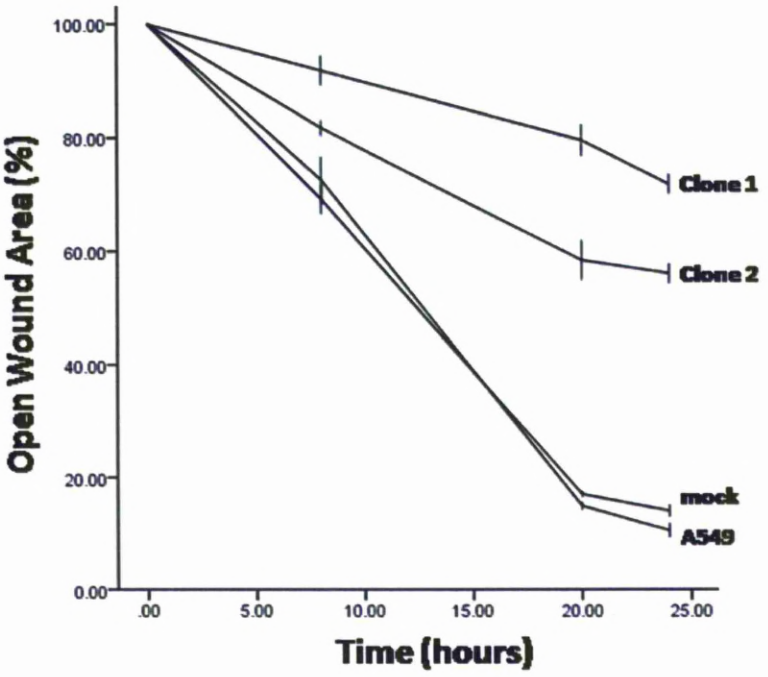

Figure 39 Diagrammatic representation of the migration rates of parental, mock and UHRF1 knock down clones in scratch assays. The open wound area (OWA) was quantified using TScratch software. The increased OWA of the UHRF1 clones indicate their reduced migration capability.

Chapter 7. Retrotransposons, DNA methylation and genomic instability

The second aim of this study was to measure the extent of global DNA hypomethylation in NSCLC and investigate its links with genomic instability and reactivation of retrotransposition We evaluated global DNA methylation by pyrosequencing, measuring the DNA methylation levels of LINE-1 and Alu transposable elements in primary non-small cell carcinomas and their paired adjacent tissues. We demonstrated a significant reduction of the methylation levels of both elements in a coordinated manner suggesting a possible common mechanism for their methylation maintenance. Moreover we assessed genomic instability of this lung tumour set and demonstrated that hypomethylation of both transposable elements was associated with increased genomic instability. The reduction of the methylation index of LINE-1 and Alu following treatment of three lung cell lines with a demethylating agent, consistently resulted in increased expression of both elements. We have also demonstrated, utilising a construct which carries a full LINE-1 element tagged with a reporter cassette, that unmethylated LINE-1 can retrotranspose successfully in a lung cancer cell line.

7.1 Methylation status of LINE-1 and Alu-PV in primary NSCLC tumours

Pyrosequencing assays were designed In order to examine the methylation status of LINE-1.2 and Alu-PV elements in lung primary tissues. Both assays were used to identify the methylation status of these elements in the set of 48 paired tumour and adjacent normal NSCLC primary tissues. Representative pyrograms of the pyrosequencing runs are given in Figure 40 and 41 respectively. Detailed results are given in Table 25.

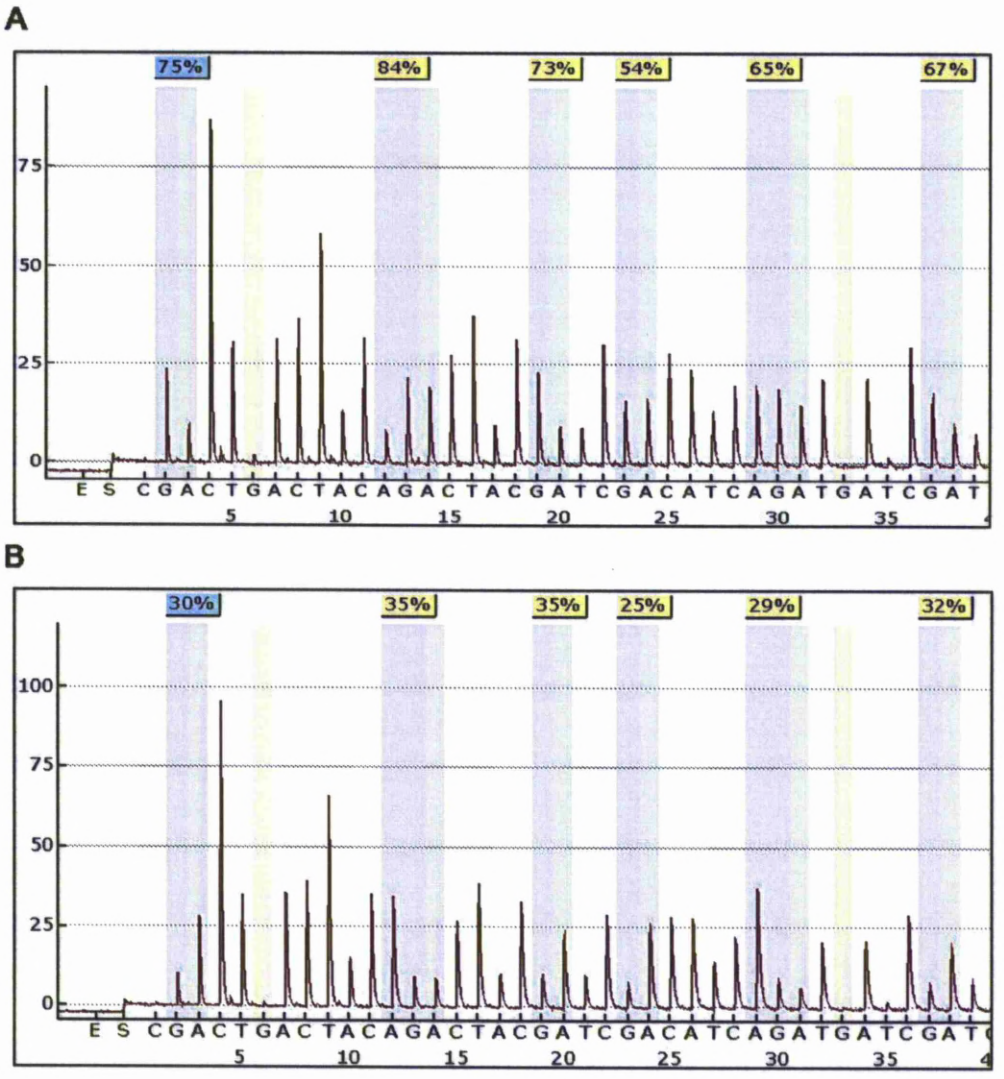

Figure 40 Representative pyrograms of the LINE-1.2 promoter sequence examined in this study. A: LINE-1.2, adjacent normal, MtI 69%. B: LINE-1.2, lung tumour, MtI 31%. The percentages in boxes represent the individual CpG methylation values. The methylation index (MtI) is calculated as the average values of the examined CpGs.

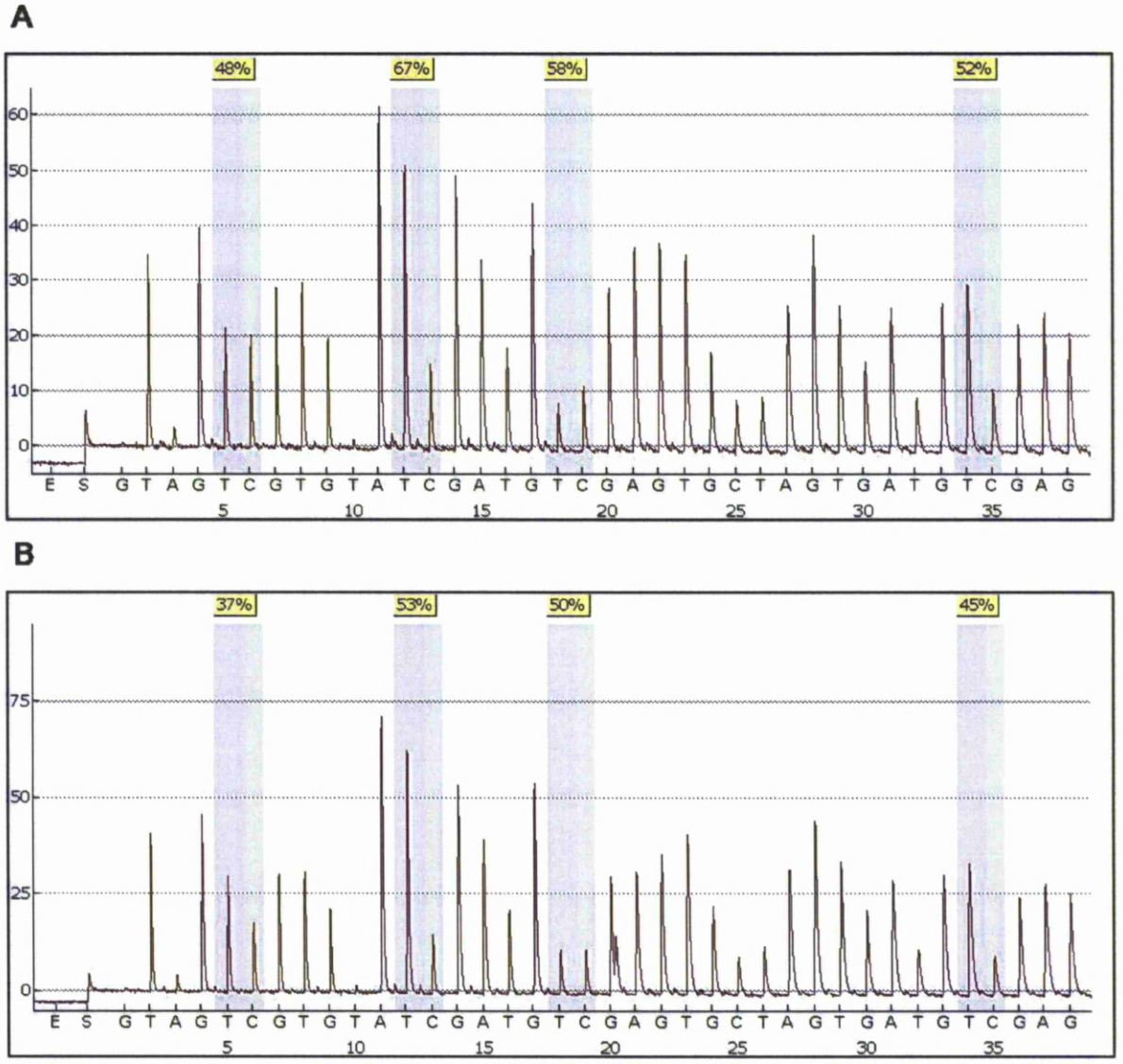

Figure 41 Representative pyrograms of the Alu-PV promoter sequence examined in this study. A: Alu-PV adjacent normal, MtI 56%. B: Alu-PV, lung tumour, MtI 46%. The percentages in boxes represent the individual CpG methylation values. The methylation index (MtI) is calculated as the average values of the examined CpGs.

Table 25 Clinical samples of the utilized cohort and results for LINE-1 and Alu methylation and genomic instability (FAL).

				Methylation Index (%)				
Sample	Gender	Age	Diagnosis	LINE-1 Normal	LINE-1 Tumour	Alu Normal	Alu Tumour	FAL
1	F	74	AdenoCa	70.3	61.3	53.3	52.7	0.455
2	M	68	AdenoCa	69.7	58.0	55.0	53.2	0.857
3	F	50	AdenoCa	69.1	56.3	50.6	53.9	0.857
4	M	52	AdenoCa	69.6	65.6	57.4	54.1	0.375
5	F	68	AdenoCa	69.7	64.7	56.6	60.0	0.400
6	F	74	AdenoCa	69.4	47.0	56.6	55.0	0.625
7	F	67	AdenoCa	69.3	67.8	53.5	54.0	0.500
8	F	53	AdenoCa	70.0	60.8	58.2	52.8	0.778
9	F	73	AdenoCa	70.6	67.6	56.7	55.7	0.000
10	F	58	AdenoCa	70.2	54.0	58.4	55.2	1.000
11	M	74	AdenoCa	69.8	48.4	60.3	51.8	0.909
12	F	69	AdenoCa	69.6	34.8	59.0	56.5	1.000
13	M	63	AdenoCa	69.3	47.2	56.7	51.6	0.900
14	F	64	AdenoCa	69.8	51.3	56.2	50.7	0.889
15	F	66	AdenoCa	70.0	68.8	56.6	56.6	0.000
16	F	61	AdenoCa	68.3	57.4	58.8	55.7	0.600
17	M	67	AdenoCa	70.2	69.4	55.9	60.5	0.143
18	M	65	AdenoCa	69.3	62.4	58.8	52.2	1.000
19	F	68	AdenoCa	68.4	59.2	56.0	52.8	0.889
20	F	69	AdenoCa	69.5	52.2	ND	ND	0.818
21	F	77	AdenoCa	69.7	54.5	55.7	54.3	1.000
22	F	53	AdenoCa	69.1	59.3	54.8	53.1	0.556
23	F	67	AdenoCa	68.1	52.1	56.9	48.6	0.500
24	F	45	SqCCL	69.4	66.8	55.3	53.4	0.250
25	M	62	SqCCL	69.7	30.9	56.4	46.3	0.833
26	M	68	SqCCL	69.9	70.3	58.7	54.5	0.000
27	M	78	SqCCL	67.1	48.2	58.7	59.9	0.556
28	M	68	SqCCL	70.8	41.5	58.8	54.1	0.375
29	M	60	SqCCL	70.2	62.7	53.4	52.4	0.333
30	M	62	SqCCL	69.5	40.8	59.9	51.7	0.556
31	M	60	SqCCL	70.3	43.9	58.2	52.2	0.636
32	M	70	SqCCL	69.6	63.1	56.5	54.4	1.000
33	F	70	SqCCL	69.6	40.0	55.4	51.2	0.900
34	M	83	SqCCL	69.6	49.8	56.4	53.8	0.900
35	M	83	SqCCL	70.5	56.8	56.5	48.8	1.000
36	M	66	SqCCL	68.3	41.0	60.6	47.6	1.000
37	M	65	SqCCL	70.4	50.5	53.0	55.9	1.000
38	M	58	SqCCL	69.0	48.2	55.6	51.8	0.714
39	M	66	SqCCL	70.1	60.3	57.2	53.4	0.182
40	M	72	SqCCL	69.8	61.9	62.5	54.9	0.300
41	F	66	SqCCL	68.8	57.1	53.9	50.9	0.667
42	M	47	SqCCL	69.4	38.6	55.7	53.4	0.700
43	M	69	SqCCL	70.3	66.4	57.2	54.1	0.636
44	M	68	SqCCL	73.5	67.7	55.2	55.1	0.100
45	F	48	SqCCL	ND	ND	56.6	57.5	0.182
46	M	63	SqCCL	65.4	34.6	55.6	52.6	0.714
47	F	71	SqCCL	69.1	41.6	54.4	53.7	0.778
48	F	69	SqCCL	70.1	52.1	ND	ND	0.667

LINE-1.2 promoter was highly methylated with minimal variability in normal lung tissues (mean MtI: 69.8%±0.14%). The corresponding tumour samples demonstrated a significant drop in the MtI values (mean MtI: 56.4%±1.4%, paired t-test, $p=7.7\times10^{-14}$, Figure 42).

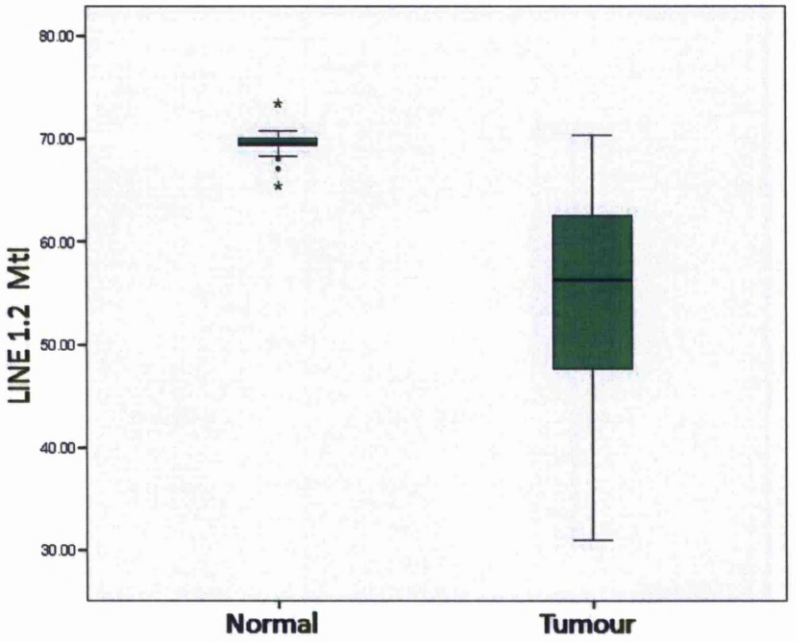

Figure 42 Box plot representation of LINE-1.2 methylation values observed in the first studied cohort. There is a profound hypomethylation of LINE-1.2 element in the lung cancer tissue compared to adjacent normal.

A highly significant difference between normal (mean MtI:56.6%±0.3%) and tumour (mean MtI: 53.5%±0.4%) tissue MtIs was found for Alu-PV promoter (paired t-test, $p=9.6\times10^{-7}$, Figure 43). Notably, LINE-1.2 and Alu-PV methylation indices in primary tumours correlated to each other (Pearson's correlation=0.401, p=0.006). The methylation status of the two promoters was analysed in comparison to clinicopathological features such as histology, age, gender, T status, differentiation and nodal metastasis. Clinicopathological parameters such as age, gender, T status, differentiation and nodal metastasis did not demonstrate any significant association with LINE-1.2 and Alu-PV methylation. LINE-1.2 hypomethylation was more

apparent in squamous carcinomas than adenocarcinomas, however only at borderline significance (p=0.052).

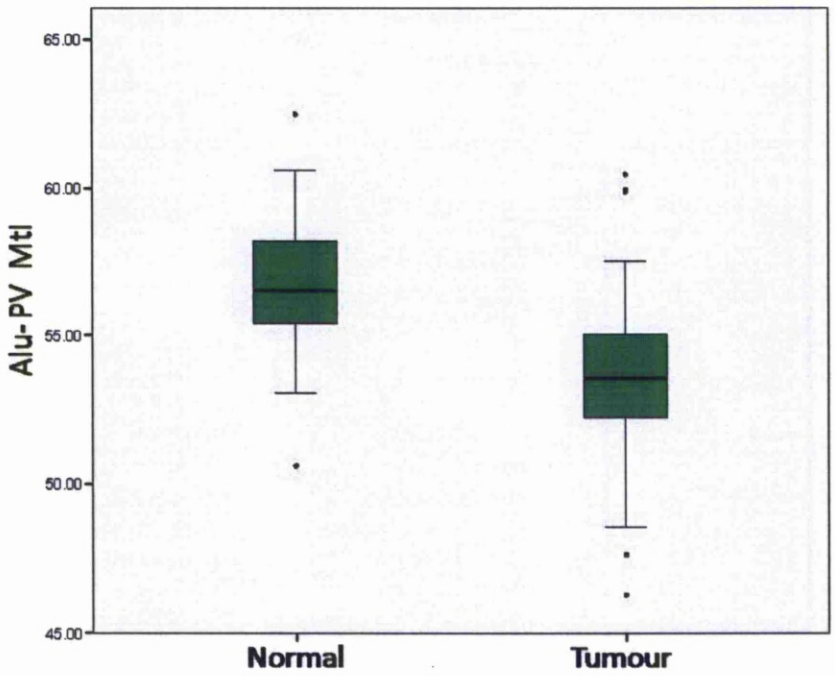

Figure 43 Box plot representation of Alu-PV methylation values observed in the first studied cohort. There is a profound hypomethylation of Alu-PV element in the lung cancer tissue compared to adjacent normal.

7.2 Correlation of LINE-1.2 and Alu-PV hypomethylation with genomic instability

We determined genomic instability in this tumour set utilising 11 microsatellite markers which have been previously shown to be hot spots for loss of heterozygosity (LOH) in lung tumours [Liloglou, 2000], [Liloglou, 2001]. Detailed results from individual microsatellites are given in appendix. Genomic instability for each sample was expressed as the fractional allele loss (FAL) value (Table 25). The fractional allele loss (FAL) value was used as an expression of overall genomic instability in each sample and was calculated as: FAL = [number of loci with loss]/[number of informative loci]. The bivariate correlation analysis between MtI and FAL demonstrated that genomic instability is associated with hypomethylation of LINE-1.2

(Pearson's correlation= -0.547, $p=7.1\times10^{-5}$) and Alu-PV elements (Pearson's correlation= -0.392, p=0.008) (Figure 44).

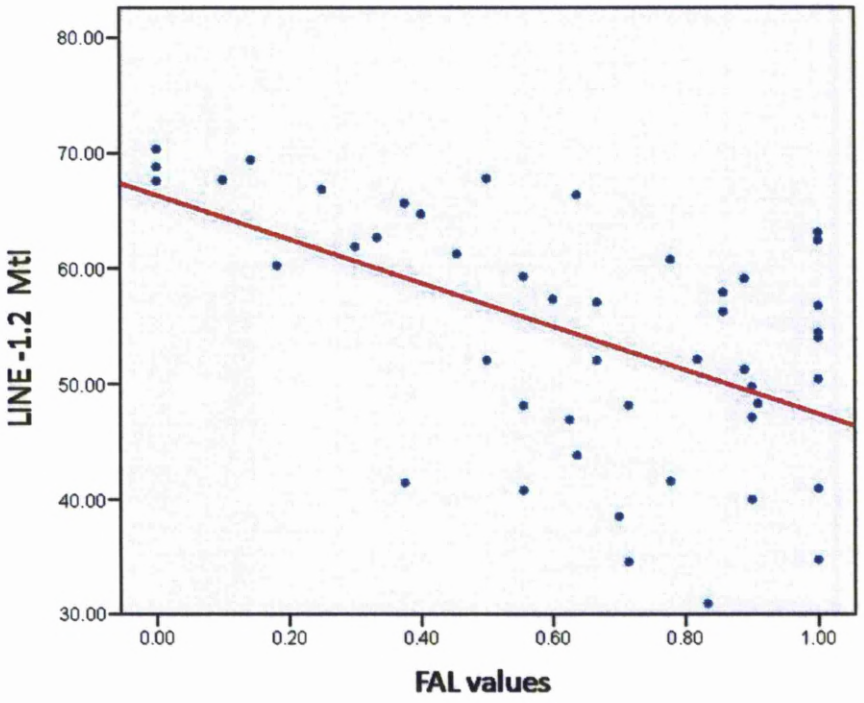

Figure 44 Scatter plot presentation of LINE-1.2 methylation values in comparison to genomic instability as measured by FAL values.

7.3 Effect of demethylating and deacetylating agents on LINE-1 and Alu expression

We examined the methylation levels of the LINE-1.2 and Alu-PV elements in nine lung cancer cell lines and one immortalized non-tumourigenic bronchial epithelial cell line (HBEC3KT). Cancer cell lines demonstrated a variable degree of methylation at these elements, while the immortalised cell line methylation status was somewhat lower of the average index of surgical normal adjacent tissue (Table 26).

Table 26 Methylation status of LINE-1.2 and Alu-PV promoters in different cell lines

Cell line	LINE-1.2 MtI	Alu-PV MtI
SKMES	58.71	45.93
CRL 5802	36.63	37.01
CALU 6	49.52	45.45
A549	58.21	40.58
DMS 53	39.94	42.83
CALU 3	64.18	45.71
CRL 5935	63.8	43.91
CORL 23	63.4	47.68
SKLU-1	61.91	45.62
HBEC 3KT	62.73	44.08

We examined the possible epigenetic control of LINE-1 and Alu expression by using the demethylating agent 5-aza-2-deoxycytidine (decitabine) and a histone deacetylase inhibitor such as trichostatin (TSA). At first we identified the optimal concentration of decitabine to achieve maximum hypomethylation level, undertaking a dose-dependent experiment. The optimal amount of decitabine was found to be 0.1 μM (Figure 45). Our results are in agreement with a dose dependent experiment showing that low concentration of decitabine caused more hypomethylation than high concentrations of the drug [Qin, 2007].

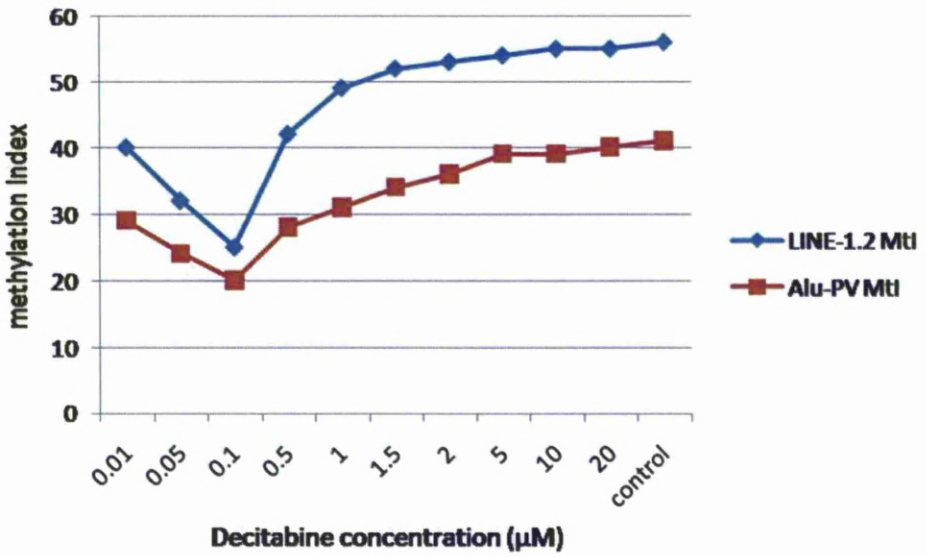

Figure 45 Dose-dependent effect of decitabine on the methylation status of LINE-1.2 and Alu-PV elements. HBEC-3kt cells were treated with decitabine concentration as shown in the figure. The methylation levels measured by pyrosequencing for LINE-1.2 and Alu-PV are shown in the figure. Both elements seem to follow a similar pattern demonstrating higher hypomethylation with lower decitabine concentrations around 0.1 µM.

We applied the optimal dose of decitabine in the A549, CRL5802 and HBEC3KT lines (one adenocarcinoma, one squamous cell carcinoma and one non-tumourigenic respectively). Treatment with decitabine resulted in hypomethylation while addition of TSA did not affect, as expected, the methylation status. Decitabine and TSA increased the expression of both elements, with the exception of LINE-1 expression in HBEC3KT were TSA had no effect. As expected the combined use of both substances resulted in enhanced transcription compared to single substance use (Figure 46).

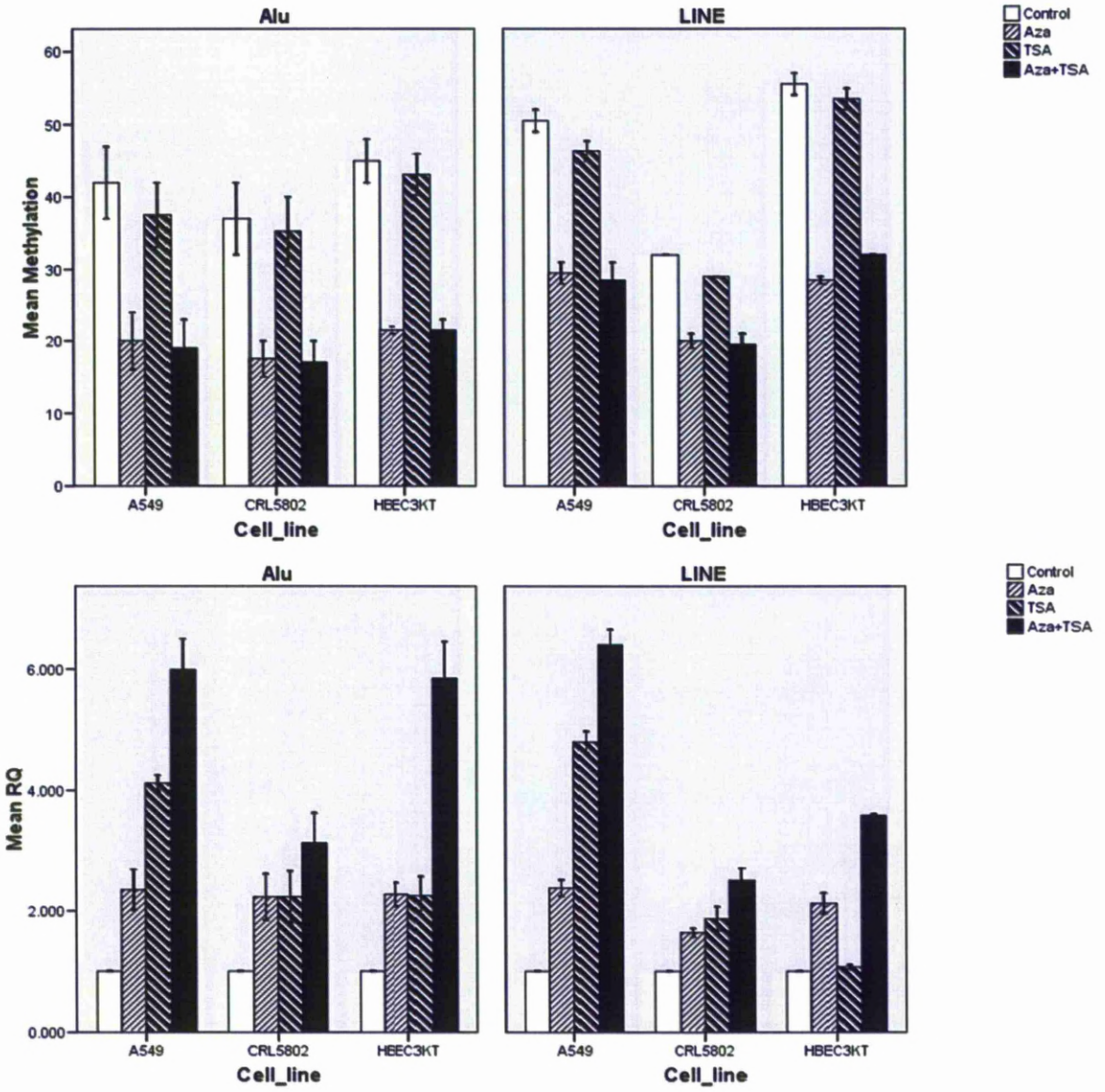

Figure 46 **Bar charts demonstrating the methylation (top panels) and expression (bottom panels) levels of** LINE-1.2 and Alu-PV **transcripts following treatment of lung cell lines with** 5-aza-2'-**deoxycitidine (Aza) and trichostatin (TSA). The addition of azacytidine reduces methylation and increases expression of both** Alu-PV and LINE-1.2 elements**. The addition of TSA does not affect** methylation but has an **effect in expression of both** elements with the exception of LINE-**1.2 in HBEC3KT cells. Simultaneous use of both compounds has a profound synergistic effect in expression of** both elements**. Expression is given in relative quantification** (RQ) values which are calculated as $RQ=2^{(-\Delta\Delta Ct)}$ **value using the untreated control cell population as the calibrator.** Means and standard error (SE) bars **have been calculated from**3 biological replicates.

7.4 LINE-1 activity in lung cell lines.

In order to identify the retrotransposition ability of a full LINE-1 element in a lung cell environment we have utilised the KS-101 vector system (described in materials and methods). IMR-90, A549, CRL5802, CRL5935, CALU-1 and CALU-6 cell lines were transfected with the reporter plasmid KS-101. After selection with G418, formation of colonies was visible only in the CRL5802 cell line (Figure 47) while the rest of the cell lines did not demonstrate any colonies and therefore no retrotransposition events. As expected, transfection with the control retrotransposition-incompetent KS-105 vector did not demonstrate any colonies in any of the above cell lines (Figure 47).

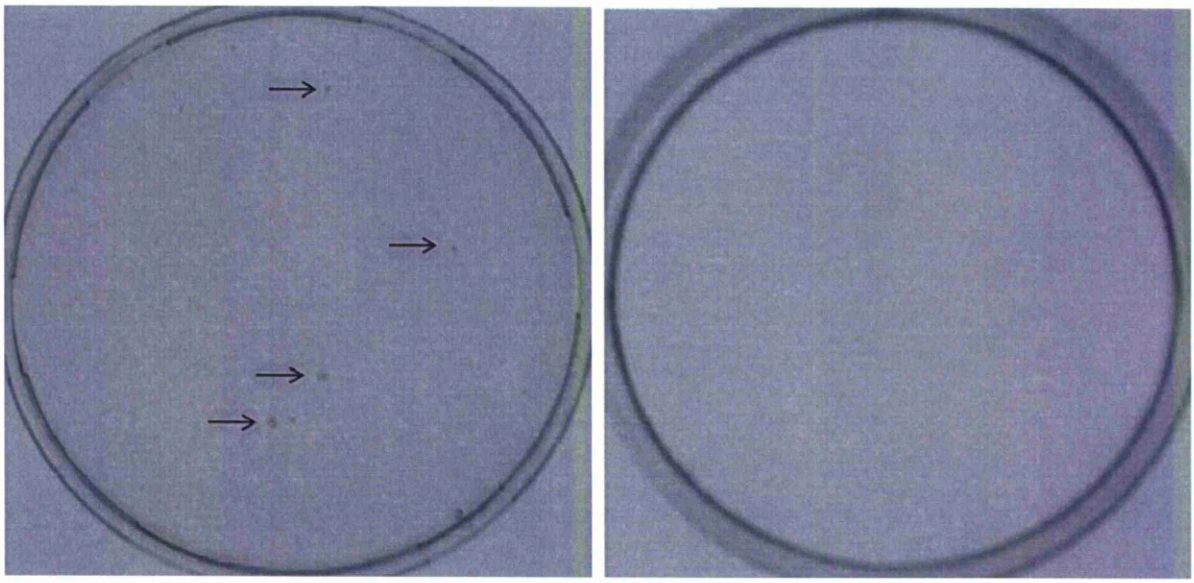

Figure 47 CRL5802 cells transfected with KS-101 (left) and KS-105 (right) after two weeks selection with G418.

Interestingly the CRL5802 cell line which demonstrated LRE3 activity has the lowest LINE-1 methylation levels as measured by pyrosequencing compared to the other cell lines (Table 27).

Table 27 **Cell lines, methylation status of LINE-1.2 element and retrotransposition events of LRE3 element**

Cell line	LINE-1.2 Mtl	LINE-1.3 retrotransposition
IMR-90	60	N
CRL 5802	37	Y
CALU-6	50	N
A549	51	N
CALU-3	64	N
CRL 5935	64	N

In order to identify the role of decitabine-induced global hypomethylation in the retrotransposition ability of the LRE3 element we have treated the above cell lines with decitabine after transfection with the KS-101 plasmid, allowed at least two cell duplications and then selected with G418. Again, only CRL5802 demonstrated the formation of colonies which in the presence of decitabine did not change significantly while at the rest of the cell lines no colonies were observed even after the addition of decitabine (Figure 48).

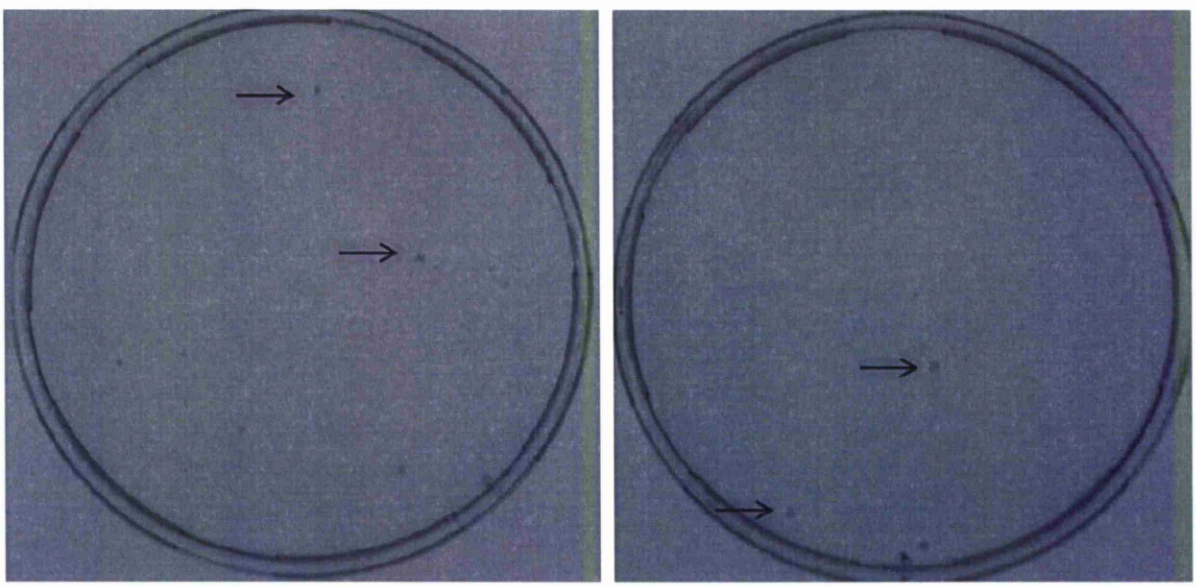

Figure 48 CRL5802 cells transfected with KS-101, untreated (left) and treated with decitabine (right) after two weeks selection with G418.

7.5 LINE-1 activity in cell lines utilising the KS101B and KS105B plasmids

The use of the KS101 plasmid in cell lines in order to identify the activity of LINE-1 element poses a significant limitation. No selection marker is available on the plasmid and therefore the transformation efficiency cannot be estimated. We have seen that LRE3 remains inactive in most cell lines even after decitabine treatment. In addition, it was observed that activity of the LRE3 element did not change significantly after decitabine treatment in the CRL 5802 cell line. Although these data suggest that global hypomethylation induced by decitabine does not affect LINE-1 activity, however we cannot be certain since transformation efficiency is unknown. Furthermore, the methylation status of the LRE3 element of the KS-101 plasmid can only be examined in selected colonies. To overcome these problems we have inserted the blasticidin resistance market in the KS-101 and KS105 plasmids in order to be able to examine the status of the plasmid before selection with G418 and to correct for transfection differences. The colonies with the new KS-101B and KS-105B plasmids carrying the blasticidin resistance gene can be seen in Figure 49.

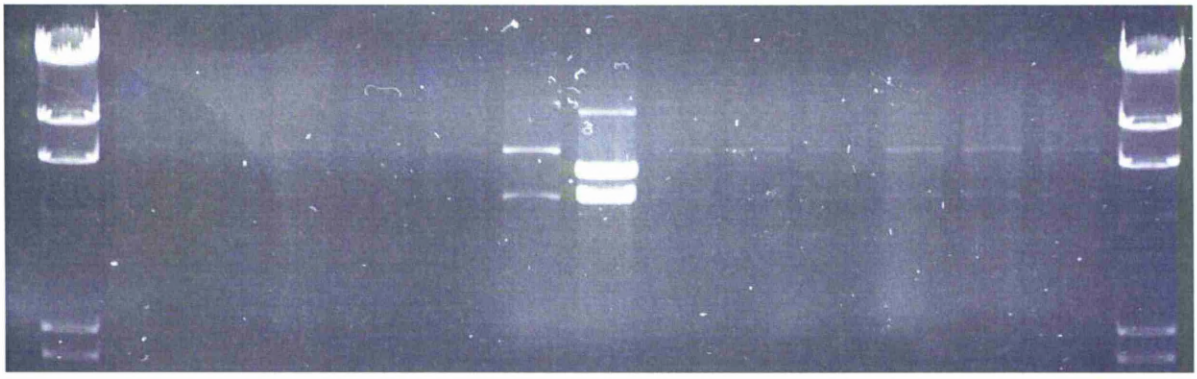

Figure 49 KS-101B (lanes 1-6), and KS-105B (lanes 8-13) plasmids from minipreps digested with Sal I (NEB) and ECOR I run in a 1% agarose gel in TBE together with the λ DNA-HindIII marker (lanes 1, 15) . KS-101 (lane 7) was also digested with the two enzymes to serve as controls. The lower fragment is common in all minipreps and control while the upper fragment which carries the blasticidin fragment runs higher compared with the KS-101 plasmid. All the minipreps carry the blasticidin fragment. Two plasmids were picked and grown further to generate the KS-101B and KS105B plasmids.

The KS-101B and KS105B plasmids were transfected into the CRL5802 cell line and stable colonies were obtained after selection with blasticidin. DNA was extracted from the colonies in order to identify the methylation status of the KS101B plasmids in each colony. Utilising the LRE3 methylation assay we have identified using pyrosequencing the methylation status of the LRE3 promoter in each colony. A representative pyrogram of LRE3 run is shown in Figure 50.

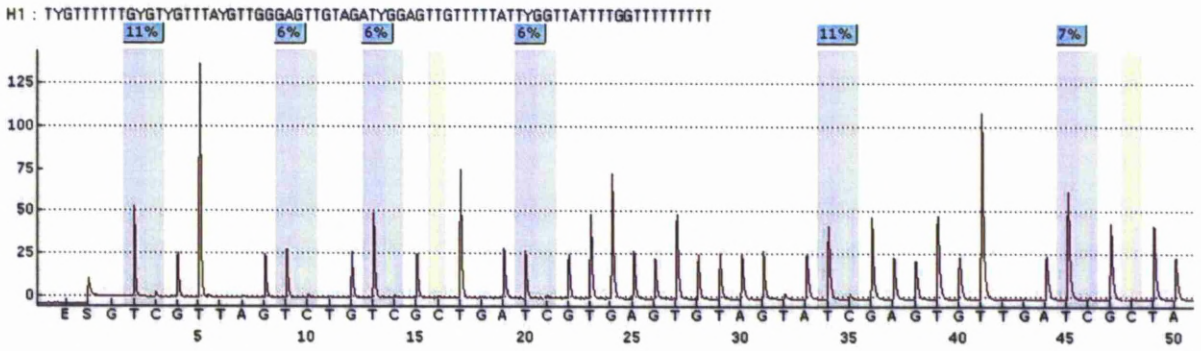

Figure 50 Representative pyrogram of the LRE3 promoter sequence examined in this study. MtI: 8%. The percentages in boxes represent the individual CpG methylation values. The methylation index (MtI) is calculated as the average values of the examined CpGs. Yellow column indicate the bisulphite control sites.

CRL 5802 KS101B colonies demonstrated variable methylation levels of the LRE3 element promoter which remained at low levels less than 10% (Table 28). In order to examine the effect of global hypomethylation on the retrotransposition efficiency of the LRE3 element in the selected CRL5802 clones, we have treated them with decitabine and then selected them using G418 in order to identify the number of retrotransposition events. Since the methylation status of each promoter was low, decitabine treatment would lead to global LINE-1 hypomethylation without affecting directly the methylation status of the LRE3

promoter. As expected no colonies were observed in the CRL 5802 KS105B transfected cells after selection with G418.

Table 28 Four CRL 5802 KS101B colonies and the corresponding methylation status of the LRE3 element.

CRL 5802 KS101B colonies	LRE3 promoter MtI (%)
1	8
2	5
3	10
4	9

Treatment with decitabine did not lead to any significant change in the number of colonies with retrotransposition events of the KS101B plasmid (Figure 51).

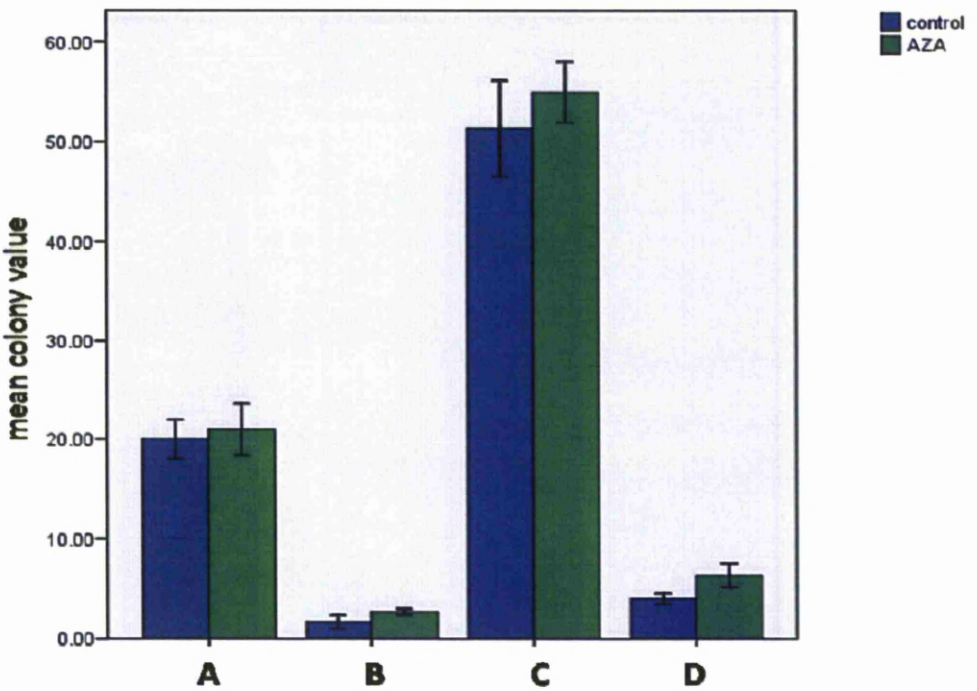

Figure 51 Mean colony values of CRL5802 KS-101B transfected clones (A-B) with (green) and without (blue) decitabine treatment after selection for two weeks with G418. The number of retrotransposition events does not change significantly with decitabine treatment in any of the four clones.

Chapter 8. Discussion

Lung cancer is among the most frequent cancer types and the number one cancer killer in the western countries. There is compelling evidence to demonstrate that epigenetic changes are of key importance in lung carcinogenesis, with DNA methylation taking up the largest part of the existing relevant literature on cancer epigenetics [Esteller, 2007], [Esteller,2008].

Human cancers are characterised by a somewhat paradoxical coincidence of global genome hypomethylation and regional hypermethylation and lung cancer is no exception to this. Global genome hypomethylation affects mainly repeat sequences like LINE-1 and Alu elements while hypermethylation of CpG island-bearing promoters frequent leads to TSGs transcriptional silencing. Our understanding of epigenetic deregulation is continuously advancing as the list of genes and mechanisms mediating the DNA methylation process is growing [Bestor, 2000], [Bird, 1999], [Webster, 2005], [Lopez-Serra, 2008], [Ooi, 2007].

The main objectives of this study was to explore further the molecular mechanisms involved in the observed deregulation of DNA methylation in lung cancer and to investigate the potential epigenetically controlled re-activation of retrotransposable elements and their implication in lung cancer development.

8.1 DNMTs and UHRF1 overexpression in lung cancer

DNMTs are the only enzymes up to date with known methyltransferase activity and are therefore considered as the main players in establishing and maintaining the methylation patterns. However, UHRF1 was also recently shown to exert critical function in DNA methylation maintenance [Bostick, 2007] by assisting the recruitment of DNMT1 on hemimethylated substrates. In order to identify potential causes of the observed methylation

aberrations in lung cancers we have examined the expression status of DNMTs and UHRF1 genes.

The expression of DNMTs has been studied widely in various cancer types. Overexpression of DNMT1, DNMT3A and DNMT3B has been reported in human tumours [Girault, 2003], [Robertson, 2001], [Ehrlich, 2006]. In this study we observed that all three DNMTs are overexpressed in NSCLC tissues when compared to their normal adjacent tissues, in accordance with previous studies [Robertson, 1999], [Kim, 2006], [Vallbohmer, 2006]. We also demonstrated a significant overexpression of UHRF1 mRNA in NSCLC tumour tissues. Similar observations have been reported in a small set of human lung tumours [Jenkins, 2005], a cDNA microarray study in breast tumours [Unoki, 2004] and proteomic analysis in breast [Hopfner, 2000] and pancreatic carcinomas [Crnogorac-Jurcevic, 2005]. The expression of UHRF1 was higher in squamous carcinomas underlying further the differences in the molecular evolution of these tumour types. Further research is required to provide evidence on whether this difference could be utilized in the clinical management of these two histological types.

A strong correlation between the expression levels of all the DNMTs was observed in our primary lung tumours set suggesting a coordinated expression of DNMTs in cancers [Robertson, 1999], [Lin, 2007]. The E2F1 transcription factor, which is most frequently overexpressed in cancers, has been shown to regulate expression of both DNMT1 [Kimura, 2003], [McCabe, 2005] and UHRF1 [Mousli, 2003] [Unoki, 2004]. In order to find out whether up-regulation of DNMT1 and UHRF1 was due to E2F1 regulation, we examined the levels of E2F1 in our tissue set. We found a strong relationship between the expression of E2F1 and both DNMT1 and UHRF1 suggesting that this transcription factor is, at least partially, responsible for the observed overexpression of DNMT1 and UHRF1 in lung cancers. It appears

that the pRb/E2F pathway regulates the expression of DNMT1 and UHRF1 increasing their abundance during S and G2 phases [Vogel, 1988], [Jeanblanc, 2005] in order to replicate the DNA methylation patterns onto the newly synthesized strands. Furthermore, the expression levels of DNMT3A and DNMT3B examined in this set correlated with the expression of E2F1. Our data suggest that DNMT3A and DNMT3B may be also regulated by E2F1. Recent evidence on the participation of DNMT3A and DNMT3B in DNA methylation maintenance following DNA replication [Liang, 2002], [Jones, 2009] provides a biological reason behind the E2F1 dependence. However, this hypothesis requires further confirmation with functional studies in order to prove a direct regulation of DNMT3A and DNMT3B by E2F1.

The presence of dense CpG islands in DNMTs and UHRF1 promoters led us to examine the hypothesis of a possible negative feedback loop through DNA methylation. However, no methylation was found within these promoters in any of the lung tumours, or adjacent normal tissue examined, thus excluding this possibility. Interestingly we found that overexpression of DNMT3B correlates with worse survival in NSCLC patients. This is in accordance with a previous study demonstrating prognostic significance of DNMT3B expression but only in younger patients <65 years [Xing, 2008]. Although in our present study survival data are available only for a small subset (n=52), the potential clinical exploitation of this observation should be further investigated.

8.2 Expression of DNMTs and UHRF1 in relation to hypermethylation

During the past years many studies have examined the aberrant expression patterns of DNMTs in comparison to regional hypermethylation in primary tumours. In some cases the expression of DNMTs could not be associated with promoter hypermethylation [Ehrlich,

2006], [Sato, 2002], [Park, 2006], while other studies demonstrated correlations between the expression of particular DNMTs and hypermethylation status of certain promoters such as RASSF1 or CDKN2A [Wang, 2007], [Kim, 2006], [Lin, 2007]. Here we investigated the potential relationship between DNMTs or UHRF1 overexpression with regional hypermethylation of tumour suppressor genes in NSCLCs. We examined the methylation status of RASSF1 and CDKN2A TSGs as they are two of the most frequently hypermethylated genes in lung cancers [Virmani, 2000], [Zöchbauer-Müller, 2001]. Statistical analysis in primary tumours demonstrated a correlation between DNMT1 overexpression and a hypermethylated CDKN2A promoter, being in agreement with two previous studies [Lin, 2007] [Kim, 2006]. We also found that DNMT3B overexpression correlates with RASSF1 promoter hypermethylation. It has been reported that a specific DNMT3B subfamily, ΔDNMT3B, correlates with RASSF1 hypermethylation but not CDKN2A hypermethylation in NSCLC suggesting that ΔDNMT3B can regulate methylation in a promoter specific manner [Wang, 2007]. The primer set we used to amplify the DNMT3B transcript, amplifies all different DNMT3B transcripts and since ΔDNMT3B is the predominant form of DNMT3B in NSCLCs [Wang, 2006] we believe that our result reflects the observed correlation between ΔDNMT3B and RASSF1. Our data together with previous reports [Wang, 2007], [Lin, 2007], [Kim, 2006] suggest that DNMT1 and DNMT3B can regulate DNA methylation in a promoter-specific manner. In concordance to this suggestion is the classification of common and distinct promoter groups identified following RNAi-mediated suppression of DNMT1 and DNMT3B [Foltz, 2009].

UHRF1 plays a critical function in DNA methylation maintenance [Bostick, 2007], however, its involvement in TSG promoter hypermethylation in cancer is not yet clear. Here we investigated in NSCLCs the relationship of UHRF1 expression with the hypermethylation status

of CDKN2A and RASSF1 promoters. UHRF1 overexpression correlated with increased DNA methylation of both CDKN2A and RASSF1 promoters. Moreover, a much stronger association was observed when analyzing UHRF1 expression against a combined CDKN2A/RASSF1 methylation epigenotype. Thus, these data suggest that UHRF1 activity is important in maintaining the hypermethylation of certain TSGs. This is also supported by findings in breast tumours, where UHRF1 overexpression correlated to BRCA1 promoter hypermethylation [Jin, 2009].

The importance of both DNMT1 and DNMT3B expression in the maintenance of aberrant CpG island methylation of TSGs has been adequately demonstrated in mammalian cell models [Robert, 2003], [Suzuki, 2004], [Rhee, 2002], [Wang, 2007]. However, this is not the case for UHRF1, which was only recently found to play a role in methylation maintenance [Bostick, 2007]. There is only one study up to date connecting the overexpression of UHRF1 in a breast cancer cell line with hypermethylation of BRCA1 promoter in sporadic breast cancers [Jin, 2009]. We therefore choose to provide additional evidence to our *ex vivo* observations regarding UHRF1 and TSG hypermethylation. In order to do that we knocked down the expression of UHRF1 in the A549 lung adenocarcinoma cell line. Both UHRF1 knockdown derived clones demonstrated reduced methylation of RASSF1, CYGB and CDH13 promoters, which are hypermethylated in A549 cells. Since CDKN2A promoter was completely unmethylated in this cell line we could not assess the effect of UHRF1 downregulation on the hypermethylation of this promoter. The UHRF1 knockdown clones presented with reduced proliferation rates and migration efficiency in comparison to those characteristics of the parental and mock cell lines. This is in acquiescence with UHRF1's reported association with proliferation [Fujimori, 1998] and tumour cell growth [Jenkins, 2005]. E2F1 levels did not

change upon UHRF1 knockdown indicating a lack of a feedback loop. Both our *ex vivo* and *in vitro* data suggest that UHRF1-mediated cell cycle control is mainly facilitated by the epigenetic silencing of key cell cycle regulators, such as RASSF1 and CDKN2A or other tumour suppressor genes such as CDH13 or CYGB.

Interestingly, while the expression levels of DNMT1 and DNMT3A remained unchanged in the UHRF1 knockdown clones, there was a significant increase of DNMT3B expression in the absence of any methylation change of its promoter. The reasons behind the increase of DNMT3B expression upon UHRF1 knockdown are not currently clear. It is not known whether this is a directly UHRF1-related effect or whether unprompted high-DNMT3B expression provides a selective advantage which eventually takes over the cell population in the culture environment. Nevertheless, the incomplete RASSF1, CYGB and CDH13 promoter hypomethylation observed in the UHRF1 knockdown clones suggests that DNMTs can maintain a degree of methylation in the presence of low abundance of UHRF1 protein.

It is worth noting that UHRF1 was recently found to bind strongly to DNMT3A and DNMT3B proteins [Meilinger, 2009]. This, in combination with the proven ability of DNMT1 to act as a de novo methyltransferase as well, could therefore imply a potential role of UHRF1 in de novo methylation apart from its role on methylation maintenance. In support of this, is a recent study which demonstrates that UHRF1 overexpression can lead to methylation of the BRCA1 promoter in sporadic breast cancers [Jin, 2009].

This study provides compelling new evidence to suggest that the overexpression of UHRF1 in NSCLC is critical, alongside the overexpression of DNMTs, for the maintenance of hypermethylated TSG promoters. UHRF1 is thus emerging as key epigenetic switch for cell cycle control and can be utilized as a new target for epigenetic therapies.

8.3 Expression of DNMTs and UHRF1 in relation to hypomethylation

We have also examined the role of DNMTs and UHRF1 expression in the global hypomethylation observed in lung cancers. In order to do this we have examined the methylation status of LINE-1 which can serve as a global DNA methylation surrogate [Weisenberger, 2005]. Interestingly, when examining the expression status of DNMTs and UHRF1 in relation to LINE-1 methylation we found an inverse correlation. This result appears to be a great paradox since one would expect that high expression of DNMTs and/or UHRF1 would lead to higher global methylation or at least would be enough to maintain the methylation patterns of repeated sequences. Indeed, double knockdowns of DNMT1 and DNMT3B in a cancer cell line have been shown to reduce the genome methylation up to 95% affecting repeated sequences including Alu [Rhee, 2002] and LINE-1 [Weisenberger, 2005]. Knockout of UHRF1 in mouse embryonic stem cells has lead to global hypomethylation in mouse IAP and LINE-1 elements [Bostick, 2007]. In the same direction we observed here that downregulation of UHRF1 in the A549 cell line has lead to global hypomethylation as measured by LINE-1.

Nevertheless, it must be noted that an association between two parameters does not indicate which of the two affects the other. Moreover, it is also possible that the two phenomena are associated because they are affected by a third unknown parameter. Based on previous reports and our observations that loss of DNMTs or UHRF1 leads to global hypomethylation we suggest that LINE-1 hypomethylation observed in our lung set cannot be the cause of DNMTs and /or UHRF1 overexpression. The opposite effect is more likely. Global hypomethylation is thought to be an early event in human carcinogenesis [Fraga, 2004], [Suter, 2004]. It is possible that early induced global hypomethylation is sensed by the cell which in response induces the overexpression of DNMTs and/or UHRF1 proteins in order to

balance this effect. However this is only one possible explanation lacking any functional data and needs to be further investigated.

Previous studies investigating the expression of DNTMT1 in relation to proliferation measuring the levels of PCNA reported that although DNMT1 is overexpressed in cancers, when compared to a housekeeping gene, it is underexpressed when normalised to a proliferation marker such as PCNA. They suggest that, although DNMT1 is overexpressed, the proliferation rates of cancer cells are quite high and the enzyme is not able to maintain the methylation patterns during replications and thus global hypomethylation occurs passively through subsequent cell cycles. However they failed to prove a relationship between LINE-1 hypomethylation and DNMT1/PCNA expression [Kimura, 2003]. This concept could explain the observed inverse correlation in our sample set between LINE-1 hypomethylation and E2F1 expression. Since E2F1 is a measure of cell proliferation it is possible that tissues with higher proliferation fail to maintain methylation patterns demonstrating greater hypomethylation of the genome. This suggestion also explains the relationships between LINE-1 hypomethylation and DNMT1, DNMT3B and UHRF1 expression since they are E2F1 targets and demonstrate similar expression patterns. This suggestion needs to be further investigated exploring the expression status of DNMTs and UHRF1 normalised to proliferation markers in comparison to global hypomethylation. Nevertheless, if this suggestion is true the paradox remains since the inability of DNMT1 or UHRF1 to maintain DNA methylation is in contrast to the observed hypermethylated genes and the role of these proteins in their maintenance.

It is also worth noting that we have observed an inverse relationship between global hypomethylation and regional hypermethylation of RASSF1 promoter. The same relationship was not significant for CDKN2A hypermethylation as well, however, when combining the two

promoters the relationship was apparent. This implies that the two phenomena, global hypomethylation and regional hypermethylation are inverse correlated in lung cancers. A similar association between LINE-1 hypomethylation and CpG island methylator phenotype was observed in colorectal cancers [Ogino, 2008], [Nosho, 2008].

Cancer-associated global hypomethylation is a very important event which has been linked with tumour formation [Gaudet, 2003], [Eden, 2003]. Many studies have demonstrated several causes of passive hypomethylation in cell models most of them including the knockdown of DNMTs or UHRF1. In addition a number of studies have searched for a demethylase enzyme that could actively promote hypomethylation [Ooi, 2008]. However, an enzyme with a demethylase activity is not yet proven to exist while DNMTs irregular activity is not yet associated with global hypomethylation in primary tumours. Although in this study we demonstrate that UHRF1 downregulation leads to global demethylation of a lung cancer cell line, we fail to provide any evidence regarding the expression status of UHRF1 and/or DNMTs that would explain the observed hypomethylation in primary lung tumours.

8.4 Hypomethylation of retrotransposable elements and genomic instability in NSCLC

The second aim of this study was to examine the link between global hypomethylation and tumour formation in NSCLC [Gaudet, 2003], [Eden, 2003]. As we already described in the introduction global hypomethylation in cancer cells mainly affect repeated sequences. The vast majority of these sequences are comprised of retrotransposable elements. The LINE-1 and Alu elements are non-LTR containing retrotransposons which comprise a long stretch of the human repeat DNA sequences [Cordaux, 2009]. Although only a small number of these elements are considered to be retrotranspositionally active in the human genome, spontaneous retrotransposition events are associated with insertional mutagenesis and can

lead to genetic disorders [Babushok, 2007], [Kazazian, 2004], [Sassaman,1997], [Cordaux, 2009], [Lin, 1988]. LINE-1 and Alu elements are methylated in normal somatic cells and are frequently demethylated in cancer following global genome hypomethylation [Ehrlich, 2002]. Indeed, because of their abundance in the genome they have been shown to be a good measure of such global hypomethylation in cancer [Weisenberger, 2005]. However, the possible involvement of hypomethylation-mediated activation of LINE-1 and Alu in the genome stability and cancer development has not been widely studied, although there is recent evidence to fuel such investigations [Schulz, 2006], [Gilbert, 2002], [Kazazian, 2002], [Belgnaoui, 2006], [Roman-Gomez, 2005]. As demethylating agents are increasingly used in cancer treatment, it is imperative to understand how cancer-related and/or drug-induced hypomethylation may initiate retrotransposition and subsequent genomic alterations, thus drawing valuable conclusions for implications in cancer therapy.

Here, we quantitatively determined in NSCLC the methylation status of LINE and Alu elements utilizing the sequences of LINE-1.2 and Alu-PV species respectively. These particular LINE and SINE species were selected based on their activity in the human genome [Sassaman, 1999], [Mighell, 1997], [Wallace, 1991]. Of course, due to the high degeneracy of these sequences the final amplified products most probably contain copies of different families [Schulz, 2006]. We demonstrated a significant reduction of the methylation levels of both LINE-1.2 and Alu-PV elements in primary NSCLC. These findings suggest a potentially important role for LINEs and SINEs in lung cancer development, adding to the limited information for retro-element methylation in this cancer type [Chalitchagorn, 2004], [Rauch, 2007], [Rauch, 2008].

There are profound differences on the detected methylation levels of LINE-1.2 and Alu-PV in normal and tumour specimens. More precisely, the observed average change in LINE is 13.2%

while in Alu is only 3.1%. The small decrease of Alu-PV element methylation was expected since we have used as a template the Alu-PV element which comprises an evolutionary young Alu family. It has been demonstrated that hypomethylation of Alu elements is greater in older retrotranspositionally inactive families, while at younger transpositionally active families, as in the Alu-PV family, hypomethylation occurs in a much lesser extent [Rodriguez, 2007]. This data suggest that younger Alu families in which the most active elements exist and are closer to genes are under a stronger silencing pressure [Rodriguez, 2007].

From the clinicopathological point of view, it is notable that the observed hypomethylation was widespread among tumours of variable stage, nodal metastasis and differentiation status, most probably suggesting an early onset of this molecular abnormality in the course of lung cancer development [Morey Kinney, 2008]. When examining LINE-1 hypomethylation further in a second set of NSCLC tissues we verified the observed trend of greater LINE-1 hypomethylation in squamous cell carcinomas compared to adenocarcinomas.

Our study confirms that NSCLC follows a similar global hypomethylation pattern as other human tumours [Ehrlich, 2002], [Weisenberger, 2005]. Of particular note here is the finding that the methylation status of LINE-1.2 is highly correlated to that of Alu-PV ($p=0.004$). This suggests a common mechanism of methylation maintenance of these elements in cancer and receives further supporting evidence from data in prostate cancer [Cho, 2007] and the reported correlation of both elements methylation with global genome methylation as measured by HPLC [Weisenberger, 2005].

In order to assess the potential implication of LINE-1 and Alu elements demethylation in genome stability maintenance in NSCLCs, we have examined LOH at loci which are hotspots for lung cancer [Liloglou, 2001] and used fractional allele loss (FAL) as a measure of the overall

genomic instability. We demonstrated that hypomethylation of both transposable elements correlates with high FAL values indicating a strong link between genome stability and transposable element methylation. A similar observation has been reported in colorectal carcinomas where LINE-1 hypomethylation correlated with microsatellite instability [Estecio, 2007], [Ogino, 2008], although the mechanisms responsible for chromosomal instability (expressed by FAL) and microsatellite instability (MSI) are different. Genomic hypomethylation has been shown to induce chromosomal instability and tumourigenesis in mice models [Gaudet, 2003], [Eden, 2003]. Genomic hypomethylation may promote genomic instability and tumourigenesis by unmasking transposable elements and therefore allowing retrotransposition events to take place. It is well established that LINE-1 retrotransposition in model systems induces genomic instability and deletions promoting carcinogenesis [Gilbert, 2002], [Symer, 2002], [Kazazian, 2002].

8.5 Re-Expression of LINE-1 and Alu elements due to demethylation in lung cancer

A triangular relationship between global hypomethylation - transposable elements -genomic instability has been suggested for many types of human tumours [Schulz, 2006], [Kazazian, 2002] and the correlation between genomic instability and hypomethylation in our study is in agreement to this. This hypothesis suggests that hypomethylation of retrotransposable elements leads to their re-expression and subsequent retrotransposition in cancer. The information on LINE-1 expression in human tumours is very limited but suggests a degree of transcriptional activation in leukaemias [Roman-Gomez, 2005], breast [Bratthauer, 1994], urothelial and renal carcinomas [Florl, 1999].

However, identification of LINE-1 or Alu-PV elements expression levels at the RNA levels poses significant limitations. These elements are intronless and thus primers designed to amplify the

LINE-1 or Alu RNAs will inevitably amplify gDNA copies of these elements as well. Bearing in mind the great number of copies of these elements in the human genome one understands that even minimum amounts of gDNA contamination of RNA samples will lead to false results. In order to circumvent this problem one needs to treat RNA samples with DNAse extensively. However this leads to the loss of the greater percentage of the starting RNA material and can also lead to RNA degradation due to long incubation times. The problem becomes greater when comparing RNA samples from tumour and adjacent normal tissues. Tumour cells are characterised by genomic instability (chromosome amplifications, loss of chromosome arms) compared to their normal adjacent tissues which have a normal human genome, therefore providing different starting backgrounds.

To overcome these problems we chose to study the potential epigenetic re-expression of LINE-1 and Alu elements by utilizing decitabine and TSA (common inhibitors of methylation and histone deacetylation, respectively) on two lung cancer cell lines and a non-tumourigenic bronchial epithelial cell line to verify hypomethylation-mediated activation of transcription. The study of expression of these elements in a cell line can be more accurate providing more trustful results than when working with RNA from primary tumours. Firstly, cell lines can provide endless amount of RNA and therefore we were able to treat our RNAs with DNase at three different steps without compromising RNA integrity or quantity. We performed on column DNase digestion during RNA extraction, we treated our RNAs with turbo DNAse and finally we have included a gDNA elimination step during cDNA preparation. Secondly, comparing the effect of hypomethylating and de-acetylating agents in a cell line provide us with the ability to compare the differences of LINE-1 and Alu expression on an almost identical genomic background. Finally, we have undertaken PCR reactions amplifying p21 promoter in

order to check for any possible gDNA contamination on our final cDNA samples. Only 'clean' cDNAs were used for our experiments.

We have identified the optimal dose of decitabine in order to achieve maximum hypomethylation of LINE-1 and Alu-PV elements and found that decitabine shows greater activity in low concentrations. This is in agreement with another study demonstrating similar results [Qin, 2008]. In higher doses decitabine gradually lost any effect which probably is caused by the induction of cell cycle arrest [Qin, 2008]. In all three cell lines, the use of decitabine, which led to experimentally confirmed hypomethylation of LINE-1.2 and Alu-PV elements, resulted in increased transcription of both elements. Notably, simultaneous use of TSA further increased transcription level. It has to be noted at this point that the observed increased expression of LINE-1.2 and Alu-PV could be partly due to incomplete elements encompassed in genes that are overexpressed in the presence of decitabine.

While we are clearly demonstrating that expression of LINE-1.2 and Alu-PV elements is under epigenetic control in a lung cancer environment, it has to be noted that retrotransposition could be impaired by methylation-independent mechanisms. siRNAs produced by the LINE-1 5'antisense promoter have been shown to inhibit its retrotransposition [Yang, 2006], [Soifer, 2006]. In addition, LINE and Alu retrotransposition is controlled by APOBEC3 proteins [Muckenfuss, 2006], [Esnault, 2005] and sequestration into stress granules [Goodier, 2007]. Last, it must be also noted that hypomethylation of LINE and Alu is not necessarily uniform [Schulz, 2006], [Rodriguez, 2008] thus it is not totally clear to which extent our data can be extrapolated.

We have found an association between hypomethylation of retrotransposable elements and genomic instability in primary NSCLCs. In addition, we ascertained that demethylation of these

elements can lead to their re-expression in lung cancer cell lines. Together these data imply a possible re-activation of LINE-1 and Alu elements in NSLCs which could lead after successful or unsuccessful retrotransposition cycles to genomic instability therefore promoting tumour progression. In support of this notion is a recent study demonstrating the activation and retrotransposition of endogenous retroviral elements in hypomethylation induced tumours in mice [Howard, 2008]. An alternative suggestion is that chromatin relaxation at such retroelement sites may promote illegitimate recombination leading to genomic instability [Schulz, 2006], [Kolomietz, 2002], [Jurka, 2004]. In fact it is possible that both phenomena could take place during lung cancer progression.

Taking into account that global hypomethylation is an early event in tumour formation it is apparent that the retrotransposable element may have a great role towards lung carcinogenesis and progression [Fraga, 2004], [Suter, 2004]. This suggestion is reflected by the findings of a study in a large number of colorectal cancer cases (n=643) where LINE-1 hypomethylation correlated with shorter survival of cancer patients [Ogino, 2008]. We were not able to establish a similar association between LINE-1 hypomethylation and survival in our data set, however, this was probably due to the small number of cases (n=52) for which we had survival information.

Although we provide evidence towards a more active role of LINE-1 and Alu elements in lung tumourigenesis there are certain limitations due to technical difficulties arising from the massive sequence homology among LINE and SINE species members. We have utilised the LINE-1.2 and Alu-PV elements to design our primers for methylation detection which are retrotranspositionally active elements. However, it is most likely that we have amplified the promoter region of thousands of family members in the genome. These could be other highly

homologous LINE-1/Alu sequences or even L1.2/Alu-PV truncated smaller sequences incapable of retrotransposition. The same problem exists regarding the expression data. It is particularly difficult to ascertain that the observed overexpression of LINE-1.2 and Alu-PV reflects exclusively retrotranspositionally active elements. In other words, as the detection of endogenous retro-elements re-insertion events is practically not feasible with current technology, the detected activation of transcription does not guarantee increased re-insertion.

8.6 Activity of a full LINE-1 element in lung cancer environment

In order to bypass these limitations and investigate further the hypomethylation induced reactivation of LINE-1 in the lung cancer environment we have created a cell culture model utilising the KS-101 construct which was a generous gift from Dr John V. Moran. The KS-101 construct carries a full LINE-1 element tagged with a retrotransposition cassette. The full LINE-1 element in this construct (LRE3) is located to chromosome 2q24.1 on the human genome and is one of the most actively retrotransposing LINE-1 elements [Brouha, 2002]. Similar constructs carrying different LINE-1 retrotransposition competent elements have been used in cell lines demonstrating variable retrotransposition efficiencies [Moran, 1996], [Morrish, 2002], [Wei, 2000], [Garcia-Perez, 2007]. In most of these studies the LINE-1 element in these constructs was under the regulation of a CMV promoter and therefore under extreme modelling conditions that do not resemble human cells where LINE-1 elements are regulated by their own 5' end promoter. The KS-101 construct we used has the advantage that its LINE-1 element is only regulated by its own promoter [Garcia-Perez, 2007]. Using this construct we have proved that LINE-1 element is active in a CRL5802 lung cancer cell line with a low LINE-1 methylation status, while it remained inactive in other 5 cell lines with high LINE-1

methylation. These data suggest that LINE-1 element may preferentially retrotranspose in cell lines with low global methylation status. However, the use of decitabine in all cell lines which leads to global demethylation has not led to an increase in the number of retrotransposition events in the CRL5802 or in any retrotransposition events in the other cell lines.

It must be noted that the methylation status of the specific LRE3 promoter could not be examined before retrotransposition using the KS-101 plasmid. In order to investigate further the effect of decitabine-induced hypomethylation we have constructed the KS101B plasmid, incorporating a blasticidin resistance gene, which enables stable transfection. Using this construct in the CRL5802 cell line we have seen that all the obtained colonies had a very low methylated LRE3 promoter. Treating these colonies with decitabine did not lead to an increase in the number of retrotransposition events. Since the LINE-1 promoter was by itself unmethylated any change would be due to global hypomethylation changes. This data confirm the hypothesis that the retrotransposition machinery of LINE-1 element has a strong cis preference for its own RNA transcript [Wei, 2001]. Since the LINE-1 promoter in the obtained colonies remained unmethylated we could not test the effect of decitabine on this specific promoter in the case that it would have become methylated. In order to bypass this problem, in vitro methylation of the KS101B plasmid before transfection should be included in future experiments. Although there are some reports demonstrating successful in vitro methylation of plasmids and subsequent transfection in mammalian cells [Qu, 1999], it remains to be discovered whether the cells will maintain the methylation status of the inserted vector long enough for the needs of the study.

Epigenetic mechanisms appear to have a key role in cancer development and thus are considered as critical targets in anticancer therapies. DNMT inhibitors are increasingly used in

clinical trials [Lyko, 2005], [Issa, 2007]. Recent studies provide very promising results [Appleton, 2007], [Oki, 2008] as epigenetic modulation of drug resistance may be critical for improving cancer drug efficiency overall [Glasspool, 2006]. It is, however, important to understand in detail the epigenetic reprogramming of cancer cells. In this direction, further to identifying the most commonly hypermethylated genes, it is crucial to understand the impact of transposable element hypomethylation in cancer biology. In addition, we need to understand how and to what extent DNA hypomethylation may be a critical adverse effect of epigenetic therapies [Ehrlich, 2006].

8.7 Conclusions

Our findings in this study demonstrate for the first time in primary human lung tumours the relationship between retro-element hypomethylation and genomic instability. In addition, we provide evidence that hypomethylation of LINE-1 and Alu elements in human lung cancer cell lines leads to enhanced transcription, which in combination with previous reports on retrotransposition-induced genomic instability and the observed ability of a full LINE-1 element to retrotranspose under the regulation of its own promoter in a lung cancer cell line, points towards a more active role of the reactivation of such retroelements in the pathogenesis of human tumours. Furthermore we demonstrate that UHRF1 is a key epigenetic switch that is overexpressed in NSCLC and can promote cancer development mediating the silencing of tumour-suppressor genes. Therefore UHRF1 might serve as a biomarker in diagnostics or therapeutic stratification of patients with lung cancer.

As mentioned above although current epigenetic therapies present some interesting data, the promotion of hypomethylation and potential re-activation of retrotransposable elements is one of their main adverse effects. Therefore new epigenetic targets, apart from DNMTs blocking, that will enable the re-expression of TSGs without affecting the methylation status of retrotransposable elements are needed. It is of great importance that in the present study we have identified an epigenetic regulator which acts towards this direction. UHRF1 downregulation has led to a profound hypomethylation on the promoter region of TSGs while at the same time it has led only to a modest hypomethylation of LINE-1 and Alu elements. These data suggest that UHRF1 protein is emerging as a new more promising target towards epigenetic therapies since it shows more specificity for TSGs than transposable elements.

8.8 Future directions

UHRF1 appears to be a key factor of epigenetic deregulation in lung cancers acting mainly through the silencing of TSGs. Although the present study provided important data regarding the role of UHRF1 in lung tumourigenesis there are a number of issues which could be further investigated.

UHRF1 protein expression should be studied in a large cohort in order to verify the data we provide regarding the expression of UHRF1 at the RNA level.

In addition the observed important effect of UHRF1 downregulation on the methylation status of TSGs should be further investigated. Towards this direction rescue experiments should be undertaken in the UHRF1 knockdown clones. The re-expression of UHRF1 would further establish the relationship between this protein and TSG hypermethylation. Furthermore this rescue experiment would demonstrate whether the indication that UHRF1 underexpression leads to DNMT3B overexpression is true or not.

We have already pointed out that UHRF1 downregulation has lead to various degrees of hypomethylation in certain TSGs while the retrotransposable elements were affected in a lesser extend. As this implies that there is a preference of UHRF1 protein for different DNA regions, methylation array experiments could be undertaken in order to identify potential groups of gene promoters that are affected in a greater extend. In addition nuclear extracts could be used in order to prove in vitro whether UHRF1 enzymatic activity preferentially methylates TSG promoters in comparison to repetitive sequences.

We also provide evidence towards a potential reactivation of retrotransposable elements due to hypomethylation in lung cancer. Whole genome sequencing in a cohort of lung cancer

tissues would reveal the potential re-activation and retrotransposition of these elements as well as their relationship to genomic instability and tumour progression.

Future work in this blooming field of cancer epigenetics will assist to fully elucidate the molecular mechanisms involved and provide the basis for the better clinical utilization of demethylating agents for the treatment of human cancer.

Appendices

Appendix 1. Expression of DNMTs, UHRF1 and E2F1 in 50 paired NSCLC tissues.

Sample	DNMT1		DNMT3A		DNMT3B		UHRF1		E2F1	
	T	N	T	N	T	N	T	N	T	N
1	7.55	4.77	20.36	13.41	16.87	14.86	0.55	0.33	3.00	1.87
2	12.96	4.17	31.56	13.07	44.70	6.88	3.90	0.16	21.61	4.57
3	11.87	5.25	16.20	15.97	36.45	11.70	3.01	0.13	12.83	2.90
4	15.36	3.88	41.98	12.67	114.16	6.35	3.89	0.33	40.38	2.98
5	3.20	2.52	15.89	12.86	6.88	8.20	2.68	0.19	7.12	2.52
6	11.86	4.80	69.70	15.33	120.41	15.70	2.60	0.14	33.28	8.94
7	6.14	8.02	7.82	60.80	110.89	60.55	1.94	1.11	8.72	13.64
8	1.75	3.20	6.96	7.78	15.80	6.64	0.56	0.15	2.10	3.18
9	9.24	4.72	30.04	19.85	77.26	11.19	5.56	0.31	18.01	4.31
10	10.21	4.56	35.39	12.87	29.91	13.44	6.67	0.15	19.85	4.28
11	13.42	5.73	26.40	56.04	40.07	40.34	5.42	0.26	45.96	18.44
12	7.10	4.12	19.79	20.79	59.42	15.91	2.45	0.30	17.10	5.61
13	20.94	11.31	61.19	33.94	99.26	26.83	6.53	0.86	31.75	7.72
14	5.29	3.39	16.55	15.53	36.97	9.50	0.79	0.12	6.31	3.78
15	10.16	3.74	59.18	46.68	119.17	50.49	2.85	0.20	37.02	14.83
16	7.78	4.67	252.93	17.68	506.79	17.08	4.06	0.32	123.37	5.08
17	13.54	3.69	24.00	18.93	38.16	14.43	2.47	0.39	16.27	6.12
18	17.24	4.60	25.38	17.44	14.58	10.28	2.99	0.42	47.00	4.32
19	10.17	6.83	53.39	52.69	75.77	38.99	3.50	0.78	14.67	12.16
20	15.19	8.68	39.45	52.20	74.76	69.66	10.01	0.56	38.70	24.24
21	10.07	5.87	75.43	69.36	45.12	94.61	5.94	0.45	16.37	20.23
22	8.95	3.85	22.21	25.46	34.46	12.06	1.84	0.17	14.28	4.99
23	3.23	5.25	9.70	20.10	22.07	10.26	1.70	0.53	6.89	5.19
24	5.77	13.10	40.63	66.44	32.16	122.80	2.00	1.58	7.89	24.58
25	10.43	3.79	31.37	17.55	26.04	9.00	1.95	0.19	6.59	3.83
26	5.96	3.66	16.73	21.77	17.63	19.71	0.61	0.26	6.37	3.54
27	17.72	3.09	25.87	8.30	57.33	5.22	7.73	0.15	23.73	2.71
28	14.07	15.89	36.33	132.62	63.00	202.41	5.54	1.27	13.76	43.47
29	5.33	7.51	44.21	30.05	70.23	42.68	2.41	0.45	16.23	5.67
30	16.03	3.39	58.86	15.71	115.61	9.74	3.27	0.16	22.61	4.56
31	5.13	1.94	20.71	8.79	10.08	7.97	2.35	0.13	14.54	3.17
32	4.80	9.27	136.37	92.58	543.70	111.79	8.27	ND	92.95	15.71
33	21.83	8.12	63.73	51.69	108.97	40.44	4.34	0.33	37.54	15.11
34	3.65	4.03	18.11	15.53	42.89	13.27	3.89	0.04	12.29	3.87
35	14.41	7.63	222.35	32.00	410.91	14.05	7.22	0.43	120.83	7.42
36	2.93	5.19	20.51	22.58	135.05	10.39	0.99	0.08	15.10	3.74
37	4.06	10.29	28.30	ND	37.16	ND	0.97	ND	6.55	ND
38	16.44	6.15	40.26	10.49	ND	19.51	9.08	3.38	9.09	19.41
39	4.64	7.38	14.55	41.08	19.18	31.07	1.44	0.59	5.75	13.17
40	8.17	7.95	32.31	30.03	67.59	18.54	6.56	0.30	27.57	5.08
41	3.87	4.05	21.17	14.85	18.04	8.36	3.76	0.05	11.92	3.95

42	7.06	5.09	17.96	12.76	11.12	4.10	1.15	0.11	3.69	2.33
43	3.60	3.03	20.66	10.84	30.11	8.12	3.82	0.15	8.59	3.83
44	13.86	5.24	60.41	20.84	221.17	15.10	2.92	0.27	29.27	2.97
45	10.49	8.64	16.33	15.23	25.09	8.95	5.63	0.21	16.27	3.23
46	2.15	3.68	21.00	23.35	61.48	14.22	1.99	0.27	7.98	4.82
47	28.96	11.72	178.98	169.42	226.66	135.82	13.30	1.58	68.58	57.98
48	4.92	4.53	16.99	29.88	26.74	32.93	4.85	2.10	20.41	9.12
49	8.85	4.49	93.43	34.54	56.93	22.44	4.18	0.74	20.51	4.40
50	13.25	4.84	116.58	53.21	136.46	49.44	5.35	0.30	36.97	14.04

Values represent the mean RQ values. The expression of IMR-90 cells was used as a calibrator.

Appendix 2. Expression of DNMTs, UHRF1 and E2F1 in 54 NSCLC tumours and survival information

Sample	DNMT1	DNMT3A	UHRF1	E2F-1	DNMT3B	Fate[1]	FU[2]
1	11.44	40.81	12.44	72.99	268.72	0	87.8
2	9.33	52.72	1.44	17.35	73.72	0	46.6
3	4.86	9.86	5.68	5.62	11.03	1	93.5
4	11.87	16.20	3.01	12.83	36.45	0	36.1
5	10.21	35.39	6.67	19.85	29.91	0	30.8
6	15.19	39.45	10.01	38.70	74.76	0	15.3
7	8.95	22.21	1.84	14.28	34.46	0	37.4
8	3.23	9.70	1.70	6.89	22.07	0	6.5
9	5.13	20.71	2.35	14.54	10.08	1	79.6
10	7.06	17.96	1.15	3.69	11.12	1	78.2
11	2.15	21.00	1.99	7.98	61.48	0	14.2
12	4.92	16.99	4.85	20.41	26.74	0	5.8
13	40.53	87.09	20.64	57.55	211.37	0	35.2
14	2.90	3.60	1.20	17.38	167.14	0	14.2
15	2.80	8.21	0.25	1.36	6.41	1	37.5
16	2.32	6.51	0.78	6.01	3.87	0	18.3
17	7.54	24.02	2.40	5.29	29.64	0	10.9
18	23.47	4.85	4.83	10.49	16.58	1	26.6
19	5.26	7.32	1.15	3.38	7.34	1	25.4
20	5.49	6.90	2.02	8.96	14.36	1	25.3
21	7.11	9.16	2.54	6.98	56.48	1	18.3
22	4.27	10.29	1.11	3.64	9.02	1	17.5
23	7.24	73.34	4.69	44.94	46.25	1	22.5
24	2.22	7.70	0.74	4.36	12.50	1	16.5
25	3.99	23.20	2.86	17.58	28.68	1	21.7
26	5.77	22.50	3.04	32.23	77.75	0	12.9
27	7.53	24.84	6.13	29.45	26.57	1	15.1
28	2.47	10.84	3.01	7.12	37.27	0	6.5
29	5.49	33.69	1.10	25.01	78.23	0	2.1
30	3.43	19.90	0.65	7.85	40.82	0	24.9
31	2.89	10.11	0.71	7.40	14.09	1	14.4

32	5.51	24.41	3.30	33.99	54.94	1	11.7
33	2.07	7.86	0.81	3.36	8.71	1	11.7
34	1.36	6.36	2.10	4.80	2.88	1	10.5
35	4.42	16.59	2.08	14.66	44.61	1	26.2
36	2.06	9.44	1.93	5.52	33.09	1	12.0
37	5.23	29.00	3.44	31.81	171.15	1	7.5
38	1.77	7.51	1.83	7.40	15.22	1	7.4
39	1.82	7.49	2.14	7.73	9.61	1	6.3
40	1.74	7.25	0.92	4.14	6.52	1	6.5
41	2.20	19.17	3.80	19.21	49.45	1	5.9
42	1.27	5.98	0.78	2.37	8.84	0	19.9
43	1.55	7.55	0.23	2.14	8.23	1	5.3
44	3.15	15.25	0.48	10.56	26.84	1	5.2
45	2.65	6.45	1.09	7.74	63.58	1	3.1
46	2.80	8.53	3.04	10.73	15.98	1	2.5
47	1.97	10.48	0.73	4.39	7.21	1	3.5
48	2.04	8.13	0.68	5.53	8.46	1	3.5
49	3.42	19.21	3.36	23.92	22.92	1	2.3
50	2.73	13.51	0.21	8.21	23.73	1	2.7
51	2.52	7.46	1.70	6.94	38.33	1	2.6
52	4.14	12.40	1.12	10.58	24.35	0	1.7
53	2.17	16.26	2.98	11.50	30.32	0	8.9
54	2.42	13.64	1.90	9.80	20.67	1	4.8

Values represent the mean RQ values. The expression of IMR-90 cells was used as a calibrator

[1]:Fate 1: diseased, 0: alive

[2]FU: Time in months post surgery with available follow up information

Appendix 3. Expression of UHRF1, DNMTs, and DNA methylation of CDKN2A and RASSF1 promoters in NSCLC.

			mRNA expression (mean RQ value)[1]					DNA methylation status[2]	
Sample	Gender	Histology	UHRF1	DNMT1	DNMT3A	DNMT3B	E2F1	CDKN2A	RASSF1
1	M	SqCCL	12.44	11.44	40.81	268.72	72.99	0	1
2	M	SqCCL	1.44	9.33	52.72	73.72	17.35	0	0
3	M	SqCCL	5.68	4.86	9.86	11.03	5.62	1	0
4	M	SqCCL	0.55	7.55	20.36	16.87	3.00	0	0
5	M	SqCCL	3.90	12.96	31.56	44.70	21.61	0	1
6	M	SqCCL	3.01	11.87	16.20	36.45	12.83	ND	1
7	M	AdenoCa	3.89	15.36	41.98	114.16	40.38	1	0
8	F	AdenoCa	2.68	3.20	15.89	6.88	7.12	0	0
9	F	AdenoCa	2.60	11.86	69.70	120.41	33.28	1	1
10	M	AdenoCa	1.94	6.14	7.82	110.89	8.72	1	1
11	M	SqCCL	0.56	1.75	6.96	15.80	2.10	0	0
12	M	AdenoCa	5.56	9.24	30.04	77.26	18.01	1	1
13	M	SqCCL	6.67	10.21	35.39	29.91	19.85	0	0
14	M	SqCCL	5.42	13.42	26.40	40.07	45.96	0	1
15	F	AdenoCa	2.45	7.10	19.79	59.42	17.10	0	0
16	F	SqCCL	6.53	20.94	61.19	99.26	31.75	1	0
17	F	AdenoCa	0.79	5.29	16.55	36.97	6.31	0	0
18	F	AdenoCa	2.85	10.16	59.18	119.17	37.02	0	0
19	M	SqCCL	4.06	7.78	252.93	506.79	123.37	1	0
20	M	SqCCL	2.47	13.54	24.00	38.16	16.27	1	1
21	M	SqCCL	2.99	17.24	25.38	14.58	47.00	0	0
22	M	AdenoCa	3.50	10.17	53.39	75.77	14.67	0	0
23	M	SqCCL	10.01	15.19	39.45	74.76	38.70	0	0
24	F	AdenoCa	5.94	10.07	75.43	45.12	16.37	1	1
25	M	AdenoCa	1.84	8.95	22.21	34.46	14.28	0	0
26	M	SqCCL	1.70	3.23	9.70	22.07	6.89	0	0
27	F	AdenoCa	2.00	5.77	40.63	32.16	7.89	0	0
28	M	SqCCL	1.95	10.43	31.37	26.04	6.59	1	0
29	F	AdenoCa	0.61	5.96	16.73	17.63	6.37	0	1
30	M	SqCCL	7.73	17.72	25.87	57.33	23.73	0	0
31	F	SqCCL	5.54	14.07	36.33	63.00	13.76	0	1
32	F	AdenoCa	2.41	5.33	44.21	70.23	16.23	0	1
33	M	AdenoCa	3.27	16.03	58.86	115.61	22.61	1	1
34	M	SqCCL	2.35	5.13	20.71	10.08	14.54	0	1
35	F	AdenoCa	8.27	4.80	136.37	543.70	92.95	0	1
36	F	SqCCL	4.34	21.83	63.73	108.97	37.54	0	0
37	M	SqCCL	3.89	3.65	18.11	42.89	12.29	0	1
38	M	AdenoCa	7.22	14.41	222.35	410.91	120.83	ND	0
39	F	AdenoCa	0.99	2.93	20.51	135.05	15.10	0	1
40	F	AdenoCa	0.97	4.06	28.30	37.16	6.55	0	0
41	F	AdenoCa	9.08	16.44	40.26		9.09	1	1
42	M	AdenoCa	1.44	4.64	14.55	19.18	5.75	0	0
43	M	SqCCL	6.56	8.17	32.31	67.59	27.57	1	0
44	M	SqCCL	3.76	3.87	21.17	18.04	11.92	0	0
45	M	AdenoCa	1.15	7.06	17.96	11.12	3.69	0	0
46	F	AdenoCa	3.82	3.60	20.66	30.11	8.59	1	0
47	F	AdenoCa	2.92	13.86	60.41	221.17	29.27	0	0
48	M	SqCCL	5.63	10.49	16.33	25.09	16.27	1	1
49	F	SqCCL	1.99	2.15	21.00	61.48	7.98	0	0
50	M	SqCCL	13.30	28.96	178.98	226.66	68.58	0	0
51	F	AdenoCa	4.85	4.92	16.99	26.74	20.41	0	0
52	M	SqCCL	4.18	8.85	93.43	56.93	20.51	ND	0

53	F	SqCCL	5.35	13.25	116.58	136.46	36.97	ND	0
54	F	AdenoCa	20.64	40.53	87.09	211.37	57.55	0	1
55	M	AdenoCa	1.20	2.90	3.60	167.14	17.38	1	1
56	F	SqCCL	0.25	2.80	8.21	6.41	1.36	0	0
57	F	AdenoCa	0.78	2.32	6.51	3.87	6.01	0	0
58	M	AdenoCa	2.40	7.54	24.02	29.64	5.29	1	0
59	M	AdenoCa	4.83	23.47	4.85	16.58	10.49	1	0
60	M	SqCCL	1.15	5.26	7.32	7.34	3.38	0	0
61	F	SqCCL	2.02	5.49	6.90	14.36	8.96	1	1
62	F	SqCCL	2.54	7.11	9.16	56.48	6.98	0	0
63	F	AdenoCa	1.11	4.27	10.29	9.02	3.64	0	0
64	M	AdenoCa	4.69	7.24	73.34	46.25	44.94	0	1
65	M	AdenoCa	1.08	4.29	20.28	48.36	7.34	0	0
66	M	AdenoCa	0.74	2.22	7.70	12.50	4.36	1	0
67	F	AdenoCa	2.86	3.99	23.20	28.68	17.58	0	0
68	F	AdenoCa	3.04	5.77	22.50	77.75	32.23	0	1
69	F	SqCCL	6.13	7.53	24.84	26.57	29.45	0	1
70	M	AdenoCa	3.01	2.47	10.84	37.27	7.12	0	0
71	M	AdenoCa	1.10	5.49	33.69	78.23	25.01	0	0
72	M	AdenoCa	0.65	3.43	19.90	40.82	7.85	0	0
73	F	SqCCL	2.84	6.78	35.17	57.50	20.49	1	0
74	F	SqCCL	0.71	2.89	10.11	14.09	7.40	0	0
75	M	SqCCL	3.30	5.51	24.41	54.94	33.99	0	0
76	F	AdenoCa	0.81	2.07	7.86	8.71	3.36	0	0
77	M	AdenoCa	2.10	1.36	6.36	2.88	4.80	0	1
78	M	SqCCL	2.08	4.42	16.59	44.61	14.66	0	0
79	M	AdenoCa	1.93	2.06	9.44	349.04	5.52	0	1
80	F	AdenoCa	0.24	2.31	23.70	14.27	6.07	0	1
81	F	SqCCL	0.30	3.57	18.17	33.09	5.22	0	0
82	F	SqCCL	3.44	5.23	29.00	171.15	31.81	0	1
83	M	AdenoCa	1.83	1.77	7.51	15.22	7.40	0	0
84	F	SqCCL	2.14	1.82	7.49	9.61	7.73	1	0
85	F	SqCCL	0.92	1.74	7.25	6.52	4.14	0	0
86	M	SqCCL	3.80	2.20	19.17	49.45	19.21	1	1
87	M	AdenoCa	0.78	1.27	5.98	8.84	2.37	0	0
88	M	AdenoCa	0.23	1.55	7.55	8.23	2.14	0	0
89	F	AdenoCa	0.48	3.15	15.25	26.84	10.56	0	0
90	M	SqCCL	1.09	2.65	6.45	63.58	7.74	0	0
91	M	SqCCL	3.04	2.80	8.53	15.98	10.73	1	0
92	M	AdenoCa	0.73	1.97	10.48	7.21	4.39	0	1
93	F	AdenoCa	0.68	2.04	8.13	8.46	5.53	0	0
94	F	AdenoCa	3.36	3.42	19.21	22.92	23.92	0	0
95	M	SqCCL	0.21	2.73	13.51	23.73	8.21	0	0
96	F	AdenoCa	1.70	2.52	7.46	38.33	6.94	1	0
97	F	AdenoCa	0.17	1.45	6.69	6.03	3.38	0	0
98	M	SqCCL	1.12	4.14	12.40	24.35	10.58	0	0
99	F	AdenoCa	2.98	2.17	16.26	30.32	11.50	0	0
100	F	SqCCL	3.21	1.73	5.33	15.42	8.25	0	1
101	M	AdenoCa	3.98	3.64	20.36	60.57	19.83	0	0
102	F	SqCCL	1.90	2.42	13.64	20.67	9.80	1	1
103	F	AdenoCa	1.55	1.77	4.77	18.22	4.81	ND	1
104	F	SqCCL	7.73	5.31	18.89	28.86	22.54	1	0
105	M	SqCCL	4.96	4.26	16.74	43.33	18.62	0	0

[1] RQ=Relative quantification value= $2^{-\Delta\Delta Ct}$. The expression of IMR90 lung fibroblasts has been used as calibrator in all genes. The mean value was deduced by triplicate experiments.

[2] Methylation status: 1= methylated (methylation index ≥5%) , 0=unmethylated (methylation index <5%)

Appendix 4 Loss of heterozygosity data on 48 NSCLC tissues.

Sample	FAL	D13S153	D13S171	D13S263	D17S938	D3S1263	D3S1289	D3S1300	D3S1566	D5S644	D9S157	D9S161
1	0.455	HET	LOH	HET	HET	LOH	HET	LOH	LOH	LOH	HET	HET
2	0.857	LOH	LOH	LOH	LOH	HET			LOH		LOH	
3	0.857		HET			LOH	LOH	LOH	LOH	LOH	LOH	
4	0.375		HET	HET	LOH	HET	HET		HET	LOH	LOH	
5	0.400	HET	HET		HET	HET	HET	LOH	HET	LOH	LOH	LOH
6	0.625	HET		HET	LOH	LOH	LOH	LOH		LOH		HET
7	0.500	LOH	LOH	LOH	HET	HET	HET	HET		HET	LOH	LOH
8	0.778		LOH	LOH	HET	LOH		LOH	LOH	HET	LOH	LOH
9	0.000	HET	HET	HET	HET	HET	HET	HET	HET	HET	HET	
10	1.000				LOH	LOH	LOH		LOH	LOH	LOH	LOH
11	0.909	LOH	LOH	LOH	LOH	HET	LOH	LOH	LOH	LOH	LOH	LOH
12	1.000	LOH	LOH	LOH	LOH	LOH	LOH	LOH		LOH		LOH
13	0.900	LOH		LOH	LOH	LOH	LOH	LOH	LOH	LOH	LOH	HET
14	0.889	HET	LOH	LOH	LOH	LOH	LOH		LOH	LOH		LOH
15	0.000	HET	HET	HET	HET	HET		HET	HET	HET	HET	HET
16	0.600	HET	HET	HET	LOH	LOH	LOH	LOH	LOH	LOH		HET
17	0.143	HET		HET		LOH	HET			HET	HET	HET
18	1.000	LOH			LOH	LOH	LOH		LOH	LOH	LOH	LOH
19	0.889	LOH	LOH	LOH	LOH	LOH	LOH	LOH	HET	LOH		
20	0.818	HET	LOH	LOH	LOH	LOH	LOH	HET	LOH	LOH	LOH	LOH
21	1.000	LOH	LOH	LOH		LOH	LOH		LOH	LOH	LOH	LOH
22	0.556	LOH	LOH	LOH	LOH		HET		HET	HET	LOH	HET
23	0.500		HET	HET	HET	HET	LOH	LOH			LOH	LOH
24	0.250	LOH	HET	HET		HET	HET	LOH	HET		HET	
25	0.833			LOH				HET	LOH	LOH	LOH	LOH
26	0.000	HET		HET			HET		HET	HET	HET	HET
27	0.556	HET	HET	HET	LOH	HET			LOH	LOH	LOH	LOH
28	0.375	HET	HET	HET	LOH		LOH			HET	LOH	HET
29	0.333	HET		LOH	LOH	HET		HET	HET	LOH	HET	HET
30	0.556	HET	HET	HET		LOH	LOH		HET	LOH	LOH	LOH
31	0.636	HET	HET	HET	LOH	LOH	LOH	LOH	LOH	HET	LOH	LOH
32	1.000	LOH	LOH	LOH	LOH	LOH	LOH	LOH	LOH	LOH	LOH	
33	0.900	LOH	LOH		LOH	LOH	LOH	HET	LOH	LOH	LOH	LOH
34	0.900		LOH	LOH	LOH	LOH	LOH	LOH	LOH	HET	LOH	LOH
35	1.000	LOH	LOH	LOH	LOH	LOH		LOH		LOH	LOH	
36	1.000	LOH		LOH	LOH	LOH	LOH	LOH	LOH	LOH	LOH	LOH
37	1.000	LOH		LOH	LOH	LOH	LOH	LOH		LOH	LOH	LOH
38	0.714	HET		LOH	LOH	HET	LOH			LOH	LOH	
39	0.182	HET	HET	HET	HET	HET	HET	HET	HET	HET	LOH	LOH
40	0.300	HET		HET	LOH	HET	HET	HET	LOH	HET	HET	LOH
41	0.667		LOH	LOH	LOH	HET	HET		HET	LOH	LOH	LOH
42	0.700	LOH	HET	HET		LOH	LOH	LOH	LOH	HET	LOH	LOH
43	0.636	LOH	HET	HET	LOH	LOH	LOH	LOH	LOH	LOH	HET	HET
44	0.100	HET	HET	HET	HET	HET	HET	HET		HET	HET	LOH
45	0.182	HET	LOH	HET	HET	HET	HET	HET	HET	HET	LOH	HET
46	0.714	LOH	LOH			HET		LOH	HET	LOH		LOH
47	0.778	HET		LOH	HET	LOH	LOH	LOH	LOH	LOH		LOH
48	0.667	HET		HET	LOH	LOH	LOH	LOH	LOH	HET		LOH

LOH: loss of heterozygosity, HET: heterozygous, blank cells: homozygous (non-informative). FAL: fractional allele loss.

List of Reagents

ANTIBIOTICS

Name	Company	Cat. number
Ampicilin	Sigma Aldrich	A9518
Blasticidin	Invitrogen	R21001
G418	Promega	V7983
Kanamycin	Sigma Aldrich	K4000

ANTIBODIES

Name	Company	Cat. number
Anti-tubulin α goat Ab P-16	Santa Cruz	SC-31779
HRP-rabbit anti-mouse secondary antibody	Abcam	AB6728
Rabbit polyclonal anti-goat Ab HRP coupled	Abcam	AB6741
UHRF1 mouse antibody	Abcam	ab57083

CHEMICAL REAGENTS

Name	Company	Cat. number
5-Aza-2′-deoxycytidine	Sigma Aldrich	A3656
Acetic Acid	Fisher Chemicals	BP2401
Agar	Gibco BRL	30391-023
Agarose	Fisher Bioreagents	BPE-1356-50
Annealing Buffer	Biotage	40-0036
Betaine	Sigma Aldrich	B0300
Binding Buffer	Biotage	40-0033
Boric Acid (H_2BO_3)	Fluka	15663
Bovine serum Albumine (BSA)	Sigma Aldrich	A7906
Chloroform	BDH	100776B
Deoxycholate sodium	Sigma Aldrich	D6750
Dextran blue	Sigma Aldrich	D5751
Doxycycline hyclate	Sigma Aldrich	44577-1G
EDTA	BDH	100935V
Ethanol	Department of Chemistry, UoL	UN1170
Glycerol	Sigma Aldrich	G6279
Hi-Di™ Formamide	Applied Biosystems	4311320
Hydrogen chloride (HCl)	BDH	101254H
Isopropanol	Fisher Scientific	P17490/17
Leupeptin	Sigma Aldrich	L2884

Low-melting point agarose	Sigma Aldrich	A9414
Methanol	BDH	10158BG
Nonidet P-40	BDH	56009
NuPAGE® Antioxidant	Invitrogen	NP0005
NuPAGE® LDS Sample Preparation Buffer	Invitrogen	MP0007
NuPAGE® MES SDS Running Buffer	Invitrogen	NP0002
NuPage® Sample Reducing Agent	Invitrogen	NP0009
NuPAGE® Tris-Acetate SDS Running Buffer	Invitrogen	LA0041
Phenol : chloroform : isoamyl alcohol (50:49:1)	Fisher Bioreagents	BPE-1752p-400
Phenylmethanesulfonyl (PMSF)	Sigma Aldrich	P7626
Phosphate Buffered Saline (PBS)	Invitrogen	18912-014
SafeView solution	NBS Biologicals	NBS-SV1
Simple Blue™ SafeStain	Invitrogen	LC6060
Sodium chloride (NaCl)	Sigma Aldrich	S9625
Sodium dodecyl sulphate (SDS)	BDH	444464T
Sodium flouride (NaF)	Fluka	71519
Sodium hydroxide (NaOH)	Fluka	7169
Sodium orthovanadate (Na_3VO_4)	Sigma Aldrich	S6508
Streptavidin Coated Dynabeads	Invitrogen	112-05D
Thiazolyl Blue Tetrazolium Bromide (MTT)	Sigma Aldrich	M5655
Trichostatin A	Sigma Aldrich	T8552
Trizma® Acetate	Fluka	93337
Trizma® base	Sigma Aldrich	T1503
Trypton	BIO101	3066-022
Tween 20	Sigma Aldrich	P7949
Yeast extract	Gibco BRL	30393-029
Yeast tRNA	Invitrogen	15401-011

ENZYMES AND BUFFERS

Name	Company	Cat. number
Alkaline phosphatase	NEB	M0290S
Apa I	NEB	R0114S
Bgl II	NEB	R0144S
EcoR I	NEB	R0101S
Hind III	NEB	R0104S
NEB buffer 2	NEB	B7002S
NEB buffer 3	NEB	B7003S
NEB buffer 4	NEB	B7004S
PCR buffer	Roche	11 699 105 001
Proteinase K	Qiagen	19133
RNase A	Qiagen	19101

Sal I	NEB	R0138S
T4 DNA Ligase	NEB	M0202S
T4 ligase reaction buffer	NEB	B0202S
XhoI	NEB	R0146S

KITS AND ASSAYS

Name	Company	Cat. number
Agilent RNA 6000 Nano Kit	Agilent	5067-1511
DC Biorad Assay	Biorad	500-0119
DNeasy Blood and Tissue kit (96-well protocol)	Qiagen	69581
DNeasy Blood and Tissue kit (Spin column protocol)	Qiagen	69504
ECL Western Blotting Detection Reagents	GE Healthcare	RPN2109
EZ DNA Methylation-Gold™ kit	Zymo Research	D5005
EZ-96 DNA Methylation-Gold™ Kit	Zymo Research	D5007
High Capacity cDNA Reverse Transcription Kit	Applied Biosystems	4368813
HotStarTaq Plus DNA Polymerase Master Mix Kit	Qiagen	203645
Mini RNA Isolation II Kit™	Zymo Research	R1030
Multiplex PCR Master Mix	Qiagen	206143
ProtoBlock Solution	National Diagnostics	CL-252
Pyro Gold™ SQA Reagents	Qiagen	40-0045
QIAquick Gel Extraction Kit	Qiagen	28704
QIAquick Nucleotide Removal Kit	Qiagen	28304
Quantitect reverse transcription kit	Qiagen	205311
R.E.A.L.® Prep 96 Kit	Qiagen	26171
RNeasy Mini Kit	Qiagen	74104
TaqMan® Gene Expression Master Mix	Applied Biosystems	4369542
BigDye® Terminator v3.1 Cycle Sequencing Kit	Applied Biosystems	4337456
TURBO DNAse Free kit	Ambion	AM1907
Venor®GeM-qEP Mycoplasma PCR Detection Kit	Minerva Biolabs	11-4025
Zyppy Plasmid Miniprep kit	Zymo Research	D4036
Zyppy™ Plasmid Maxiprep Kit	Zymo Research	D4028

MOLECULAR MASS LADDERS

Name	Company	Cat. number
Full Range Amersham™ Rainbow™ Marker	GE Healthcare	RPN800E
HyperLadder I	Bioline	BIO-33025
HyperLadder IV	Bioline	BIO-33029
λ DNA-HindIII Digest	NEB	N3012L
ROX400 size standard	Applied Biosystems	402985

PLASMIDS AND BACTERIA

Name	Company	Cat. number
One Shot® TOP10 Chemically Competent *E. coli* bacteria	Invitrogen	C4040-10
pCMV/Bsd vector	Invitrogen	V51020

PRIMERS

Name	Company	Cat. number
Actin-β (ACTB)	Applied Biosystems	4326315E
DNMT1	Applied Biosystems	Hs00945898_g1
DNMT3A	Applied Biosystems	Hs01027167_g1
DNMT3B	Applied Biosystems	Hs01003404_g1
E2F1	Applied Biosystems	HS01566605_g1
UHRF1	Applied Biosystems	Hs00273589_m1

TISSUE CULTURE MEDIA AND REAGENTS

Name	Company	Cat. number
Attractene Transfection Reagent	Qiagen	301007
Cell Freezing Medium Serum-free	Sigma Aldrich	C2639
D-MEM/F-12, liquid 1:1 with Glutamax™-L	Invitrogen	31331-093
Dulbecco Phosphate Buffered Saline (DPBS)	Invitrogen	14040-174
Foetal bovine serum	Biosera	S1810
Keratinocyte-SFM medium	Invitrogen	17005-59
Supplements for K-SFM medium	Invitrogen	37005-059
*Trans*IT®-2020 Transfection Reagent	Mirus	MIR 5404
Tryple Express	Gibco Invitrogen	12605-036

Bibliography

1. Aapola U, Kawasaki K, Scott HS, et al. Isolation and initial characterization of a novel zinc finger gene, DNMT3L, on 21q22.3, related to the cytosine-5-methyltransferase 3 gene family. Genomics 2000; 65: 293-8.

2. Appleton K, Mackay HJ, Judson I, et al. Phase I and pharmacodynamic trial of the DNA methyltransferase inhibitor decitabine and carboplatin in solid tumours. J Clin Oncol 2007; 25: 4603-9.

3. Arima Y, Hirota T, Bronner C, et al. Down-regulation of nuclear protein ICBP90 by p53/p21Cip1/WAF1-dependent DNA-damage checkpoint signals contributes to cell cycle arrest at G1/S transition. Genes Cells 2004; 9: 131-42.

4. Arita K, Ariyoshi M, Tochio H, Nakamura Y, Shirakawa M. Recognition of hemi-methylated DNA by the SRA protein UHRF1 by a base-flipping mechanism. Nature 2008; 455: 818-21.

5. Aviel-Ronen S, Blackhall FH, Shepherd FA, Tsao MS. K-ras mutations in non-small-cell lung carcinoma: a review. Clin Lung Cancer 2006; 8: 30-8.

6. Avvakumov GV, Walker JR, Xue S, et al. Structural basis for recognition of hemi-methylated DNA by the SRA domain of human UHRF1. Nature 2008; 455: 822-5.

7. Babushok DV, Kazazian HH, Jr. Progress in understanding the biology of the human mutagen LINE-1. Hum Mutat 2007; 28: 527-39.

8. Bailey-Wilson JE, Amos CI, Pinney SM, et al. A major lung cancer susceptibility locus maps to chromosome 6q23-25. Am J Hum Genet 2004; 75: 460-74.

9. Barreto G, Schafer A, Marhold J, et al. Gadd45a promotes epigenetic gene activation by repair-mediated DNA demethylation. Nature 2007; 445: 671-5.

10. Beasley MB, Brambilla E, Travis WD. The 2004 World Health Organization classification of lung tumours. Semin Roentgenol 2005; 40: 90-7.

11. Belgnaoui SM, Gosden RG, Semmes OJ, Haoudi A. Human LINE-1 retrotransposon induces DNA damage and apoptosis in cancer cells. Cancer Cell Int 2006; 6: 13.

12. Bestor TH. Cloning of a mammalian DNA methyltransferase. Gene 1988; 74: 9-12.

13. Bestor TH. The DNA methyltransferases of mammals. Hum Mol Genet 2000; 9: 2395-402.

14. Bhattacharya SK, Ramchandani S, Cervoni N, Szyf M. A mammalian protein with specific demethylase activity for mCpG DNA. Nature 1999; 397: 579-83.

15. Bird AP, Wolffe AP. Methylation-induced repression--belts, braces, and chromatin. Cell 1999; 99: 451-4.

16. Bonapace IM, Latella L, Papait R, et al. Np95 is regulated by E1A during mitotic reactivation of terminally differentiated cells and is essential for S phase entry. J Cell Biol 2002; 157: 909-14.

17. Bostick M, Kim JK, Esteve PO, Clark A, Pradhan S, Jacobsen SE. UHRF1 plays a role in maintaining DNA methylation in mammalian cells. Science 2007; 317: 1760-4.

18. Bourc'his D, Bestor TH. Meiotic catastrophe and retrotransposon reactivation in male germ cells lacking Dnmt3L. Nature 2004; 431: 96-9.

19. Boyes J, Bird A. DNA methylation inhibits transcription indirectly via a methyl-CpG binding protein. Cell 1991; 64: 1123-34.

20. Bratthauer GL, Cardiff RD, Fanning TG. Expression of LINE-1 retrotransposons in human breast cancer. Cancer 1994; 73: 2333-6.

21. Brena RM, Costello JF. Genome-epigenome interactions in cancer. Hum Mol Genet 2007; 16 Spec No 1: R96-105.

22. Breuer RH, Postmus PE, Smit EF. Molecular pathology of non-small-cell lung cancer. Respiration 2005; 72: 313-30.

23. Bronner C, Achour M, Arima Y, Chataigneau T, Saya H, Schini-Kerth VB. The UHRF family: oncogenes that are drugable targets for cancer therapy in the near future? Pharmacol Ther 2007; 115: 419-34.

24. Brouha B, Meischl C, Ostertag E, et al. Evidence consistent with human L1 retrotransposition in maternal meiosis I. Am J Hum Genet 2002; 71: 327-36.

25. Brouha B, Schustak J, Badge RM, et al. Hot L1s account for the bulk of retrotransposition in the human population. Proc Natl Acad Sci U S A 2003; 100: 5280-5.

26. Brown KD, Robertson KD. DNMT1 knockout delivers a strong blow to genome stability and cell viability. Nat Genet 2007; 39: 289-90.

27. Bruske-Hohlfeld I. Environmental and occupational risk factors for lung cancer. Methods Mol Biol 2009; 472: 3-23.

28. Burris HA, 3rd. Shortcomings of current therapies for non-small-cell lung cancer: unmet medical needs. Oncogene 2009; 28 Suppl 1: S4-13.

29. Cassidy A, Myles JP, van Tongeren M, et al. The LLP risk model: an individual risk prediction model for lung cancer. Br J Cancer 2008; 98: 270-6.

30. Chalitchagorn K, Shuangshoti S, Hourpai N, et al. Distinctive pattern of LINE-1 methylation level in normal tissues and the association with carcinogenesis. Oncogene 2004; 23: 8841-6.

31. Chen T, Li E. Establishment and maintenance of DNA methylation patterns in mammals. Curr Top Microbiol Immunol 2006; 301: 179-201.

32. Chen T, Ueda Y, Dodge JE, Wang Z, Li E. Establishment and maintenance of genomic methylation patterns in mouse embryonic stem cells by Dnmt3a and Dnmt3b. Mol Cell Biol 2003; 23: 5594-605.

33. Cheng X, Blumenthal RM. Mammalian DNA methyltransferases: a structural perspective. Structure 2008; 16: 341-50.

34. Cheng X, Kumar S, Posfai J, Pflugrath JW, Roberts RJ. Crystal structure of the Hhal DNA methyltransferase complexed with S-adenosyl-L-methionine. Cell 1993; 74: 299-307.

35. Cheng X, Roberts RJ. AdoMet-dependent methylation, DNA methyltransferases and base flipping. Nucleic Acids Res 2001; 29: 3784-95.

36. Cho NY, Kim BH, Choi M, et al. Hypermethylation of CpG island loci and hypomethylation of LINE-1 and Alu repeats in prostate adenocarcinoma and their relationship to clinicopathological features. J Pathol 2007; 211: 269-77.

37. Choi IS, Estecio MR, Nagano Y, et al. Hypomethylation of LINE-1 and Alu in well-differentiated neuroendocrine tumours (pancreatic endocrine tumours and carcinoid tumours). Mod Pathol 2007; 20: 802-10.

38. Cordaux R, Batzer MA. The impact of retrotransposons on human genome evolution. Nat Rev Genet 2009; 10: 691-703.

39. Costello JF, Fruhwald MC, Smiraglia DJ, et al. Aberrant CpG-island methylation has non-random and tumour-type-specific patterns. Nat Genet 2000; 24: 132-8.

40. Crnogorac-Jurcevic T, Gangeswaran R, Bhakta V, et al. Proteomic analysis of chronic pancreatitis and pancreatic adenocarcinoma. Gastroenterology 2005; 129: 1454-63.

41. CRUK. Cancer Stats. CRUK website 2007.

42. Daskalakis M, Nguyen TT, Nguyen C, et al. Demethylation of a hypermethylated P15/INK4B gene in patients with myelodysplastic syndrome by 5-Aza-2'-deoxycytidine (decitabine) treatment. Blood 2002; 100: 2957-64.

43. Dewannieux M, Esnault C, Heidmann T. LINE-mediated retrotransposition of marked Alu sequences. Nat Genet 2003; 35: 41-8.

44. Eden A, Gaudet F, Waghmare A, Jaenisch R. Chromosomal instability and tumours promoted by DNA hypomethylation. Science 2003; 300: 455.

45. Ehrlich M. DNA methylation in cancer: too much, but also too little. Oncogene 2002; 21: 5400-13.

46. Ehrlich M, Woods CB, Yu MC, et al. Quantitative analysis of associations between DNA hypermethylation, hypomethylation, and DNMT RNA levels in ovarian tumours. Oncogene 2006; 25: 2636-45.

47. el-Deiry WS, Nelkin BD, Celano P, et al. High expression of the DNA methyltransferase gene characterizes human neoplastic cells and progression stages of colon cancer. Proc Natl Acad Sci U S A 1991; 88: 3470-4.

48. Esnault C, Heidmann O, Delebecque F, et al. APOBEC3G cytidine deaminase inhibits retrotransposition of endogenous retroviruses. Nature 2005; 433: 430-3.

49. Estecio MR, Gharibyan V, Shen L, et al. LINE-1 hypomethylation in cancer is highly variable and inversely correlated with microsatellite instability. PLoS ONE 2007; 2: e399.

50. Esteller M. Epigenetic gene silencing in cancer: the DNA hypermethylome. Hum Mol Genet 2007; 16 Spec No 1: R50-9.

51. Esteller M. Epigenetics in cancer. N Engl J Med 2008; 358: 1148-59.

52. Esteller M, Sanchez-Cespedes M, Rosell R, Sidransky D, Baylin SB, Herman JG. Detection of aberrant promoter hypermethylation of tumour suppressor genes in serum DNA from non-small cell lung cancer patients. Cancer Res 1999; 59: 67-70.

53. Feinberg AP, Ohlsson R, Henikoff S. The epigenetic progenitor origin of human cancer. Nat Rev Genet 2006; 7: 21-33.

54. Feinberg AP, Vogelstein B. Hypomethylation distinguishes genes of some human cancers from their normal counterparts. Nature 1983; 301: 89-92.

55. Ferlay J, Autier P, Boniol M, Heanue M, Colombet M, Boyle P. Estimates of the cancer incidence and mortality in Europe in 2006. Ann Oncol 2007; 18: 581-92.

56. Field JK, Liloglou T, Warrak S, et al. Methylation discriminators in NSCLC identified by a microarray based approach. Int J Oncol 2005; 27: 105-11.

57. Florl AR, Lower R, Schmitz-Drager BJ, Schulz WA. DNA methylation and expression of LINE-1 and HERV-K provirus sequences in urothelial and renal cell carcinomas. Br J Cancer 1999; 80: 1312-21.

58. Foltz G, Yoon JG, Lee H, et al. DNA methyltransferase-mediated transcriptional silencing in malignant glioma: a combined whole-genome microarray and promoter array analysis. Oncogene 2009; 28: 2667-77.

59. Fraga MF, Herranz M, Espada J, et al. A mouse skin multistage carcinogenesis model reflects the aberrant DNA methylation patterns of human tumours. Cancer Res 2004; 64: 5527-34.

60. Fujimori A, Matsuda Y, Takemoto Y, et al. Cloning and mapping of Np95 gene which encodes a novel nuclear protein associated with cell proliferation. Mamm Genome 1998; 9: 1032-5.

61. Garcia-Perez JL, Marchetto MC, Muotri AR, et al. LINE-1 retrotransposition in human embryonic stem cells. Hum Mol Genet 2007; 16: 1569-77.

62. Gaudet F, Hodgson JG, Eden A, et al. Induction of tumours in mice by genomic hypomethylation. Science 2003; 300: 489-92.

63. Geback T, Schulz MM, Koumoutsakos P, Detmar M. TScratch: a novel and simple software tool for automated analysis of monolayer wound healing assays. Biotechniques 2009; 46: 265-74.

64. Geradts J, Fong KM, Zimmerman PV, Minna JD. Loss of Fhit expression in non-small-cell lung cancer: correlation with molecular genetic abnormalities and clinicopathological features. Br J Cancer 2000; 82: 1191-7.

65. Gilbert N, Lutz-Prigge S, Moran JV. Genomic deletions created upon LINE-1 retrotransposition. Cell 2002; 110: 315-25.

66. Girault I, Tozlu S, Lidereau R, Bieche I. Expression analysis of DNA methyltransferases 1, 3A, and 3B in sporadic breast carcinomas. Clin Cancer Res 2003; 9: 4415-22.

67. Glasspool RM, Teodoridis JM, Brown R. Epigenetics as a mechanism driving polygenic clinical drug resistance. Br J Cancer 2006; 94: 1087-92.

68. Goll MG, Bestor TH. Eukaryotic cytosine methyltransferases. Annu Rev Biochem 2005; 74: 481-514.

69. Goll MG, Kirpekar F, Maggert KA, et al. Methylation of tRNAAsp by the DNA methyltransferase homolog Dnmt2. Science 2006; 311: 395-8.

70. Gonzalo S, Jaco I, Fraga MF, et al. DNA methyltransferases control telomere length and telomere recombination in mammalian cells. Nat Cell Biol 2006; 8: 416-24.

71. Goodier JL, Zhang L, Vetter MR, Kazazian HH, Jr. LINE-1 ORF1 protein localizes in stress granules with other RNA-binding proteins, including components of RNA interference RNA-induced silencing complex. Mol Cell Biol 2007; 27: 6469-83.

72. Hall GL, Shaw RJ, Field EA, et al. p16 Promoter methylation is a potential predictor of malignant transformation in oral epithelial dysplasia. Cancer Epidemiol Biomarkers Prev 2008; 17: 2174-9.

73. Hamilton W, Peters TJ, Round A, Sharp D. What are the clinical features of lung cancer before the diagnosis is made? A population based case-control study. Thorax 2005; 60: 1059-65.

74. Hamm S, Just G, Lacoste N, Moitessier N, Szyf M, Mamer O. On the mechanism of demethylation of 5-methylcytosine in DNA. Bioorg Med Chem Lett 2008; 18: 1046-9.

75. Han JS, Szak ST, Boeke JD. Transcriptional disruption by the L1 retrotransposon and implications for mammalian transcriptomes. Nature 2004; 429: 268-74.

76. Haoudi A, Semmes OJ, Mason JM, Cannon RE. Retrotransposition-Competent Human LINE-1 Induces Apoptosis in Cancer Cells With Intact p53. J Biomed Biotechnol 2004; 2004: 185-94.

77. Hecht SS. Cigarette smoking and lung cancer: chemical mechanisms and approaches to prevention. Lancet Oncol 2002; 3: 461-9.

78. Hermann A, Schmitt S, Jeltsch A. The human Dnmt2 has residual DNA-(cytosine-C5) methyltransferase activity. J Biol Chem 2003; 278: 31717-21.

79. Hoffman PC, Mauer AM, Vokes EE. Lung cancer. Lancet 2000; 355: 479-85.

80. Hollstein M, Sidransky D, Vogelstein B, Harris CC. p53 mutations in human cancers. Science 1991; 253: 49-53.

81. Hopfner R, Mousli M, Jeltsch JM, et al. ICBP90, a novel human CCAAT binding protein, involved in the regulation of topoisomerase IIalpha expression. Cancer Res 2000; 60: 121-8.

82. Hopfner R, Mousli M, Oudet P, Bronner C. Overexpression of ICBP90, a novel CCAAT-binding protein, overcomes cell contact inhibition by forcing topoisomerase II alpha expression. Anticancer Res 2002; 22: 3165-70.

83. Howard G, Eiges R, Gaudet F, Jaenisch R, Eden A. Activation and transposition of endogenous retroviral elements in hypomethylation induced tumours in mice. Oncogene 2008; 27: 404-8.

84. Hung RJ, McKay JD, Gaborieau V, et al. A susceptibility locus for lung cancer maps to nicotinic acetylcholine receptor subunit genes on 15q25. Nature 2008; 452: 633-7.

85. Issa JP. DNA methylation as a therapeutic target in cancer. Clin Cancer Res 2007; 13: 1634-7.

86. Issa JP, Kantarjian HM. Targeting DNA methylation. Clin Cancer Res 2009; 15: 3938-46.

87. Jackman DM, Johnson BE. Small-cell lung cancer. Lancet 2005; 366: 1385-96.

88. Jeanblanc M, Mousli M, Hopfner R, et al. The retinoblastoma gene and its product are targeted by ICBP90: a key mechanism in the G1/S transition during the cell cycle. Oncogene 2005; 24: 7337-45.

89. Jeltsch A. On the enzymatic properties of Dnmt1: specificity, processivity, mechanism of linear diffusion and allosteric regulation of the enzyme. Epigenetics 2006; 1: 63-6.

90. Jemal A, Siegel R, Ward E, Hao Y, Xu J, Thun MJ. Cancer statistics, 2009. CA Cancer J Clin 2009; 59: 225-49.

91. Jenkins Y, Markovtsov V, Lang W, et al. Critical role of the ubiquitin ligase activity of UHRF1, a nuclear RING finger protein, in tumour cell growth. Mol Biol Cell 2005; 16: 5621-9.

92. Jin W, Chen L, Chen Y, et al. UHRF1 is associated with epigenetic silencing of BRCA1 in sporadic breast cancer. Breast Cancer Res Treat 2009.

93. Jones PA, Baylin SB. The fundamental role of epigenetic events in cancer. Nat Rev Genet 2002; 3: 415-28.

94. Jones PA, Baylin SB. The epigenomics of cancer. Cell 2007; 128: 683-92.

95. Jones PA, Liang G. Rethinking how DNA methylation patterns are maintained. Nat Rev Genet 2009; 10: 805-11.

96. Jones PL, Veenstra GJ, Wade PA, et al. Methylated DNA and MeCP2 recruit histone deacetylase to repress transcription. Nat Genet 1998; 19: 187-91.

97. Jost JP. Nuclear extracts of chicken embryos promote an active demethylation of DNA by excision repair of 5-methyldeoxycytidine. Proc Natl Acad Sci U S A 1993; 90: 4684-8.

98. Jurka J. Evolutionary impact of human Alu repetitive elements. Curr Opin Genet Dev 2004; 14: 603-8.

99. Kangaspeska S, Stride B, Metivier R, et al. Transient cyclical methylation of promoter DNA. Nature 2008; 452: 112-5.

100. Kazazian HH, Jr. Mobile elements: drivers of genome evolution. Science 2004; 303: 1626-32.

101. Kazazian HH, Jr., Goodier JL. LINE drive. retrotransposition and genome instability. Cell 2002; 110: 277-80.

102. Kim DS, Kim MJ, Lee JY, Kim YZ, Kim EJ, Park JY. Aberrant methylation of E-cadherin and H-cadherin genes in nonsmall cell lung cancer and its relation to clinicopathologic features. Cancer 2007; 110: 2785-92.

103. Kim H, Kwon YM, Kim JS, et al. Elevated mRNA levels of DNA methyltransferase-1 as an independent prognostic factor in primary nonsmall cell lung cancer. Cancer 2006; 107: 1042-9.

104. Kimura F, Seifert HH, Florl AR, et al. Decrease of DNA methyltransferase 1 expression relative to cell proliferation in transitional cell carcinoma. Int J Cancer 2003; 104: 568-78.

105. Knight LJ, Burrage J, Bujac SR, et al. Epigenetic silencing of the endothelin-B receptor gene in non-small cell lung cancer. Int J Oncol 2009; 34: 465-71.

106. Kolomietz E, Meyn MS, Pandita A, Squire JA. The role of Alu repeat clusters as mediators of recurrent chromosomal aberrations in tumours. Genes Chromosomes Cancer 2002; 35: 97-112.

107. Lander ES, Linton LM, Birren B, et al. Initial sequencing and analysis of the human genome. Nature 2001; 409: 860-921.

108. Levanon K, Eisenberg E, Rechavi G, Levanon EY. Letter from the editor: Adenosine-to-inosine RNA editing in Alu repeats in the human genome. EMBO Rep 2005; 6: 831-5.

109. Li LH, Olin EJ, Buskirk HH, Reineke LM. Cytotoxicity and mode of action of 5-azacytidine on L1210 leukemia. Cancer Res 1970; 30: 2760-9.

110. Liang G, Chan MF, Tomigahara Y, et al. Cooperativity between DNA methyltransferases in the maintenance methylation of repetitive elements. Mol Cell Biol 2002; 22: 480-91.

111. Liloglou T, Maloney P, Xinarianos G, Fear S, Field JK. Sensitivity and limitations of high throughput fluorescent microsatellite analysis for the detection of allelic imbalance: application in lung tumours. Int J Oncol 2000; 16: 5-14.

112. Liloglou T, Maloney P, Xinarianos G, et al. Cancer-specific genomic instability in bronchial lavage: a molecular tool for lung cancer detection. Cancer Res 2001; 61: 1624-8.

113. Lin CS, Goldthwait DA, Samols D. Identification of Alu transposition in human lung carcinoma cells. Cell 1988; 54: 153-9.

114. Lin RK, Hsu HS, Chang JW, Chen CY, Chen JT, Wang YC. Alteration of DNA methyltransferases contributes to 5'CpG methylation and poor prognosis in lung cancer. Lung Cancer 2007; 55: 205-13.

115. Lips EH, Gaborieau V, McKay JD, et al. Association between a 15q25 gene variant, smoking quantity and tobacco-related cancers among 17 000 individuals. Int J Epidemiol 2010; 39: 563-77.

116. Littman AJ, Thornquist MD, White E, Jackson LA, Goodman GE, Vaughan TL. Prior lung disease and risk of lung cancer in a large prospective study. Cancer Causes Control 2004; 15: 819-27.

117. Lopez-Serra L, Esteller M. Proteins that bind methylated DNA and human cancer: reading the wrong words. Br J Cancer 2008; 98: 1881-5.

118. Lyko F, Brown R. DNA methyltransferase inhibitors and the development of epigenetic cancer therapies. J Natl Cancer Inst 2005; 97: 1498-506.

119. Matakidou A, Eisen T, Houlston RS. Systematic review of the relationship between family history and lung cancer risk. Br J Cancer 2005; 93: 825-33.

120. McCabe MT, Davis JN, Day ML. Regulation of DNA methyltransferase 1 by the pRb/E2F1 pathway. Cancer Res 2005; 65: 3624-32.

121. McKay JD, Hung RJ, Gaborieau V, et al. Lung cancer susceptibility locus at 5p15.33. Nat Genet 2008; 40: 1404-6.

122. Meilinger D, Fellinger K, Bultmann S, et al. Np95 interacts with de novo DNA methyltransferases, Dnmt3a and Dnmt3b, and mediates epigenetic silencing of the viral CMV promoter in embryonic stem cells. EMBO Rep 2009; 10: 1259-64.

123. Metivier R, Gallais R, Tiffoche C, et al. Cyclical DNA methylation of a transcriptionally active promoter. Nature 2008; 452: 45-50.

124. Mighell AJ, Markham AF, Robinson PA. Alu sequences. FEBS Lett 1997; 417: 1-5.

125. Miki Y, Katagiri T, Kasumi F, Yoshimoto T, Nakamura Y. Mutation analysis in the BRCA2 gene in primary breast cancers. Nat Genet 1996; 13: 245-7.

126. Miki Y, Nishisho I, Horii A, et al. Disruption of the APC gene by a retrotransposal insertion of L1 sequence in a colon cancer. Cancer Res 1992; 52: 643-5.

127. Momparler RL, Bouchard J, Onetto N, Rivard GE. 5-aza-2'-deoxycytidine therapy in patients with acute leukemia inhibits DNA methylation. Leuk Res 1984; 8: 181-5.

128. Moran JV, Holmes SE, Naas TP, DeBerardinis RJ, Boeke JD, Kazazian HH, Jr. High frequency retrotransposition in cultured mammalian cells. Cell 1996; 87: 917-27.

129. Morey Kinney SR, Smiraglia DJ, James SR, Moser MT, Foster BA, Karpf AR. Stage-specific alterations of DNA methyltransferase expression, DNA hypermethylation, and DNA hypomethylation during prostate cancer progression in the transgenic adenocarcinoma of mouse prostate model. Mol Cancer Res 2008; 6: 1365-74.

130. Morrish TA, Garcia-Perez JL, Stamato TD, Taccioli GE, Sekiguchi J, Moran JV. Endonuclease-independent LINE-1 retrotransposition at mammalian telomeres. Nature 2007; 446: 208-12.

131. Morrish TA, Gilbert N, Myers JS, et al. DNA repair mediated by endonuclease-independent LINE-1 retrotransposition. Nat Genet 2002; 31: 159-65.

132. Mortusewicz O, Schermelleh L, Walter J, Cardoso MC, Leonhardt H. Recruitment of DNA methyltransferase I to DNA repair sites. Proc Natl Acad Sci U S A 2005; 102: 8905-9.

133. Mousli M, Hopfner R, Abbady AQ, et al. ICBP90 belongs to a new family of proteins with an expression that is deregulated in cancer cells. Br J Cancer 2003; 89: 120-7.

134. Muckenfuss H, Hamdorf M, Held U, et al. APOBEC3 proteins inhibit human LINE-1 retrotransposition. J Biol Chem 2006; 281: 22161-72.

135. Nan X, Ng HH, Johnson CA, et al. Transcriptional repression by the methyl-CpG-binding protein MeCP2 involves a histone deacetylase complex. Nature 1998; 393: 386-9.

136. Nosho K, Irahara N, Shima K, et al. Comprehensive biostatistical analysis of CpG island methylator phenotype in colorectal cancer using a large population-based sample. PLoS One 2008; 3: e3698.

137. Ogino S, Kawasaki T, Nosho K, et al. LINE-1 hypomethylation is inversely associated with microsatellite instability and CpG island methylator phenotype in colorectal cancer. Int J Cancer 2008; 122: 2767-73.

138. Okano M, Bell DW, Haber DA, Li E. DNA methyltransferases Dnmt3a and Dnmt3b are essential for de novo methylation and mammalian development. Cell 1999; 99: 247-57.

139. Oki Y, Jelinek J, Shen L, Kantarjian HM, Issa JP. Induction of hypomethylation and molecular response after decitabine therapy in patients with chronic myelomonocytic leukemia. Blood 2008; 111: 2382-4.

140. Ooi SK, Bestor TH. The colorful history of active DNA demethylation. Cell 2008; 133: 1145-8.

141. Ooi SK, Bestor TH. Cytosine methylation: remaining faithful. Curr Biol 2008; 18: R174-6.

142. Ooi SK, Qiu C, Bernstein E, et al. DNMT3L connects unmethylated lysine 4 of histone H3 to de novo methylation of DNA. Nature 2007; 448: 714-7.

143. Ostertag EM, Kazazian HH, Jr. Biology of mammalian L1 retrotransposons. Annu Rev Genet 2001; 35: 501-38.

144. Oyer JA, Chu A, Brar S, Turker MS. Aberrant epigenetic silencing is triggered by a transient reduction in gene expression. PLoS ONE 2009; 4: e4832.

145. Park HJ, Yu E, Shim YH. DNA methyltransferase expression and DNA hypermethylation in human hepatocellular carcinoma. Cancer Lett 2006; 233: 271-8.

146. Parkin DM, Bray F, Ferlay J, Pisani P. Global cancer statistics, 2002. CA Cancer J Clin 2005; 55: 74-108.

147. Plimack ER, Kantarjian HM, Issa JP. Decitabine and its role in the treatment of hematopoietic malignancies. Leuk Lymphoma 2007; 48: 1472-81.

148. Qin T, Youssef EM, Jelinek J, et al. Effect of cytarabine and decitabine in combination in human leukemic cell lines. Clin Cancer Res 2007; 13: 4225-32.

149. Qu GZ, Ehrlich M. Demethylation and expression of methylated plasmid DNA stably transfected into HeLa cells. Nucleic Acids Res 1999; 27: 2332-8.

150. Rauch T, Wang Z, Zhang X, et al. Homeobox gene methylation in lung cancer studied by genome-wide analysis with a microarray-based methylated CpG island recovery assay. Proc Natl Acad Sci U S A 2007; 104: 5527-32.

151. Rauch TA, Zhong X, Wu X, et al. High-resolution mapping of DNA hypermethylation and hypomethylation in lung cancer. Proc Natl Acad Sci U S A 2008; 105: 252-7.

152. Rhee I, Bachman KE, Park BH, et al. DNMT1 and DNMT3b cooperate to silence genes in human cancer cells. Nature 2002; 416: 552-6.

153. Richardson GE, Johnson BE. The biology of lung cancer. Semin Oncol 1993; 20: 105-27.

154. Risch A, Plass C. Lung cancer epigenetics and genetics. Int J Cancer 2008; 123: 1-7.

155. Robert MF, Morin S, Beaulieu N, et al. DNMT1 is required to maintain CpG methylation and aberrant gene silencing in human cancer cells. Nat Genet 2003; 33: 61-5.

156. Robertson KD. DNA methylation, methyltransferases, and cancer. Oncogene 2001; 20: 3139-55.

157. Robertson KD, Uzvolgyi E, Liang G, et al. The human DNA methyltransferases (DNMTs) 1, 3a and 3b: coordinate mRNA expression in normal tissues and overexpression in tumours. Nucleic Acids Res 1999; 27: 2291-8.

158. Rodriguez J, Vives L, Jorda M, et al. Genome-wide tracking of unmethylated DNA Alu repeats in normal and cancer cells. Nucleic Acids Res 2008; 36: 770-84.

159. Roman-Gomez J, Jimenez-Velasco A, Agirre X, et al. Promoter hypomethylation of the LINE-1 retrotransposable elements activates sense/antisense transcription and marks the progression of chronic myeloid leukemia. Oncogene 2005; 24: 7213-23.

160. Santos FP, Kantarjian H, Garcia-Manero G, Issa JP, Ravandi F. Decitabine in the treatment of myelodysplastic syndromes. Expert Rev Anticancer Ther 2010; 10: 9-22.

161. Sassaman DM, Dombroski BA, Moran JV, et al. Many human L1 elements are capable of retrotransposition. Nat Genet 1997; 16: 37-43.

162. Sato M, Horio Y, Sekido Y, Minna JD, Shimokata K, Hasegawa Y. The expression of DNA methyltransferases and methyl-CpG-binding proteins is not associated with the methylation status of p14(ARF), p16(INK4a) and RASSF1A in human lung cancer cell lines. Oncogene 2002; 21: 4822-9.

163. Schabath MB, Delclos GL, Martynowicz MM, et al. Opposing effects of emphysema, hay fever, and select genetic variants on lung cancer risk. Am J Epidemiol 2005; 161: 412-22.

164. Schulz WA. L1 retrotransposons in human cancers. J Biomed Biotechnol 2006; 2006: 83672.

165. Schulz WA, Steinhoff C, Florl AR. Methylation of endogenous human retroelements in health and disease. Curr Top Microbiol Immunol 2006; 310: 211-50.

166. Schwartz AG, Prysak GM, Bock CH, Cote ML. The molecular epidemiology of lung cancer. Carcinogenesis 2007; 28: 507-18.

167. Sekido Y, Fong KM, Minna JD. Molecular genetics of lung cancer. Annu Rev Med 2003; 54: 73-87.

168. Sharif J, Muto M, Takebayashi S, et al. The SRA protein Np95 mediates epigenetic inheritance by recruiting Dnmt1 to methylated DNA. Nature 2007; 450: 908-12.

169. Sharma S, Kelly TK, Jones PA. Epigenetics in cancer. Carcinogenesis 2010; 31: 27-36.

170. Sharma SV, Bell DW, Settleman J, Haber DA. Epidermal growth factor receptor mutations in lung cancer. Nat Rev Cancer 2007; 7: 169-81.

171. Shaw RJ, Akufo-Tetteh EK, Risk JM, Field JK, Liloglou T. Methylation enrichment pyrosequencing: combining the specificity of MSP with validation by pyrosequencing. Nucleic Acids Res 2006; 34: e78.

172. Shaw RJ, Liloglou T, Rogers SN, et al. Promoter methylation of P16, RARbeta, E-cadherin, cyclin A1 and cytoglobin in oral cancer: quantitative evaluation using pyrosequencing. Br J Cancer 2006; 94: 561-8.

173. Shields PG. Molecular epidemiology of smoking and lung cancer. Oncogene 2002; 21: 6870-6.

174. Soifer HS, Rossi JJ. Small interfering RNAs to the rescue: blocking L1 retrotransposition. Nat Struct Mol Biol 2006; 13: 758-9.

175. Stresemann C, Lyko F. Modes of action of the DNA methyltransferase inhibitors azacytidine and decitabine. Int J Cancer 2008; 123: 8-13.

176. Suter CM, Martin DI, Ward RL. Hypomethylation of L1 retrotransposons in colorectal cancer and adjacent normal tissue. Int J Colorectal Dis 2004; 19: 95-101.

177. Suzuki M, Sunaga N, Shames DS, Toyooka S, Gazdar AF, Minna JD. RNA interference-mediated knockdown of DNA methyltransferase 1 leads to promoter demethylation and gene re-expression in human lung and breast cancer cells. Cancer Res 2004; 64: 3137-43.

178. Symer DE, Connelly C, Szak ST, et al. Human l1 retrotransposition is associated with genetic instability in vivo. Cell 2002; 110: 327-38.

179. Unoki M, Nishidate T, Nakamura Y. ICBP90, an E2F-1 target, recruits HDAC1 and binds to methyl-CpG through its SRA domain. Oncogene 2004; 23: 7601-10.

180. Vaissiere T, Hung RJ, Zaridze D, et al. Quantitative analysis of DNA methylation profiles in lung cancer identifies aberrant DNA methylation of specific genes and its association with gender and cancer risk factors. Cancer Res 2009; 69: 243-52.

181. Vallbohmer D, Brabender J, Yang D, et al. DNA methyltransferases messenger RNA expression and aberrant methylation of CpG islands in non-small-cell lung cancer: association and prognostic value. Clin Lung Cancer 2006; 8: 39-44.

182. Virmani AK, Rathi A, Zochbauer-Muller S, et al. Promoter methylation and silencing of the retinoic acid receptor-beta gene in lung carcinomas. J Natl Cancer Inst 2000; 92: 1303-7.

183. Vogel MC, Papadopoulos T, Muller-Hermelink HK, Drahovsky D, Pfeifer GP. Intracellular distribution of DNA methyltransferase during the cell cycle. FEBS Lett 1988; 236: 9-13.

184. Vousden KH, Lane DP. p53 in health and disease. Nat Rev Mol Cell Biol 2007; 8: 275-83.

185. Wallace MR, Andersen LB, Saulino AM, Gregory PE, Glover TW, Collins FS. A de novo Alu insertion results in neurofibromatosis type 1. Nature 1991; 353: 864-6.

186. Wang J, Bhutani M, Pathak AK, et al. Delta DNMT3B variants regulate DNA methylation in a promoter-specific manner. Cancer Res 2007; 67: 10647-52.

187. Wang L, Wang J, Sun S, et al. A novel DNMT3B subfamily, DeltaDNMT3B, is the predominant form of DNMT3B in non-small cell lung cancer. Int J Oncol 2006; 29: 201-7.

188. Webster KE, O'Bryan MK, Fletcher S, et al. Meiotic and epigenetic defects in Dnmt3L-knockout mouse spermatogenesis. Proc Natl Acad Sci U S A 2005; 102: 4068-73.

189. Wei W, Gilbert N, Ooi SL, et al. Human L1 retrotransposition: cis preference versus trans complementation. Mol Cell Biol 2001; 21: 1429-39.

190. Wei W, Morrish TA, Alisch RS, Moran JV. A transient assay reveals that cultured human cells can accommodate multiple LINE-1 retrotransposition events. Anal Biochem 2000; 284: 435-8.

191. Weisenberger DJ, Campan M, Long TI, et al. Analysis of repetitive element DNA methylation by MethyLight. Nucleic Acids Res 2005; 33: 6823-36.

192. Welman A, Barraclough J, Dive C. Generation of cells expressing improved doxycycline-regulated reverse transcriptional transactivator rtTA2S-M2. Nat Protoc 2006; 1: 803-11.

193. Wild L, Flanagan JM. Genome-wide hypomethylation in cancer may be a passive consequence of transformation. Biochim Biophys Acta 2010; 1806: 50-7.

194. Wilson AS, Power BE, Molloy PL. DNA hypomethylation and human diseases. Biochim Biophys Acta 2007; 1775: 138-62.

195. Xinarianos G, McRonald FE, Risk JM, et al. Frequent genetic and epigenetic abnormalities contribute to the deregulation of cytoglobin in non-small cell lung cancer. Hum Mol Genet 2006; 15: 2038-44.

196. Xing J, Stewart DJ, Gu J, Lu C, Spitz MR, Wu X. Expression of methylation-related genes is associated with overall survival in patients with non-small cell lung cancer. Br J Cancer 2008; 98: 1716-22.

197. Yang AS, Estecio MR, Garcia-Manero G, Kantarjian HM, Issa JP. Comment on "Chromosomal instability and tumours promoted by DNA hypomethylation" and "Induction of tumours in nice by genomic hypomethylation". Science 2003; 302: 1153; author reply

198. Yang N, Kazazian HH, Jr. L1 retrotransposition is suppressed by endogenously encoded small interfering RNAs in human cultured cells. Nat Struct Mol Biol 2006; 13: 763-71.

199. Yoder JA, Soman NS, Verdine GL, Bestor TH. DNA (cytosine-5)-methyltransferases in mouse cells and tissues. Studies with a mechanism-based probe. J Mol Biol 1997; 270: 385-95.

200. Zochbauer-Muller S, Fong KM, Maitra A, et al. 5' CpG island methylation of the FHIT gene is correlated with loss of gene expression in lung and breast cancer. Cancer Res 2001; 61: 3581-5.

201. Zochbauer-Muller S, Fong KM, Virmani AK, Geradts J, Gazdar AF, Minna JD. Aberrant promoter methylation of multiple genes in non-small cell lung cancers. Cancer Res 2001; 61: 249-55.

Supporting Papers

Original Article

UHRF1-Mediated Tumor Suppressor Gene Inactivation in Nonsmall Cell Lung Cancer

Alexandros Daskalos, BSc[1]; Urszula Oleksiewicz, MSc[1]; Anastasia Filia, BSc[1]; George Nikolaidis, MSc[1]; George Xinarianos, PhD[1]; John R. Gosney, MD, PhD[2]; Angeliki Malliri, PhD[3]; John K. Field, BDS, PhD[1]; and Triantafillos Liloglou, PhD[1]

BACKGROUND: The *UHRF1* gene possesses an essential role in DNA methylation maintenance, but its contribution to tumor suppressor gene hypermethylation in primary human cancers currently remains unclear. **METHODS:** mRNA expression levels of *UHRF1*, *DNMT1*, *DNMT3A*, *DNMT3B*, and *E2F1* were evaluated in 105 primary nonsmall cell lung carcinomas by quantitative polymerase chain reaction. The methylation status of *CDKN2A* and *RASSF1* promoters was examined by pyrosequencing. *UHRF1* was knocked down by short hairpin RNA in A549 lung adenocarcinoma cells. **RESULTS:** All 4 genes were overexpressed in a coordinated manner in the lung tumor tissues, and their expression correlated with that of E2F1. Higher *UHRF1* expression in tumor tissues correlated with the hypermethylation of *CDKN2A* ($P = .005$) and *RASSF1* promoters ($P = .034$), and the relationship with a combined epigenotype was even stronger ($P = 2.3 \times 10^{-4}$). When *UHRF1* was knocked down in A549 lung adenocarcinoma cells, lower methylation levels of *RASSF1*, *CYGB*, and *CDH13* promoters were observed. Also, UHRF1 knockdown clones demonstrated reduced proliferation and decreased cell migration properties. **CONCLUSIONS:** Our data demonstrate that *UHRF1* is a key epigenetic switch, which controls cell cycle in nonsmall cell lung carcinoma through its ability to sustain the transcriptional silencing of tumor suppressor genes by maintaining their promoters in a hypermethylated status. Thus, *UHRF1* should be considered, along with DNMTs, among the potential targets for cancer treatment and/or therapeutic stratification. ***Cancer* 2010;000:000–000.** © *2010 American Cancer Society.*

KEYWORDS: UHRF1, DNMT, DNA methylation, tumor suppressor genes.

Epigenetic silencing of tumor suppressor genes (TSGs) is a hallmark in human cancers affecting multiple cellular pathways, such as cell signaling, adhesion and invasion, cell cycle, angiogenesis, DNA repair and apoptosis.[1,2] Nonsmall cell lung carcinomas (NSCLCs) are no exception to this, with a plethora of TSG promoters affected, including *RASSF1*,[3] *CDKN2A*,[4] *CYGB*,[5], *EDNRB*,[6] *RARbeta*,[7,8] *MGMT*,[8] and *CDH13*.[9]

DNMTs (DNA methyltransferases) are the key enzymes responsible for the establishment and maintenance of DNA methylation profiles.[10-12] Until recently, DNMT1 was considered to be the maintenance enzyme after DNA replication, whereas DNMT3A and DNMT3B were characterized as de novo methyltransferases.[13] The revised model suggests that DNMT1 carries out the bulk of the DNA methylation maintenance, whereas DNMT3A and DNMT3B, being compartmentalized to particular chromosome regions, can complete the methylation process and correct errors.[14] In addition, there is increasing evidence suggesting the involvement of histone modifications and nucleosome positioning in both de novo and maintenance methylation processes.[15,16] Numerous studies have demonstrated frequent overexpression of the DNMTs in many cancer types,[17-19] which in some cases correlated with the hypermethylation of particular TSGs.[20-22] However, other reports suggest that DNMT overexpression does not by itself seem to sufficiently account for the hypermethylation of TSG promoters.[19,21,23,24]

UHRF1 (also known as ICBP90) has recently been shown to play an important role in methylation maintenance.[25] It has the ability to bind hemimethylated DNA through its SET- and RING-associated domain,[26,27] triggering the recruitment of DNMT1[25,28] and histone deacetylace-1.[29] UHRF1-knockout mouse embryonic stem cells exhibit significant loss of genomic methylation.[25] The *UHRF1* gene is a target for the transcriptional activator E2F1,[29] and its

Corresponding author: Triantafillos Liloglou, PhD, University of Liverpool, Department of Clinical and Molecular Cancer Medicine, 200 London Road, Liverpool L3 9TA, United Kingdom; Fax: (011) +44 151 7948989; tliloglo@liv.ac.uk

[1]Roy Castle Lung Cancer Research Programme, University of Liverpool, Department of Clinical and Molecular Cancer Medicine, Liverpool, United Kingdom; [2]Pathology Unit, Department of Clinical and Molecular Cancer Medicine, University of Liverpool, Liverpool, United Kingdom; [3]Paterson Institute for Cancer Research, University of Manchester, Manchester, United Kingdom

DOI: 10.1002/cncr.25531, Received: March 3, 2010; Revised: May 21, 2010; Accepted: June 14, 2010, Published online in Wiley Online Library (wileyonlinelibrary.com)

expression is associated with increased cell proliferation.[30,31] Accumulating evidence suggests that UHRF1 has a putative oncogene function.[32] Despite the importance of UHRF1 function in DNA methylation, the current data regarding its contribution to the epigenetic silencing of TSGs in primary human tumors are limited to a single report associating UHRF1 overexpression with BRCA1 promoter methylation in sporadic breast cancer.[33]

In this study, we examined the mRNA expression profile of *UHRF1* as well as *DNMT1*, *DNMT3A*, and *DNMT3B* in NSCLC and examined their relationship to the methylation status of *CDKN2A* and *RASSF1* gene promoters. In addition, we further investigated the role of UHRF1 in regional hypermethylation by knocking its expression down in a lung cancer cell line.

MATERIALS AND METHODS

Human Tissues and Cell Lines

Frozen tissue from 105 NSCLCs (55 adenocarcinomas and 50 squamous cell carcinomas), as well as 50 adjacent normal lung tissues were obtained from Liverpool Heart and Chest Hospital (Liverpool, UK). Fifty-seven patients were male, and 48 were female. Specimens comprised the following pathological stages (pT): 10 T1, 81 T2, 10 T3, and 4 T4. Ethical approval was obtained from the Liverpool Ethics Committee for this study, and informed consent was obtained from each individual. The A549 adenocarcinoma cell line and its transfectant derivatives used in this study were grown in Dulbecco modified Eagle medium:F12 with L-glutamine and 10% fetal bovine serum, at 37°C supplemented with 5% CO_2.

DNA, RNA, and cDNA Synthesis

DNA and RNA extraction from tissues used 20 × 40 μm frozen sections from each patient sample. The first and last sections underwent pathological review to ensure ≥80% tumor cell content. DNA and RNA extraction from tissues and cell lines were performed using the DNeasy and RNeasy kits (Qiagen, Crawley, UK), respectively, after the manufacturer's protocol. Five hundred nanograms total RNA was reverse transcribed in a 20 μL reaction using the Quantitect kit (Qiagen) following the supplier's protocol.

Quantitative Polymerase Chain Reaction Expression Assays

TaqMan Gene Expression Assays for *DNMT1* (Hs00945898_g1), *DNMT3A* (Hs01027167_g1), *DNMT3B* (Hs01003404_g1), *UHRF1* (Hs00273589_m1), and *E2F1* (HS01566605_g1) (FAM-labeled) as well as *ACTB* (4326315E) as endogenous control (VIC-labeled) were purchased from Applied Biosystems, Warrington, UK. Assays were performed in 15 μL containing 7.5 μL Taqman expression master mix (Applied Biosystems), 0.75 μL of the target primer/probe mix, 0.75 μL endogenous control, and 2 μL of cDNA per the universal conditions (2 minutes at 50°C, 95°C for 10 minutes, 50 cycles of 94°C for 30 seconds, 60°C for 45 seconds) on an Applied Biosystems 7500 real-time polymerase chain reaction (PCR) machine. mRNA levels were expressed as relative quantification values, which were calculated as relative quantification = $2^{(-\Delta\Delta C_t)}$, where the mRNA expression of IMR-90 cells was used as a calibrator in each run. All assays were run in triplicate, and the mean value was used for the analysis.

DNA Methylation Analysis

Pyrosequencing assays (Qiagen) were developed to measure the DNA methylation levels of *CDKN2A*, RASSF1, CYGB, CDH13, *DNMT1*, *DNMT3A*, *DNMT3B*, and *UHRF1* promoters. The locations of the interrogated CG dinucleotides (CpGs) and relevant primers in each promoter are shown in Figure 1. The primer sequences used are the following:

(CDKN2A) F: 5′-AGGGGTTGGTTGGTTATTAG-3′, R: 5′-biotin-CTACCTACTCTCCCCCTCTC-3′, S: 5′-GGTTGGTTATTAGAGGGT-3′; (RASSF1) F: 5′-AGTATAGTAAAGTTGGTTTTTAGAAA-3′, R: 5′-biotin-CCCTTCCTTCCCTCCTT-3′, S: 5′-AAGTTGGTTTTTAGAAATA-3′; (CDH13) F: 5′-biotin-TTAGGGAAAATATGTTTAGTGTAGT-3′, R: 5′-ACCCCTCTTCCCTACCTA-3′, S: 5′-ACCCCTCTTCCCTACCT-3′; (CYGB) F: 5′-biotin-GGGAATTGATTTAAAGTTTA-3′, R: 5′-AAAAAACCCAACTAAATCCAC-3′, S: 5′-ACCCAACTAAATCCAC-3′; (UHRF1) F: 5′-GGTTAATTAGGAGGTAGG-3′, R: 5′-biotin-ACTCCACATTTAAAAATTAC-3′, S: 5′-GGTTAATTAGGAGGTAG-3′; (DNMT1) F: 5′-GATATTTTGTGTAGAAGGATGGAA-3′, R: 5′-biotin-ACCCACCTCCCAACAAAC-3′, S: 5′-ATTTTGTGTAGAAGGATG-3′; (DNMT3A) F: 5′-GATTTTGGTTTTGTAGAGTAGAG-3′, R: 5′-biotin-TCTACCTACCTCAACACTAAAACT-3′, S: 5′-ATTCACCTCCCAACAAAC-3′; (DNMT3B) F: 5′-GAGTTAGGTTTATTTGGGTT

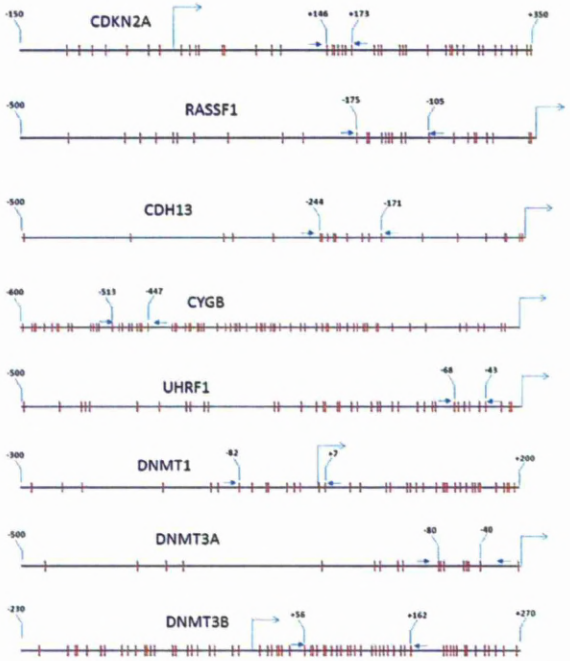

Figure 1. Diagrammatic map of the promoter regions examined is shown. CG dinucleotides are represented by vertical lines and primers as arrows. Numbering refers to the transcriptions start site depicted by the gamma-shaped arrow.

AT-3′, R: 5′-biotin-CTTCCTCCCAACAACTACT-3′, S: 5′-TTATTTGGGTTATTTAA-3′.

One microgram of genomic DNA was treated with sodium bisulphite (EZ DNA methylation Kit, Zymo Research, Orange, Calif) following the manufacturer's protocol. All primers were designed using Pyromark Assay Design 2.0 software (Qiagen) and supplied by Eurofins MWG Operon (Ebersberg, Germany). PCR amplifications were performed in a final volume of 25 μL using Qiagen HotStarTaq Master Mix, 200 nM biotinylated primer, 400 nM nonbiotinylated primer, and approximately 60 ng of bisulfite-treated genomic DNA. The thermal profile was: 95°C for 5 minutes followed by 40 cycles consisting of 94°C for 30 seconds, 51 to 57°C for 30 seconds, 72°C for 30 seconds. The annealing temperature for each gene was: CDKN2A, 55°C; RASSF1, 50°C; CYGB, 50°C; CDH13, 52°C; UHRF1, 51°C; DNMT1, 57°C; DNMT3A, 54°C; DNMT3B, 57°C. For pyrosequencing analysis, the PyroMark Gold Q96 SQA Reagents and the PyroMark Q96 ID instrument (Qiagen) were used following the supplier's protocol. The methylation index for each promoter was calculated as the mean value of mC/(mC + C), where C is unmethylated cytosine and mC is 5′ methyl-cytosine, for all examined CpGs in the target sequence.[34]

Construction of a Short Hairpin RNA UHRF1 Knockdown Stable Cell Line

The short hairpin RNA (shRNA) oligonucleotides used were (bold characters indicate the target sequence): UHRF1-sense, 5′GATCCC **GGACGGCG CGGGAACTCTA**TTCAAGAGA**TAGAGTTCCCGCG CCGTCC**TTTTTGGAAA 3′; UHRF1-antisense, 5′AGC TTTTCCAAAAA**GGACGGCGCGGGAACTCTA**TCT CTTGAA**TAGAGTTCCCGCGCCGTCC**GG 3′; scrambled-sense, 5′GATCCC**ATGAAGTCG CATGGTGCAG**TT CAAGAGA**CTGCACCATGCGACTTCAT**TTTTTGG AAA 3′; scrambled-antisense, 5′AGCTTTTCCAAAAA **ATGAAGTCGCATGGTGCAG**TCTCTTGAA**CTGCA CCATGCGACTTCAT**GG 3′.

Oligonucleotides were annealed and ligated into the pGEM-T-easy shuttle vector (Promega, Madison, Wis) containing the H1 promoter. Constructs were verified by sequencing analysis on a 3130 capillary sequencer using the BigDye 1.1 kit (Applied Biosystems). The shRNA module was then excised and ligated into the vector backbone of the pN1pβactin-rtTA2S-M2-IRESEGFP plasmid[35] containing the tetracycline repressor and a neomycin resistance gene. The final pN1pβactin-rtTA2S-M2-IRESEGFP-UHRF1 and pN1pβactin-rtTA2S-M2-IRESEGFP-scrambled constructs were transfected into the A549 cell line using the Attractene reagent (Invitrogen, Carlsbad, Calif). Stable cell lines were selected after 2 weeks using 600 ng/μL G418 antibiotics. Twenty different clones were checked for UHRF1 down-regulation at both RNA (quantitative PCR) and protein (Western blot) level in the presence/absence of 1 μg/mL doxycycline. The clones demonstrating inducible knockdown of UHRF1 did not produce >45% reduction of the UHRF1 mRNA. In contrast, 2 clones (named clone 1 and 2 thereafter) demonstrated constitutive, noninducible >80% knockdown of UHRF1 mRNA. Thus, it was decided to proceed to the subsequent experiments with these 2 clones.

MTT Proliferation Assay

The viability of A549 parental and UHRF1 knockdown clones was measured using the MTT proliferation assay; 5×10^3 of A549 parental, mock, A549 PAXUHRF1 clone 1 and clone 2 cells were seeded in 12-well plates. The next day, cells were washed with phosphate-buffered saline (PBS) and incubated with fresh medium containing 0.5

mg/mL of MTT (3-[4,5-dimethylthiazol-2-yl]-2,5-diphenyltetrazolium bromide) (Sigma-Aldrich, St Louis, Mo) for 2.5 hours at 37°C supplemented with 5% CO2. The medium was subsequently removed, and cells were washed with PBS. The converted formazan was solubilized by adding 1 mL of isopropyl alcohol-0.04 M HCl. After 5 minutes, viability of the cells was determined by measuring the difference in absorbance at 570 nm with reference at 630 nm. Time point measurements were performed every 24 hours for 5 days in total. The average proliferation rate was deduced from 3 biological replicates.

Western Blot

A549 cells were lysed at 80% confluence using RIPA buffer supplemented with protease inhibitors (1 mM phenylmethylsulfonyl fluoride [Sigma Aldrich], 10 μg/mL leupeptin [Sigma Aldrich], 10 mM NaF [Fluka, Neu-Ulm, Germany], 1 mM Na_3VO_4 [Sigma Aldrich]). Total protein concentration was measured with the DC Biorad Assay [Biorad, Hercules, Calif]. Twenty micrograms of total protein were denatured, separated on a 3%-8% NuPAGE Novex Tris-Acetate Mini gel (Invitrogen), and blotted onto a polyvinylidene difluoride membrane using an iBLOT platform (Invitrogen). Membranes were blocked in 5% Protoblock Reagent A (National Diagnostics) for 1 hour, incubated overnight with 2 μg/mL of the primary anti-UHRF1 mouse antibody (ab57083, Abcam, Cambridge, UK) at 4°C, and probed with horseradish peroxidase-rabbit antimouse secondary antibody (ab6741, Abcam). Antitubulin primary antibody (SC31779, Santa Cruz Biotechnology, Santa Cruz, Calif) was used as an internal control of total protein concentration. The bands were observed with the ECL western blotting detection kit (Amersham, Piscataway, NJ).

Wound Healing Assay

Wound-healing capacity of the A549 parental, mock, and A549 UHRF1 knockdown colonies was measured using scratch assays. Approximately 3 to 5×10^3 of A549 parental, mock, A549 PAXUHRF1 clone 1 and clone 2 cells were seeded in 24-well plates. The next day, when cells had reached confluence, monolayers were scratched using a tip. Time-lapsed images were digitally captured with a charge-coupled device camera over a period of 24 hours. The area that was covered by the migrating cells was calculated using TScratch software.[36]

Table 1. mRNA Expression of Examined Genes in Lung Tumor and Paired Normal Lung Tissue (n=50)

Gene	mRNA Expression (RQ Values, Mean±SE)		P (Wilcoxon Test)
	Tumor	Normal Lung	
UHRF1	3.9 ± 0.4	0.5 ± 0.1	1.7×10^{-9}
DNMT1	9.8 ± 0.8	5.8 ± 0.4	2.0×10^{-5}
DNMT3A	47.9 ± 7.4	32.9 ± 4.5	3.9×10^{-4}
DNMT3B	89.0 ± 16.7	31.8 ± 5.8	4.4×10^{-6}
E2F1	25.3 ± 3.8	9.5 ± 1.5	1.9×10^{-6}

RQ indicates relative quantification value = $2^{-\Delta\Delta Ct}$; SE, standard error. The expression of IMR90 lung fibroblasts has been used as calibrator in all genes. The mean value was deduced by 2 repeats.

Statistical Analysis

The fitness of continuous data into a normal distribution was tested by the one-sample Kolmogorov-Smirnov test. As none of the variable data fitted into normal distribution, nonparametric tests such as Mann-Whitney and Wilcoxon were used to analyze expression values among different groups. Spearman correlation was used to assess the relationship between continuous values. All statistical tests were performed by SPSS version 16.0 (SPSS Inc. Chicago, Ill).

RESULTS

UHRF1, DNMT1, DNMT3A, and DNMT3B Are Overexpressed in Primary NSCLCs

We measured by quantitative PCR the mRNA expression levels of *UHRF1*, *DNMT1*, *DNMT3A*, *DNMT3B*, and E2F1 in 105 primary NSCLC tumors, 50 of which had available paired adjacent nontumor tissue. Analysis of normal/tumor paired tissue sets demonstrated higher mRNA levels for all these genes in the tumors (Table 1). Bivariate analysis of the expression of the above genes in the set of 105 tumors demonstrated significant correlations between all of them (Table 2). In addition, expression of *UHRF1*, *DNMTs*, and *E2F1* was comparatively analyzed with the clinicopathological data. *UHRF1* was found to be expressed at higher levels in squamous carcinomas (mean relative quantification, 3.8 ± 0.4) than adenocarcinomas (mean relative quantification, 2.8 ± 0.4, Mann-Whitney, $P = .019$). No further associations were observed between other clinical parameters (age, sex, T stage, nodal metastasis and differentiation) and any of the examined genes with the exception of the correlation between *DNMT3B* mRNA overexpression and poor prognosis. In particular, patients with lower than median *DNMT3B* expression (relative quantification ≤24.4) had a mean estimated survival of 70.2 ± 10.4 months,

Table 2. Coordinated Expression of UHRF1, DNMTs, and E2F1 in Nonsmall Cell Lung Carcinoma (N=105)

Gene	*DNMT1*	*DNMT3A*	*DNMT3B*	*E2F1*
UHRF1				
Spearman correlation coefficient	0.633	0.583	0.514	0.754
P	4.5×10^{-13}	6.6×10^{-11}	2.4×10^{-8}	1.5×10^{-20}
DNMT1				
Spearman correlation coefficient		0.737	0.558	0.659
P		3.2×10^{-19}	7.3×10^{-10}	2.3×10^{-14}
DNMT3A				
Spearman correlation coefficient			0.688	0.744
P			6.9×10^{-16}	1.1×10^{-19}
DNMT3B				
Spearman correlation coefficient				0.732
P				1.1×10^{-18}

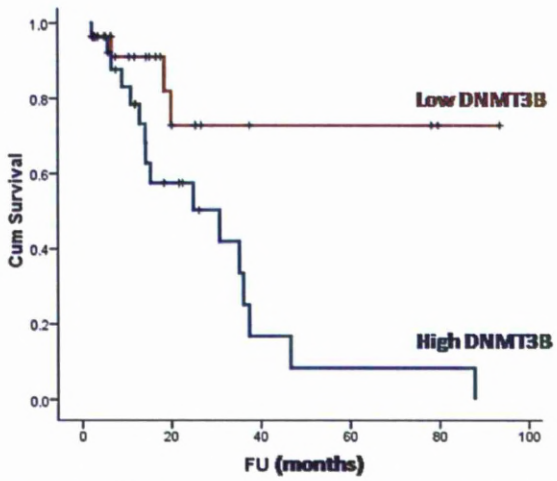

Figure 2. Kaplan-Meier survival analysis of nonsmall cell lung carcinoma patients in relation to DNMT3B mRNA expression is shown. X axis represents follow-up (FU) time; cumulative (Cum) survival is represented on the Y axis. Tumors with DNMT3B relative quantification value >24.4 (median) demonstrate a lower survival rate than those with lower than the median DNMT3B expression. It must be noted that none of the patients received postoperative chemo- or radiotherapy.

whereas the corresponding figure for those with higher *DNMT3B* expression was 29.3 ± 5.7 months (log-rank test, $P = .013$, Fig. 2).

The presence of CpG islands in the promoters of *UHRF1* and all *DNMTs* led us to examine their DNA methylation status in this NSCLC set. All 4 promoters were found to be unmethylated in both normal and tumor tissues examined.

UHRF1 and DNMT Overexpression Correlates With Hypermethylation of TSGs

The methylation levels of *CDKN2A* and *RASSF1* promoters were measured by pyrosequencing in this set of 105 NSCLC tissues. Representative pyrograms are given in Figure 3. The threshold for scoring hypermethylated samples was conservatively set to 10%, which is higher than previously established thresholds,[37,38] to increase the prospect of the detected methylation for biologically relevance. DNA hypermethylation was observed in 32.4% of the tumors for *RASSF1* and 26% of the tumors for *CDKN2A*. The expression of the *UHRF1* and *DNMTs* genes was analyzed in relation to the hypermethylation status of the TSGs (Table 3). Tumors with hypermethylated *CDKN2A* demonstrated higher levels of *DNMT1* (Mann-Whitney, $P = .018$) and UHRF1 ($P = .005$) expression compared with the *CDKN2A*-unmethylated tumors. Also, tumors with hypermethylated *RASSF1* demonstrated higher levels of *DNMT3B* (Mann-Whitney, $P = .043$) and *UHRF1* ($P = .034$) expression. *DNMT3A* expression did not demonstrate a correlation with any of the 2 examined promoters. Interestingly, when combining the methylation status of both *CDKN2A* and *RASSF1* (positive = at least 1 methylated), the correlation between *UHRF1* expression and hypermethylation becomes more significant ($P = 2.3 \times 10^{-4}$, Table 3).

UHRF1 Down-Regulation Leads to Hypomethylation of TSGs in A549 Cells

After the observations regarding the relationship between *UHRF1* expression and TSG hypermethylation in primary NSCLCs, we further investigated the role of UHRF1 in a cell line model by knocking down UHRF1

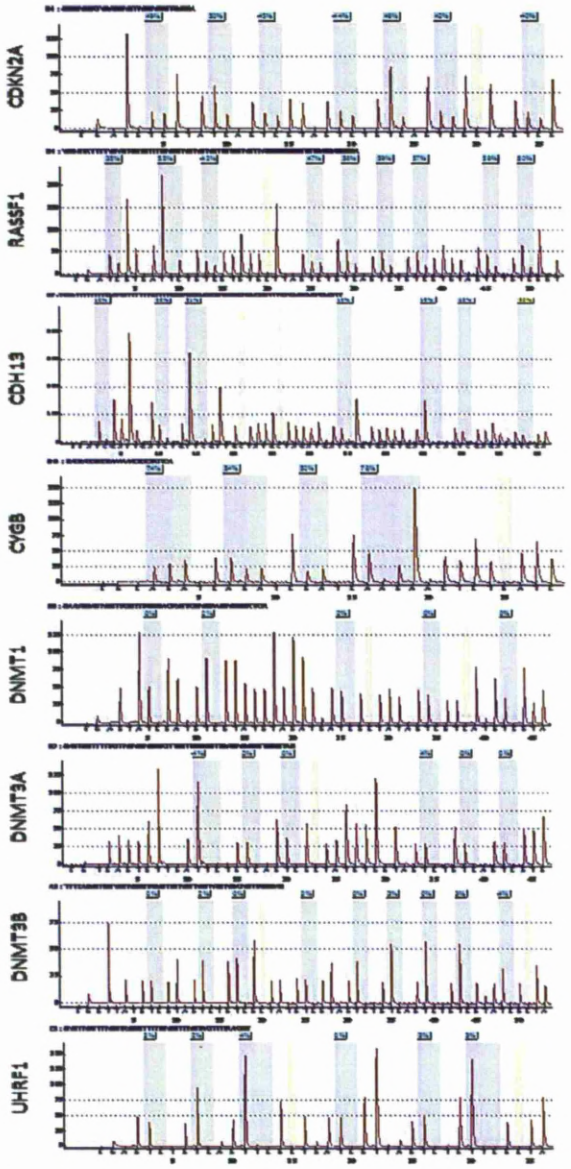

Figure 3. Representative pyrograms from the DNA methylation analysis are shown. X axis shows the dispensation order; the examined sequence is shown at the top of each pyrogram. Gray lanes are indicative of individual CG dinucleotides; yellow lanes indicate the bisulfite conversion controls.

in A549 lung adenocarcinoma cell line and acquiring stable transfectants. Both derived clones demonstrated 80% knockdown at the RNA level (Fig. 4A), whereas the protein was almost undetectable in Western blotting (Fig. 4B). The mRNA expression levels of *DNMT1* and *DNMT3A* demonstrated no significant changes between A459, the mock, and the UHRF1 knockdown clones. In contrast, *DNMT3B* was consistently up-regulated in both UHRF1 knockdown clones (Table 4). *UHRF1* and *DNMT* promoters were unmethylated in the A549 cells, and no change was observed in the UHRF1 knockdown clones (Table 4). To examine the UHRF1 knockdown effect on regional hypermethylation, we examined by pyrosequencing the promoters of *RASSF1*, *CYGB*, and *CDH13*, which were known from previous unpublished work to be methylated in the A549 parental line (*CDKN2A* promoter was found to be unmethylated in A549 cells). Although no difference was observed in the mock cell line, the methylation status of all 3 promoters was consistently, although variably, reduced in both UHRF1 knockdown clones (Fig. 5).

Phenotypic Effects of UHRF1 Down-Regulation

The phenotypic characteristics of the UHRF1 knockdown clones were significantly different from those of A549 and mock cell lines. Both UHRF1 knockdown clones had reduced proliferation rates (Fig. 6). In addition, scratch assays (Fig. 7) demonstrated lower migration efficiency of the UHRF1 knockdown clones. In particular, TScratch software analysis demonstrated that after 24 hours, the open wound area was 10.5% ± 1.3% in the parental A549, 14.1% ± 1.1% in mock cells, 71.9% ± 1.8% in UHRF1 clone 1, and 56.1% ± 1.8% in clone 2 (Fig. 8).

DISCUSSION

Inactivation of TSGs by promoter hypermethylation is among the most frequent abnormalities in human cancers.[1] Our understanding of epigenetic deregulation is advancing as the list of genes and mechanisms mediating the DNA methylation process grows.[39-43]

UHRF1 performs a critical function in DNA methylation maintenance[25]; however, its involvement in TSG promoter hypermethylation in cancer is not yet clear. In the present study, we investigated in NSCLCs the relationship of UHRF1 expression with the hypermethylation status of *CDKN2A* and *RASSF1* promoters, which are among the most frequently hypermethylated genes in this tumor type. *UHRF1* mRNA was overexpressed in NSCLC tumor tissues in comparison to their normal adjacent tissue, confirming in a large sample set a

Table 3. mRNA Expression Levels of UHRF1, DNMT1, DNMT3A, and DNMT3B in Groups of NSCLCs With Different Methylation Status of CDKN2A and RASSF1

Gene	*CDKN2A* Methylation		*P*	*RASSF1* Methylation		*P*	*CDKN2A* and/or *RASSF1*		*P*
	−	+		−	+		−	+	
UHRF1	2.9 ± 0.4	3.9 ± 0.4	.005[a]	2.8 ± 0.3	4.1 ± 0.7	.034[a]	2.4 ± 0.3	4.1 ± 0.5	2.3×10^{-4}[a]
DNMT1	6.5 ± 0.8	8.8 ± 1.2	.018[a]	6.8 ± 0.7	8.1 ± 1.3	.301	6.0 ± 0.7	8.2 ± 1.0	.058
DNMT3A	26.4 ± 3.2	35.3 ± 9.6	.604	31.7 ± 5.3	31.4 ± 4.9	.314	23.7 ± 3.6	33.3 ± 5.9	.151
DNMT3B	59.5 ± 10.0	73.1 ± 20.0	.200	54.8 ± 9.7	90.8 ± 19.8	.043[a]	41.9 ± 6.1	84.6 ± 16.8	.037[a]

Values are presented as mean relative quantification±standard error. *P* values originate from Mann-Whitney tests.
[a] Statistically significant.

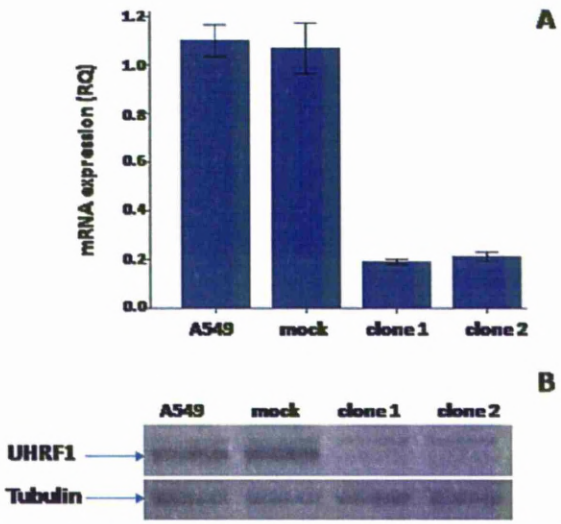

Figure 4. (A) Quantitative polymerase chain reaction and (B) Western blotting demonstrate UHRF1 mRNA and protein expression, respectively, of the A549-derived UHRF1 knockdown clones. A >80% reduction of mRNA levels is observed in both clones; UHRF1 protein is hardly detectable in the Western blot in comparison to the strong UHRF1 expression in A549 and mock cells. RQ indicates relative quantification.

preliminary observation.[44] UHRF1 overexpression was more profound in squamous carcinomas than adenocarcinomas, further underlying the differences in the molecular evolution of these tumor types. Further research is required to provide evidence on whether this difference could be used in the clinical management of these 2 histological types. Although *UHRF1* promoter bears a CpG island, no DNA methylation was found in normal or tumor tissue, excluding the possibility of an epigenetic expression feedback loop. As *UHRF1* is a known E2F1 target,[29,45] we also examined E2F1 mRNA expression levels in this sample set. Indeed, a strong relationship was observed between the expression levels of the 2 genes, supporting the concept that UHRF1 regulation is under the control of the pRb/E2F1pathway.[46]

It is of note that UHRF1 overexpression in the NSCLC tissue set was correlated with increased DNA methylation of both *CDKN2A* and *RASSF1* promoters, and moreover that a much stronger association was observed when analyzing UHRF1 expression against a combined *CDKN2A*/*RASSF1* methylation epigenotype. Thus, UHRF1 activity is important in maintaining the hypermethylation of certain TSGs. This is also supported by findings in breast tumors, where UHRF1 overexpression was correlated with BRCA1 promoter hypermethylation.[33]

To provide additional support to our ex vivo observations, we knocked down the expression of UHRF1 in A549 lung adenocarcinoma cell line. Both UHRF1 knockdown derived clones demonstrated reduced methylation of *RASSF1*, CYGB, and CDH13 promoters, which are hypermethylated in A549. The UHRF1 knockdown clones presented with reduced proliferation rates and migration efficiency in comparison to those of the parent and the mock cell lines. This is consistent with the reported association between UHRF1, proliferation,[30] and tumor cell growth.[44] E2F1 levels did not change upon UHRF1 knockdown, indicating a lack of a feedback loop. Both our ex vivo and in vitro data suggest that UHRF1 can influence the cell cycle control mainly through the epigenetic silencing of relevant tumor suppressors.

To gain a wider view of the DNA methylation machinery status, we also measured the mRNA expression of *DNMT1*, *DNMT3A*, and *DNMT3B*. All these genes were overexpressed in NSCLC tissues, in concordance with previous reports in other human cancer types.[17-19,21,47,48] A strong correlation between the

Table 4. mRNA Expression and DNA Methylation of DNMTs in UHRF1 Knockdown Clones

Cells	mRNA Expression (Mean RQ±SE)			Promoter Methylation Index			
	DNMT1	*DNMT3A*	*DNMT3B*	*UHRF1*	*DNMT1*	*DNMT3A*	*DNMT3B*
A549	1.00 ± 0.21	1.02 ± 0.08	1.02 ± 0.08	2%	1%	0%	1%
Mock	1.07 ± 0.19	0.96 ± 0.04	1.2 ± 0.13	3%	2%	1%	0%
Clone 1	0.78 ± 0.15	1.16 ± 0.06	**6.03 ± 0.39**	2%	0%	2%	1%
Clone 2	0.94 ± 0.18	1.27 ± 0.06	**4.15 ± 0.19**	2%	1%	1%	1%

RQ indicates relative quantification; SE, standard error.
Means and SE have been calculated from 6 replicates (2 biological × 3 technical). The average value of the A549 cells was used as calibrator for calculating RQ.

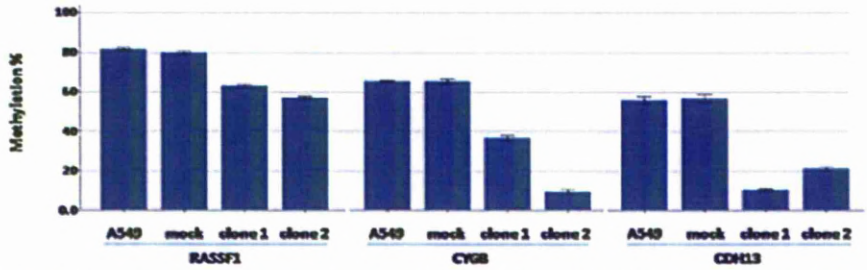

Figure 5. Effect of UHRF1 expression knockdown on the DNA methylation levels of RASSF1, CYGB, and CHD13 is shown. A consistent reduction of the DNA methylation of all 3 promoters is observed across biological replicates in both UHRF1 knockdown clones. The Y axis represents the mean methylation index detected by triplicate pyrosequencing experiments. Error bars represent standard error of the mean.

expression levels of all the *DNMTs* was observed, in accordance with a reported coordinated expression of *DNMTs*.[22,47] Furthermore, the expression levels of all *DNMTs* examined in this set was correlated with the expression of *E2F1*. Although the E2F1 dependence of *DNMT1* transcription is well established,[49] our data suggest that *DNMT3A* and *DNMT3B* may also be regulated by E2F1. Recent evidence of the participation of DNMT3A and DNMT3B in DNA methylation maintenance after DNA replication[14,50] provides a biological reason behind the E2F1 dependence. However, this requires further confirmation with functional studies. The overexpression of *DNMT3B* correlated with poor survival in our NSCLC set, and this is in agreement with a previous study demonstrating prognostic significance of DNMT3B expression but only in younger patients aged <65 years.[51] The potential clinical implementation of these observations should be further investigated.

Statistical analysis in primary tumors demonstrated that DNMT1 overexpression was correlated with hypermethylation of *CDKN2A* promoter, in accordance with previous reports.[21,22] In addition, *DNMT3B* overexpression was correlated with hypermethylation of RASSF1 but not *CDKN2A* promoter. Interestingly, the same finding was reported for ΔDNMT3B in NSCLC.[20] The amplicon detected in our study includes all different DNMT3B transcripts, and because ΔDNMT3B is the predominant form of DNMT3B in NSCLCs,[52] it is likely that our results reflect the observed correlation between

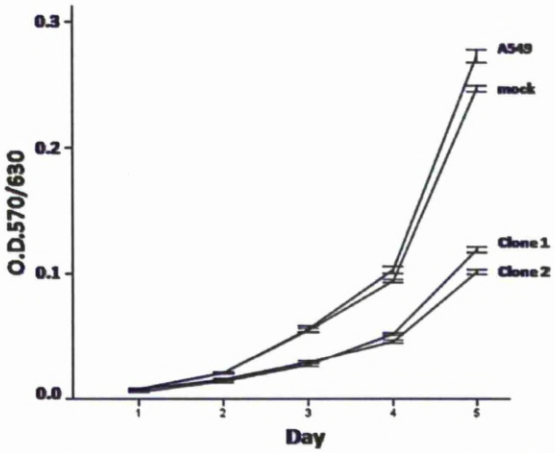

Figure 6. Proliferation rates over 5 days, measured by MTT experiments, are shown. Proliferation is significantly reduced in both UHRF1 knockdown clones in comparison to A549 cells and mock (scrambled short hairpin RNA) cell lines.

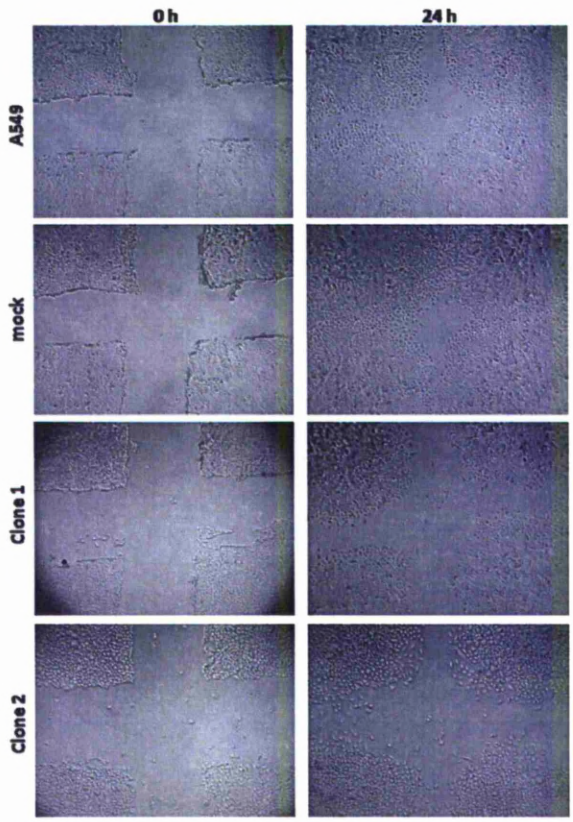

Figure 7. Scratch assays demonstrate the reduced migration efficiency of UHRF1 knockdown clones in comparison to A549 cells and mock (scrambled short hairpin RNA) cell lines. Photographs of t = 0 and t = 24 hours are presented.

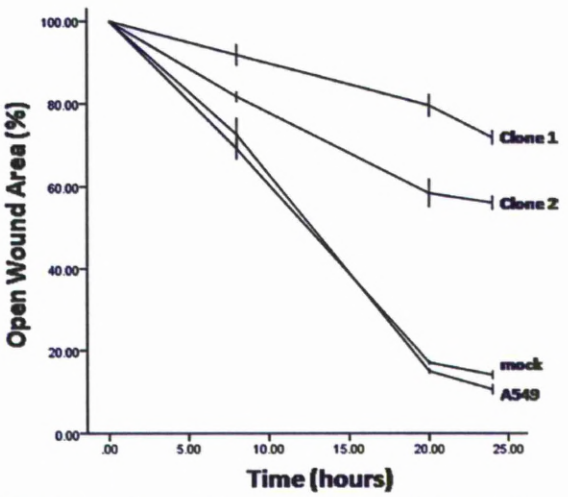

Figure 8. Diagrammatic representation shows the migration rates of parental, mock, and UHRF1 knockdown clones in scratch assays. The open wound area (OWA) was quantified using TScratch software. The increased OWAs of the UHRF1 clones indicate their reduced migration capability.

ΔDNMT3B and RASSF1. The importance of both DNMT1 and DNMT3B expression in the maintenance of aberrant CpG island methylation of TSGs in mammalian cell models[20,53-55] has been demonstrated. Our data together with previous reports[20-22] suggest that DNMT1 and DNMT3B can regulate DNA methylation in a promoter-specific manner. In concordance with this suggestion is the classification of common and distinct promoter groups identified after RNA interference-mediated suppression of DNMT1 and DNMT3B.[56]

Interestingly, whereas the expression levels of *DNMT1* and *DNMT3A* remained unchanged in the UHRF1 knockdown clones, there was a significant increase of *DNMT3B* expression in the absence of any methylation change of its promoter. The reasons behind the increase of *DNMT3B* expression upon UHRF1 knockdown are not currently clear. It is not known whether this is a directly UHRF1-related effect or whether unprompted high-DNMT3B expression provides a selective advantage that eventually takes over the cell population in the culture environment. Nevertheless, the incomplete *RASSF1*, *CYGB*, and *CDH13* promoter hypomethylation observed in the UHRF1 knockdown clones suggests that DNMTs can maintain a degree of methylation in the presence of low abundance of UHRF1 protein.

This study provides compelling new evidence to suggest that the overexpression of UHRF1 in NSCLC is critical, alongside the overexpression of DNMTs, for the maintenance of hypermethylated TSG promoters. UHRF1 is thus emerging as key epigenetic switch for cell cycle control and can be used as a new target for epigenetic therapies.

CONFLICT OF INTEREST DISCLOSURES

Supported by a grant from the Roy Castle Lung Cancer Foundation, United Kingdom.

REFERENCES

1. Esteller M. Epigenetic gene silencing in cancer: the DNA hypermethylome. *Hum Mol Genet.* 2007;16 Spec No 1: R50-R59.
2. Esteller M. Epigenetics in cancer. *N Engl J Med.* 2008;358: 1148-1159.

3. Vaissiere T, Hung RJ, Zaridze D, et al. Quantitative analysis of DNA methylation profiles in lung cancer identifies aberrant DNA methylation of specific genes and its association with gender and cancer risk factors. *Cancer Res.* 2009;69:243-252.
4. Zochbauer-Muller S, Fong KM, Virmani AK, Geradts J, Gazdar AF, Minna JD. Aberrant promoter methylation of multiple genes in non-small cell lung cancers. *Cancer Res.* 2001;61:249-255.
5. Xinarianos G, McRonald FE, Risk JM, et al. Frequent genetic and epigenetic abnormalities contribute to the deregulation of cytoglobin in non-small cell lung cancer. *Hum Mol Genet.* 2006;15:2038-2044.
6. Knight LJ, Burrage J, Bujac SR, et al. Epigenetic silencing of the endothelin-B receptor gene in non-small cell lung cancer. *Int J Oncol.* 2009;34:465-471.
7. Virmani AK, Rathi A, Zochbauer-Muller S, et al. Promoter methylation and silencing of the retinoic acid receptor-beta gene in lung carcinomas. *J Natl Cancer Inst.* 2000;92:1303-1307.
8. Field JK, Liloglou T, Warrak S, et al. Methylation discriminators in NSCLC identified by a microarray based approach. *Int J Oncol.* 2005;27:105-111.
9. Kim DS, Kim MJ, Lee JY, Kim YZ, Kim EJ, Park JY. Aberrant methylation of E-cadherin and H-cadherin genes in nonsmall cell lung cancer and its relation to clinicopathologic features. *Cancer.* 2007;110:2785-2792.
10. Bestor TH, Ingram VM. Two DNA methyltransferases from murine erythroleukemia cells: purification, sequence specificity, and mode of interaction with DNA. *Proc Natl Acad Sci U S A.* 1983;80:5559-5563.
11. Yoder JA, Soman NS, Verdine GL, Bestor TH. DNA (cytosine-5)-methyltransferases in mouse cells and tissues. *Studies with a mechanism-based probe. J Mol Biol.* 1997;270:385-395.
12. Okano M, Bell DW, Haber DA, Li E. DNA methyltransferases Dnmt3a and Dnmt3b are essential for de novo methylation and mammalian development. *Cell.* 1999;99:247-257.
13. Chen T, Li E. Establishment and maintenance of DNA methylation patterns in mammals. *Curr Top Microbiol Immunol.* 2006;301:179-201.
14. Jones PA, Liang G. Rethinking how DNA methylation patterns are maintained. *Nat Rev Genet.* 2009;10:805-811.
15. Cedar H, Bergman Y. Linking DNA methylation and histone modification: patterns and paradigms. *Nat Rev Genet.* 2009;10:295-304.
16. Sharma S, Kelly TK, Jones PA. Epigenetics in cancer. *Carcinogenesis.* 2010;31:27-36.
17. Girault I, Tozlu S, Lidereau R, Bieche I. Expression analysis of DNA methyltransferases 1, 3A, and 3B in sporadic breast carcinomas. *Clin Cancer Res.* 2003;9:4415-4422.
18. Robertson KD. DNA methylation, methyltransferases, and cancer. *Oncogene.* 2001;20:3139-3155.
19. Ehrlich M, Woods CB, Yu MC, et al. Quantitative analysis of associations between DNA hypermethylation, hypomethylation, and DNMT RNA levels in ovarian tumors. *Oncogene.* 2006;25:2636-2645.
20. Wang J, Bhutani M, Pathak AK, et al. Delta DNMT3B variants regulate DNA methylation in a promoter-specific manner. *Cancer Res.* 2007;67:10647-10652.
21. Kim H, Kwon YM, Kim JS, et al. Elevated mRNA levels of DNA methyltransferase-1 as an independent prognostic factor in primary nonsmall cell lung cancer. *Cancer.* 2006;107:1042-1049.
22. Lin RK, Hsu HS, Chang JW, Chen CY, Chen JT, Wang YC. Alteration of DNA methyltransferases contributes to 5'CpG methylation and poor prognosis in lung cancer. *Lung Cancer.* 2007;55:205-213.
23. Sato M, Horio Y, Sekido Y, Minna JD, Shimokata K, Hasegawa Y. The expression of DNA methyltransferases and methyl-CpG-binding proteins is not associated with the methylation status of p14(ARF), CDKN2A(INK4a) and RASSF1A in human lung cancer cell lines. *Oncogene.* 2002;21:4822-4829.
24. Park HJ, Yu E, Shim YH. DNA methyltransferase expression and DNA hypermethylation in human hepatocellular carcinoma. *Cancer Lett.* 2006;233:271-278.
25. Bostick M, Kim JK, Esteve PO, Clark A, Pradhan S, Jacobsen SE. UHRF1 plays a role in maintaining DNA methylation in mammalian cells. *Science.* 2007;317:1760-1764.
26. Arita K, Ariyoshi M, Tochio H, Nakamura Y, Shirakawa M. Recognition of hemi-methylated DNA by the SRA protein UHRF1 by a base-flipping mechanism. *Nature.* 2008;455:818-821.
27. Avvakumov GV, Walker JR, Xue S, et al. Structural basis for recognition of hemi-methylated DNA by the SRA domain of human UHRF1. *Nature.* 2008;455:822-825.
28. Sharif J, Muto M, Takebayashi S, et al. The SRA protein Np95 mediates epigenetic inheritance by recruiting Dnmt1 to methylated DNA. *Nature.* 2007;450:908-912.
29. Unoki M, Nishidate T, Nakamura Y. ICBP90, an E2F-1 target, recruits HDAC1 and binds to methyl-CpG through its SRA domain. *Oncogene.* 2004;23:7601-7610.
30. Fujimori A, Matsuda Y, Takemoto Y, et al. Cloning and mapping of Np95 gene which encodes a novel nuclear protein associated with cell proliferation. *Mamm Genome.* 1998;9:1032-1035.
31. Hopfner R, Mousli M, Jeltsch JM, et al. ICBP90, a novel human CCAAT binding protein, involved in the regulation of topoisomerase IIalpha expression. *Cancer Res.* 2000;60:121-128.
32. Bronner C, Achour M, Arima Y, Chataigneau T, Saya H, Schini-Kerth VB. The UHRF family: oncogenes that are drugable targets for cancer therapy in the near future? *Pharmacol Ther.* 2007;115:419-434.
33. Jin W, Chen L, Chen Y, et al. UHRF1 is associated with epigenetic silencing of BRCA1 in sporadic breast cancer. *Breast Cancer Res Treat.* 2010;123:359-373.
34. Shaw RJ, Akufo-Tetteh EK, Risk JM, Field JK, Liloglou T. Methylation enrichment pyrosequencing: combining the specificity of MSP with validation by pyrosequencing. *Nucleic Acids Res.* 2006;34:e78.
35. Rooney C, White G, Nazgiewicz A, et al. The Rac activator STEF (Tiam2) regulates cell migration by microtubule-mediated focal adhesion disassembly. *EMBO Rep.* 2010;11:292-298.
36. Geback T, Schulz MM, Koumoutsakos P, Detmar M. TScratch: a novel and simple software tool for automated analysis of monolayer wound healing assays. *Biotechniques.* 2009;46:265-274.
37. Shaw RJ, Liloglou T, Rogers SN, et al. Promoter methylation of CDKN2A, RARbeta, E-cadherin, cyclin A1 and cytoglobin in oral cancer: quantitative evaluation using pyrosequencing. *Br J Cancer.* 2006;94:561-568.
38. Hall GL, Shaw RJ, Field EA, et al. CDKN2A promoter methylation is a potential predictor of malignant transformation in

oral epithelial dysplasia. *Cancer Epidemiol Biomarkers Prev.* 2008;17:2174-2179.
39. Bestor TH. The DNA methyltransferases of mammals. *Hum Mol Genet.* 2000;9:2395-2402.
40. Bird AP, Wolffe AP. Methylation-induced repression—belts, braces, and chromatin. *Cell.* 1999;99:451-454.
41. Webster KE, O'Bryan MK, Fletcher S, et al. Meiotic and epigenetic defects in Dnmt3L-knockout mouse spermatogenesis. *Proc Natl Acad Sci U S A.* 2005;102:4068-4073.
42. Lopez-Serra L, Esteller M. Proteins that bind methylated DNA and human cancer: reading the wrong words. *Br J Cancer.* 2008;98:1881-1885.
43. Ooi SK, Qiu C, Bernstein E, et al. DNMT3L connects unmethylated lysine 4 of histone H3 to de novo methylation of DNA. *Nature.* 2007;448:714-717.
44. Jenkins Y, Markovtsov V, Lang W, et al. Critical role of the ubiquitin ligase activity of UHRF1, a nuclear RING finger protein, in tumor cell growth. *Mol Biol Cell.* 2005;16:5621-5629.
45. Mousli M, Hopfner R, Abbady AQ, et al. ICBP90 belongs to a new family of proteins with an expression that is deregulated in cancer cells. *Br J Cancer.* 2003;89:120-127.
46. Jeanblanc M, Mousli M, Hopfner R, et al. The retinoblastoma gene and its product are targeted by ICBP90: a key mechanism in the G1/S transition during the cell cycle. *Oncogene.* 2005;24:7337-7345.
47. Robertson KD, Uzvolgyi E, Liang G, et al. The human DNA methyltransferases (DNMTs) 1, 3a and 3b: coordinate mRNA expression in normal tissues and overexpression in tumors. *Nucleic Acids Res.* 1999;27:2291-2298.
48. Vallbohmer D, Brabender J, Yang D, et al. DNA methyltransferases messenger RNA expression and aberrant methylation of CpG islands in non-small-cell lung cancer: association and prognostic value. *Clin Lung Cancer.* 2006;8:39-44.
49. McCabe MT, Davis JN, Day ML. Regulation of DNA methyltransferase 1 by the pRb/E2F1 pathway. *Cancer Res.* 2005;65:3624-3632.
50. Liang G, Chan MF, Tomigahara Y, et al. Cooperativity between DNA methyltransferases in the maintenance methylation of repetitive elements. *Mol Cell Biol.* 2002;22:480-491.
51. Xing J, Stewart DJ, Gu J, Lu C, Spitz MR, Wu X. Expression of methylation-related genes is associated with overall survival in patients with non-small cell lung cancer. *Br J Cancer.* 2008;98:1716-1722.
52. Wang L, Wang J, Sun S, et al. A novel DNMT3B subfamily, DeltaDNMT3B, is the predominant form of DNMT3B in non-small cell lung cancer. *Int J Oncol.* 2006;29:201-207.
53. Robert MF, Morin S, Beaulieu N, et al. DNMT1 is required to maintain CpG methylation and aberrant gene silencing in human cancer cells. *Nat Genet.* 2003;33:61-65.
54. Suzuki M, Sunaga N, Shames DS, Toyooka S, Gazdar AF, Minna JD. RNA interference-mediated knockdown of DNA methyltransferase 1 leads to promoter demethylation and gene re-expression in human lung and breast cancer cells. *Cancer Res.* 2004;64:3137-3143.
55. Rhee I, Bachman KE, Park BH, et al. DNMT1 and DNMT3b cooperate to silence genes in human cancer cells. *Nature.* 2002;416:552-556.
56. Foltz G, Yoon JG, Lee H, et al. DNA methyltransferase-mediated transcriptional silencing in malignant glioma: a combined whole-genome microarray and promoter array analysis. *Oncogene.* 2009;28:2667-2677.

Cancer Letters 300 (2011) 79–86

Contents lists available at ScienceDirect

Cancer Letters

journal homepage: www.elsevier.com/locate/canlet

Global DNA hypomethylation-induced ΔNp73 transcriptional activation in non-small cell lung cancer

Alexandros Daskalos [a], Stella Logotheti [b], Soultana Markopoulou [a], George Xinarianos [a], John R. Gosney [c], Anastasia N. Kastania [d], Vassilis Zoumpourlis [b], John K. Field [a], Triantafillos Liloglou [a,*]

[a] Roy Castle Lung Cancer Research Programme, The University of Liverpool, Department of Clinical and Molecular Cancer Medicine, 200 London Road, Liverpool L3 9TA, United Kingdom
[b] National Hellenic Research Foundation, 48 Vassileos Constantinou Ave., 11635 Athens, Greece
[c] The University of Liverpool, School of Cancer Studies, Division of Pathology, Duncan Building, Liverpool, United Kingdom
[d] Bioinformatics and Medical Informatics Team, Biomedical Research Foundation of the Academy of Athens, 4 Soranou Ephessiou, 115 27 Athens, Greece

ARTICLE INFO

Article history:
Received 21 July 2010
Received in revised form 2 September 2010
Accepted 6 September 2010

Keywords:
Lung cancer
p73
DNA methylation
ΔNp73
TAp73

ABSTRACT

p73 possesses an extrinsic P1 promoter and an intrinsic P2 promoter controlling the expression of the pro-apoptotic TAp73 isoforms and the anti-apoptotic ΔNp73 isoforms respectively. In this study, we investigated the DNA methylation status of both promoters as a means of epigenetic transcriptional control of their corresponding isoforms in 102 primary non-small cell lung carcinomas (NSCLCs). We demonstrated that while P1 hypermethylation-associated reduction of TAp73 mRNA levels is relatively infrequent, the P2 hypomethylation-associated over-expression of ΔNp73 mRNA is a frequent event, particularly among squamous cell carcinomas. P2 hypomethylation strongly correlated with LINE-1 element hypomethylation, indicating that ΔNp73 over-expression may be a passive consequence of global DNA hypomethylation.

1. Introduction

p73 is a p53-family member which, despite its high homology with *p53*, is not a typical Knudson-type gene. It encodes a number of protein isoforms with a suggested dual role in cancer. In detail, the full-length TAp73 isoforms induce cell cycle arrest and apoptosis by transactivating a number of *p53* target genes, whereas the N-terminal truncated ΔNp73 isoforms hamper apoptosis either by directly inhibiting TAp73 and p53 or through indirect inhibition of p53-mediated transcription, therefore exerting ongogenic activities in the cells [1–4]. The synthesis of isoforms with opposing properties by only one gene is mainly achieved by the alternative usage of two different promoters in *p73* gene, the extrinsic promoter (P1) located upstream to exon 1, which gives rise to the transactivation domain (TA)-containing (TAp73) isoforms and the intrinsic promoter (P2) located in intron 3, which controls the transcription of TA-deprived (ΔNp73) isoforms. Isoforms lacking the TA domain (p73Δex2, p73Δex2/3 and ΔN′-p73) can also be produced through alternative splicing of transcripts driven by the extrinsic promoter [5,6].

DNA methylation is a dynamic, reversible mode of epigenetic regulation which can modify functionality of numerous genes within the cell. Alterations of the pattern of DNA methylation are common in cancer cells. On the one hand, hypermethylation of CpG islands within certain gene promoter regions inhibits transcription, thus contributing in the silencing of crucial tumour suppressor genes, such as $p16^{INK4\alpha}$, *Rb*, *E-cadherin* and *BRCA1* [7]. On the other hand, hypomethylation of specific loci reactivates expression of genes with an oncogenic potential. For example, hypomethylation-linked activation has been reported in some cancers for genes such as *H-Ras*, *c-myc* [7], *PAX2* [8], *Cros* [9] and *NGALR* [10]. DNA demethylation occurs through

* Corresponding author. Tel.: +44 0151 7948958.
E-mail address: liloglout@roycastle.liv.ac.uk (T. Liloglou).

0304-3835/$ - see front matter © 2010 Elsevier Ireland Ltd. All rights reserved.
doi:10.1016/j.canlet.2010.09.009

two distinct processes, referred as passive demethylation, which results from improper preservation of methylation marks during DNA replication due to the lack of methylation maintenance activities; and active demethylation, which involves a demethylase that erases methylation marks from DNA in a replication-independent manner [11]. Global hypomethylation of the genome occurs simultaneously with hypermethylation of CpG islands in cancer cells, involving genes implicated in cell cycle regulation, DNA repair and apoptosis [7]. These changes are usually tumour-type specific [12].

Methylation of *p73* has been reported in certain types of cancer, such as leukemias/lymphomas and neuroblastomas. Specifically, *p73* hypermethylation poses as a common event in acute lymphoblastic leukemia, responsible for inhibition of transcription of the corresponding gene product [13], whereas it is very rare and has no effect on pathogenesis in acute myeloblastic leukemia [14]. In non-Hodgkins lymphomas, P1 *p73* promoter has been found methylated in B-cell lymphomas, accompanied by absence or low levels of TAp73, but unmethylated in T-cell lymphomas [15]. The highest *p73* methylation frequency up to 94% has been reported in natural killer cell lymphomas, while *p73* transcript was not detectable in these malignancies [16]. Other studies indicate that extrinsic and intrinsic *p73* promoters are differentially affected by methylation. In detail, P1 promoter is unmethylated independently from TAp73 transcription in neuroblastomas [17]. In contrast, P2 promoter is partially methylated in ΔNp73-expressing primary neuroblastomas and fully methylated in ΔNp73-non-expressing primary neuroblastomas, suggesting that expression of ΔNp73, but not TAp73, is at least in part, controlled by epigenetic events [18].

Recently, *p73* promoter methylation was investigated in the context of lung cancer. Using qualitative methods, Di Vinci et al. showed that both ΔNp73 and TAp73 proteins are overexpressed in NSCLCs and that P1 promoter was unmethylated in most cases examined (39/41), whereas P2 was partially unmethylated in 24/41 cases examined. Both TAp73 and ΔNp73 protein levels were variably elevated in these tumours in comparison with normal adjacent tissues, however no correlation was established between P1 and P2 methylation status and the expression of the corresponding protein products in tumours [19]. Following this work and expanding the analysis to a larger number of patients, we used sensitive quantitative assays to thoroughly determine the methylation levels of P1 and P2 promoters and to further investigate their correlation with TAp73 and ΔNp73 mRNA levels, as well as with LINE-1 promoter methylation, the surrogate marker of global hypomethylation [20,21], in lung cancer. We also evaluated the association of P1 and P2 promoter methylation with their corresponding products in the context of distinct histological NSCLC types, mainly adenocarcinomas and squamous cell carcinomas.

2. Materials and methods

2.1. Patients and tissues

Frozen tumour samples for 102 NSCLC patients were obtained from Liverpool Heart and Chest Hospital. Corresponding normal lung tissues were available for 38 of these patients. The patients comprised 56 males and 46 females and ranged in age between 49 and 81 years (mean, 64 years). Fifty-three of the NSCLCs were adenocarcinomas, whereas the remaining 49 were squamous cell carcinomas. Tissues were dissected by the pathologist within 30 min from surgical resection and were immediately stored to a −80 °C freezer. The study protocol was approved by the Liverpool Ethics Committee and all patients provided written, informed consent in accordance with the Declaration of Helsinki.

2.2. DNA extraction and methylation analysis

For the DNA extraction 20 μm-thick sections were cut from frozen tissue. Tumour sections were stained with H&E and microscopically reviewed to ensure a >80% tumour cell content. Genomic DNA was extracted from the samples using the DNeasy kit (Qiagen, Hilden, Germany) according to the manufacturer's protocol. Quality and quantity of the DNA was assessed by spectrophotometry at 260/280 nm. For the methylation analysis, CpG rich regions of both *p73* gene promoters were identified by CpG island searcher (http://cpgislands.usc.edu/). For P1 a target region upstream to exon 1 containing eight CpGs was chosen, whereas for P2 a target region containing six CpGs upstream to the alternative 3′ exon was chosen. The following primers were designed for pyrosequencing methylation analysis of P1 using the Assay Design Software (Biotage, Uppsala, Sweden): FWD: 5′-GGTTATATTTTTTGTTTTTTG-GA-3′, REV (biotinylated): 5′-ACCCATCTTTCCTAACACC-3′, SEQ: 5′-GTTTTTTGGATTTTAAG-3′. For the P2 promoter, the primers were: FWD: 5′-AGGAGTTTTGGTGGGTTTAAT-TAT-3′, REV (biotinylated): 5′-CCCACCCCTTTATTCCTC-3′, SEQ: 5′-GGTGGGTTTAATTATGG-3′. One μg of genomic DNA was treated with sodium bisulfite, using the EZ DNA methylation Kit™ (ZymoResearch, CA, USA). Fifty nanograms of bisulfite-treated genomic DNA, 5 μM of each primer and GoTaq mix (Promega, Madison, WI) were used in a 25 μl-PCR reaction. The thermal profile was: 95 °C for 2 min, [−94 °C for 30 s, 51 °C for 45 s at, 72 °C for 45 s] 40 cycles, 72 °C for 10 min. Pyrosequencing was performed as previously described [22]. The methylation index (MtI) for each promoter was calculated as the average methylation% of the examined CpGs.

2.3. RNA extraction, cDNA synthesis and mRNA expression analysis by qPCR

RNA extraction was performed using the RNeasy kit (Qiagen, Hilden, Germany) following the manufacturer's protocol and the quality and the quantity of the RNA was assessed by capillary electrophoresis on an Agilent 2100 Bioanalyser (Agilent Technologies, CA, USA). For cDNA synthesis, the Quantitect kit (Qiagen, Hilden, Germany) was used. Primers/probe designed to specifically amplify the TAp73 transcript were: FWD: 5′ GGTTATATTTTTT-GTTTTTTGGA 3′, REV: 5′ Biotin-ACCCATCTTTCCTAACACC 3′, sequencing: 5′ GTTTTTTGGATTTTAAG 3′. Primers/probe for ΔNp73 transcript were: FWD: 5′-GCCCGCATGTTCCC-CAG-3′, REV: 5′-TTGAACTGGGCCGTGGC-3′ and Probe:

5′-FAM-TCACCGACGTACAGCATGGTAGGCG-TAMRA-3′. Each amplification reaction was performed using 1 μl of the reverse transcription reaction, 900 nM of each primer, 250 nM probe, 1 μl of the endogenous control ACTB-VIC (Applied Biosystems, CA, USA) and Taqman expression master mix (Applied Biosystems, CA, USA) under universal conditions (50 °C for 2 min, 95 °C for 10 min, [94 °C for 30 s, 60 °C for 45 s] 50 cycles, on a 7500 real time PCR system (Applied Biosystems, CA, USA). Relative quantification (RQ) values were calculated using the expression of A549 cells as a calibrator. All qPCR experiments were performed in triplicate from a single RNA preparation from each tumour specimen.

2.4. Cell lines and in vitro experiments

CRL5802 and A549 lung cancer cell lines, obtained from American Type Culture Collection (Rockville, MD, USA), were grown in DMEM: F12 with L-glutamine and 10% FBS. Cell lines were treated with 100 nM 5-aza-2′-deoxycytidine (Sigma–Aldrich, St. Louis, MO) alone or combined with 100 nM Trichostatin-A (TSA) (Sigma–Aldrich, St. Louis, MO) for 24 h as previously described [22] and ΔNp73 mRNA expression was measured by qPCR. All qPCR experiments were performed in triplicate from two biological replicates for each condition (overall six measurements taken).

2.5. Statistical analysis

The SPSS Statistics 17.0 (SPSS Inc.) was used for statistical analysis. Non-parametric tests were selected, since Kolmogorov Smirnov test revealed that the distribution of each study parameter was not normal both in squamous cell cancer patients and in adenocarcinoma patients. The Mann–Whitney test was employed to examine the differences in mRNA expression levels of TAp73 RQ and the ΔNp73 RQ between the sample groups with hypermethylated and hypomethylated promoters, as well as between sample groups with different histologies. The P2 MtI was correlated with LINE-1 promoter MtI also using the Spearman correlation test. The statistical significance was defined by $p < 0.05$.

3. Results

3.1. Methylation status of P1 and P2 p73 promoters in NSCLCs

We used pyrosequencing to quantitatively determine the methylation levels of P1 and P2 *p73* promoters in NSCLC tissues, as well as in the available adjacent normal tissues. Representative pyrograms of the pyrosequencing assays for both promoters are given in Fig. 1 while detailed methylation index values for all examined specimens are provided in Table 1. Hypermethylation in tumours was designated at the 10% level as has been previously used [22]. Similarly, we set a threshold of 10% reduction to classify tumours as hypomethylated [22]. Very low methylation levels of P1 promoter were observed in normal adjacent tissues. Only seven tumour samples (6.8%) exceeded the 10% hypermethylation threshold (Table 1). The P2 promoter was heavily methylated in normal tissues (mean MtI: 91 ± 0.2%) while a variable degree of demethylation was observed in the tumour tissues. Fifty-seven (55.9%) of the examined tumours demonstrated P2 hypomethylation (Table 1). Simultaneous P1 hypermethylation and P2 hypomethylation was observed in 5/102 (4.91%) tumour samples, whereas 2/102 (0.02%) tumour samples presented only P1 hypermethylation and 50/102 (49.1%) tumour samples presented only P2 hypomethylation.

We have also assessed global DNA methylation by examining the methylation levels of the LINE-1 retrotransposable element. A variable degree of LINE-1 hypomethylation was observed in tumour tissue (mean MtI 58.5% ± 0.9) as compared to the normal adjacent lung tissue (mean MtI 69.5% ± 0.1, Mann–Whitney test $p < 0.05$). Notably, a significant association was observed between the DNA methylation levels of P2 and LINE-1 promoters (Spearman's $R = 0.340$, $p = 0.001$).

No significant associations were observed between the methylation status of any of the *p73* promoters or LINE-1 element and clinicopathological parameters, such as age, gender, T status, nodal metastasis and differentiation.

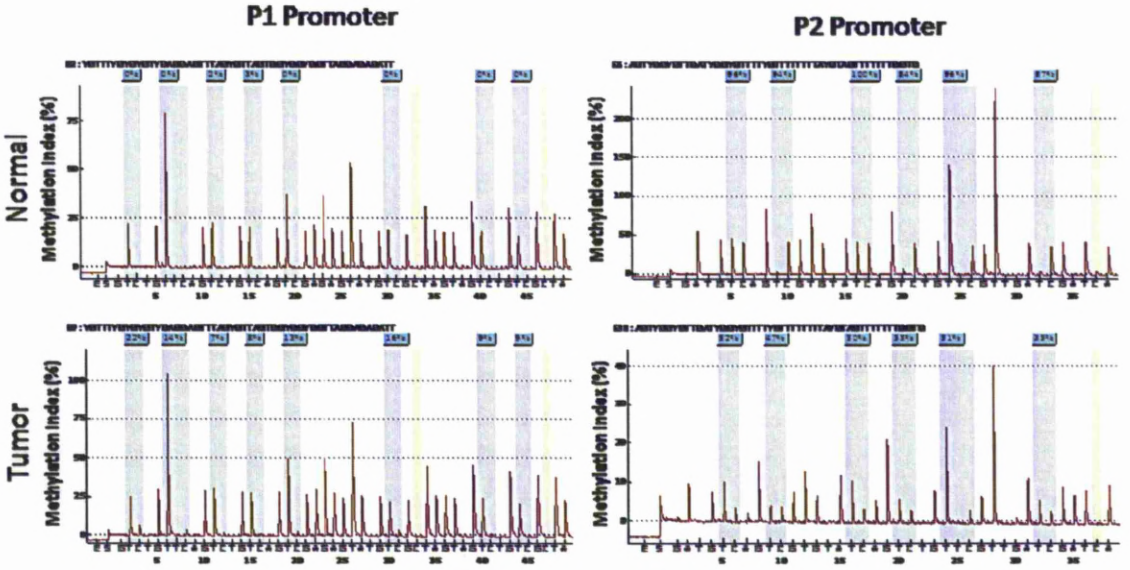

Fig. 1. Representative pyrograms from the DNA methylation analysis of the P1 and P2 promoters. *X*-axis shows the dispensation order and *Y*-axis the fluorescence level. The percentage of methylation is calculated as the C/(C + T) peak ratio per CpG. The C dispensation at position 35 controls for the full bisulfite conversion of DNA. Normal adjacent tissue (top) demonstrates high levels of DNA methylation while lung cancer tissue (bottom) has lower levels of methylation.

Table 1
mRNA expression of p73 isoforms and DNA methylation levels of their promoters in NSCLC specimens, in comparison to their clinicopathological parameters. M = male, F = female, Sq = squamous carcinoma, Ad = adenocarcinoma, ND = not determined.

Sample	Clinicopathological parameters					Methylation index (%)				mRNA expression (RQ value)	
	Gender	Histology	Differentiation	T status	N status	P1 tumour	P2 tumour	P2 normal	LINE-1 tumour	TAp73 RQ tumour	ΔNp73 RQ tumour
1	M	Sq	Moderate	2	0	4.23	58.43	91.2	45.5	1.12	0.46
2	M	Sq	Good	2	1	5.00	93.79	ND	70.5	0.18	0.00
3	M	Sq	Moderate	2	1	2.85	63.83	90.7	64.8	0.42	0.45
4	M	Sq	Moderate	2	0	7.34	88.04	91.3	66.5	0.22	0.28
5	M	Sq	Poor	2	1	4.24	47.13	ND	53.0	0.62	0.04
6	M	Sq	Moderate	3	1	6.04	68.41	89.7	51.2	0.46	0.07
7	M	Ad	Poor	2	0	3.29	92.06	92.8	58.3	1.08	0.16
8	F	Ad	Moderate	2	1	2.72	90.74	ND	64.1	0.15	0.00
9	F	Ad	Moderate	2	0	46.89	56.02	ND	58.4	0.06	0.00
10	M	Ad	Poor	2	1	15.85	48.24	ND	40.6	0.03	0.00
11	M	Sq	Moderate	2	1	0.47	69.51	92.6	60.0	0.07	0.19
12	M	Ad	Poor	2	2	5.18	93.30	92.1	67.7	0.98	0.07
13	M	Sq	Moderate	2	1	6.82	92.93	91.4	43.1	ND	ND
14	M	Sq	Poor	2	1	3.39	47.39	ND	50.1	0.41	2.30
15	F	Ad	Poor	2	2	5.65	60.56	92.7	49.8	0.41	0.08
16	F	Sq	Poor	2	1	10.12	60.78	92.3	58.8	0.12	0.04
17	F	Ad	Moderate	2	0	6.15	60.19	92.4	ND	0.30	0.99
18	F	Ad	Moderate	2	0	3.83	94.12	91.9	64.2	0.33	0.03
19	M	Sq	Moderate	2	0	4.07	80.68	90.1	50.2	0.26	0.00
20	M	Sq	Moderate	2	0	3.41	59.79	91	55.0	3.18	15.89
21	M	Sq	Moderate	2	1	2.66	54.28	92.5	45.9	0.75	0.22
22	M	Ad	Moderate	3	0	6.11	75.18	ND	69.2	0.24	0.06
23	M	Sq	Poor	3	1	3.98	90.91	ND	58.2	0.10	0.00
24	F	Ad	Moderate	2	0	1.83	84.06	ND	66.9	0.77	0.26
25	F	Ad	Moderate	2	0	4.03	91.88	ND	41.5	ND	ND
26	M	Ad	Poor	2	0	2.46	45.98	ND	64.3	0.12	0.47
27	M	Sq	Poor	2	1	3.48	86.93	91	58.9	0.91	0.39
28	M	Sq	Good	3	1	3.03	62.32	ND	53.7	0.55	0.13
29	F	Ad	Moderate	1	0	3.18	61.49	ND	69.1	0.26	0.29
30	M	Sq	Moderate	2	1	5.95	94.37	ND	22.9	0.28	0.04
31	F	Sq	Moderate	2	1	0.30	12.77	ND	63.9	0.42	9.99
32	F	Ad	Moderate	2	0	2.68	54.50	92.2	52.7	0.48	0.07
33	M	Ad	Poor	2	1	2.66	93.08	ND	62.0	0.11	0.00
34	M	Sq	Moderate	2	0	0.59	72.05	ND	50.4	1.44	0.23
35	F	Ad	Poor	2	2	7.65	54.47	90.2	57.4	0.25	0.10
36	M	Sq	Moderate	2	2	3.32	94.75	90.9	44.1	1.67	0.00
37	M	Ad	Poor	2	0	4.78	52.23	ND	50.5	0.29	0.08
38	F	Ad	Poor	3	0	5.05	61.82	ND	33.1	0.93	0.88
39	F	Ad	Poor	2	2	4.14	36.43	91.3	67.0	0.06	0.00
40	M	Ad	Poor	2	1	3.43	94.46	93.3	60.8	0.11	0.00
41	M	Sq	Moderate	4	2	5.13	92.77	ND	43.1	0.15	0.00
42	M	Sq	Moderate	2	1	2.83	50.72	ND	43.4	1.00	0.65
43	M	Ad	Poor	2	0	2.50	52.29	90.3	68.0	0.32	0.32
44	F	Ad	Poor	2	2	2.45	93.00	93.3	64.6	0.25	0.07
45	F	Ad	Poor	2	0	2.56	92.48	91.4	63.1	0.42	0.00
46	M	Sq	Moderate	2	1	6.53	71.60	ND	44.6	0.23	ND
47	F	Sq	Moderate	2	1	7.19	29.01	ND	ND	0.18	0.00
48	M	Sq	Moderate	2	0	3.05	62.68	91	51.2	0.28	0.41
49	F	Ad	Moderate	2	1	3.29	62.20	85.8	64.2	3.03	9.71
50	M	Sq	Poor	3	1	2.81	90.59	92.2	68.9	1.00	0.02
51	F	Sq	Poor	2	0	3.86	75.91	ND	58.9	2.97	0.77
52	M	Ad	Poor	2	1	3.04	65.23	93.5	56.8	1.35	1.04
53	F	Sq	Nd	2	0	4.73	72.00	ND	67.0	0.02	0.00
54	F	Ad	Poor	2	2	4.86	93.75	ND	66.1	0.09	0.00
55	M	Ad	Moderate	2	2	3.24	71.38	90.6	64.0	0.90	0.45
56	M	Ad	Poor	1	0	28.04	67.58	ND	47.1	0.09	0.00
57	M	Sq	Moderate	2	0	6.59	89.25	92.2	60.3	0.13	0.02
58	F	Sq	Moderate	2	0	3.05	49.05	91.6	52.3	0.42	0.29
59	F	Sq	Moderate	1	0	3.99	71.49	ND	58.5	0.31	0.04
60	F	Ad	Poor	2	1	3.96	75.82	90.3	ND	0.08	0.54
61	M	Ad	Poor	1	0	3.25	52.69	90	47.4	1.16	2.10
62	M	Ad	Good	2	0	5.49	92.53	91.2	ND	0.19	0.00
63	M	Ad	Poor	2	0	4.69	80.36	ND	67.9	0.33	0.44
64	F	Ad	Poor	1	0	5.10	91.42	ND	55.9	0.47	0.00
65	F	Ad	Moderate	2	2	4.18	88.41	ND	66.3	0.55	0.30
66	F	Sq	Moderate	2	0	3.42	59.23	90.9	64.1	0.96	0.01

Table 1 (*continued*)

Sample	Clinicopathological parameters					Methylation index (%)				mRNA expression (RQ value)	
	Gender	Histology	Differentiation	T status	N status	P1 tumour	P2 tumour	P2 normal	LINE-1 tumour	TAp73 RQ tumour	ΔNp73 RQ tumour
67	M	Ad	Moderate	2	0	2.97	94.42	91.3	69.1	0.29	0.00
68	M	Ad	Moderate	2	1	4.77	93.29	ND	ND	0.07	0.00
69	M	Ad	Moderate	2	1	5.13	91.35	ND	63.8	0.31	0.39
70	F	Sq	Moderate	2	0	3.36	81.21	92.5	60.1	2.48	1.10
71	F	Sq	Moderate	2	2	3.45	88.46	91.7	64.6	0.10	0.00
72	M	Sq	Poor	2	0	5.53	93.60	ND	63.0	0.10	0.00
73	F	Ad	Poor	2	1	4.98	91.71	ND	64.9	0.38	0.58
74	M	Ad	Moderate	2	0	5.51	93.93	ND	68.0	0.15	0.00
75	M	Sq	Moderate	3	0	4.22	92.25	ND	64.7	0.15	0.13
76	M	Ad	Poor	2	0	32.06	84.48	ND	45.2	0.05	0.00
77	F	Ad	Good	1	0	5.81	94.16	ND	61.1	0.02	0.00
78	F	Sq	Moderate	2	0	4.93	94.14	ND	71.0	0.07	0.00
79	F	Sq	Moderate	2	0	4.64	79.34	ND	65.8	0.88	1.46
80	M	Ad	Moderate	2	1	7.81	91.28	ND	67.3	0.04	0.00
81	F	Sq	Moderate	2	1	3.74	72.74	ND	67.0	0.14	0.04
82	F	Sq	Poor	1	2	5.71	93.93	ND	66.4	0.28	0.01
83	M	Sq	Poor	2	0	6.89	47.57	ND	60.2	0.48	0.05
84	M	Ad	Poor	4	1	6.99	91.45	ND	66.1	0.04	0.00
85	M	Ad	Moderate	4	0	3.79	91.49	ND	67.7	0.06	0.11
86	F	Ad	Moderate	1	1	4.38	89.66	ND	68.6	0.55	0.41
87	M	Sq	Moderate	2	0	5.31	75.11	ND	58.8	0.24	0.06
88	M	Sq	Moderate	2	2	3.37	66.26	ND	45.5	0.22	0.13
89	M	Ad	Moderate	4	0	4.66	92.56	ND	65.4	0.07	0.00
90	F	Ad	Moderate	1	0	14.12	91.57	ND	67.4	0.09	0.00
91	F	Ad	Poor	1	0	2.72	53.84	ND	51.9	0.73	1.69
92	M	Sq	Poor	2	1	3.46	92.96	ND	68.4	0.06	0.00
93	F	Ad	Moderate	2	0	2.97	72.49	ND	65.9	0.43	0.14
94	F	Ad	Moderate	3	2	3.95	92.46	ND	60.9	0.02	0.02
95	M	Sq	Poor	2	2	10.77	89.74	ND	59.2	0.10	0.00
96	F	Ad	Moderate	2	0	5.29	92.22	ND	66.7	0.09	0.00
97	F	Sq	Moderate	3	2	3.17	65.56	ND	50.0	0.41	0.10
98	M	Ad	Poor	2	0	5.05	81.15	ND	67.9	1.06	0.04
99	F	Sq	Poor	2	1	7.76	92.51	ND	61.9	0.18	0.00
100	F	Ad	Moderate	2	2	8.73	93.31	ND	57.9	0.05	0.01
101	F	Sq	Moderate	2	0	3.34	60.62	ND	44.4	0.27	0.08
102	M	Sq	Poor	3	1	4.09	64.67	ND	55.6	0.25	0.04

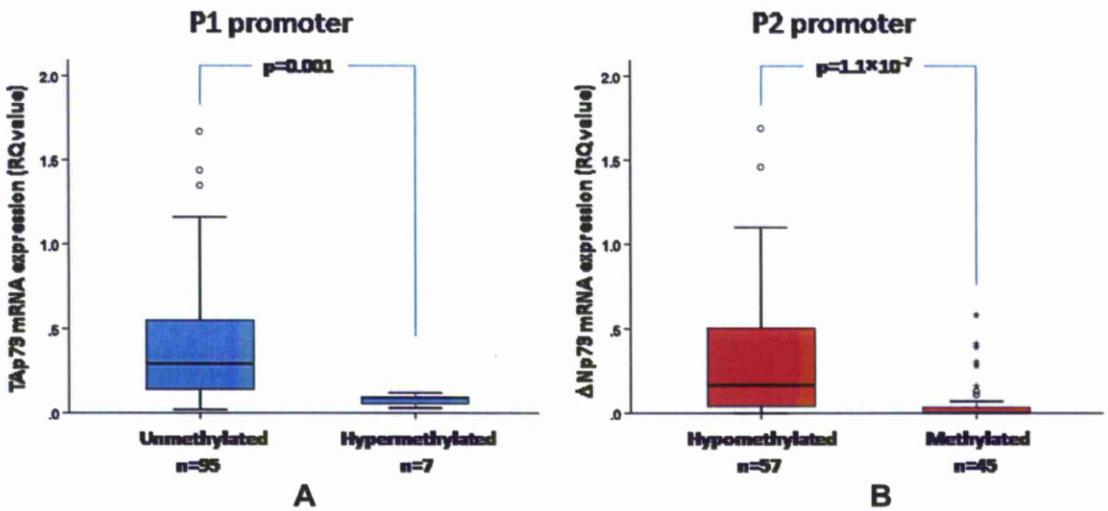

Fig. 2. (A) Box plot representation of the distribution of TAp73 RQ values in lung cancer tissues bearing an unmethylated P1 promoter versus lung cancer tissues bearing a hypermethylated P1 promoter. (B) Box plot representation of the distribution of ΔNp73 RQ values in lung cancer tissues bearing a methylated P2 promoter versus lung cancer tissues bearing a hypomethylated P2 promoter. Stars and circles in the plot indicate outliers.

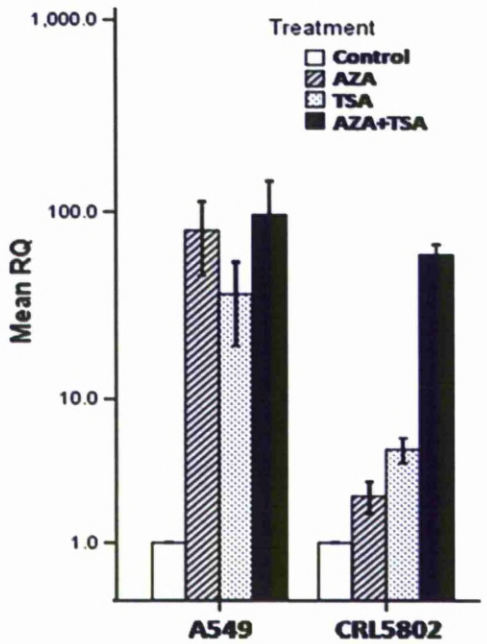

Fig. 3. ΔNp73 expression analysis in lung cancer cell lines treated with 5′-aza-2′-deoxycytidine (AZA) and trichostatin (TSA). The addition of compounds separately triggers the over-expression of ΔNp73 in both cell lines while an additive effect is profound in CRL5802 cells. ΔNp73 mRNA expression (*Y*-axis) is given as relative quantification (RQ) values in logarithmic scale. For each cell line, the untreated control was used as calibrator, thus the control expression is set to 1.

3.2. TAp73 and ΔNp73 mRNA levels correlated to the methylation status of their corresponding promoters

The TAp73 and ΔNp73 mRNA levels were measured in primary NSCLCs by qPCR. Particular attention was given experimentally to ensure the use of primers that amplify only the ΔNp73 transcripts and none of P1-derived p73Δex2, p73Δex2/3 and ΔN′-p73 transcripts. We subsequently analyzed the TAp73 expression comparatively to the DNA methylation levels of P1 promoter in the panel of tumour samples. The mRNA expression in the seven samples bearing a hypermethylated P1 promoter was significantly lower to that of the sample group with an unmethylated P1 promoter (Fig. 2). However, the correlation between the ΔNp73 mRNA expression and the methylation levels of the P2 promoter was more profound (Mann–Whitney test, $p = 1.1 \times 10^{-7}$), with ΔNp73 mRNA levels being significantly higher in the tumours with a hypomethylated P2 promoter (Fig. 2). No other association was observed between TAp73 or ΔNp73 mRNA expression and any of the clinicopathological parameters of the examined specimens.

In order to further validate the impact of P2 hypomethylation on ΔNp73 expression, we monitored the effect of epigenetic modifiers on ΔNp73 mRNA levels *in vitro* by treating one adenocarcinoma lung cancer cell line (A549) and one squamous cell carcinoma lung cancer cell line (CRL5802) with the DNA methyltransferase inhibitor 5-aza-2′-deoxycytidine (AZA) and the histone deacetylase inhibitor trichostatin-A (TSA). Both cell lines bear a methylated P2 promoter, whereas methylation levels of P1 promoter are very low (data not shown). ΔNp73 mRNA expression was increased upon treatment, while an additive effect of the two compounds was observed in both cell lines. Strikingly, treatment with 5-aza-2′-deoxycytidine alone increased ΔNp73 levels as much as 100-fold in A549 cell line (Fig. 3).

3.3. Hypomethylation-induced ΔNp73 over-expression is more profound in squamous cell carcinomas than in adenocarcinomas

As shown in Fig. 4, P2 methylation levels were markedly lower in squamous cell carcinomas (mean Mtl: 68% ± 2.5) in comparison with adenocarcinomas (mean Mtl: 83% ± 3.0, Mann–Whitney test $U = 655.50$, $p < 0.05$). Consistently, ΔNp73 mRNA expression was higher in squamous carcinomas (mean RQ = 0.98 ± 0.41) than in adenocarcinomas (mean RQ = 0.19 ± 0.05, Mann–Whitney test, $p = 0.006$). The methylation levels were significantly correlated to ΔNp73 mRNA levels both in adenocarcinomas (Spearman's $R = -0.373$, $p = 0.008$) and in squamous cell carcinomas (Spearman's $R = -0.425$, $p = 0.002$). Importantly, this correlation was more intense in squamous cell carcinomas compared to adenocarcinomas. Thus, higher P2 methylation levels in adenocarcinomas result to lower ΔNp73 mRNA levels whereas lower P2 methylation levels in squamous cell carcinomas correspond to higher ΔNp73 mRNA levels (Fig. 4). In contrast, no differences were observed in P1 methylation levels between squamous cell carcinomas and adenocarcinomas (Mann–Whitney test $U = 1112.00$, $p = 0.212$) although a borderline difference of TAp73 mRNA levels was observed between squamous cell carcinomas (mean RQ = 0.57 ± 0.1) and adenocarcinomas (mean RQ = 0.4 ± 0.07) (Mann–Whitney test U = 957.50, $p = 0.044$). Therefore, inter-histological differences exist for both ΔNp73 and TAp73 mRNA levels, but only ΔNp73 mRNA levels are consistent with corresponding differences in the P2 methylation levels.

4. Discussion

In this study we demonstrated that P1 promoter of the p73 gene is rarely hypermethylated (6.8%) in NSCLCs whereas the P2 promoter is often hypomethylated (55.9%). This epigenetic deregulation is, linked with decreased TAp73 mRNA levels and increased ΔNp73 mRNA levels, respectively. Treatment of lung cancer cell lines with epigenetic modifiers confirmed the epigenetic induction of ΔNp73 transcription *in vitro*. Notably, P2 hypomethylation was associated with LINE-1 hypomethylation, an indicator of global methylation. We also demonstrated a tissue type specific difference in the hypomethylation-linked induction of ΔNp73 mRNA levels. TAp73 mRNA levels are also more increased in squamous cell carcinomas, however independently from inter-histological differences in the P1 methylation levels.

In agreement with Di Vinci et al., P1 promoter is essentially unmethylated in normal tissues and its methylation levels remain invariably low in the majority of the tumour samples. Only a few tumour samples bear a hypermethylated P1 promoter in conjunction with lower TAp73 expression when compared to the TAp73 expression of the unmethylated tumour samples ([19] and this study). Since P1 promoter remains unmethylated in the majority of tumour tissues, TAp73 expression cannot be prevented, provided that specific transcription factors are present within the nucleus. Indeed, recently it has been shown that TAp73 isoforms are overexpressed in response to over-expression of Sp1 transcription factor, which directly activates P1 promoter in lung cancer [23]. Therefore, changes in the levels of transcription factors seem to mainly deregulate P1 promoter control, whereas the infrequent methylation of P1 promoter does not pose as a major determinant of TAp73 deregulation in lung cancer.

The P2 promoter which was generally heavily methylated in normal lung tissues was found partially demethylated in the tumour samples in a percentage slightly lower than the one previously determined by methylation-specific PCR [19]. It is of note that although methylation levels were significantly correlated to the ΔNp73 mRNA expression, a clear association between the methylation status of P2 promoter and the ΔNp73 protein levels could not be established in NSCLC tissues examined previously

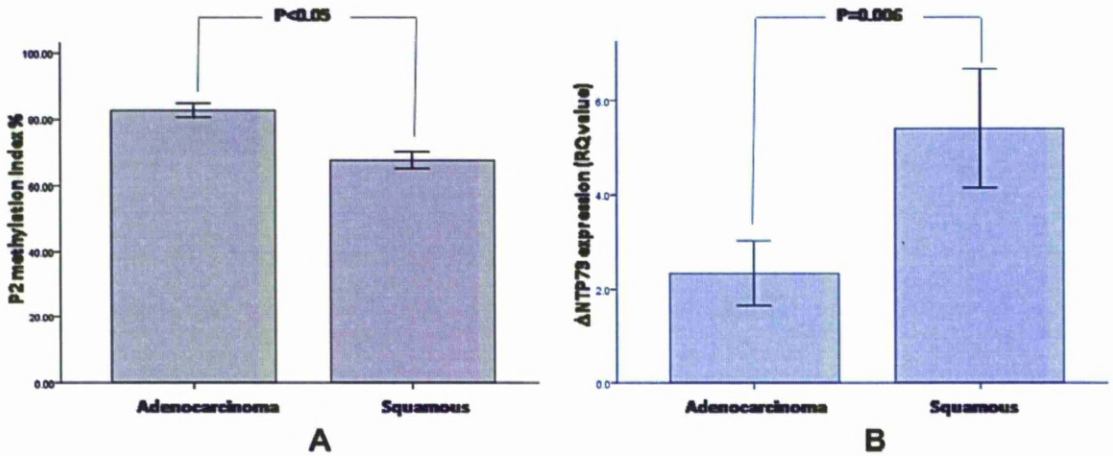

Fig. 4. Hypomethylation of P2 promoter is more profound in squamous cell carcinomas than adenocarcinomas (A). This is directly reflected in the ΔNp73 transcript levels which are higher in squamous carcinomas than adenocarcinomas (B). Histograms represent mean values and error bars are indicative of the standard error of the mean.

[19]. This discrepancy could possibly be attributed to the fact that commercially available ΔNp73-specific antibodies inevitably detect not only the translational product of the P2-derived ΔN transcript, but also the translational product of the P1-derived ΔN′ transcript, which is identical to the ΔNp73 protein [6]. Indeed, P1-derived ΔN′ transcripts have been reported to be expressed in lung cancer tumours used in the abovementioned study [19]. In contrast, quantitative RT-PCR assays detect products arising exclusively from P2 promoter and, therefore, they provide a more accurate means of estimating sheer P2 transcriptional activity, unbiased by P1 transcriptional activity. Another reason of inconsistent results between studies based on qualitative (methylation-specific PCR) versus quantitative methylation methods (pyrosequencing) could be mis-priming of methylation-specific PCR, which subsequently yields false positive results in up to 10% frequency, in assays combining small amounts of DNA input and high numbers of PCR cycles. Methylation enrichment pyrosequencing used herein overcomes these technical limitations and provides a higher degree of sensitivity in estimating methylation status, whenever clinical samples with low DNA concentrations are used [24].

Both TAp73 and ΔNp73 mRNA levels demonstrated significant inter-histological differences, but only ΔNp73 mRNA levels were dependent on the methylation levels of the corresponding promoter. Importantly, ΔNp73 expression has been previously shown to predict poor prognosis in lung cancer, with squamous cell carcinoma patients presenting lower 5-year survival rates in comparison with adenocarcinoma patients [25,26]. Thus, elevated ΔNp73 mRNA levels, consistent with lower P2 methylation levels in squamous cell lung cancer patients, may contribute, among other discrete molecular changes, to the poorer prognosis of this histological group in comparison to lung adenocarcinoma patients. In addition, the correlation of P2 promoter hypomethylation with LINE-1 hypomethylation, an accepted measure of global DNA methylation status [21,22], suggests that this reduction of P2 methylation levels is a passive consequence of global hypomethylation, which is more frequent in squamous cell carcinomas comparatively to adenocarcinomas [22,27]. In contrast, differences in TAp73 mRNA expression between distinct histological lung cancer types might be attributed to tissue type-related differences in the levels of specific transcription factors that activate P1 promoter.

Collectively, the above data suggest that epigenetic events might be crucial for the deregulation of P2 activity, whereas transcriptional events seem to be mainly implicated to deregulation of P1 activity in lung cancer [23]. ΔNp73 mRNA expression appears to be restrained by strict epigenetic control of P2 promoter in the normal lung cell. Once deregulated, specific transcription factor(s) have the opportunity to approach P2 promoter, therefore enhancing transcription of the anti-apoptotic ΔNp73 isoforms and possibly favoring oncogenic activities within the cell. In contrast, epigenetic control is looser in the case of P1 promoter and the synthesis of its corresponding products seems to be deregulated only upon presence of excess amounts of specific transcription factors.

In addition, the fact that P2 hypomethylation is markedly more frequent than P1 hypermethylation in lung cancer samples suggests that the resulting over-expression of the anti-apoptotic ΔNp73 contributes in a much greater extent to oncogenesis as compared to the under-expression of the apoptotic TAp73. Considering the strict epigenetic inhibition of ΔNp73 transcription in the normal lung cell, the question if increase of ΔNp73 rather than alterations of TAp73 may determine the ultimate effect of *p73* in lung carcinogenesis should be addressed in future studies. As demethylating agents are now entering lung cancer trials, it is imperative to gain a greater insight into the potential reactivation of oncogenic ΔNp73 in order to evaluate the risk of the usage of these agents in anti-cancer treatment and to advance for the clinical utilization of epigenetics in cancer therapy.

Our study also provides hints of a differential rather than opposing mode of regulation of *p73* promoters in lung tissues. In case that the modes of regulation of P1 and P2 promoters do present a non-yin-yang relationship, they

could offer a certain degree of freedom in the synthesis of their corresponding products in specific tissues, thus allowing their participation in distinct functions. This notion is further supported by the fact that TAp73 and ΔNp73 isoforms present not only strictly counteracting functions, i.e. TAp73 apoptotic activities versus ΔNp73 anti-apoptotic activities [3], but also unique, independent functions especially in developmental processes, in which *p73* gene is primarily implicated. For instance, ΔNp73 is essential for normal ventricular size and cortical thickness during neurogenesis in $\Delta Np73^{-/-}$ mice, whereas lack of TAp73 does not influence these parameters in $TAp73^{-/-}$ mice [28]. The investigation of this hypothesis in the future would set more light on the range of functions and the interplay of the p73 isoforms.

Conflict of interest

The authors declare no conflict of interest related to this work.

Acknowledgements

This research project was funded by the Roy Castle Lung Cancer Foundation, UK and the TOK Marie Curie program SUPRAGENE, Cont. No. MTKD-CT-2005-029508. We are grateful to the clinical resources group for providing the tissue.

References

[1] C.D. Pozniak, S. Radinovic, A. Yang, F. McKeon, D.R. Kaplan, F.D. Miller, An anti-apoptotic role for the p53 family member, p73, during developmental neuron death, Science 289 (2000) 304–306.
[2] T. Stiewe, C.C. Theseling, B.M. Putzer, Transactivation-deficient Delta TA-p73 inhibits p53 by direct competition for DNA binding: implications for tumorigenesis, J. Biol. Chem. 277 (2002) 14177–14185.
[3] T.J. Grob, U. Novak, C. Maisse, D. Barcaroli, A.U. Luthi, F. Pirnia, B. Hugli, H.U. Graber, V. De Laurenzi, M.F. Fey, G. Melino, A. Tobler, Human delta Np73 regulates a dominant negative feedback loop for TAp73 and p53, Cell Death Differ. 8 (2001) 1213–1223.
[4] T. Stiewe, S. Zimmermann, A. Frilling, H. Esche, B.M. Putzer, Transactivation-deficient DeltaTA-p73 acts as an oncogene, Cancer Res. 62 (2002) 3598–3602.
[5] U.M. Moll, N. Slade, p63 and p73: roles in development and tumor formation, Mol. Cancer Res. 2 (2004) 371–386.
[6] T. Stiewe, S. Tuve, M. Peter, A. Tannapfel, A.H. Elmaagacli, B.M. Putzer, Quantitative TP73 transcript analysis in hepatocellular carcinomas, Clin. Cancer Res. 10 (2004) 626–633.
[7] M. Esteller, J.G. Herman, Cancer as an epigenetic disease-DNA methylation and chromatin alterations in human tumours, J. Pathol. 196 (2002) 1–7.
[8] H. Wu, Y. Chen, J. Liang, B. Shi, G. Wu, Y. Zhang, D. Wang, R. Li, X. Yi, H. Zhang, L. Sun, Y. Shang, Hypomethylation-linked activation of PAX2 mediates tamoxifen-stimulated endometrial carcinogenesis, Nature 438 (2005) 981–987.
[9] H.J. Jun, S. Woolfenden, S. Coven, K. Lane, R. Bronson, D. Housman, A. Charest, Epigenetic regulation of c-ROS receptor tyrosine kinase expression in malignant gliomas, Cancer Res. 69 (2009) 2180–2184.
[10] L. Cui, L.Y. Xu, Z.Y. Shen, Q. Tao, S.Y. Gao, Z. Lv, Z.P. Du, W.K. Fang, E.M. Li, NGALR is overexpressed and regulated by hypomethylation in esophageal squamous cell carcinoma, Clin. Cancer Res. 14 (2008) 7674–7681.
[11] C. De Smet, A. Loriot, DNA hypomethylation in cancer: epigenetic scars of a neoplastic journey, Epigenetics 5 (2010) 206–213.
[12] J.F. Costello, M.C. Frühwald, D.J. Smiraglia, L.J. Rush, G.P. Robertson, X. Gao, F.A. Wright, J.D. Feramisco, P. Peltomäki, J.C. Lang, D.E. Schuller, L. Yu, C.D. Bloomfield, M.A. Caligiuri, A. Yates, R. Nishikawa, H. Su Huang, N.J. Petrelli, X. Zhang, M.S. O'Dorisio, W.A. Held, W.K. Cavenee, C. Plass, Aberrant CpG-island methylation has non-random and tumour-type-specific patterns, Nat. Genet. 24 (2000) 132–138.
[13] P.G. Corn, S.J. Kuerbitz, M.M. van Noesel, M. Esteller, N. Compitello, S.B. Baylin, J.G. Herman, Transcriptional silencing of the p73 gene in acute lymphoblastic leukemia and Burkitt's lymphoma is associated with 5′ CpG island methylation, Cancer Res. 59 (1999) 3352–3356.
[14] A. Pluta, U. Nyman, B. Joseph, T. Robak, B. Zhivotovsky, P. Smolewski, The role of p73 in hematological malignancies, Leukemia 20 (2006) 757–766.
[15] B. Martinez-Delgado, B. Melendez, M. Cuadros, M.J. Garcia, J. Nomdedeu, C. Rivas, Frequent inactivation of the *p73* gene by abnormal methylation or LOH in non-Hodgkin's lymphomas, Int. J. Cancer 102 (2002) 15–19.
[16] L.L. Siu, J.K. Chan, K.F. Wong, Y.L. Kwong, Specific patterns of gene methylation in natural killer lymphomas: p73 is consistently involved, Am. J. Pathol. 160 (2002) 59–66.
[17] B. Banelli, I. Casciano, M. Romani, Methylation-independent silencing of the *p73* gene in neuroblastoma, Oncogene 19 (2000) 4553–4556.
[18] I. Casciano, B. Banelli, M. Croce, G. Allemanni, S. Ferrini, G.P. Tonini, M. Ponzoni, M. Romani, Role of methylation in the control of ΔNp73 expression in neuroblastoma, Cell Death Differ. 9 (2002) 343–345.
[19] A. Di Vinci, F. Sessa, I. Casciano, B. Banelli, F. Franzi, C. Brigati, G. Allemanni, P. Russo, L. Dominioni, M. Romani, Different intracellular compartmentalization of TA and DeltaNp73 in non-small cell lung cancer, Int. J. Oncol. 34 (2009) 449–456.
[20] K. Chalitchagorn, S. Shuangshoti, N. Hourpai, N. Kongruttanachok, P. Tangkijvanich, D. Thong-ngam, N. Voravud, V. Sriuranpong, A. Mutirangura, Distinctive pattern of LINE-1 methylation level in normal tissues and the association with carcinogenesis, Oncogene 23 (2004) 8841–8846.
[21] D.J. Weisenberger, M. Campan, T.I. Long, M. Kim, C. Woods, E. Fiala, M. Ehrlich, P.W. Laird, Analysis of repetitive element DNA methylation by MethyLight, Nucleic Acids Res. 33 (2005) 6823–6836.
[22] A. Daskalos, G. Nikolaidis, G. Xinarianos, P. Savvari, A. Cassidy, R. Zakopoulou, A. Kotsinas, V. Gorgoulis, J.K. Field, T. Liloglou, Hypomethylation of retrotransposable elements correlates with genomic instability in non-small cell lung cancer, Int. J. Cancer 124 (2009) 81–87.
[23] S. Logotheti, I. Michalopoulos, M. Sideridou, A. Daskalos, S. Kossida, D.A. Spandidos, J.K. Field, B. Vojtesek, T. Liloglou, V. Gorgoulis, V. Zoumpourlis, Sp1 binds to the external promoter of the p73 gene and induces the expression of TAp73gamma in lung cancer, FEBS J. 277 (2010) 3014–3027.
[24] R.J. Shaw, E.K. Akufo-Tetteh, J.M. Risk, J.K. Field, T. Liloglou, Methylation enrichment pyrosequencing: combining the specificity of MSP with validation by pyrosequencing, Nucleic Acids Res. 34 (2006) e78.
[25] H. Uramoto, K. Sugio, T. Oyama, S. Nakata, K. Ono, M. Morita, K. Funa, K. Yasumoto, Expression of deltaNp73 predicts poor prognosis in lung cancer, Clin. Cancer Res. 10 (2004) 6905–6911.
[26] H. Uramoto, K. Sugio, T. Oyama, S. Nakata, K. Ono, T. Nozoe, K. Yasumoto, Expression of the p53 family in lung cancer, Anticancer Res. 26 (2006) 1785–1790.
[27] K. Saito, K. Kawakami, I. Matsumoto, M. Oda, G. Watanabe, T. Minamoto, Long interspersed nuclear element 1 hypomethylation is a marker of poor prognosis in stage IA non-small cell lung cancer, Clin. Cancer Res. 16 (2010) 2418–2426.
[28] M.T. Wilhelm, A. Rufini, M.K. Wetzel, K. Tsuchihara, S. Inoue, R. Tomasini, A. Itie-Youten, A. Wakeham, M. Arsenian-Henriksson, G. Melino, D.R. Kaplan, F.D. Miller, T.W. Mak, Isoform-specific p73 knockout mice reveal a novel role for (Delta)Np73 in the DNA damage response pathway, Genes Dev. 24 (2010) 549–560.

Int. J. Cancer: **124,** 81–87 (2009)

Hypomethylation of retrotransposable elements correlates with genomic instability in non-small cell lung cancer

Alexandros Daskalos[1], Georgios Nikolaidis[1], George Xinarianos[1], Paraskevi Savvari[2], Adrian Cassidy[1], Roubini Zakopoulou[1,2], Athanasios Kotsinas[2], Vassilis Gorgoulis[2], John K. Field[1] and Triantafillos Liloglou[1]*

[1]*Roy Castle Lung Cancer Research Programme, The University of Liverpool, School of Cancer Studies, Liverpool, United Kingdom*
[2]*Molecular Carcinogenesis Group, Histology-Embryology Lab, Medical School, University of Athens, Athens, Greece*

LINE-1 and Alu elements are non-LTR retrotransposons, constituting together over 30% of the human genome and they are frequently hypomethylated in human tumors. A relationship between global hypomethylation and genomic instability has been shown, however, there is little evidence to suggest active role for hypomethylation-mediated reactivation of retroelements in human cancer. In our study, we examined by Pyrosequencing the methylation levels of LINE-1 and Alu sequences in 48 primary nonsmall cell carcinomas and their paired adjacent tissues. We demonstrate a significant reduction of the methylation levels of both elements ($p = 7.7 \times 10^{-14}$ and 9.6×10^{-7}, respectively). The methylation indices of the 2 elements correlated ($p = 0.006$), suggesting a possible common mechanism for their methylation maintenance. Genomic instability was measured utilizing 11 fluorescent microsatellite markers located on lung cancer hot-spot regions such as 3p, 5q 9p, 13q and 17p. Hypomethylation of both transposable elements was associated with increased genomic instability (LINE, $p = 7.1 \times 10^{-5}$; Alu, $p = 0.008$). The reduction of the methylation index of LINE-1 and Alu following treatment of 3 lung cell lines with 5-aza-2′-deoxycitidine, consistently resulted in increased expression of both elements. Our study demonstrates the strong link between hypomethylation of transposable elements with genomic instability in non-small cell lung cancer and provides early evidence for a potential active role of these elements in lung neoplasia. As demethylating agents are now entering lung cancer trials, it is imperative to gain a greater insight into the potential reactivation of silent retrotransposons in order to advance for the clinical utilization of epigenetics in cancer therapy.

Key words: LINE-1; Alu; hypomethylation; genomic instability; lung cancer

LINE-1 elements are autonomous non-LTR retrotransposons comprising almost 21% of the human genome.[1] Although most of these elements are inactive, mostly due to 5′ truncations, there are a number of 80–100 intact LINE-1 elements that remain capable of retrotransposition.[2,3] The full length human LINE-1 retrotransposon is about 6 kb consisting of a 5′ UTR, two open reading frames (ORF 1 and ORF2), and a 3′ UTR with a functional polyadenylation signal and a variable length poly-A tail.[1] The bicistronic mRNA of LINE-1 is generated by an internal promoter at the 5′ UTR region. ORF1 encodes for p40, a 40 kDa RNA-binding protein with cis preference for LINE-1 RNA, while ORF2 encodes for a 150 kDa protein with 3 conserved domains.[4] LINE-1 retrotransposition is undertaken with the help of both ORF1 and ORF2 proteins through a target-primed reverse transcription mechanism (TPRT).[2]

In normal human cells, transcription and retrotransposition of LINE-1 is suppressed by a variety of control mechanisms including methylation, siRNAs and transcription regulators.[4–6] As a result, cells manage to protect themselves from a number of adverse effects exerted by LINE-1 activity. LINE-1 retrotransposition events elicit enhanced illegitimate and homologous recombination,[2,7] genomic deletions,[8] chromosome breaks and translocations[9] leading to enhanced genomic instability of the cell.[10] In addition, successful retrotransposition events may change the activity of genes at the insertion sites, either by inducing or reducing their transcription, or by generating alternative transcripts.[7]

The Alu element, the most prevalent human SINE, is another retrotransposon which, like LINE-1, can retrotranspose promoting chromosomal rearrangements, insertions/deletions and unequal recombination.[4] A typical Alu element stretches over about 300 bp and has an internal promoter. It is not known to encode a protein product, thus it is in need of other retrotransposons' machinery to undertake transposition. It is mainly suggested that LINE-1 facilitates Alu element retrotransposition.[4,11] As with LINE-1, Alu's activity in the normal cells is inhibited mostly through methylation of its sequence.[10,12]

Two phenomenically contradicting epigenetic events coexist in cancer, namely global hypomethylation of DNA, mainly associated with repeated DNA and hypermethylation in nonrepeat DNA stretches, frequently associated with gene promoter sequences.[7,13] Indeed, LINE-1 sequences are found to be hypomethylated in a large number of human cancers including colorectal, prostate, lung, bladder, teratocarcinoma, renal and gastric cancer suggesting potential activation in these cancers.[7,13–17] Although less studied, Alu element hypomethylation in cancer has been also reported.[16,18–20] Of note is the fact that in ovarian tumors this global DNA hypomethylation cannot be attributed to differential mRNA expression of any particular DNMT gene or isoform.[20]

Taking the above observations under consideration, one could hypothesize that reactivation of LINE-1 and Alu elements in normal cells through hypomethylation could potentially induce genomic instability, thus introducing cells into a precancerous state. Animal studies demonstrate that genome wide hypomethylation induces genomic instability and tumors.[21,22] However, these findings have not been directly connected to retrotransposition. In addition, LINE-1 retrotransposition was shown to induce DNA damage and apoptosis in a breast cancer cell line.[23]

Lung cancer is a major cause of cancer-related death. Numerous molecular abnormalities have associated with the development of the disease including extensive epigenetic deregulation events.[24] So far, a large number of hypermethylated and hypomethylated genes have been reported in primary lung cancers.[25–28]

To date, there is evidence linking global hypomethylation in human cancer with genomic instability. However, it remains questionable whether LINE and Alu elements are actively mediating this process. In our study we examine the methylation status of the LINE-1.2 and Alu-PV elements in a set of nonsmall cell lung carcinomas (NSCLCs) comparatively to genomic instability. In addition, we assess the epigenetic control potential on the expression levels of both elements in lung cell lines by treating these with a demethylating agent and a histone deacetylase inhibitor.

Abbreviations: FAL, fractional allele loss; FBS, fetal bovine serum; LINE, long interspersed nucleotide elements; LOH, loss of heterozygosity; LTR, long terminal repeat; NSCLC, nonsmall cell lung cancer; ORF, open reading frame; SINE, short interspersed nucleotide elements; TSA, trichostatin A.

Grant sponsors: Roy Castle Lung Cancer Foundation (UK), GENICA-FP7 EU.

***Correspondence to:** Roy Castle Lung Cancer Research Programme, The University of Liverpool, School of Cancer Studies, 200 London Road, Liverpool L3 9TA, UK. E-mail: tliloglo@liv.ac.uk

Received 23 May 2008; Accepted after revision 3 July 2008
DOI 10.1002/ijc.23849
Published online 29 September 2008 in Wiley InterScience (www.interscience.wiley.com).

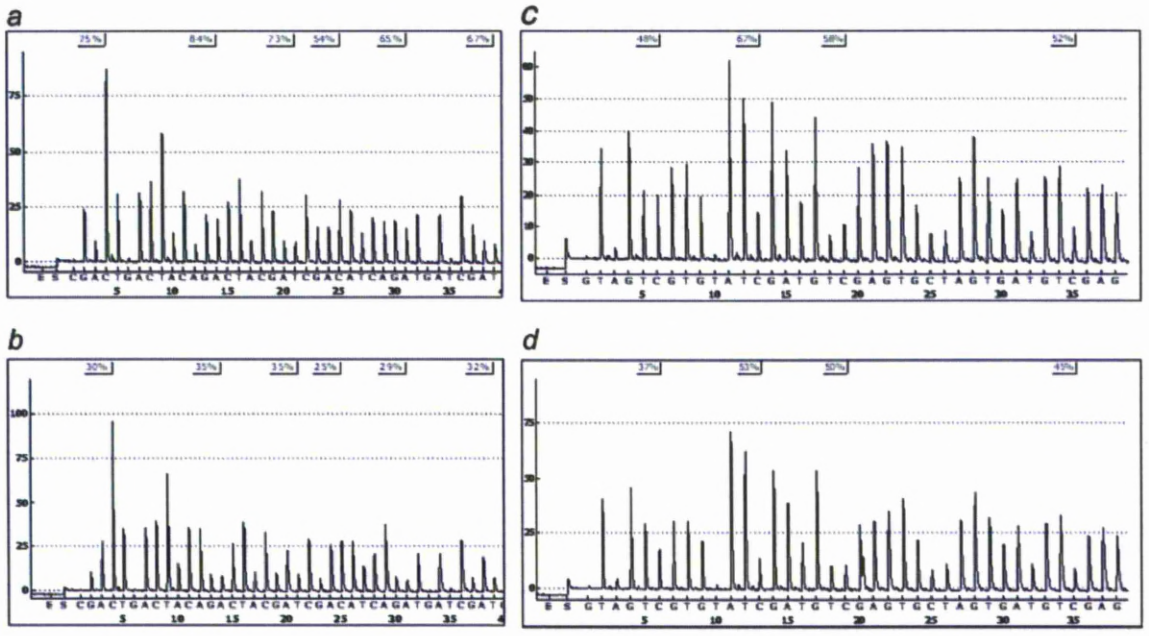

FIGURE 1 – Representative pyrograms of the LINE-1 and Alu sequences examined in our study. (*a*) LINE-1; adjacent normal, (*b*) LINE-1; lung tumor, (*c*) Alu; adjacent normal, (*d*) Alu; lung tumor. The percentages in boxes indicate the individual CpGs methylation values. The methylation index (MtI) is calculated as the average values of the examined CpGs.

Material and methods

Human tissues and cell lines

Forty-eight NSCLCs (24 adenocarcinomas and 24 squamous carcinomas) and adjacent normal tissues were collected from patients undergoing surgery at Broadgreen Cardiothoracic Centre (Liverpool, UK). Twenty-six (54%) patients were male. Age ranged between 46 and 80 years (mean = 64). All specimens were of advanced stage (43 T2, 4 T3 and 1 T4). The study protocol was approved by the Liverpool Ethics Committee and all patients provided written, informed consent in accordance with the Declaration of Helsinki. Nine cell lines of lung cancer origin were studied in parallel: CRL5802, SKMES (squamous), A549, SKLU1, CALU 3, CRL 5935 (adenocarcinoma), DMS 53 (small cell) CORL 23 (large cell), CALU 6 (anaplastic carcinoma). Cells were grown in DMEM: F12 with L-glutamine and 10% FBS. In addition one immortalized, nontumorigenic lung epithelial cell line (HBEC3KT—kindly donated by A. Gazdar) and a commercially available normal epithelial cell line (NHBE, Lonza, Basel, Switzerland) were analyzed. These cell lines were grown in Keratinocyte serum-free medium (Invitrogen) supplemented with EGF and pituitary extract (Invitrogen). All cells were grown at 37°C supplemented with 5% CO_2.

For the DNA methylation/histone acetylation inhibition experiments, we treated cell lines with 100 nM 5-aza-2′-deoxycytidine (Decitabine; Sigma-Aldrich, cat no11390) or 100 nM Trichostatin A (TSA, Sigma-Aldrich, Dorset, UK) cat no T8552) and a combination of both compounds. Cells were treated with decitabine for 2 cell duplications, with medium and fresh decitabine being replenished daily. TSA was added and were applicable for the last 16 hr before harvesting cells. All observations were confirmed by duplicate experiments at both the technical and biological level.

DNA, RNA extraction and cDNA synthesis

For the DNA extraction 20 μm × 40 μm sections were cut from frozen tissue. The first and last sections underwent pathological review to ensure at least 80% tumor cell content. DNA extraction of the samples and cell lines was performed using the DNeasy kit (Qiagen, West Sussex, UK) following the manufacturer's protocol. Quality and quantity of the DNA was assessed by spectrophotometry at 260/280 nm. RNA from cell lines was extracted using the RNeasy kit (DNAse digest protocol, Qiagen, West Sussex, UK) following the manufacturer's protocol. Quality and quantity of the RNA was assessed by capillary electrophoresis on an Agilent 2100 Bioanalyser (Agilent Technologies). cDNA was prepared from 1 μg RNA using the Quantitect kit (Qiagen, West Sussex, UK), which includes an initial genomic DNA elimination step eliminating thus the possibility of genomic DNA carry over into the cDNA preparation.

DNA methylation analysis

For the methylation analysis of the LINE-1.2 (Genebank accession no M80343) and the Alu-PV (Genebank accession no Z49816) elements, 1 μg of genomic DNA was treated with sodium bisulfite, using the EZ DNA methylation Kit™ (ZymoResearch) following the manufacturer's protocol. For the LINE-1.2 element a target region inside the CpG-rich region of the 5′ internal promoter including 6 CpGs was chosen, whereas for the Alu PV element we selected a target CpG-rich region near its 3′ end encompassing 4 CpG sites. All primers were designed using the Assay Design Software (Biotage, Uppsala, Sweden) and synthesized by MWG (Germany): LINE-1 fwd: 5′-BIO-TAG GGA GTG TTA GAT AGT GG-3′, LINE-1 rev: 5′-AAC TCC CTA ACC CCT TAC-3′, LINE-1 seq 5′-CAA ATA AAA CAA TAC CTC-3′. Alu fwd: 5′-GAG GTT GAG GTA GGA GAA-3′, Alu rev: 5′-BIO-CCC AAA CTA AAA TAC AAT AAC-3′, Alu seq: 5′-GTT GAG GTA GGA GAA-3′. PCR amplifications were performed using Qiagen HotStarTaq Master Mix Kit, (5 μM biotinylated primer, 10 μM nonbiotinylated primer and 3 μl (~60 ng) bisulfite-treated DNA. Thermal profiles were as follows: 95°C for 5 min followed by 40 cycles of 94°C for 30 sec, 58°C (LINE-1) or 49°C (Alu) for

TABLE I - CLINICAL SAMPLES OF THE UTILIZED COHORT AND RESULTS FOR LINE-1 AND ALU METHYLATION AND GENOMIC INSTABILITY (FAL)

Sample	Gender	Age	Diagnosis	Methylation index (%)				FAL
				LINE-1 normal	LINE-1 tumor	Alu normal	Alu tumor	
1	F	74	AdenoCa	70.3	61.3	53.3	52.7	0.455
2	M	68	AdenoCa	69.7	58.0	55.0	53.2	0.857
3	F	50	AdenoCa	69.1	56.3	50.6	53.9	0.857
4	M	52	AdenoCa	69.6	65.6	57.4	54.1	0.375
5	F	68	AdenoCa	69.7	64.7	56.6	60.0	0.400
6	F	74	AdenoCa	69.4	47.0	56.6	55.0	0.625
7	F	67	AdenoCa	69.3	67.8	53.5	54.0	0.500
8	F	53	AdenoCa	70.0	60.8	58.2	52.8	0.778
9	F	73	AdenoCa	70.6	67.6	56.7	55.7	0.000
10	F	58	AdenoCa	70.2	54.0	58.4	55.2	1.000
11	M	74	AdenoCa	69.8	48.4	60.3	51.8	0.909
12	F	69	AdenoCa	69.6	34.8	59.0	56.5	1.000
13	M	63	AdenoCa	69.3	47.2	56.7	51.6	0.900
14	F	64	AdenoCa	69.8	51.3	56.2	50.7	0.889
15	F	66	AdenoCa	70.0	68.8	56.6	56.6	0.000
16	F	61	AdenoCa	68.3	57.4	58.8	55.7	0.600
17	M	67	AdenoCa	70.2	69.4	55.9	60.5	0.143
18	M	65	AdenoCa	69.3	62.4	58.8	52.2	1.000
19	F	68	AdenoCa	68.4	59.2	56.0	52.8	0.889
20	F	69	AdenoCa	69.5	52.2	ND	ND	0.818
21	F	77	AdenoCa	69.7	54.5	55.7	54.3	1.000
22	F	53	AdenoCa	69.1	59.3	54.8	53.1	0.556
23	F	67	AdenoCa	68.1	52.1	56.9	48.6	0.500
24	F	45	SqCCL	69.4	66.8	55.3	53.4	0.250
25	M	62	SqCCL	69.7	30.9	56.4	46.3	0.833
26	M	68	SqCCL	69.9	70.3	58.7	54.5	0.000
27	M	78	SqCCL	67.1	48.2	58.7	59.9	0.556
28	M	68	SqCCL	70.8	41.5	58.8	54.1	0.375
29	M	60	SqCCL	70.2	62.7	53.4	52.4	0.333
30	M	62	SqCCL	69.5	40.8	59.9	51.7	0.556
31	M	60	SqCCL	70.3	43.9	58.2	52.2	0.636
32	M	70	SqCCL	69.6	63.1	56.5	54.4	1.000
33	F	70	SqCCL	69.6	40.0	55.4	51.2	0.900
34	M	83	SqCCL	69.6	49.8	56.4	53.8	0.900
35	M	83	SqCCL	70.5	56.8	56.5	48.8	1.000
36	M	66	SqCCL	68.3	41.0	60.6	47.6	1.000
37	M	65	SqCCL	70.4	50.5	53.0	55.9	1.000
38	M	58	SqCCL	69.0	48.2	55.6	51.8	0.714
39	M	66	SqCCL	70.1	60.3	57.2	53.4	0.182
40	M	72	SqCCL	69.8	61.9	62.5	54.9	0.300
41	F	66	SqCCL	68.8	57.1	53.9	50.9	0.667
42	M	47	SqCCL	69.4	38.6	55.7	53.4	0.700
43	M	69	SqCCL	70.3	66.4	57.2	54.1	0.636
44	M	68	SqCCL	73.5	67.7	55.2	55.1	0.100
45	F	48	SqCCL	ND	ND	56.6	57.5	0.182
46	M	63	SqCCL	65.4	34.6	55.6	52.6	0.714
47	F	71	SqCCL	69.1	41.6	54.4	53.7	0.778
48	F	69	SqCCL	70.1	52.1	ND	ND	0.667

45 sec and 72°C for 45 sec and a final extension step at 72°C for 10 min. The quality and quantity of the PCR product was confirmed by agarose gel (2%) electrophoresis before the clean up and Pyrosequencing analysis. For the latter, the SQA kit was used following the suppliers protocol (Biotage, Uppsala, Sweden) and the reaction was performed on a 96MA Pyrosequencer (Biotage, Uppsala, Sweden). The methylation index for the LINE-1 and Alu elements was calculated as the mean value of mC/(mC + C) for all examined CpGs in the elements.

qPCR expression assay

To investigate the expression status of the LINE-1 and Alu-PV elements in our cell lines, qPCR (real time) assays were designed using the Primer Express software (Applied Biosystems, Warrington, UK): LINE-1 fwd 5′-GAG AGG ATG CGG AGA AAT AGG A-3′, LINE-1 rev 5′-GGA TGG CTG GGT CAA ATG GT-3′ and LINE-1 probe 5′-FAM-CAA CCA TTG TGG AAG TCA GTG TGG CG-TAMRA-3′; Alu-PV fwd 5′-GAG GCG GGC GGA TCA C-3′, Alu-PV rev 5′-GTT TCA CCG TTT TAG CCA GGA T-3′ and Alu-PV probe 5′-FAM-AGG TCA GGA GAT CGA G-TAMRA-3′. Assays were performed in a final reaction volume of 20 µl containing 10 µl Taqman expression master mix, 900 nM of each primer and 250 nM probe, 1 µl of the endogenous control ACTB-VIC (Applied Biosystems, Warrington, UK) and 2 µl of cDNA following the universal conditions (2 min at 50°C, 95°C for 10 min, 50 cycles of 94°C for 30 sec, 60°C for 45 sec) on an Applied Biosystems 7500 real time PCR machine. All qPCR assays were run in triplicates.

Microsatellite analysis

The microsatellite marker panel reaction was carried out in a multiplex fashion using the Qiagen Multiplex PCR Master Mix (Qiagen, UK). Primers were selected from the LMS HD5 set (Applied Biosystems, Warrington, UK) and were custom synthesized with 5′ biotinylated reverse primers. The reaction volume was 20 µl and the loci included were D3S1300, D3S1263, D3S1566, D3S1289, D5S644, D9S157, D9S161, D13S153, D13S171, D13S263 and D17S938. The thermal profile consisted of 95°C for 15 min followed by 30 cycles consisting of 94°C for 30 sec, 56°C for 90 sec and 72°C for 60 sec and a final 30-min step extension at 72°C. PCR products were cleaned using Streptavidin coated Dynabeads (Invitrogen, Paisley, UK). Immobilized

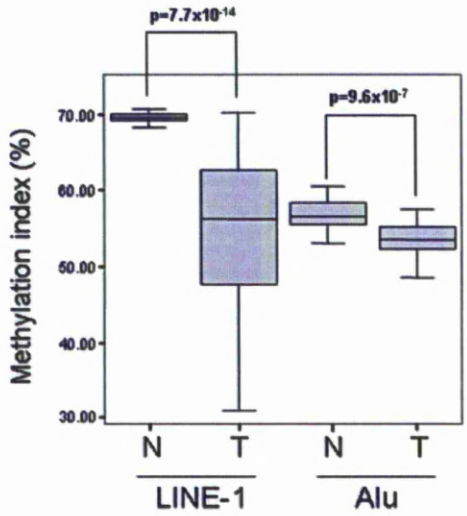

FIGURE 2 – Box plot representation of LINE-1 and Alu methylation values observed in the studied cohort. There is a profound hypomethylation of both elements in the lung cancer tissue (T) compared to adjacent normal (N). *p* values above each pair are produced by 2-tailed paired *t*-test.

PCR products were washed with 200 μl 70% ethanol and dissolved in 4 μl loading buffer containing formamide:dextran blue:-ROX400 size standard (Applied Biosystems, Warrington, UK) in a 10:2:1.5 ratio. The mixture was denatured at 95°C for 5 min, cooled on ice and loaded on a 4.2% denaturing polyacrylamide gel on a 377 ABI PRISM automated sequencer. Peak area analysis was undertaken using the GeneScan and Genotyper software (Applied Biosystems, Warrington, UK). The allelic imbalance index (AII) was calculated for each sample as follows: AII = (A1/A2)T/(A1/A2)N. The loss of heterozygosity (LOH) threshold was calculated based on the 99% reference range (= mean ± 3 × SD) created by values produced by multiple repetition of normal blood DNA samples.[29] The fractional allele loss (FAL) value was used as an expression of overall genomic instability in each sample and was calculated as: FAL = [number of loci with loss]/[number of informative loci].

Statistical analysis

Q-Q plots and the one-sample Kolmogorov-Smirnof test were used to evaluate fitness to normal distribution of continuous parameters. Paired *t*-test was used to determine if there was a statistically significant change in the methylation status of LINE-1 and AluPV in primary NSCLC tumors. Based on the fitness of parameters to normal distribution, the Pearson's (parametric) test was used to analyze correlations between LINE-1 and AluPV methylation and genomic instability. All analyses were performed using the SPSS 13.0 package. $p < 0.05$ is considered statistically significant.

Results

Methylation status of LINE-1 and AluPV in primary NSCLC tumors

We have examined the methylation levels of the 5′ promoter CpG island of LINE-1 and the 3′-end CpG island of the Alu element, utilizing Pyrosequencing assays that we developed and validated. Representative pyrograms of such assays are given in Figure 1 and the results are summarized in Table I. LINE-1 promoter was highly methylated with minimal variability in normal lung tissues (Methylation index = 69.8% ± 0.14%). The corresponding tumor samples demonstrated a significant drop in the methylation index values (56.4% ± 1.4%, paired *t*-test, $p = 7.7 \times 10^{-14}$, Fig. 2). A highly significant difference between normal (56.6% ± 0.3%) and tumor (53.5% ± 0.4%) tissue methylation indexes were found for Alu (paired *t*-test, $p = 9.6 \times 10^{-7}$, Fig. 2). Notably, LINE-1 and Alu methylation indices in primary tumors strongly correlated with each other (Pearson's correlation = 0.401, $p = 0.006$). Clinicopathological parameters such as age, gender, T status, differentiation and nodal metastasis did not correlate with LINE-1 and Alu methylation (data not shown). LINE-1 hypomethylation was more frequent in squamous carcinomas than adenocarcinomas, however only at borderline significance ($p = 0.052$). As only 4 never smokers were present in this patient cohort, no valid conclusions regarding the impact of smoking can be drawn.

TABLE II – METHYLATION LEVELS OF THE LINE-1,2 AND ALU-PV ELEMENTS IN LUNG CELL LINES

Cell line	Origin	Methylation index (%)	
		LINE-1	Alu
NHBE	Primary normal bronchial	56	52
HBEC3KT	Bronchial immortalized	56	45
A549	Adenocarcinoma	51	42
CALU 3	Adenocarcinoma	64	46
CRL 5935	Adenocarcinoma	64	44
SKLU-1	Adenocarcinoma	62	46
CALU 6	Anaplastic carcinoma	50	45
CORL 23	Large cell carcinoma	63	48
DMS 53	Small cell carcinoma	40	43
CRL 5802	Squamous carcinoma	33	37
SKMES	Squamous carcinoma	59	46

Correlation of LINE-1 and Alu elements with genomic instability

We determined genomic instability in this tumor set utilizing 11 microsatellite markers, which have been previously shown to be hot spots for LOH in lung tumors.[29,30] Detailed results from individual microsatellites are given in supplementary data. Genomic instability for each sample is expressed as the FAL value (Table I). The bivariate correlation analysis between methylation index and FAL demonstrated that genomic instability is associated with hypomethylation of LINE-1 (Pearson's correlation = −0.547, $p = 7.1 \times 10^{-5}$) and Alu (Pearson's correlation = −0.392, $p = 0.008$).

Epigenetic regulation of LINE-1 and Alu elements in lung cell lines

We measured the methylation levels of the LINE-1 and Alu elements in 9 lung cancer cell lines, 1 immortalized, nontumorigenic bronchial epithelial cell line (HBEC3KT) and a commercially available normal bronchial epithelial line (NHBE). Cancer cell lines demonstrated a variable degree of methylation in these elements, whereas the normal and immortalized cell lines methylation status was somewhat lower than the average index of surgical normal adjacent tissue (Table II). We examined the possible epigenetic control of LINE-1 and Alu expression by using the demethylating agent 5-aza-2-deoxycytidine (Decitabine) and a histone deacetylase inhibitor such as trichostatin (TSA). We selected the A549, CRL5802 and HBEC3KT lines (1 adenocarcinoma, 1 squamous and 1 nontumorigenic, respectively). Treatment with decitabine resulted in hypomethylation while addition of TSA did not affect, as expected, the methylation status. Decitabin and TSA increased the expression of both elements, with the exception of LINE expression in HBEC3KT where TSA had no effect. As expected the combined use of both substances resulted in enhanced transcription compared to single substance use (Fig. 3).

Discussion

The LINE-1 and Alu elements are non-LTR containing retrotransposons which comprise a long stretch of the human repeat

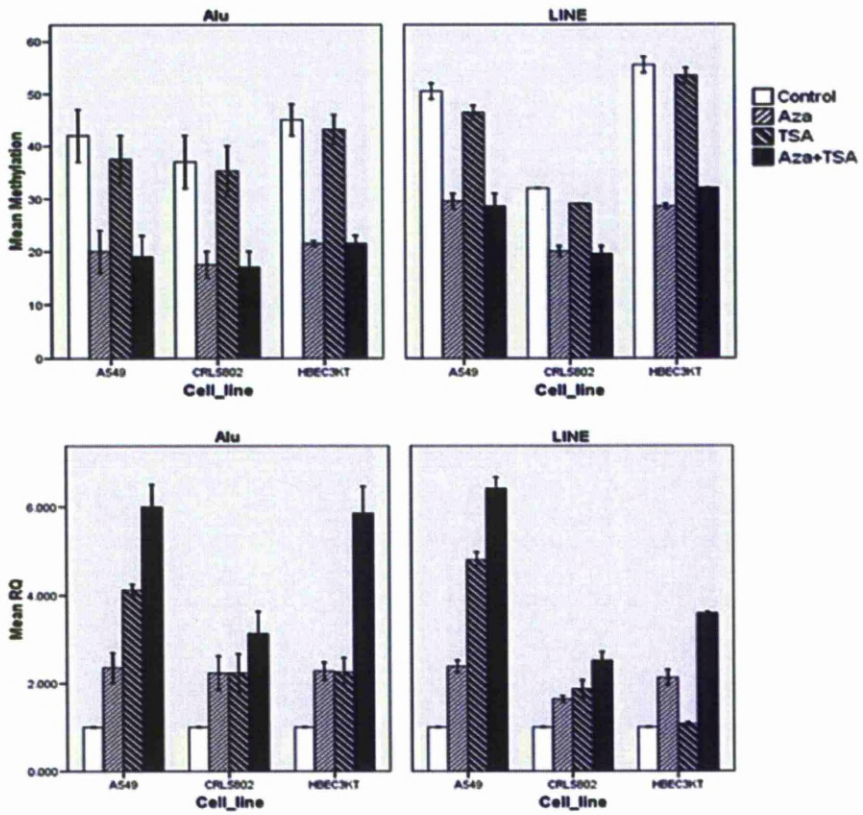

FIGURE 3 – Bar charts demonstrating the methylation (top panels) and expression (bottom panels) levels of LINE-1 and Alu transcripts following treatment of lung cell lines with 5-aza-2′-deoxycitidne (Aza) and trichostatin (TSA). The addition of azacytidine reduces methylation and increases expression of both Alu and LINE. The addition of TSA does not affect methylation, but has a significant effect in expression of both elements with the exception of LINE in HBEC3KT cells. Simultaneous use of both compounds has a profound synergistic effect in expression of Alu and LINE. Expression is given in relative quantification (RQ) values which are calculated as $RQ = 2^{(-\Delta\Delta Ct)}$ value using the untreated control cell population as the calibrator.

DNA sequences. Although only a small number of these elements are considered to be actively retrotransposing in the human genome, these are associated with insertional mutagenesis.[1,3] LINE-1 and Alu elements are methylated in normal somatic cells and are frequently demethylated in cancer following global genome hypomethylation.[13] Indeed, because of their abundance in the genome they have been shown to be a good measure of such global hypomethylation in cancer.[18] However, the possible involvement of hypomethylation-mediated activation of LINE-1 and Alu in genome stability and cancer development has not been widely studied, although there is recent evidence to fuel such investigations.[7,8,10,23,31] As demethylating agents are increasingly used in cancer treatment, it is imperative to understand how cancer-related and/or drug-induced hypomethylation may initiate retrotransposition and subsequent genomic alterations, thus drawing valuable conclusions for implications in cancer therapy.

In our study, we quantitatively determined in NSCLC the methylation status LINE and Alu elements utilizing the sequences of LINE-1.2 and Alu-PV species. These particular LINE and SINE species were selected based on their activity in the human genome.[2,12,32] We demonstrated a significant reduction of the methylation levels of both LINE and Alu elements in primary NSCLC. These findings suggest a potentially important role for LINEs and SINEs in lung cancer development, adding to the limited information for retroelement methylation in this type of cancer.[15,33,34] There are profound differences on the detected methylation levels of LINE and Alu in normal and tumor specimens. More precisely, the observed average change in LINE is 13.2%, whereas in Alu it is only 3.1%. This most probably reflects the species/subfamilies covered by the particular primers used considering the known degeneracy of the targeted sequences.

From the clinicopathological point of view, it is notable that the observed hypomethylation was widespread among tumors of variable stage, nodal metastasis and differentiation status, most probably suggesting an early onset of this molecular abnormality in the course of lung cancer development. Our study confirms that NSCLC follows a similar global hypomethylation pattern as other human tumors.[13,18] Of particular note here is the finding that the methylation status of LINE is highly correlated with that of Alu ($p = 0.004$). This suggests a common mechanism of methylation maintenance of these elements in cancer and receives further supporting evidence from data in prostate cancer[16] and the reported correlation of both elements methylation with global genome methylation as measured by HPLC.[18]

To assess the potential implication of LINE and SINE demethylation in genome stability maintenance in NSCLCs, we have examined LOH at loci which are hotspots for lung cancer[30] and used FAL as a measure of the overall genomic instability. We demonstrated that hypomethylation of both transposable elements correlates with high FAL values indicating a strong link between

genome stability and transposable element methylation. A similar observation has been reported in colorectal carcinomas where LINE-1 hypomethylation correlated with microsatellite instability,[35] although the mechanisms responsible for chromosomal instability (expressed by FAL) and MSI are different. Genomic hypomethylation has been shown to induce chromosomal instability and tumorigenesis.[21,22] A triangular relationship between global hypomethylation-transposable elements-genomic instability has been suggested for many types of human tumors[7,10] and the correlation between genomic instability and hypomethylation in our study is in agreement with this. Currently, we have no functional evidence to prove a cause-effect relationship between hypomethylation of transposable elements and genomic instability, and further studies are required toward this direction. Alternatively, it may be suggested that hypomethylation of transposable elements and genomic instability could be consequences of the overall genetic and epigenetic reprogramming in human tumors. LINE-1 overexpression in model systems has been shown to induce genomic instability and deletions.[8–10] Other models have demonstrated successful retrotransposition events of such elements.[3,36–38] The information on LINE-1 expression in human tumors is very limited but suggests a degree of transcriptional activation in leukemias,[31] breast,[39] urothelial and renal carcinomas.[40] As RNA was not available from this set of NSCLCs examined for methylation, we are unable to comment on whether the observed hypomethylation leads to overexpression of LINE-1 and Alu. To examine the potential epigenetic control of LINE-1 and Alu in lung cancer, we utilized decitabine and TSA (common inhibitors of methylation and histone deacetylation, respectively) on 2 lung cancer cell lines and a nontumorigenic bronchial epithelial cell line to verify hypomethylation-mediated activation of transcription. In all 3 cell lines, the use of decitabine (which lead to experimentally confirmed hypomethylation of LINE-1 and Alu) resulted in increased transcription of both elements (Fig. 3). Notably, simultaneous use of TSA further increased transcription level. It has to be noted at this point that the observed increased expression of LINE and Alu could be partly due to incomplete elements encompassed in genes that are overexpressed in the presence of decitabine.

Although we are clearly demonstrating that expression of LINE and Alu is under epigenetic control in a lung cancer environment, it has to be noted that retrotransposition could be impaired by methylation-independent mechanisms. siRNAs produced by the LINE-1 5′antisense promoter have been shown to inhibit its retrotransposition.[5,6] In addition, LINE and Alu retrotransposition is controlled by APOBEC3 proteins ([41,42]) and sequestration into stress granules.[43] Last, it must also be noted that hypomethylation of LINE and Alu is not necessarily uniform,[7,44] thus it is not totally clear to which extent our data can be extrapolated.

Thus, further investigation involving a new patient cohort with available DNA and RNA is required to confirm this as a mechanism contributing to genomic instability. An alternative suggestion, on the other hand, is that chromatin relaxation at such retroelement sites may promote illegitimate recombination leading to genomic instability.[7]

Epigenetics appear to have a key role to play in anticancer therapies. DNMT inhibitors are increasingly used in clinical trials.[45,46] Recent studies provide very promising results[47,48] as epigenetic modulation of drug resistance may be critical for improving cancer drug efficiency overall.[49] It is, however, important to understand in detail the epigenetic reprogramming of cancer cells. In this direction, further to identify the most commonly hypermethylated genes, it is crucial to understand the impact of transposable element hypomethylation in cancer biology. In addition, we need to understand how and to what extent DNA hypomethylation may be a critical adverse effect of epigenetic therapies.[50]

Findings in our study demonstrate for the first time in primary human lung tumors the relationship between retroelement hypomethylation and genomic instability. In addition, we provide evidence that hypomethylation of LINE-1 and Alu elements in human lung cancer cell lines leads to enhanced transcription, which in combination with previous reports on retrotransposition-induced genomic instability points towards a more active role of the reactivation of such retroelements in the pathogenesis of human tumors. Further work is required to fully elucidate the molecular mechanisms involved and to provide the basis for the better clinical utilization of demethylating agents for the treatment of human cancer.

Acknowledgements

The authors are grateful to Drs. Gazdar and Minna (University of Texas Southwestern Medical Centre, Dallas, TX) for donating the HBEC3KT lung epithelial cell line.

References

1. Babushok DV, Kazazian HH, Jr. Progress in understanding the biology of the human mutagen LINE-1. Hum Mutat 2007;28:527–39.
2. Kazazian HH, Jr. Mobile elements: drivers of genome evolution. Science 2004;303:1626–32.
3. Sassaman DM, Dombroski BA, Moran JV, Kimberland ML, Naas TP, DeBerardinis RJ, Gabriel A, Swergold GD, Kazazian HH, Jr. Many human L1 elements are capable of retrotransposition. Nat Genet 1997;16:37–43.
4. Ostertag EM, Kazazian HH, Jr. Biology of mammalian L1 retrotransposons. Annu Rev Genet 2001;35:501–38.
5. Yang N, Kazazian HH, Jr. L1 retrotransposition is suppressed by endogenously encoded small interfering RNAs in human cultured cells. Nat Struct Mol Biol 2006;13:763–71.
6. Soifer HS, Rossi JJ. Small interfering RNAs to the rescue: blocking L1 retrotransposition. Nat Struct Mol Biol 2006;13:758–9.
7. Schulz WA. L1 retrotransposons in human cancers. J Biomed Biotechnol 2006;2006:83672.
8. Gilbert N, Lutz-Prigge S, Moran JV. Genomic deletions created upon LINE-1 retrotransposition. Cell 2002;110:315–25.
9. Symer DE, Connelly C, Szak ST, Caputo EM, Cost GJ, Parmigiani G, Boeke JD. Human l1 retrotransposition is associated with genetic instability in vivo. Cell 2002;110:327–38.
10. Kazazian HH, Jr, Goodier JL. LINE drive. retrotransposition and genome instability. Cell 2002;110:277–80.
11. Dewannieux M, Esnault C, Heidmann T. LINE-mediated retrotransposition of marked Alu sequences. Nat Genet 2003;35:41–8.
12. Mighell AJ, Markham AF, Robinson PA. Alu sequences. FEBS Lett 1997;417:1–5.
13. Ehrlich M. DNA methylation in cancer: too much, but also too little. Oncogene 2002;21:5400–13.
14. Suter CM, Martin DI, Ward RL. Hypomethylation of L1 retrotransposons in colorectal cancer and adjacent normal tissue. Int J Colorectal Dis 2004;19:95–101.
15. Chalitchagorn K, Shuangshoti S, Hourpai N, Kongruttanachok N, Tangkijvanich P, Thong-ngam D, Voravud N, Sriuranpong V, Mutirangura A. Distinctive pattern of LINE-1 methylation level in normal tissues and the association with carcinogenesis. Oncogene 2004;23:8841–6.
16. Cho NY, Kim BH, Choi M, Yoo EJ, Moon KC, Cho YM, Kim D, Kang GH. Hypermethylation of CpG island loci and hypomethylation of LINE-1 and Alu repeats in prostate adenocarcinoma and their relationship to clinicopathological features. J Pathol 2007;211:269–77.
17. Wilson AS, Power BE, Molloy PL. DNA hypomethylation and human diseases. Biochim Biophys Acta 2007;1775:138–62.
18. Weisenberger DJ, Campan M, Long TI, Kim M, Woods C, Fiala E, Ehrlich M, Laird PW. Analysis of repetitive element DNA methylation by methylight. Nucleic Acids Res 2005;33:6823–36.
19. Choi IS, Estecio MR, Nagano Y, Kim do H, White JA, Yao JC, Issa JP, Rashid A. Hypomethylation of LINE-1 and Alu in well-differentiated neuroendocrine tumors (pancreatic endocrine tumors and carcinoid tumors). Mod Pathol 2007;20:802–10.
20. Ehrlich M, Woods CB, Yu MC, Dubeau L, Yang F, Campan M, Weisenberger DJ, Long T, Youn B, Fiala ES, Laird PW. Quantitative analysis of associations between DNA hypermethylation, hypomethylation, and DNMT RNA levels in ovarian tumors. Oncogene 2006;25:2636–45.
21. Gaudet F, Hodgson JG, Eden A, Jackson-Grusby L, Dausman J, Gray JW, Leonhardt H, Jaenisch R. Induction of tumors in mice by genomic hypomethylation. Science 2003;300:489–92.

22. Eden A, Gaudet F, Waghmare A, Jaenisch R. Chromosomal instability and tumors promoted by DNA hypomethylation. Science 2003; 300:455.
23. Belgnaoui SM, Gosden RG, Semmes OJ, Haoudi A. Human LINE-1 retrotransposon induces DNA damage and apoptosis in cancer cells. Cancer Cell Int 2006;6:13.
24. Sato M, Shames DS, Gazdar AF, Minna JD. A translational view of the molecular pathogenesis of lung cancer. J Thorac Oncol 2007; 2:327–43.
25. Ehrich M, Nelson MR, Stanssens P, Zabeau M, Liloglou T, Xinarianos G, Cantor CR, Field JK, van den Boom D. Quantitative high-throughput analysis of DNA methylation patterns by base-specific cleavage and mass spectrometry. Proc Natl Acad Sci USA 2005; 102:15785–90.
26. Ehrich M, Field JK, Liloglou T, Xinarianos G, Oeth P, Nelson MR, Cantor CR, van den Boom D. Cytosine methylation profiles as a molecular marker in non-small cell lung cancer. Cancer Res 2006; 66:10911–18.
27. Field JK, Liloglou T, Warrak S, Burger M, Becker E, Berlin K, Nimmrich I, Maier S. Methylation discriminators in NSCLC identified by a microarray based approach. Int J Oncol 2005;27:105–11.
28. Shames DS, Girard L, Gao B, Sato M, Lewis CM, Shivapurkar N, Jiang A, Perou CM, Kim YH, Pollack JR, Fong KM, Lam CL, et al. A genome-wide screen for promoter methylation in lung cancer identifies novel methylation markers for multiple malignancies. PLoS Med 2006;3:e486.
29. Liloglou T, Maloney P, Xinarianos G, Fear S, Field JK. Sensitivity and limitations of high throughput fluorescent microsatellite analysis for the detection of allelic imbalance: application in lung tumors. Int J Oncol 2000;16:5–14.
30. Liloglou T, Maloney P, Xinarianos G, Hulbert M, Walshaw MJ, Gosney JR, Turnbull L, Field JK. Cancer-specific genomic instability in bronchial lavage: a molecular tool for lung cancer detection. Cancer Res 2001;61:1624–8.
31. Roman-Gomez J, Jimenez-Velasco A, Agirre X, Cervantes F, Sanchez J, Garate L, Barrios M, Castillejo JA, Navarro G, Colomer D, Prosper F, Heiniger A, et al. Promoter hypomethylation of the LINE-1 retrotransposable elements activates sense/antisense transcription and marks the progression of chronic myeloid leukemia. Oncogene 2005; 24:7213–23.
32. Wallace MR, Andersen LB, Saulino AM, Gregory PE, Glover TW, Collins FS. A de novo Alu insertion results in neurofibromatosis type 1. Nature 1991;353:864–6.
33. Rauch T, Wang Z, Zhang X, Zhong X, Wu X, Lau SK, Kernstine KH, Riggs AD, Pfeifer GP. Homeobox gene methylation in lung cancer studied by genome-wide analysis with a microarray-based methylated CpG island recovery assay. Proc Natl Acad Sci USA 2007;104:5527–32.
34. Rauch TA, Zhong X, Wu X, et al. High-resolution mapping of DNA hypermethylation and hypomethylation in lung cancer. Proc Natl Acad Sci USA 2008;105:252–7.
35. Estecio MR, Gharibyan V, Shen L, Ibrahim AE, Doshi K, He R, Jelinek J, Yang AS, Yan PS, Huang TH, Tajara EH, Issa JP. LINE-1 hypomethylation in cancer is highly variable and inversely correlated with microsatellite instability. PLoS ONE 2007;2:e399.
36. Lin CS, Goldthwait DA, Samols D. Identification of Alu transposition in human lung carcinoma cells. Cell 1988;54:153–9.
37. Kubo S, Seleme MC, Soifer HS, Perez JL, Moran JV, Kazazian HH, Jr, Kasahara N. L1 retrotransposition in nondividing and primary human somatic cells. Proc Natl Acad Sci USA 2006;103:8036–41.
38. Morrish TA, Garcia-Perez JL, Stamato TD, Taccioli GE, Sekiguchi J, Moran JV. Endonuclease-independent LINE-1 retrotransposition at mammalian telomeres. Nature 2007;446:208–12.
39. Bratthauer GL, Cardiff RD, Fanning TG. Expression of LINE-1 retrotransposons in human breast cancer. Cancer 1994;73:2333–6.
40. Florl AR, Lower R, Schmitz-Drager BJ, Schulz WA. DNA methylation and expression of LINE-1 and HERV-K provirus sequences in urothelial and renal cell carcinomas. Br J Cancer 1999;80:1312–21.
41. Muckenfuss H, Hamdorf M, Held U, Perkovic M, Löwer J, Cichutek K, Flory E, Schumann GG, Münk C. APOBEC3 proteins inhibit human LINE-1 retrotransposition. J Biol Chem 2006;281:22161–72.
42. Esnault C, Heidmann O, Delebecque F, Dewannieux M, Ribet D, Hance AJ, Heidmann T, Schwartz O. APOBEC3G cytidine deaminase inhibits retrotransposition of endogenous retroviruses. Nature 2005; 433:430–3.
43. Goodier JL, Zhang L, Vetter MR, Kazazian HH, Jr. LINE-1 ORF1 protein localizes in stress granules with other RNA-binding proteins, including components of RNA interference RNA-induced silencing complex. Mol Cell Biol 2007;27:6469–83.
44. Rodriguez J, Vives L, Jordà M, Morales C, Muñoz M, Vendrell E, Peinado MA. Genome-wide tracking of unmethylated DNA Alu repeats in normal and cancer cells. Nucleic Acids Res 2008;36:770–84.
45. Lyko F, Brown R. DNA methyltransferase inhibitors and the development of epigenetic cancer therapies. J Natl Cancer Inst 2005;97: 1498–506.
46. Issa JP. DNA methylation as a therapeutic target in cancer. Clin Cancer Res 2007;13:1634–7.
47. Appleton K, Mackay HJ, Judson I, Plumb JA, McCormick C, Strathdee G, Lee C, Barrett S, Reade S, Jadayel D, Tang A, Bellenger K, et al. Phase I and pharmacodynamic trial of the DNA methyltransferase inhibitor decitabine and carboplatin in solid tumors. J Clin Oncol 2007;25:4603–9.
48. Oki Y, Jelinek J, Shen L, Kantarjian HM, Issa JP. Induction of hypomethylation and molecular response after decitabine therapy in patients with chronic myelomonocytic leukemia. Blood 2008;111: 2382–4.
49. Glasspool RM, Teodoridis JM, Brown R. Epigenetics as a mechanism driving polygenic clinical drug resistance. Br J Cancer 2006;94:1087–92.
50. Ehrlich M. The controversial denouement of vertebrate DNA methylation research. Biochemistry 2005;70:568–75.

the FEBS Journal

Sp1 binds to the external promoter of the *p73* gene and induces the expression of TAp73γ in lung cancer

Stella Logotheti[1], Ioannis Michalopoulos[2], Maria Sideridou[3], Alexandros Daskalos[4], Sophia Kossida[2], Demetrios A. Spandidos[5], John K. Field[4], Borek Vojtesek[6], Triantafyllos Liloglou[4], Vassilis Gorgoulis[3] and Vassilis Zoumpourlis[1]

1 Biomedical Applications Unit, Institute of Biological Research and Biotechnology, National Hellenic Research Foundation, Athens, Greece
2 Bioinformatics & Medical Informatics, Foundation for Biomedical Research of the Academy of Athens, Greece
3 Molecular Carcinogenesis Group, Department of Histology and Embryology, Medical School of Athens, Greece
4 Roy Castle Lung Cancer Research Programme, Division of Surgery and Oncology, University of Liverpool Cancer Research Centre, University of Liverpool, UK
5 Laboratory of Clinical Virology, Faculty of Medicine, University of Crete, Heraklion, Greece
6 Department of Oncological and Experimental Pathology, Masaryk Memorial Cancer Institute, Brno, Czech Republic

Keywords
lung cancer; P1 promoter; p73 isoforms; Sp1; TAp73γ; ΔNp73

Correspondence
V. Zoumpourlis, Biomedical Application Unit, Institute of Biological Research and Biotechnology, National Hellenic Research Foundation, 48 Vas. Constantinou Ave, 116 35 Athens, Greece
Fax: +210 7273677
Tel: +210 7273730
E-mail: vzub@eie.gr

(Received 16 February 2010, revised 1 May 2010, accepted 12 May 2010)

doi:10.1111/j.1742-4658.2010.07710.x

The *p73* gene possesses an extrinsic P1 promoter and an intrinsic P2 promoter, resulting in TAp73 and ΔNp73 isoforms, respectively. The ultimate effect of *p73* in oncogenesis is thought to depend on the apoptotic TA to antiapoptotic ΔN isoforms' ratio. This study was aimed at identifying novel transcription factors that affect TA isoform synthesis. With the use of bioinformatics tools, *in vitro* binding assays, and chromatin immunoprecipitation analysis, a region extending −233 to −204 bp upstream of the transcription start site of the human *p73* P1 promoter, containing conserved Sp1-binding sites, was characterized. Treatment of cells with Sp1 RNAi and Sp1 inhibitor functionally suppress TAp73 expression, indicating positive regulation of P1 by the Sp1 protein. Notably Sp1 inhibition or knockdown also reduces ΔNp73 protein levels. Therefore, Sp1 directly regulates TAp73 transcription and affects ΔNp73 levels in lung cancer. TAp73γ was shown to be the only TA isoform overexpressed in several lung cancer cell lines and in 26 non-small cell lung cancers, consistent with Sp1 overexpression, thereby questioning the apoptotic role of this specific *p73* isoform in lung cancer.

Introduction

Lung cancer is one of the most common and fatal types of cancer in developed countries. Despite scientific advances, the overall number of associated deaths has only slightly decreased during the last 20 years [1]. The well-known tumour suppressor gene *p53* has been found to be mutated in 70–90% of lung cancer cases and in less than 50% of all cancer cases [1]. However, the involvement of *p73*, its structural and functional homologue, in this type of cancer is not clearly understood [2].

The *p73* gene is a member of the *p53* family that encodes an N-terminal transactivation domain (TA), a highly conserved DNA-binding domain (DBD), and a C-terminal oligomerization domain [3]. Despite its high degree of sequence similarity with *p53*, especially in the DBD, and its ability to activate various *p53*

Abbreviations
ChIP, chromatin immunoprecipitation; DBD, DNA-binding domain; EMSA, electrophoretic mobility shift assay; NSCLC, non-small cell lung cancer; siRNA, small interfering RNA; TA, transactivation domain; TSS, transcription start site; VEGF, vascular endothelial growth factor.

targets [4] as well as to induce apoptosis in cancer cells [5], *p73* has unique characteristics that differentiate it from a classical Knudson-type gene. Unlike *p53*, *p73* rarely mutates in cancer [6], and $p73^{-/-}$ mice do not develop spontaneous tumours, but show severe abnormalities in neuronal development [7]. The gene produces numerous isoforms as a result of: (a) alternative splicing in the 3′-end (leading to the formation of α, β, γ, δ, ε, ζ and η isoforms) [8–12]; (b) the use of an extrinsic promoter (P1) and an alternative, intrinsic promoter (P2) in the 5′-end (leading to the formation of TA and ΔN classes of isoforms, respectively) [13]; and (c) alternative splicing in the 5′-end (resulting in truncated transcripts p73Δex2, p73Δex2/3, and ΔN′-p73, which partially or entirely lack the TA, collectively called ΔTA) [14]. The numerous isoforms derive from several combinations between differential N-terminal domain and C-terminal domain [15].

Despite the rarity of *p73* mutations, overexpression of p73 isoforms is common in several types of cancer [14,16], including lung cancer [2]. Elevated levels of expression of p73 isoforms have also been correlated with lung cancer, as ΔNp73 overexpression predicts a poorer prognosis in patients with squamous cell carcinoma and adenocarcinoma [17]. In addition, TAp73 is overexpressed in lung cancer tumour tissues [18,19].

The 'two genes in one' idea has been suggested for *p73*, whereby the same gene is thought to generate products with opposing roles, mainly the apoptotic TA isoform(s) and the antiapoptotic ΔN isoforms. In general, TAp73 isoforms regulate the transcription of ΔNp73 isoforms, which, in turn, act as dominant negative regulators of both TAp73 and p53, thus giving a dominant negative feedback loop [13]. Consequently, the ultimate effect of p73 isoforms in cancer progression is attributed to the TA/ΔN ratio, rather than the overexpression of a specific p73 isoform or a specific class of p73 isoforms *per se* [20,21].

In line with this concept, the selective promoter activation could result in the activation of either oncogenic or tumour suppressor isoform(s) of this gene, thereby shifting the TA/ΔN equilibrium towards an oncogenic or a tumour suppressor direction. For example, the *p73* P1 promoter contains functional E2F1-binding sites [22], through which the E2F1 transcription factor induces TAp73 overexpression and consequent apoptosis [23,24]. It has been reported that the *p73* P1 promoter is not completely inactivated by site-directed mutagenesis of its functional E2F1 sites [23], implying that additional transcription factor(s) play a significant role in its regulation. This study focused on the identification of novel transcriptional factors that control the use of the *p73* P1 promoter and, subsequently, the relative expression of p73 isoforms in lung cancer by using lung cancer cell lines and tumour samples. Sp1 was found to activate the transcription of TAp73γ in lung cancer via highly conserved Sp1-binding sites on the *p73* P1 promoter. In addition, TAp73γ and Sp1 are co-overexpressed both *in vitro* and *in situ* in lung cancer. Sp1 also affected the ΔNp73 levels in lung cancer.

Results

The *p73* P1 promoter has multiple putative Sp1-binding sites

In order to identify transcription factors that control the use of the *p73* P1 promoter, we searched for conserved binding sites located in regions of its sequence that show high homology among various species, including *Bos taurus*, *Equus caballus*, *Erinaceus europaeus*, *Loxodonta africana*, *Macaca mulatta*, *Mus musculus*, *Ornithorhynchus anatinus*, *Otolemur garnettii*, *Pan troglodytes*, *Rattus norvegicus* and *Tupaia belangeri*. The transcription start site (TSS) of the human transcripts ENST00000346387, ENST00000354437, ENST00000357733, ENST00000378290, and ENST00000378295, which is located at chr1:3558989 (Ensembl v54, May 2009), was selected. The analysis focused on the first 250 bp upstream of the TSS, which shows most conservation among mammals. Four conserved human *p73* P1 promoter regions (A–D), containing potential Sp1-binding sites, were identified (Fig. 1). Region A is located −233 to −204 bp upstream of the human *p73* P1 TSS, and contains two putative Sp1-binding elements. Regions B, C, and D, which are located −61 to −33, −20 to −1, and −4 to +20 bp upstream of the TSS, respectively, all contain one putative Sp1-binding element. Our *in silico* prediction of candidate Sp1 motifs in regions A, C and D is in accordance with a previous study, in which MATINSPECTOR V2.2 at the TRANSFAC website was used [25]. Furthermore, CONTRA analysis also suggested another candidate Sp1 motif in region B. Our study demonstrated a canonical, conserved TATA box at position −32, based on the mapping of the TSS by Ensembl, which is identical to the TATA box previously described for the human *p73* P1 promoter [22].

Regions A, B and C on the *p73* P1 promoter can bind Sp1 *in vitro*

We evaluated the affinity of the *in silico*-identified region A, B, C and D oligonucleotides for *in vitro*

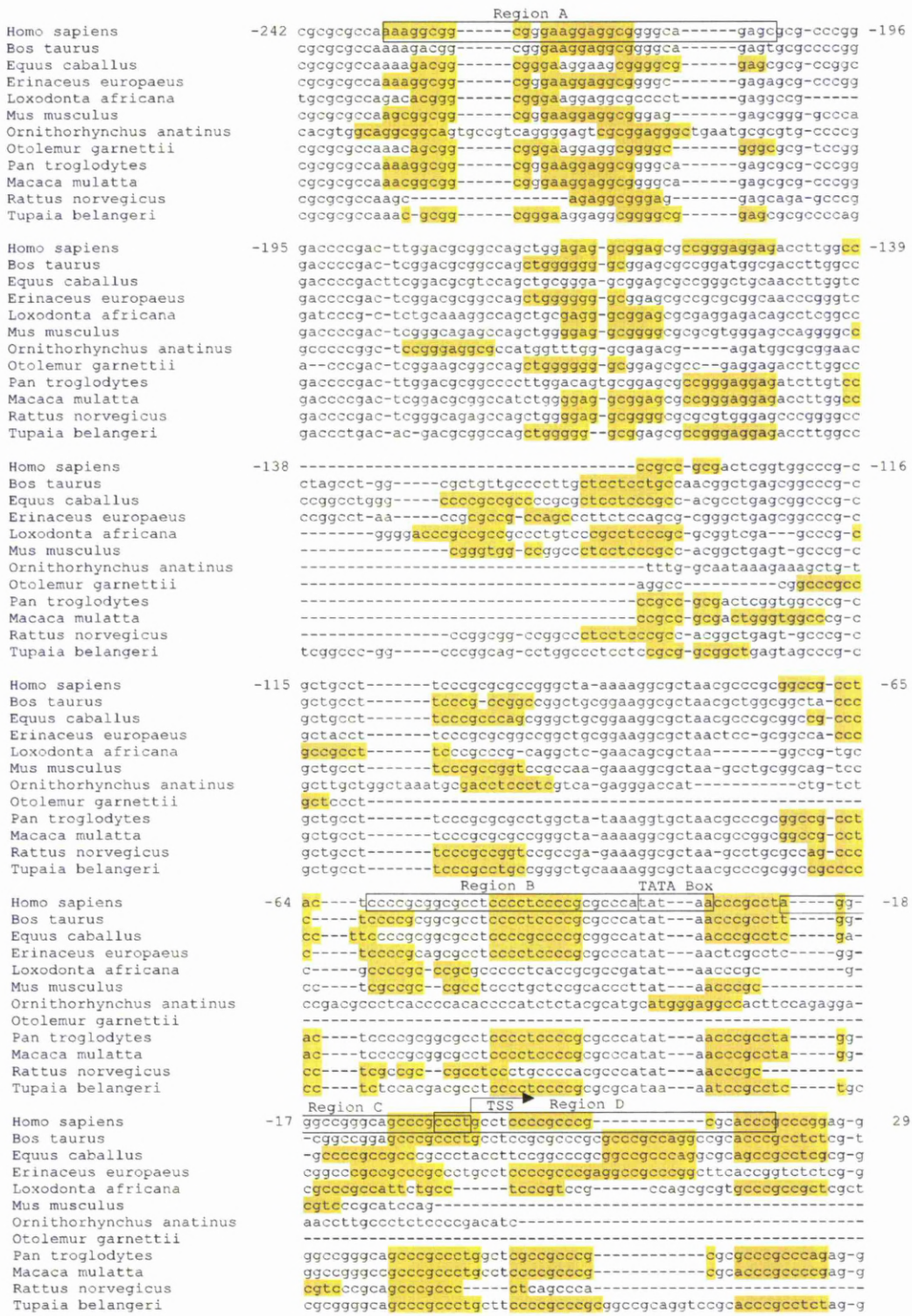
Region A
Region B
TATA Box
Region C
TSS
Region D
Homo sapiens
Bos taurus
Equus caballus
Erinaceus europaeus
Loxodonta africana
Mus musculus
Ornithorhynchus anatinus
Otolemur garnettii
Pan troglodytes
Macaca mulatta
Rattus norvegicus
Tupaia belangeri

synthesized Sp1 protein using electrophoretic mobility shift assay (EMSA) experiments. *In vitro*, Sp1 can bind to region A, B and C oligonucleotides (Fig. 2A, lanes 6 and 11, and Fig. 2B, lane 6, respectively). Self-competition experiments, as well as competition experiments using an excess of unlabelled control oligonucleotide (containing a control Sp1 binding site) for region A radiolabelled oligonucleotide, abolished the formation of the Sp1–radiolabelled region A oligonucleotide complex (Fig. 2A, lanes 7 and 8, respectively). The addition of the mSp1 oligonucleotide (containing a mutated Sp1 binding site) did not affect protein–DNA binding (Fig. 2A, lane 9), whereas the addition of antibody against Sp1 strongly supershifted the Sp1–DNA complex (Fig. 2A, lane 10). Similar experiments for regions B (Fig. 2A) and C (Fig. 2B) confirmed specific *in vitro* Sp1–DNA binding. Notably, the binding activity of the region A oligonucleotide was markedly higher than those of all other oligonucleotides that were tested, possibly indicating that both putative Sp1 binding elements in region A are active. Therefore, region A appears to be a better binding site for Sp1. In contrast, region D failed to bind *in vitro* synthesized Sp1 protein (Fig. 2B, lanes 11–15), and it was excluded from further analysis.

Binding of endogenous Sp1 from lung cancer cell lines to the *p73* P1 promoter

In order to validate the ability of endogenous Sp1 to bind to the *p73* P1 promoter within the cellular environment, we performed additional EMSA experiments using nuclear extracts from 11 representative lung cancer cell lines. We used only region A radiolabelled oligonucleotide, as it was found to bind *in vitro* to Sp1 more effectively. We observed that the binding of endogenous Sp1 to region A in the fibroblast cell line IMR90 was almost equal to that in the normal HNBE cells (Fig. 2C, lanes 1 and 2). A marked increase in the level of region A oligonucleotide–Sp1 complexes was noted in the anaplastic carcinoma cell line (Fig. 2C, lane 3), and the levels of the complexes appeared to remain equivalently high in the small cell lung cancer cell line (Fig. 2C, lane 4), the squamous cell carcinoma cell lines (Fig. 2C, lanes 5–7), the adenocarcinoma cell lines (Fig. 2C, lanes 8–10), and the large cell lung carcinoma cell line (Fig. 2C, lane 11). The region A oligonucleotide–Sp1 complex was supershifted in the representative cell line A549 (Fig. 2C, lane 12), demonstrating the specificity of region A for Sp1 of the nuclear cell lysates. The Sp1–DNA binding pattern for the region A oligonucleotide is consistent with that of the control oligonucleotide (Fig. 2D).

Binding of Sp1 to the *p73* P1 promoter within the cellular environment is further supported by chromatin immunoprecipitation (ChIP) assays. Sp1 antibody immunoprecipitated the *p73* P1 promoter in A549 cells in a dose-dependent manner (Fig. 2E). In contrast, no PCR signal was observed when the irrelevant β-actin antibody was used for ChIP. The sheared and cross-linked DNA that was produced prior to the immunoprecipitation step (input) was used as a positive control PCR template.

TAp73 synthesis is regulated by Sp1 through region A in lung cancer cell lines

Next, we tested the ability of Sp1 to regulate TAp73 expression *in vivo* by treating the standard TAp73-expressing cell line A549 with either Sp1 small interfering RNA (siRNA) or an Sp1 protein inhibitor. The resulting changes in TAp73 expression were monitored by western blot analysis. The known Sp1 target vascular endothelial growth factor (VEGF) [26] was used as a positive control. A549 cells were transiently transfected with Sp1 siRNA, and the nonsilencing control siRNA was the negative control for Sp1 siRNA interference. As shown in Fig. 3A, treatment with Sp1 siRNA resulted in the downregulation of TAp73 and VEGF levels as compared with the corresponding levels in the siRNA-untreated cells, revealing positive regulation of the *p73* P1 promoter by Sp1. In contrast, TAp73 and VEGF levels were not affected by treatment with negative control Sp1 siRNA. Similarly, TAp73 levels gradually decreased after a 48 h treatment of A549 cells with increasing concentrations of the Sp1 inhibitor mithramycin A (Fig. 3B), which not only interferes with the transcription of genes containing GC-rich regions in their promoters, but also, at high concentrations, reduces recruitment of Sp1 to its own promoter [27].

We then performed transient transfection of A549 cells with region A double-stranded phosphorothioate oligonucleotides, which are able to antagonize region A for Sp1 binding, in order to examine whether

Fig. 1. The P1 *p73* promoter has multiple putative Sp1-binding sites, conserved among 12 mammalian species. Alignment using CONTRA analysis revealed four conserved, putative Sp1 element-containing regions, spanning from −233 to −204 bp (region A), −61 to −33 bp (region B), −20 to −1 bp (region C) and −4 to +20 bp (region D) relative to the TSS of the human *p73* P1 promoter. The four regions are box-highlighted, and the human Sp1-binding sites are yellow-shaded. The TATA box is also box-highlighted.

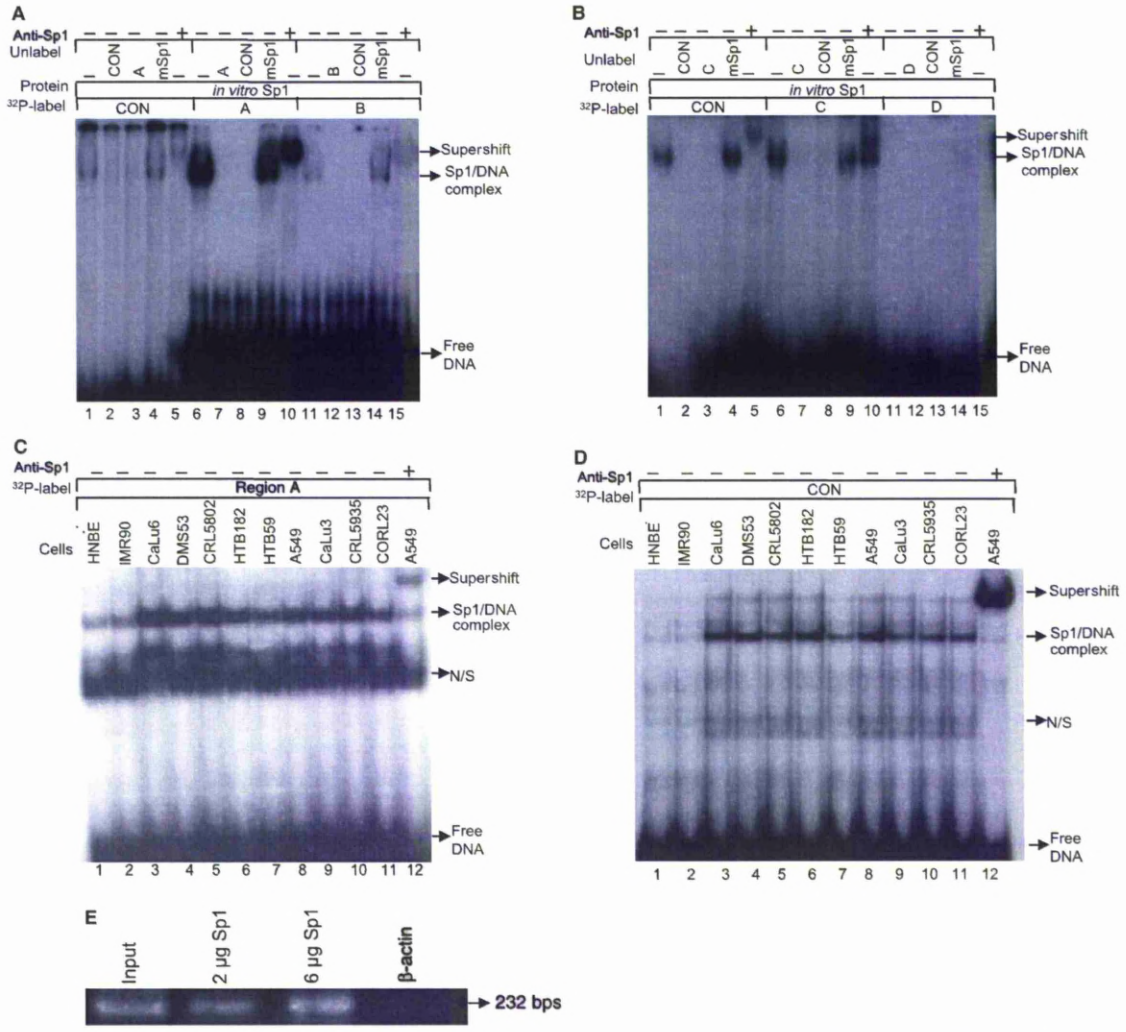

Fig. 2. Sp1 binds to the *p73* P1 promoter both *in vitro* and *in vivo*. (A) The ^{32}P-labelled region A target was incubated with the *in vitro* Sp1 protein either alone (lane 6) or in the presence of cold region A oligonucleotide (self-competition reaction) (lane 7), cold control oligonucleotide (CON) (competition reaction with positive control) (lane 8), or cold mutant Sp1 oligonucleotide (mSp1) (competition reaction with negative control) (lane 9). In lane 10, the protein–DNA complexes are supershifted with polyclonal antibody against Sp1 (supershift reaction). Lanes 11–15 correspond to a similar set of reactions for the ^{32}P-labelled region B target. Lanes 1–5 correspond to the positive control reactions for the Sp1-containing oligonucleotide (CON). (B) Lanes 6–10 correspond to a similar set of reactions for the ^{32}P-labelled region C target, and lanes 11–15 correspond to a similar set of reactions for the ^{32}P-labelled region D target. Lanes 1–5 correspond to the positive control reactions for the Sp1-containing oligonucleotide (CON). EMSAs using *in vitro* Sp1 and region A, B, C or D oligonucleotides revealed that regions A, B and C can bind to Sp1. (C) Lanes 1–11 contain radiolabelled region A oligonucleotide incubated with nuclear extracts from 11 lung cancer cell lines and electrophoresed on polyacrylamide gel. The specificity of the region A oligonucleotide–Sp1 protein complex is confirmed by a supershift reaction with polyclonal antibody against Sp1 in the representative A549 cell line (lane 12). (D) Lanes 1–11 show the corresponding positive control EMSA experiments demonstrating specific binding of endogenous Sp1 of the same cell lines to radiolabelled control Sp1 oligonucleotide (CON). The CON–Sp1 protein complex was supershifted in the representative cell line, A549 (lane 12). Unlabel., unlabelled oligonucleotides; ^{32}P-label, ^{32}P-labelled oligonucleotides; N/S, nonspecific DNA–protein complexes. (E) ChIP assay with DNA from A549 cells. Immunoprecipitation was performed with 2 µg and 6 µg of antibody against Sp1. PCR primer pairs were specific for the −265 to +61 bp region of the *p73* P1 promoter. Chromatin incubated with antibody against β-actin was used as a negative immunoprecipitation control, whereas input was used as a positive PCR control.

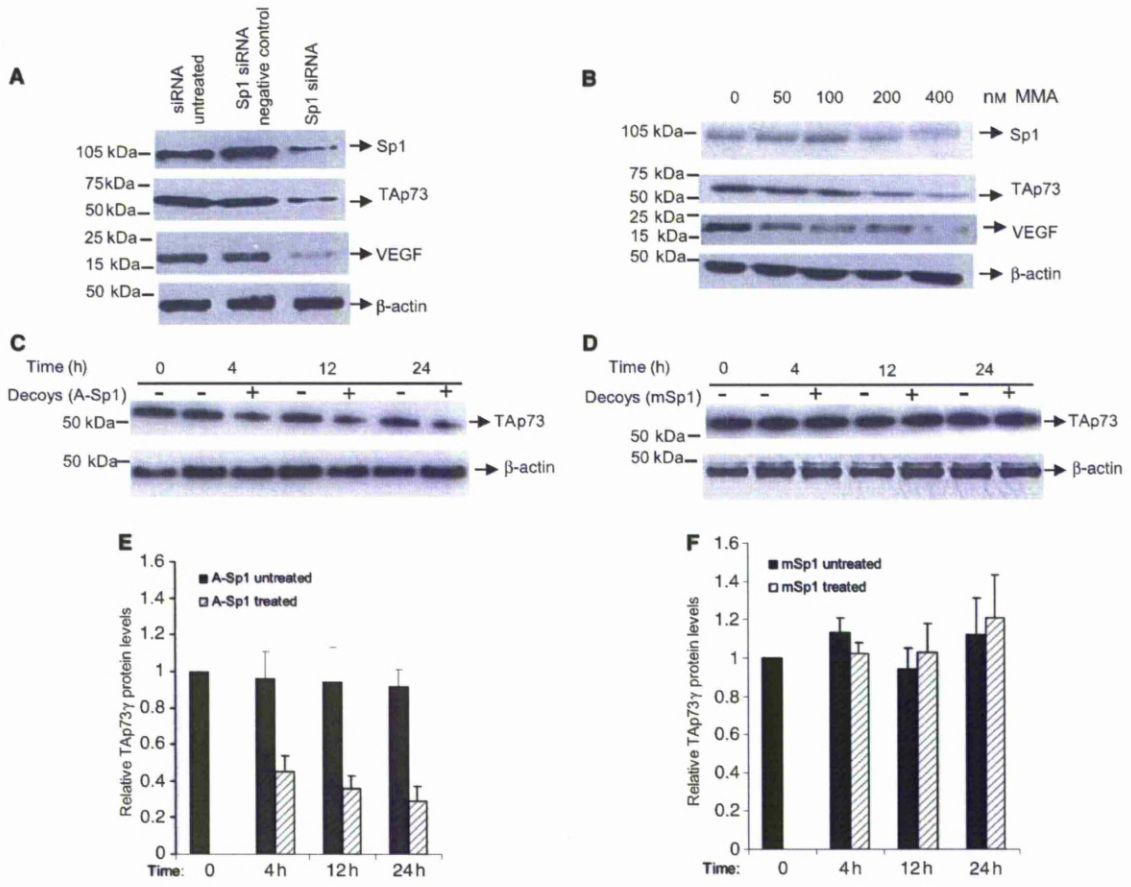

Fig. 3. Sp1 mediates TAp73 overexpression through P1 activation. (A) Transient transfection with Sp1 siRNA results in the reduction of Sp1 and TAp73 levels in A549 cells. VEGF levels were used as a positive control for Sp1 siRNA interference. β-actin levels were used as a loading control. Nonspecific Sp1 siRNA was used as a negative control. (B) A 48-h treatment of A549 cells with increasing concentrations of the Sp1 inhibitor mithramycin A results in reductions in Sp1 and TAp73 levels. VEGF levels were used as a positive control (C) A549 cells were transiently transfected with region A decoy, total protein extracts were prepared from these cells after 4, 12 and 24 h of decoy treatment, and the TAp73 levels were estimated by western blot analysis. (D) Similar transient transfection experiments with mutant Sp1 (mSp1) decoys were performed as a negative control of interference. The experiment was performed in triplicate. (E) TAp73 levels were quantified by IMAGEQUANT and compared with the corresponding levels of the untreated cells. As shown in the graph, TAp73 levels decreased with time upon region A decoy treatment. (F) Quantification of the TAp73 levels and comparison with the corresponding levels of decoy-untreated cells (black bars) demonstrated no change in TAp73 levels of mSp1-treated cells over time (grey bars). The protein amounts in all experiments were normalized to β-actin.

region A of the *p73* P1 promoter is specifically responsible for Sp1-mediated TAp73 expression in lung cancer cells. Mutant (mSp1) double-stranded phosphorothioate oligonucleotides were used as the corresponding negative control. Region A phosphorothioate oligonucleotides were able to reduce TAp73 expression over a 24 h treatment period (Fig. 3C,E), whereas mSp1 phosphorothioate oligonucleotides failed to affect TAp73 expression (Fig. 3D,F). In contrast, region B and C phosphorothioate oligonucleotides had a negligible effect on TAp73 expression, even after 48 h of treatment (data not shown).

TAp73γ and Sp1 are co-overexpressed in lung cancer cell lines and non-small cell lung cancers (NSCLCs)

Western blot analysis for TAp73 isoforms using total protein extracts from 15 lung cancer cell lines revealed that the abundantly expressed TAp73 isoform in all

tested cell lines was TAp73γ, whereas TAp73α and TAp73β were not detected. The level of TAp73γ was low in the normal HNBE cells, slightly increased in the fetal lung fibroblast cell lines (CCL171 and IMR90), and substantially increased in the lung epithelial anaplastic carcinoma cell line (CALU6), the small cell carcinoma cell line (DMS53), the squamous lung cancer cell lines (CRL5802, HTB182, HTB58, HTB59, and SKMES1), the adenocarcinoma cell lines (A549, CALU3, CRL5935, and SKLU1), and the large cell lung cancer cell line (CORL23). The corresponding Sp1 expression pattern was consistent with that of TAp73γ (Fig. 4A), as well as with the Sp1–DNA binding pattern revealed by the EMSA experiments. Quantification of TAp73γ and Sp1 levels is shown in Fig. 4B.

To verify our findings *in situ*, we analysed the expression of TAp73 isoforms in a group of 26 lung cancer patients. TAp73γ was exclusively overexpressed in 68.42% (13/19) of squamous cell lung cancer samples and in 57.14% (4/7) of adenocarcinoma samples as compared with their corresponding adjacent normal tissues. TAp73α and TAp73β were undetectable in the tumour tissues of all patients. Sp1 levels were also examined, and Sp1 was found to be overexpressed in 57.89% (11/19) of squamous cell lung cancer samples and in 42.86% (3/7) of adenocarcinoma samples. Sp1 and TAp73γ were co-overexpressed in 42.86% (3/7) of adenocarcinoma samples, in 52.63% (10/19) of squamous cell lung cancer samples, and in 50% (13/26) of total lung cancer samples. Figure 4C shows TAp73 and Sp1 levels in representative squamous cell carcinoma and adenocarcinoma samples (Fig. S1). The mean TAp73γ levels showed an approximately 12-fold increase in tumour tissues with respect to the corresponding normal levels. Similarly, an approximately eight-fold increase in the mean Sp1 levels was observed in the examined tumour samples (Fig. 4D).

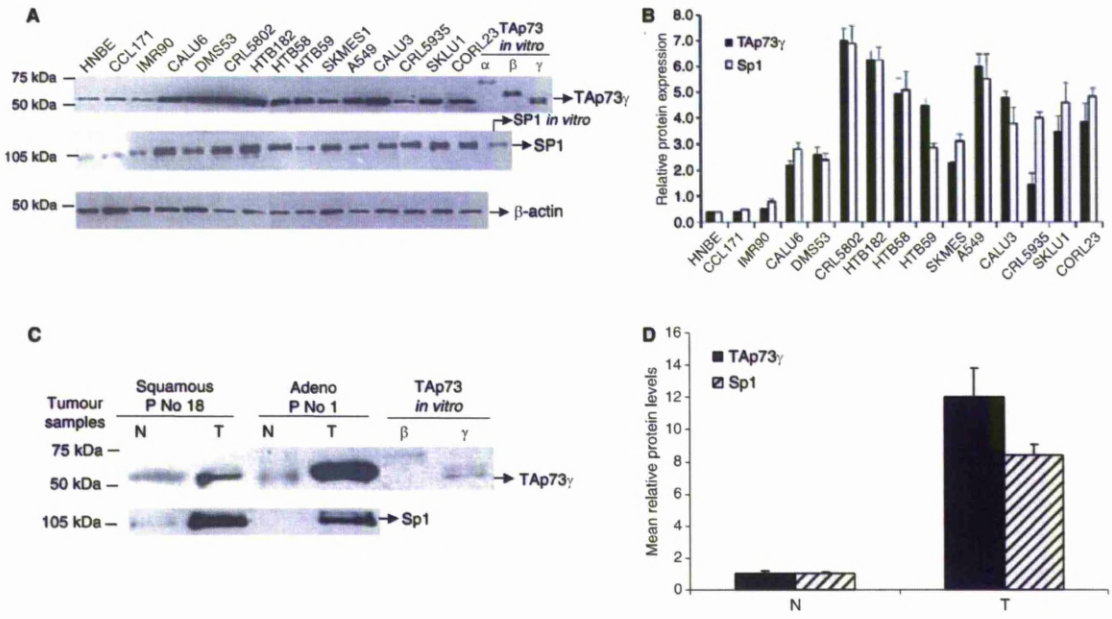

Fig. 4. TAp73γ and Sp1 are co-overexpressed in lung cancer cell lines and tumour samples. (A) Western blot analysis of total extracts from 15 lung cancer cell lines revealed coelevation of Sp1 and TAp73γ protein levels in these cells. *In vitro*-translated TAp73α, TAp73β and TAp73γ were used as controls for the identification of TAp73 isoforms, *in vitro* Sp1 was used as a control for the expression of Sp1, and β-actin was used as a loading control. (B) Sp1 and TAp73γ levels were quantified by IMAGEQUANT and expressed relative to the normal HNBE cell line. (C) Western blot analysis demonstrated a significant increase in both TAp73γ and Sp1 levels in the representative squamous cell carcinoma (patient No. 1) and adenocarcinoma (patient No. 18) samples as compared with the corresponding normal tissues. *In vitro*-synthesized TAp73β and TAp73γ were used as controls, for the identification of the exact TAp73 isoform expressed in these samples. (D) The mean levels of TAp73γ and Sp1 in 26 NSCLCs samples were compared with the corresponding mean levels in the normal samples. Relative mean TAp73γ levels showed an almost 12-fold increase (grey bars), and relative mean Sp1 levels showed a greater than eight-fold increase (black bars). The experiment was performed in triplicate.

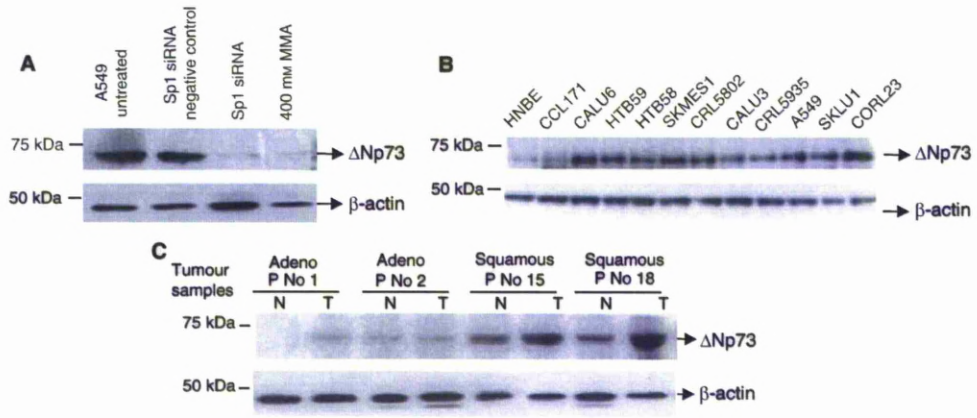

Fig. 5. ΔNp73 levels are affected by Sp1, and ΔNp73 is overexpressed in lung cancer cells. (A) Transient transfection with Sp1 siRNA resulted in the downregulation of both ΔNp73 proteins in A549 cells. Nonspecific Sp1 siRNA was used as a negative control, and β-actin levels were used as a loading control. The Sp1 inhibitor mithramycin A at 400 nM also caused a marked decrease in ΔNp73 levels. (B) Western blot analysis of total extracts from 12 lung cancer cell lines revealed elevated ΔNp73 levels in these cells. (C) Western blot analysis demonstrated an increase in ΔNp73 in representative squamous cell carcinoma and adenocarcinoma samples relative to the adjacent normal tissues.

ΔNp73 levels are affected by Sp1 and enhanced in lung cancer cells

As the outcome of the action of TAp73 is dependent on the presence of the dominant negative ΔNp73 [13], an important issue to be considered is whether Sp1 also affects ΔNp73 levels in the context of lung cancer. It is also important to investigate whether ΔNp73 is co-overexpressed, along with TAp73γ, in lung cancer. In this respect, we first assessed the effect of Sp1 siRNA treatment of A549 cells on ΔNp73 levels. As shown in Fig. 5A, ΔNp73 levels were markedly reduced in the Sp1 siRNA-treated A549 cells as compared with the untreated cells, in contrast to the ΔNp73 levels of nonsilencing control-treated A549 cells, which remained unchanged. Similarly, ΔNp73 levels showed a marked decrease upon treatment of the A549 cell line with 400 nM mithramycin A (Fig. 5A). A CONTRA analysis was performed in order to examine whether a direct interaction of Sp1 with the *p73* P2 promoter is possible. Interestingly, our analysis showed a conserved region of 124 bp upstream of the ΔN-TP73 TSS. A highly conserved Sp1 candidate site was found at position −17 to −26. This sequence was flanked by two candidate TATA boxes at positions −3 to −9 and −26 to +32. Another Sp1 site was identified at the 5′-end of the conserved promoter region (−115 to −124). The TSS was located at chr1:3597096 (Ensemble v54, May 2009) of the ΔN-TP73 promoter (transcripts ENST00000378280 and ENST00000378285) (data not shown).

Next, ΔNp73 levels were monitored in 12 lung cancer cell lines, as well as in four representative paired samples of the 26-membered panel of lung cancer patients. Figure 5B shows that ΔNp73 protein expression was low in the normal HNBE and fetal lung fibroblast CCL171 cell lines, whereas it was significantly increased in the lung epithelial anaplastic carcinoma cell line (CALU6), in the squamous lung cancer cell lines (HTB59, HTB58, and SKMES1), in the adenocarcinoma cell lines (CALU3, CRL5935, A549, and SKLU1), and in the large cell lung cancer cell line (CORL23). In agreement with the data concerning cell lines, as well as previous data on clinical samples [17,19], ΔNp73 was also overexpressed in the representative tumour samples as compared with their corresponding normal tissues (Fig. 5C). Thus, ΔNp73 levels are not only enhanced in lung cancer cells, along with those of TAp73γ, but are also affected by Sp1.

Discussion

In the search for transcription factors that affect the use of the *p73* P1 promoter, we identified a region −233 to −204 bp upstream of the TSS of the human *p73* P1 promoter containing conserved, functional Sp1-binding sites. Reduction of the endogenous Sp1 levels or inhibition of Sp1 binding to this region downregulates TAp73 expression in lung cancer cells. Importantly, Sp1 also affected the expression of ΔNp73 in lung cancer cells.

Sp1 has traditionally been considered to be a ubiquitous transcription factor, responsible for the basal/

constitutive activation of a wide range of viral and mammalian genes. However, novel data strongly correlate deregulated Sp1 expression with tumour development, growth and metastasis, as it is significantly overexpressed in pancreatic, breast, thyroid and colon tumours, and it transactivates genes with a substantial role in cancer progression, cell cycle regulation, and antiapoptotic procedures [28]. Our study makes Sp1 the second transcription factor identified, so far, after E2F1 as directly controlling the *p73* P1 promoter. In addition, it indicates an association between Sp1 overexpression and TAp73 overexpression in lung cancer.

Sp families of transcription factors can form complexes with TAp73 isoforms [29]. Recently, it was shown that TAp73 isoforms interfere with Sp1 transcriptional activity, thus acting as repressors of Sp1-mediated activation of genes, such as those encoding enhancer II of the core protein of hepatitis B virus [30], human telomerase reverse transcriptase [31,32], the potent angiogenic factor VEGF [33] and the cell cycle G_2/M checkpoint controller cyclin B [34]. It is proposed that this repression may be achieved via formation of Sp1–TAp73 complexes, resulting in the abrogation of Sp1 binding to corresponding elements on target gene promoters [30,32]. This tumour suppression mechanism parallels that of p53 [35,36]. The above-mentioned negative effect of p73 on Sp1-mediated transcription is specific only to the TAp73 isoforms, and not the ΔNp73 [31] or ΔTAp73 isoforms [30,32], and its efficiency fluctuates depending on the type of TAp73 isoform, with TAp73β being the most effective suppressor and TAp73γ being the least effective [32]. It remains to be elucidated whether TAp73 interference in the Sp1-mediated transactivation of oncogenes also applies to lung cancer, suggesting that the interactions between Sp1 and TAp73 isoforms extend beyond the level of transcriptional control of the *p73* P1 promoter.

In this study, we also demonstrated that the full-length p73 isoform overexpressed in cancer cells both *in vitro* and *in situ* is TAp73γ. TA isoforms were found to be elevated in lung cancer samples in the past, but the exact TAp73 isoform(s) overexpressed were not determined [2,19]. To the best of our knowledge, this is the first time that this particular isoform has been found to be specifically and exclusively overexpressed in cancer cells. Typically, TAp73 isoforms activate genes that mediate either cell cycle arrest or apoptosis, such as *p21*, *bax*, *mdm2*, *gadd45*, *cyclin G*, *IGFBP3*, and *14-3-3*, and trigger cell death [5]. *In vivo* evidence supports the proposed role of TA isoforms as tumour suppressors, as *TAp73*$^{-/-}$ mice are tumour-prone and develop tumours upon treatment with carcinogens,

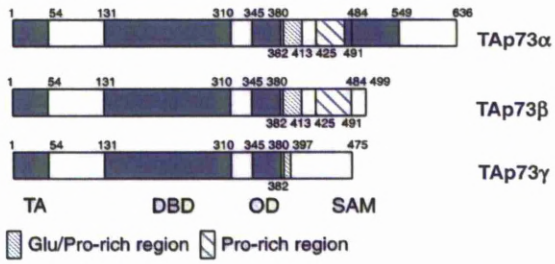

Fig. 6. Comparison between the primary structure of TAp73α, TAp73β, and TAp73γ. Alternative splicing results in the loss of the Pro-rich domain and in the truncation of the Glu/Pro-rich domain, which contains a newly identified N-terminal transactivation domain. OD, oligodimerization domain; SAM, sterile α-motif (based on [40]).

with lung adenocarcinoma being the most frequent cancer diagnosed in these knockout animals [37]. Therefore, our finding raises questions about the presumed role of TAp73γ in cancer, suggesting that its function may diverge from the traditionally proposed apoptotic function of TAp73 isoforms. Indeed, TAp73γ has been almost ineffective in activating the *p21Waf1/Cip1* promoter and inhibiting colony formation of Saos cells, in contrast to the more efficient TAp73α and TAp73β [9]. Similarly, it only poorly transactivates a p53-binding consensus sequence-containing promoter in *p53*-null cell lines [11].

The failure of TAp73γ to exert the same drastic transactivation activities as the more extensively studied TAp73α and TAp73β might be associated with differences in its C-terminal domain (Fig. 6). In this respect, a newly highlighted difference in TAp73γ is that its C-terminal domain is basic and forms weak sequence-specific DNA–protein complexes, whereas the corresponding domains of TAp73α and TAp73β are neutral and form strong DNA–protein complexes, reflecting differential promoter binding and target gene transactivation [38]. Another difference in the C-terminal domain of TAp73γ is that, owing to the excision of exon 11 during alternative splicing, it lacks most of the Glu/Pro-rich domain and the Pro-rich domain, which are located in a region extending from 382 to 491 amino acids and are thought to enhance the transactivation activities of TAp73α and TAp73β [39,40]. In addition, lack of exon 11 in TAp73γ results in the truncation of a second transactivation domain, located within amino acids 381–399, which was recently shown to regulate genes involved in cell cycle progression [41]. The above data imply a transactivational deficit for TAp73γ as compared with other TAp73 isoforms, which could influence its apoptotic function.

In agreement with previous clinical studies [19], we demonstrated that ΔNp73 levels are also elevated in

lung cancer cell lines and in exemplary tumour samples. Furthermore, and for the first time, we showed that ΔNp73 levels are reduced *in vitro* upon inhibition or knockdown of the Sp1 transcription factor. The effect of Sp1 on ΔNp73 expression may be direct, as highly conserved, putative Sp1-binding sites on the *p73* P2 promoter were identified by bioinformatic analysis. This possibly means that Sp1 controls both TAp73 and ΔNp73 expression via regulation of their respective promoters. Alternatively, it is possible that this effect may be indirect, as the overexpression of P2-derived ΔN isoforms could be attributed to the overexpression of TAp73, which is known to activate the P2 promoter [13]. In this case, downregulation of ΔNp73 expression upon Sp1 inhibition or reduction could be caused by subsequent downregulation of TAp73 expression. Furthermore, the possibility that the *p73* P1 promoter is able to produce a fraction of ΔNp73 molecules in lung cancer cannot be excluded, as the P1-derived ΔN′ transcripts, which have been reported to be expressed in lung cancer tumours [19], are also translated to ΔNp73 [14]. In other words, as ΔNp73 proteins are the translational products of both P1-derived ΔN′ and P2-derived ΔN transcripts, the decreased ΔNp73 levels may be attributed, at least in part, to the reduced activity of the *p73* P1 promoter. Finally, it is also possible that the influence of Sp1 on ΔNp73 levels might be the combinational and/or synergistic result of all the above-mentioned processes. Therefore, all of these issues should be addressed in the future.

Taken together, our findings make it clear that there is a link between the expression of Sp1 and p73 isoforms in lung cancer. Not only does Sp1 have the potential to affect the TA and ΔN protein isoform levels, but its deregulated expression is also implicated in lung cancer. On the other hand, TAp73 overexpression in lung cancer could be linked to oncogene-induced DNA damage, as induction of p73 is DNA damage response-dependent [42,43]. The mechanisms that underlie the interplay between Sp1 and full-length or N-terminal-truncated p73 isoform(s) should be further investigated.

Experimental procedures

Bioinformatics

The CONTRA [44] web tool was used for *tp73* P1 promoter analysis, as follows. The direction of transcription of *tp73* was identified, and the most upstream TSS of all *tp73* Ensembl [45] transcripts was selected. One thousand base pairs of the UCSC multiz 28-way 5000 upstream alignment, homologous to the human *tp73* P1 promoter genomic sequences, were used for the initial analysis. The sequences were compared against the V$SP1_Q2_01 TRANSFAC position weight matrix of Sp1 target motifs with a core cut-off of 0.90 and a similarity matrix cut-off of 0.75. The sequence alignment and its accompanying information regarding potential Sp1 sites were downloaded and viewed by JALVIEW [46]. Through BIOEDIT [47], the alignments were imported to Microsoft Word 2003 (http://www.microsoft.com/) for further manipulation.

Cell lines and culture conditions

The following human lung carcinoma cell lines used in this study were obtained from the American Type Culture Collection (Rockville, MD, USA): HNBE, CCL171, IMR90, CALU6, DMS53, CRL5802, HTB182, HTB58, HTB59, SKMES1, A549, CALU3, CRL5935, SKLU1 and CORL23. All cell lines were maintained in DMEM supplemented with 10% fetal bovine serum (Invitrogen, Carlsbad, CA, USA). To evaluate the effects of mithramycin A (Sigma-Aldrich, St Louis, MO, USA), 60–70% confluent cells were incubated with 50–400 nM mithramycin A in 60-mm cell culture dishes for 48 h.

Patient characteristics and tumour specimens

Tumour specimens and their corresponding normal tissues were derived from 26 lung cancer patients, 18 males and eight females. Of the 26 patients, 19 were diagnosed with squamous cell carcinoma and seven with adenocarcinoma. The patients' mean age was 68.6 years. All of the above-mentioned patients underwent surgical tumour excision at the Cardiothoracic Centre of Broadgreen, Liverpool, UK. The study protocol was approved by the Liverpool Ethics Committee and all of the patients provided written, informed consent.

Preparation of total cell lysates and nuclear extracts

For the preparation of total cell lysates, cells were lysed in lysis buffer (20 mmol·L^{-1} Tris, pH 7.6, 0.5% Triton X-100, 250 mmol·L^{-1} NaCl, 3 mmol·L^{-1} EDTA, 3 mmol·L^{-1} EGTA, 10 g·mL^{-1} Pefabloc, 2 mmol·L^{-1} sodium orthovanadate, 10 g·mL^{-1} aprotinin, 10 g·mL^{-1} leupeptin, and 1 mmol·L^{-1} dithiothreitol). Lysates were incubated on ice for 30 min and then centrifuged at 8000 × *g* at 4 °C for 10 min. The supernatant was aliquoted and stored at −70 °C.

For the preparation of nuclear extracts, cells were pelleted and homogenized in ice-cold hypotonic buffer (25 mM Tris, pH 7.5, 5 mM KCl, 0.5 mM $MgCl_2$, 0.5 mM dithiothreitol, 0.5 mM phenylmethanesulfonyl fluoride) with a Teflon–

glass homogenizer. The nuclear fraction was pelleted, washed with isotonic buffer (25 mM Tris, pH 7.5, 5 mM KCl, 0.5 mM $MgCl_2$, 0.5 mM dithiothreitol, 1 mM phenylmethanesulfonyl fluoride, 0.2 mM sucrose) and lysed with extraction buffer (25 mM Tris, pH 7.5, 1 mM EDTA, 0.1% Triton X-100, 0.5 mM dithiothreitol, 0.5 mM phenylmethanesulfonyl fluoride). Nuclear debris was removed by centrifugation at 55 000 *g* for 1 h at 4 °C. Estimations of the protein concentrations for both total cell lysates and nuclear extracts were performed using the Bio-Rad protein assay (Bio-Rad Laboratories, Hercules, CA, USA).

Protein extraction from tumour samples

Frozen tissue samples mixed with ice-cold RIPA buffer [1 × NaCl/P_i, 1% (v/v) Nonidet P-40, 0.5% (w/v) sodium deoxycholate, 0.1% (v/v) SDS] (Sigma-Aldrich) containing protease inhibitors (Roche Applied Science, Hague Road, IN, USA) at a tissue/buffer volume ratio of 1 : 1. The mixture was incubated on ice for 1 h and homogenized with frequent vortexing. The homogenate was centrifuged at 13 000 *g* for 15 min at 4 °C, and the resulting supernatant was collected in a clean Eppendorf tube.

In vitro proteins

In vitro Sp1 was purchased from Promega (Madison, WI, USA). TAp73α, TAp73β and TAp73γ were synthesized from the corresponding expression plasmids [9], using the TnT *in vitro* translation system (Promega).

EMSAs

Annealed oligonucleotides representing regions A, B, C and D of the human *p73* P1 promoter were used (Invitrogen). A consensus Sp1-binding site and a mutant Sp1-binding site were used as positive and negative control, respectively (Santa Cruz Biotechnology, Santa Cruz, CA, USA). Oligonucleotide sequences are summarized in Table 1. Annealed oligonucleotides were end-labelled with [^{32}P]ATP[γP], using T4 polynucleotide kinase (New England Biolabs, Ipwich, MA, USA), following the manufacturer's instructions. Radiolabelled products were purified on Microspin G-25 columns (GE Healthcare, Little Chalfont, UK), according to the manufacturer's instructions. The reaction mixture was prepared by mixing 2000 c.p.m. of γ-^{32}P-labelled oligonucleotide with 20 μg of nuclear cell protein in binding buffer (50 mM Hepes, pH 8.0, 500 mM NaCl, 0.5 M phenylmethanesulfonyl fluoride, 0.5 mg·mL^{-1} BSA, 20% glycerol, 1 mM EDTA) plus 1 mM dithiothreitol and 150 μg·mL^{-1} poly(dI-dC) (Sigma-Aldrich), and left at room temperature for 30 min. The reaction mixtures were subsequently electrophoresed on a 6% polyacrylamide gel at 150 V for 90 min, and the gel was dried and visualized by autoradiography. For the supershift assay, the reaction mixture was incubated with antibody against human Sp1 (PEP2) (Santa Cruz Biotechnology) for 30 min at 4 °C.

ChIP assay

Cells were crosslinked at a final concentration of 1% formaldehyde for 10 min at 37 °C. Crosslinked cells were washed twice in ice-cold NaCl/P_i and collected by centrifugation for 5 min at 300 × *g* The pellet was resuspended in 600 μL of buffer (50 mM Tris/HCl, pH 8.0, 85 mM KCl, 0.5% NP40) and incubated for 10 min on ice. The solution was centrifuged for 5 min at 1700 × *g*, and the pellet was resuspended in 600 μL of lysis buffer (50 mM Hepes/KOH, pH 7.5, 150 mM NaCl, 1 mM EDTA, pH 8.0, 1% Triton X-100, 0.1% sodium deoxycholate, 0.1% SDS) containing protease inhibitors. Lysate was sonicated to shear DNA to an average fragment size of 500–1000 bp, and the debris was pelleted by centrifugation for 5 min at 11 000 × *g* and 4 °C. The soluble chromatin material was further treated with salmon sperm DNA/protein A agarose 50% slurry (Upstate Biotechnology, Lake Placid, NY, USA). After overnight incubation with antibody against Sp1 (sc-59x) (Santa Cruz Biotechnology), the immune complexes were

Table 1. Oligonucleotides used in EMSA experiments. F, forward; R, reverse.

Name	Position (relative to the TSS)	Direction	Oligonucleotides (5′- to 3′)
Region A	−233 to −204 bp	F	aaaggcggcgggaaggaggcggggcagagc
		R	gctctgccccgcctccttcccgccgccttt
Region B	−61 to −33 bp	F	cccgcggcgcctcccctccccgcgccca
		R	tgggcgcggggaggggaggcgccgcggg
Region C	−20 to −1 bp	F	aggggccgggcagcccgccct
		R	agggcgggctgcccggcccct
Region D	−4 to +20 bp	F	ccctgcctcccgcccgcgcaccc
		R	gggtgcgcgggcggggaggcaggg
Cold control oligonucleotide	None	F	attcgatcggggcggggcgag
		R	ctcgccccgccccgatcgaat
mSp1	None	F	attcgatcggttcggggcgag
		R	ctcgccccgaaccgatcgaat

treated with 60 μL of salmon sperm DNA/protein A agarose 50% slurry (Upstate Biotechnology) for 2 h at 4 °C. The beads were then washed sequentially for 5 min at room temperature in 1 mL of lysis buffer without SDS, in 1 mL of lysis buffer plus 500 mM NaCl, in 1 mL of buffer (10 mM Tris/HCl, pH 8.0, 1 mM EDTA, pH 8.0, 250 mM LiCl, 1% NP40, 1% sodium deoxycholate), and finally twice in Tris/EDTA. Immune complexes were eluted with 200 μL of elution buffer (1% SDS, 50 mM Tris/HCl, pH 7.5, 10 mM EDTA) and incubated for 5 min at 65 °C. The pooled elutes were incubated with RNase for 1 h and with proteinase K for 4 h at 65 °C to reverse crosslinks. DNA was extracted by phenol/chloroform treatment and precipitated with 10 μg of glycogen and ethanol overnight at – 20 °C. The pelleted DNA was resuspended in 10 μL of nuclease free water and amplified by PCR. The PCR primers used were as follows: forward, 5′-TCG CCG GGC TCT GCA GGA G-3′; and reverse, 5′-GTT TCG CTG CGT CCC CTT CGC-3′.

siRNA transient transfection

Sp1 Validated Stealth RNAi DuoPak and its medium-GC content siRNA control (Invitrogen) were used for knockdown of *p73* and *VEGF*. A549 cells were harvested in six-well plates and transfected with Lipofectamine RNAiMAX according to the manufacturer's instructions. Lipofectamine-containing medium was replaced after 6 h. Cells were collected following a 48-h incubation at 37 °C, and total proteins were isolated for western blot analysis.

Double-stranded oligonucleotide functional analysis

We used phosphorothioate oligonucleotides for regions A, B and C (Invitrogen) to transiently transfect the A549 cell line, as previously described [48]. Cells were harvested in six-well plates and transfected with 150 nM Sp1-decoy oligonucleotides, using Fugene transfection reagent (Roche Applied Science), according to the manufacturer's instructions. After 4 h, the medium was replaced with fresh medium, without Fugene and oligonucleotides. The cells were collected 4, 12 and 24 h after transfection, and total proteins extracted from these cells were subjected to western blot analysis.

Western blot analysis

Protein extracts (10 μg) were electrophoresed on an 8% SDS/polyacrylamide gel under reducing conditions, transferred to nitrocellulose membranes, and blocked for 2 h at room temperature. The blots were subsequently incubated overnight at 4 °C with the following primary antibodies: rabbit immunoglobulin against human Sp1 (PEP2) (Santa Cruz Biotechnology), mouse immunoglobulin against human β-actin (Abcam, Cambridge, UK), mouse immunoglobulin against human full length p73 (which has been shown to recognize TAp73α, TAp73β, and TAp73γ [49]), rabbit immunoglobulin against human VEGF (sc-507) (Santa Cruz Biotechnology), and mouse immunoglobulin against human ΔNp73 (Abcam), in 1 : 600, 1 : 1000, 1 : 4000, 1 : 500 and 1 : 500 dilutions, respectively. The blots were incubated with the appropriate secondary horseradish peroxidase-conjugated antibodies (Santa Cruz, Santa Cruz, CA, USA) in corresponding dilutions of 1 : 8000, 1 : 5000, 1 : 10 000, 1 : 3000 and 1 : 10 000 for 2 h at room temperature. Detection of protein levels was carried out using an enhanced chemiluminescence system (Pierce, Rockford, IL, USA). The protein amounts were normalized to β-actin and quantified using IMAGEQUANT software (GE Healthcare, Little Chalfont, UK).

Acknowledgements

We thank G. Melino for kindly providing us with the TAp73 constructs. S. Logotheti and V. Zoumpourlis were supported by 05NON-EU-3. A. Daskalos, T. Liloglou and J. K. Field were supported by the Roy Castle Lung Cancer Foundation, UK. B. Vojtesek was supported by grants IGA MZ CR NS/9812-4 and MZOMOU2005. V Gorgoulis is financially supported by European commition grants FP-7 GENICA and FP-7 INLACARE.

References

1 Minna JD, Roth JA & Gazdar AF (2002) Focus on lung cancer. *Cancer Cell* **1**, 49–52.
2 Tokuchi Y, Hashimoto T, Kobayashi Y, Hayashi M, Nishida K, Hayashi S, Imai K, Nakachi K, Ishikawa Y, Nakagawa K *et al.* (1999) The expression of p73 is increased in lung cancer, independent of p53 alteration. *Br J Cancer* **80**, 1623–1629.
3 Melino G, Lu X, Gasco M, Crook T & Knight RA (2003) Functional regulation of p73 and p63: development and cancer. *Trends Biochem Sci* **28**, 663–670.
4 De Laurenzi V & Melino G (2000) Evolution of functions within the p53/p63/p73 family. *Ann NY Acad Sci* **926**, 90–100.
5 Melino G, Bernassola F, Ranalli M, Yee K, Zong WX, Corazzari M, Knight RA, Green DR, Thompson C & Vousden KH (2004) p73 Induces apoptosis via PUMA transactivation and Bax mitochondrial translocation. *J Biol Chem* **279**, 8076–8083.
6 Nomoto S, Haruki N, Kondo M, Konishi H, Takahashi T, Takahashi T & Takahashi T (1998) Search for mutations and examination of allelic expression imbalance of the p73 gene at 1p36.33 in human lung cancers. *Cancer Res* **58**, 1380–1383.

7 Yang A, Walker N, Bronson R, Kaghad M, Oosterwegel M, Bonnin J, Vagner C, Bonnet H, Dikkes P, Sharpe A *et al.* (2000) p73-deficient mice have neurological, pheromonal and inflammatory defects but lack spontaneous tumours. *Nature* **404**, 99–103.

8 Kaghad M, Bonnet H, Yang A, Creancier L, Biscan JC, Valent A, Minty A, Chalon P, Lelias JM, Dumont X *et al.* (1997) Monoallelically expressed gene related to p53 at 1p36, a region frequently deleted in neuroblastoma and other human cancers. *Cell* **90**, 809–819.

9 De Laurenzi V, Costanzo A, Barcaroli D, Terrinoni A, Falco M, Annicchiarico-Petruzzelli M, Levrero M & Melino G (1998) Two new p73 splice variants, gamma and delta, with different transcriptional activity. *J Exp Med* **188**, 1763–1768.

10 De Laurenzi VD, Catani MV, Terrinoni A, Corazzari M, Melino G, Costanzo A, Levrero M & Knight RA (1999) Additional complexity in p73: induction by mitogens in lymphoid cells and identification of two new splicing variants epsilon and zeta. *Cell Death Differ* **6**, 389–390.

11 Ueda Y, Hijikata M, Takagi S, Chiba T & Shimotohno K (1999) New p73 variants with altered C-terminal structures have varied transcriptional activities. *Oncogene* **18**, 4993–4998.

12 Ishimoto O, Kawahara C, Enjo K, Obinata M, Nukiwa T & Ikawa S (2002) Possible oncogenic potential of DeltaNp73: a newly identified isoform of human p73. *Cancer Res* **62**, 636–641.

13 Grob TJ, Novak U, Maisse C, Barcaroli D, Lüthi AU, Pirnia F, Hügli B, Graber HU, De Laurenzi V, Fey MF *et al.* (2001) Human ΔNp73 regulates a dominant negative feedback loop for TAp73 and p53. *Cell Death Differ* **8**, 1213–1223.

14 Stiewe T, Tuve S, Peter M, Tannapfel A, Elmaagacli AH & Putzer BM (2004) Quantitative TP73 transcript analysis in hepatocellular carcinomas. *Clin Cancer Res* **10**, 626–633.

15 Marabese M, Vikhanskaya F & Broggini M (2007) p73: a chiaroscuro gene in cancer. *Eur J Cancer* **43**, 1361–1372.

16 Tuve S, Wagner SN, Schittek B & Putzer BM (2004) Alterations of DeltaTA-p73 splice transcripts during melanoma development and progression. *Int J Cancer* **108**, 162–166.

17 Uramoto H, Sugio K, Oyama T, Nakata S, Ono K, Morita M, Funa K & Yasumoto K (2004) Expression of deltaNp73 predicts poor prognosis in lung cancer. *Clin Cancer Res* **10**, 6905–6911.

18 Mai M, Yokomizo A, Qian C, Yang P, Tindall DJ, Smith DI & Liu W (1998) Activation of p73 silent allele in lung cancer. *Cancer Res* **58**, 2347–2349.

19 Di Vinci A, Sessa F, Casciano I, Banelli B, Franzi F, Brigati C, Allemanni G, Russo P, Dominioni L & Romani M (2009) Different intracellular compartmentalization of TA and ΔNp73 in non-small cell lung cancer. *Int J Oncol* **34**, 449–456.

20 Nyman U, Sobczak-Pluta A, Vlachos P, Perlmann T, Zhivotovsky B & Joseph B (2005) Full-length p73alpha represses drug-induced apoptosis in small cell lung carcinoma cells. *J Biol Chem* **280**, 34159–34169.

21 Muller M, Schilling T, Sayan AE, Kairat A, Lorenz K, Schulze-Bergkamen H, Oren M, Koch A, Tannapfel A, Stremmel W *et al.* (2005) TAp73/DNp73 influences apoptotic response, chemosensitivity and prognosis in hepatocellular carcinoma. *Cell Death Differ* **12**, 1564–1577.

22 Seelan RS, Irwin M, van der Stoop P, Qian C, Kaelin WG & Liu W (2002) The human p73 promoter: characterization and identification of functional E2F binding sites. *Neoplasia* **4**, 195–203.

23 Irwin M, Marin MC, Phillips AC, Seelan RS, Smith DI, Liu W, Flores ER, Tsai KY, Jacks T, Vousden KH *et al.* (2000) Role for the p53 homologue p73 in E2F-1-induced apoptosis. *Nature* **407**, 645–648.

24 Stiewe T & Pützer BM (2001) Role of the p53-homologue p73 in E2F1-induced apoptosis. *Nat Genet* **26**, 464–469.

25 Ding Y, Inoue T, Kamiyama J, Tamura Y, Ohtani-Fujita N, Igata E & Sakai T (1999) Molecular cloning and functional characterization of the upstream promoter region of the human p73 gene. *DNA Res* **6**, 347–351.

26 Shi Q, Le X, Abbruzzese JL, Peng Z, Qian CN, Tang H, Xiong Q, Wang B, Li XC & Xie K (2001) Constitutive Sp1 activity is essential for differential constitutive expression of vascular endothelial growth factor in human pancreatic adenocarcinoma. *Cancer Res* **61**, 4143–4154.

27 Jia Z, Zhang J, Wei D, Wang L, Yuan P, Le X, Li Q, Yao J & Xie K (2007) Molecular basis of the synergistic antioncogenic activity of bevacizumab and mithramycin A. *Cancer Res* **67**, 4878–4885.

28 Safe S & Abdelrahim M (2005) Sp transcription factor family and its role in cancer. *Eur J Cancer* **41**, 2438–2448.

29 Koutsodontis G, Vasilaki E, Chou WC, Papakosta P & Kardassis D (2005) Physical and functional interactions between members of the tumour suppressor p53 and the Sp families of transcription factors: importance for the regulation of genes involved in cell-cycle arrest and apoptosis. *Biochem J* **389**, 443–455.

30 Buhlmann S, Racek T, Schwarz A, Schaefer S & Pützer BM (2008) Molecular mechanism of p73-mediated regulation of hepatitis B virus core promoter/enhancer II: implications for hepatocarcinogenesis. *J Mol Biol* **378**, 20–30.

31 Beitzinger M, Oswald C, Beinoraviciute-Kellner R & Stiewe T (2006) Regulation of telomerase activity by

the p53 family member p73. *Oncogene* **25**, 813–826.
32 Racek T, Mise N, Li Z, Stoll A & Pützer BM (2005) C-terminal p73 isoforms repress transcriptional activity of the human telomerase reverse transcriptase (hTERT) promoter. *J Biol Chem* **280**, 40402–40405.
33 Salimath B, Marmé D & Finkenzeller G (2000) Expression of the vascular endothelial growth factor gene is inhibited by p73. *Oncogene* **19**, 3470–3476.
34 Innocente SA & Lee JM (2005) p73 is a p53-independent, Sp1-dependent repressor of cyclin B1 transcription. *Biochem Biophys Res Commun* **329**, 713–718.
35 Kanaya T, Kyo S, Hamada K, Takakura M, Kitagawa Y, Harada H & Inoue M (2000) Adenoviral expression of p53 represses telomerase activity through down-regu lation of human telomerase reverse transcriptase transcription. *Clin Cancer Res* **6**, 1239–1247.
36 Xu D, Wang Q, Gruber A, Björkholm M, Chen Z, Zaid A, Selivanova G, Peterson C, Wiman KG & Pisa P (2000) Downregulation of telomerase reverse transcriptase mRNA expression by wild type p53 in human tumor cells. *Oncogene* **19**, 5123–5133.
37 Tomasini R, Tsuchihara K, Wilhelm M, Fujitani M, Rufini A, Cheung CC, Khan F, Itie-Youten A, Wakeham A, Tsao MS *et al.* (2008) TAp73 knockout shows genomic instability with infertility and tumor suppressor functions. *Genes Dev* **22**, 2677–2691.
38 Sauer M, Bretz AC, Beinoraviciute-Kellner R, Beitzinger M, Burek C, Rosenwald A, Harms GS & Stiewe T (2008) C-terminal diversity within the p53 family members account for differences in DNA binding and transcriptional activity. *Nucleic Acids Res* **36**, 1900–1912.
39 Takada N, Ozaki T, Ichimiya S, Todo S & Nakagawara A (1999) Identification of a transactivation activity in the COOH-terminal region of p73 which is impaired in the naturally occurring mutants found in human neuroblastomas. *Cancer Res* **59**, 2810–2814.
40 Ozaki T, Naka M, Takada N, Tada M, Sakiyama S & Nakagawara A (1999) Deletion of the COOH-terminal region of p73α enhances both its transactivation function and DNA-binding activity but inhibits induction of apoptosis in mammalian cells. *Cancer Res* **59**, 5902–5907.
41 Nyman U, Vlachos P, Cascante A, Hermanson O, Zhivotovsky B & Joseph B (2009) Protein kinase C-dependent phosphorylation regulates the cell cycle-inhibitory function of the p73 carboxy terminus transactivation domain. *Mol Cell Biol* **29**, 1814–1825.
42 Liontos M, Niforou K, Velimezi G, Vougas K, Evangelou K, Apostolopoulou K, Vrtel R, Damalas A, Kontovazenitis P, Kotsinas A *et al.* (2009) Modulation of the E2F1-driven cancer cell fate by the DNA damage response machinery and potential novel E2F1 targets in osteosarcomas. *Am J Pathol* **175**, 376–391.
43 Halazonetis TD, Gorgoulis VG & Bartek J (2008) An oncogene-induced DNA damage model for cancer development. *Science* **319**, 1352–1355.
44 Hooghe B, Hulpiau P, van Roy F & De Bleser P (2008) ConTra: a promoter alignment analysis tool for identification of transcription factor binding sites across species. *Nucleic Acids Res* **36**, W128–W132.
45 Hubbard TJ, Aken BL, Ayling S, Ballester B, Beal K, Bragin E, Brent S, Chen Y, Clapham P, Clarke L *et al.* (2009) Ensembl 2009. *Nucleic Acids Res* **37**, D690–D697.
46 Waterhouse AM, Procter JB, Martin DM, Clamp M & Barton GJ (2009) Jalview Version 2 – a multiple sequence alignment editor and analysis workbench. *Bioinformatics* **25**, 1189–1191.
47 Hall TA (1999) BioEdit: a user-friendly biological sequence alignment editor and analysis program for Windows 95/98/NT. *Nucleic Acids Symp Ser* **41**, 95–98.
48 Park YG, Nesterova M, Agrawal S & Cho-Chung YS (1999) Dual blockade of cyclic AMP response element-(CRE) and AP-1-directed transcription by CRE-transcription factor decoy oligonucleotide. *J Biol Chem* **274**, 1573–1580.
49 Sayan AE, Paradisi A, Vojtesek B, Knight RA, Melino G & Candi E (2005) New antibodies recognizing p73: comparison with commercial antibodies. *Biochem Biophys Res Commun* **330**, 186–193.

Supporting information

The following supplementary material is available:
Fig. S1. (A) TAp73 and Sp1 protein expression in 26 lung cancer patients. N, normal tissue; T, tumour tissue; PNo, patient number. (B) TAp73γ/Sp1 ratio in lung cancer patient samples.

This supplementary material can be found in the online version of this article.

Please note: As a service to our authors and readers, this journal provides supporting information supplied by the authors. Such materials are peer-reviewed and may be re-organized for online delivery, but are not copy-edited or typeset. Technical support issues arising from supporting information (other than missing files) should be addressed to the authors.